ECRイオン源の基礎と今後の課題

(Basics of ECR ion sources and future challenges)

阪大　加藤　裕史*, **

Yushi Kato (Osaka Univ.) *, **

Background:

*1984-90 Compact Torus(Magnetized coaxial gun, reconnection, MHD, m-probe, VIS, VUV…etc)

1990-2005 ECRIS(multicharged, B cofig., implantation, & several processes)(Toyama Pref. Univ.)

2005-13(IH vapor sources, etc.), 2013-25 ECRIS (ecr efficiency, accecibilities) (Osaka Univ.)

2016.1-2 (On-campus relocation and restructuring), 2018.6.8-2019 (Earthquake and recovery), 2020-2023(Conona

**実験的研究推進の立場で　(我々のECRISに関しての)

2025(R7)0220 FSS 於理研

**From the standpoint of promoting experimental research　(Regarding our ECRIS)

Contents

Diamagnetic:properties of charged particles:

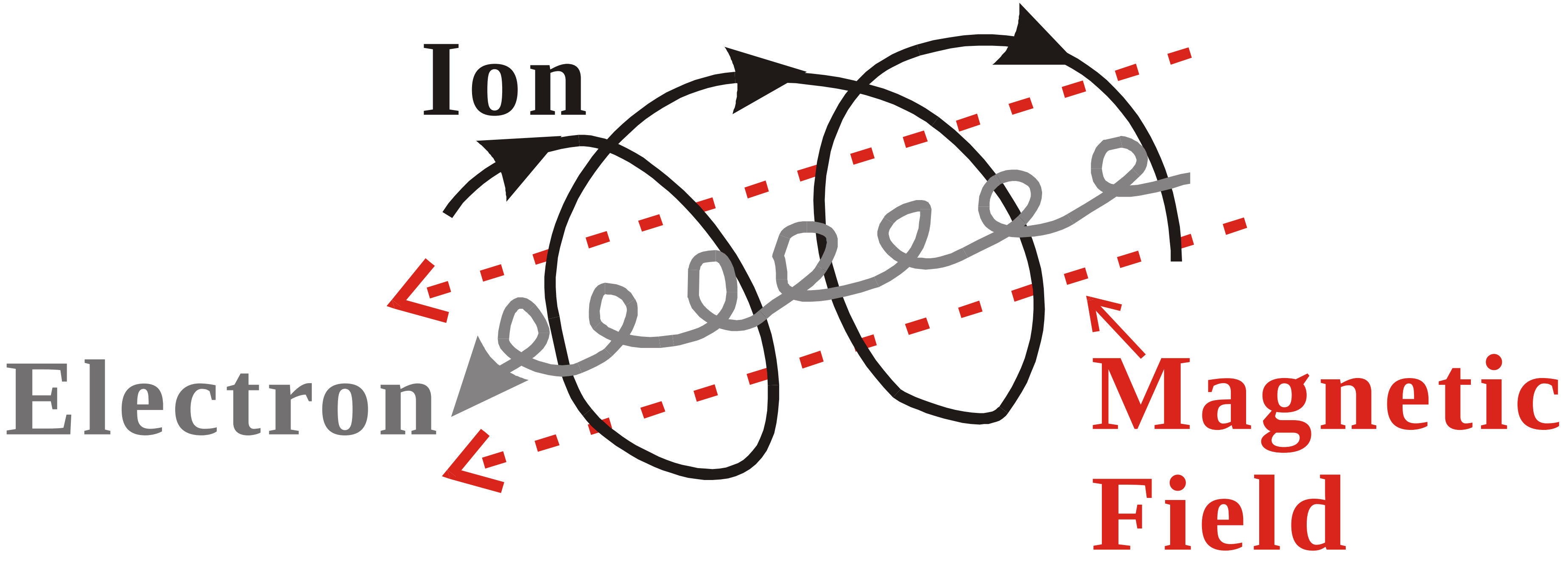

サイクロトロン角周波数: $\omega_c = 2\pi f_c$

電子: $\omega_{ce} \equiv \frac{|-e|B}{m_e} = \frac{eB}{m_e}$

イオン: $\omega_{ci} \equiv \frac{|q|B}{m_i} = \frac{eZB}{Am_p}$

- ECR heating $\left(\omega_{ce}\left(\equiv \frac{eB}{m_e}\right) \sim \omega \text{ (applied electromagnetic waves)}\right)$

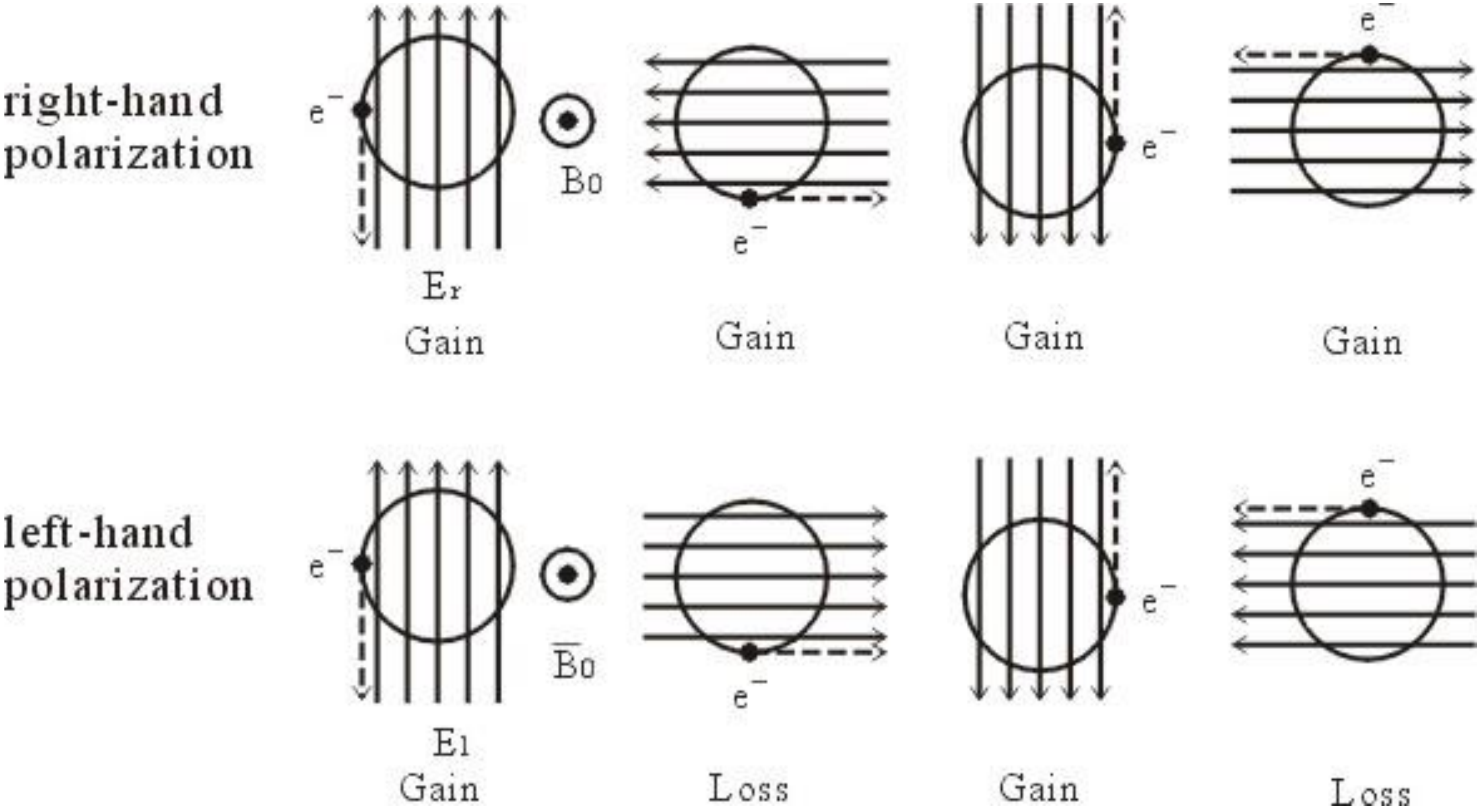

History

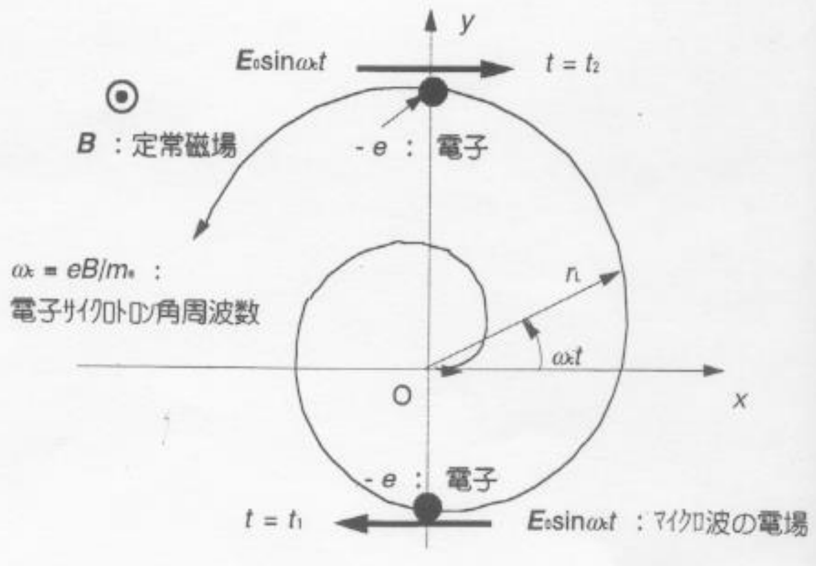

$\omega = \omega_c$ の時，電子は常に加速される．電子の走行距離が長いので低ガス圧で放電が可能である．

電子サイクロトロン共鳴(ECR)による電子の加速

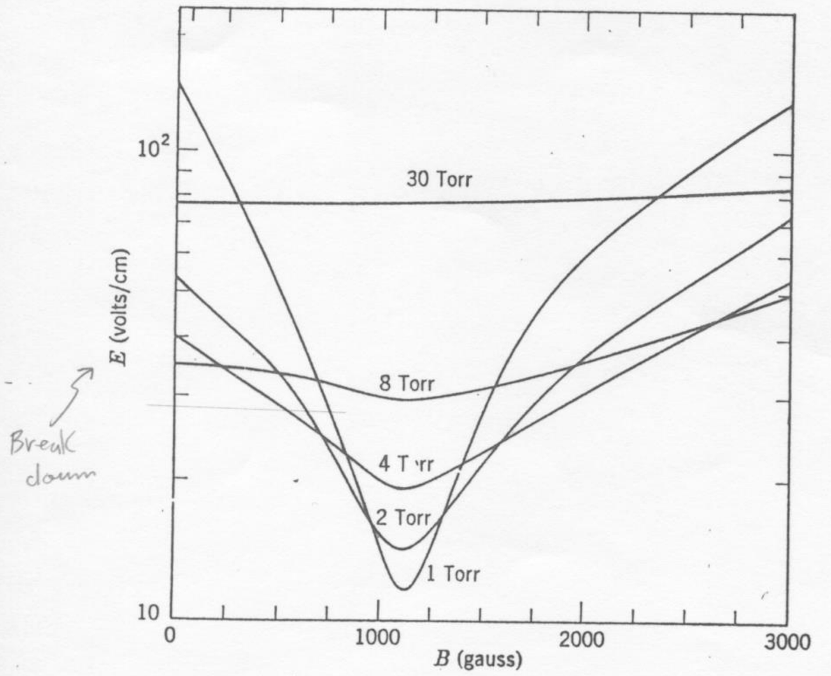

Figure 6-10 Breakdown electric fields in helium as a function of value of transverse magnetic field for different pressures at 3.1 Gc/sec with $\Lambda = 1.51$ cm.

キャビティー中のECR
Bardet, Consoli and Geller (1965)

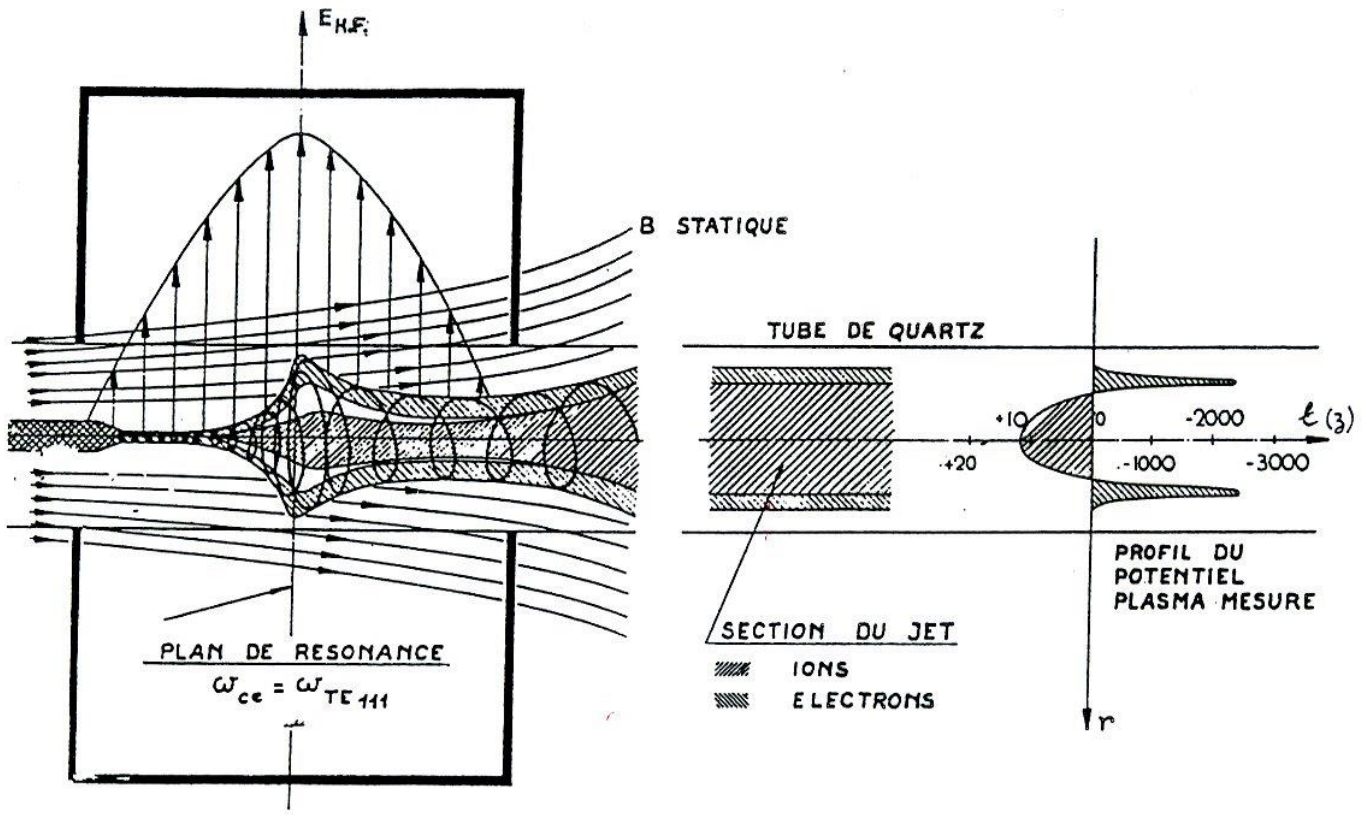

Fig. 5 Représentation du mécanisme d'entraînement et profil réel relevé expérimentalement du potentiel flottant du faisceau.

Vacuum & Operating pressure on ECRIS

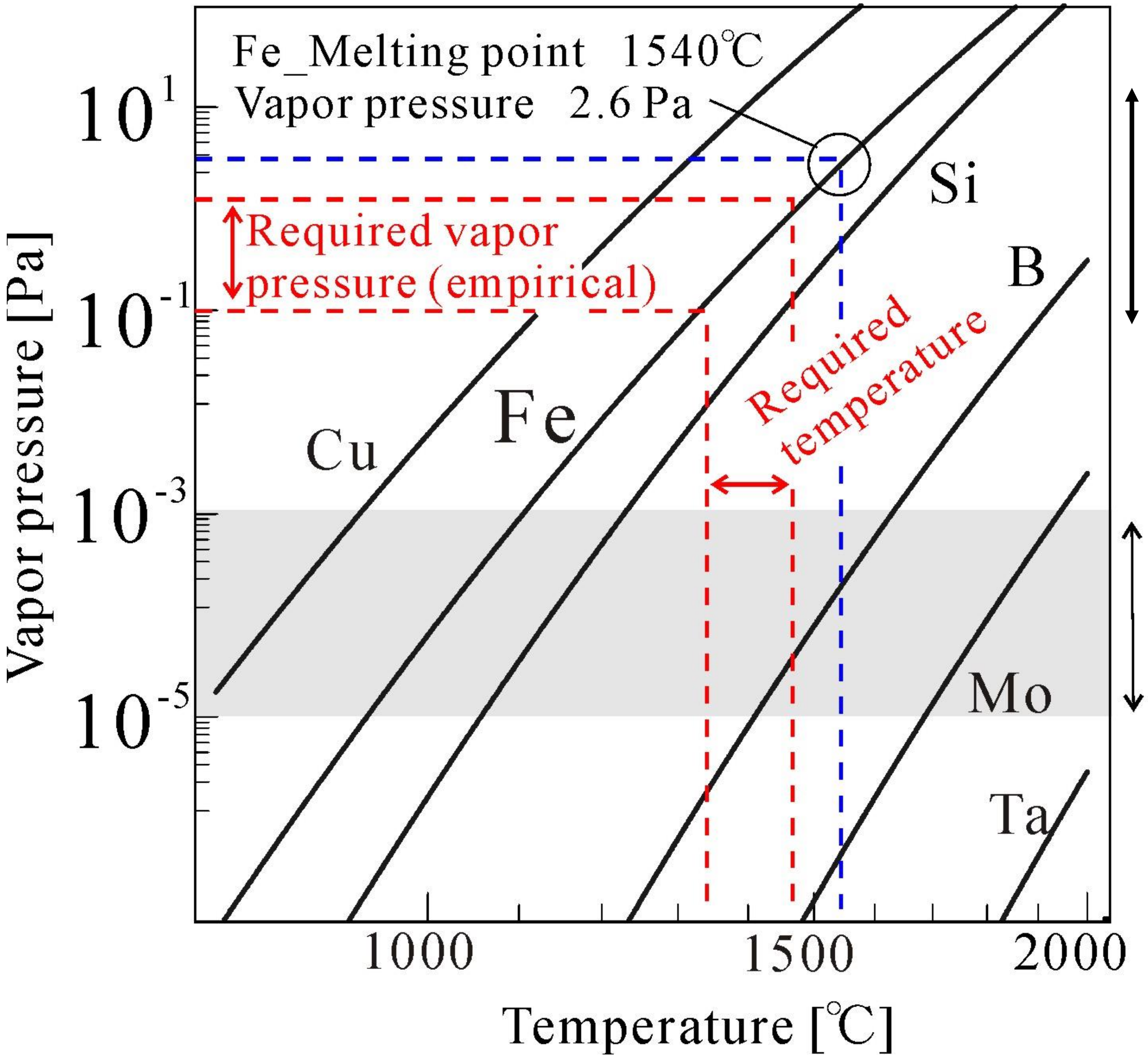

Operating pressure in process plasma $10^{-1\sim+2}$ Pa

$n_0 = 10^{19\sim22}$ m^{-3}

Operating pressure in ECRIS $10^{-5\sim-3}$ Pa

$n_0 = 10^{15\sim17}$ m^{-3}

↓

~cutoff n_c

・ミラー磁場による荷電粒子閉じ込め原理 （Plasma confinement）

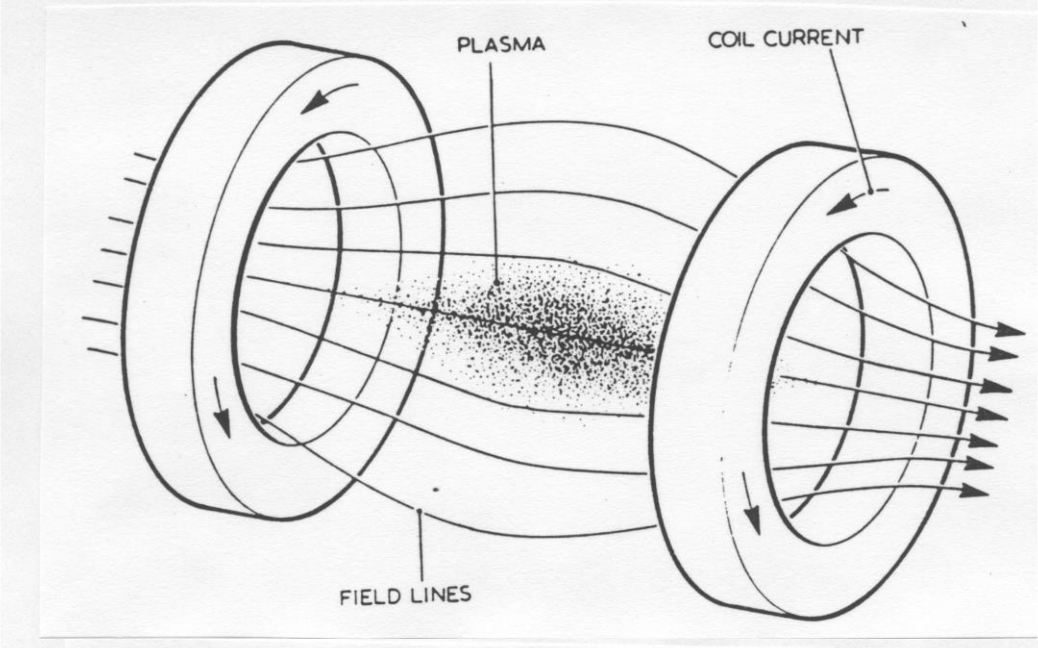

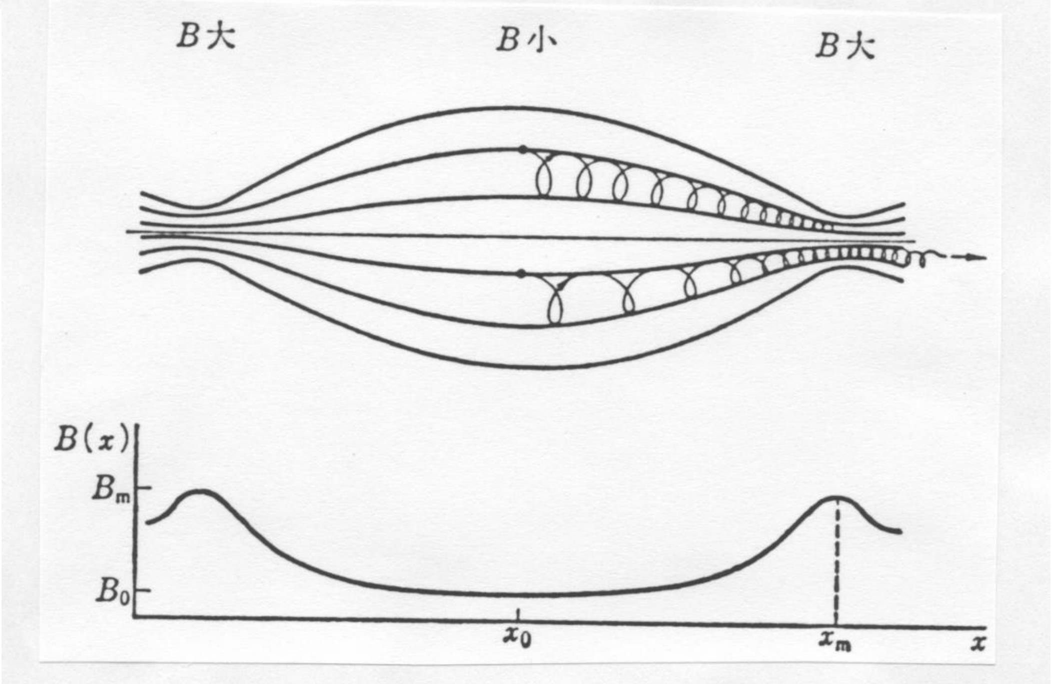

・磁気モーメントμ $\qquad \mu = \dfrac{\frac{1}{2}mv_\perp^2}{B} = const.$

・運動エネルギーE $\qquad E = \frac{1}{2}mv_{//}^2 + \frac{1}{2}mv_\perp^2 = const.$

Larmor半径: $r_L = v_\perp / \omega_c$
サイクロトロン角周波数: $\omega_c = qB/m$
(サイクロトロン周波数: $f_c = \omega_c / 2\pi$)

・Magnetics & Equilibrium:
A.I. Morozov and L.S. Solov'ev, \`The structure of magnetic fields\`; Review of Plasma Physics II
V.D. Shafranov, \`Plasma equilibrium in magnetic field\`, *ibid*.

・Mirror Confinement: *ibid,* XII

Confinement:
Minimum ***B*** configuration (極小磁場配位)*

- Mirror + Multipole field

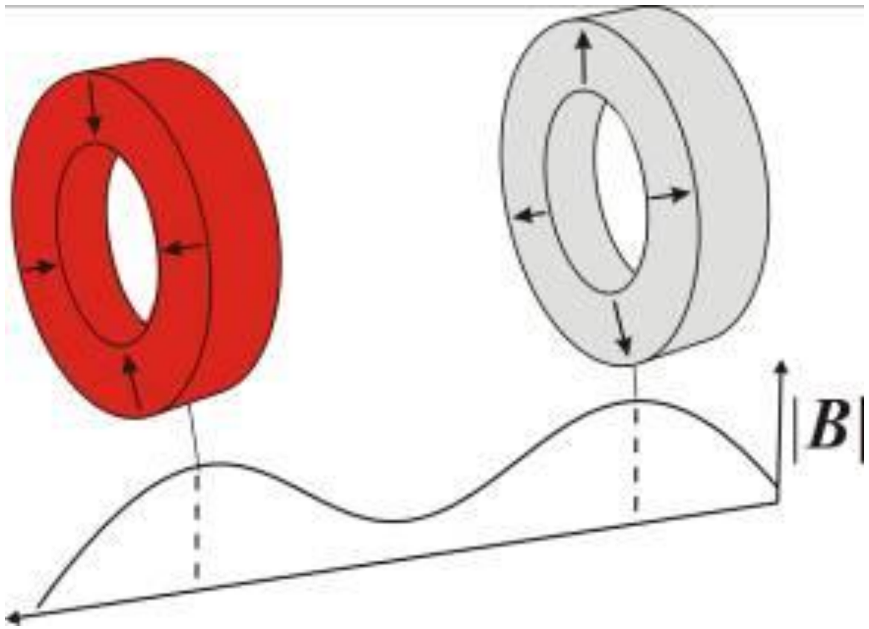

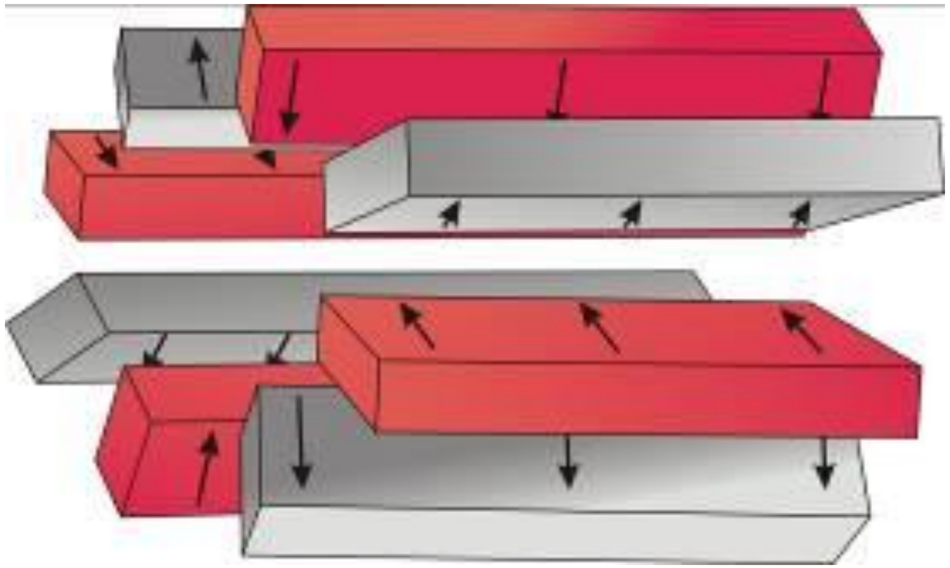

F.F.Chen, `Introduction to Plasma Physics`, Chapter 9.

＊宮本健郎,「核融合のためのプラズマ物理」(1987)p.23, 206, 475, 511

実際の装置構成

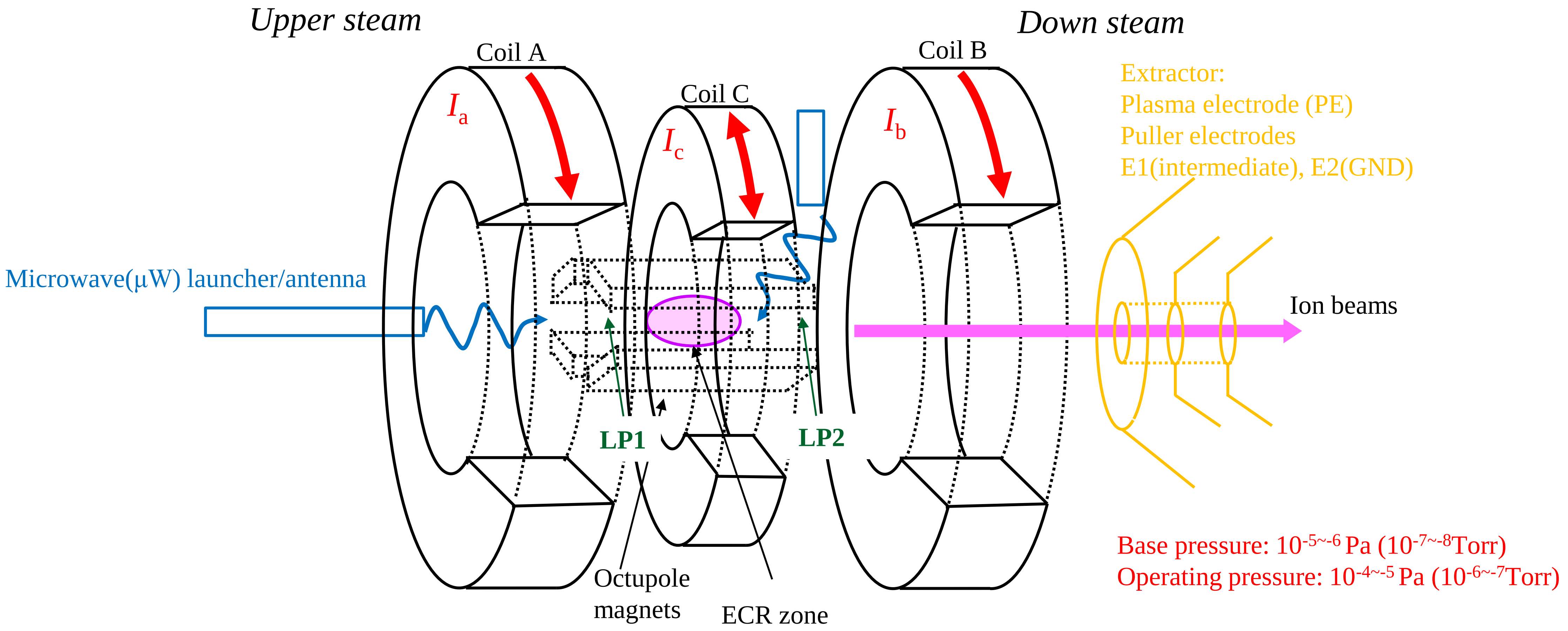

ミラー磁場＋多極磁場：極小磁場配位

Mirror field + Multipole field : Minimum B Configuration

μW launch to ECR zone (points) at bottom of mirror field

→小型重粒子線癌治療機等:All magnets & f-variable

Multipole and Race-track fields
- our experience in ECR process plasma -

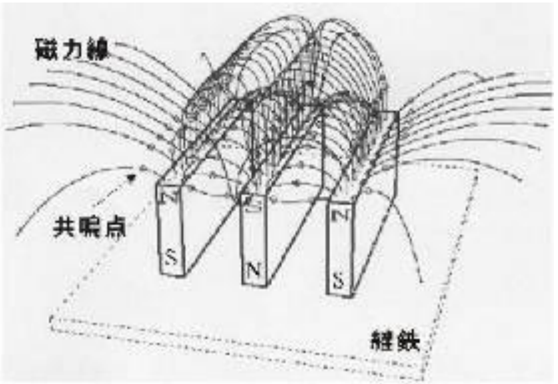

開いたアーチ形ミラー磁場

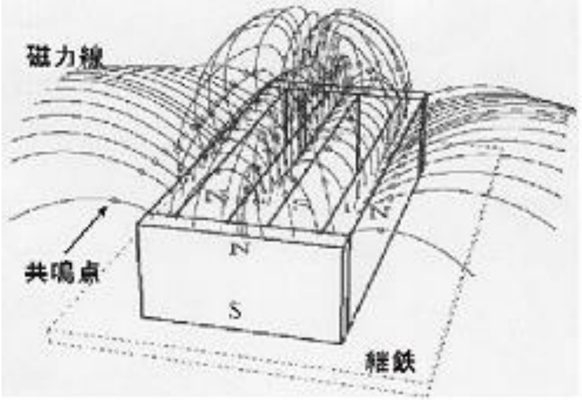

閉じたアーチ形ミラー磁場

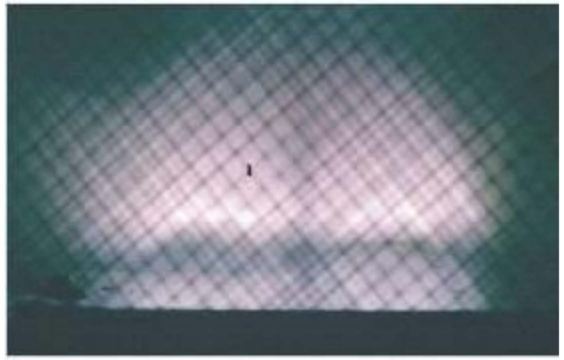

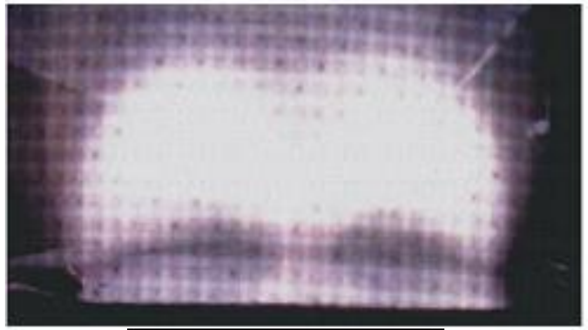

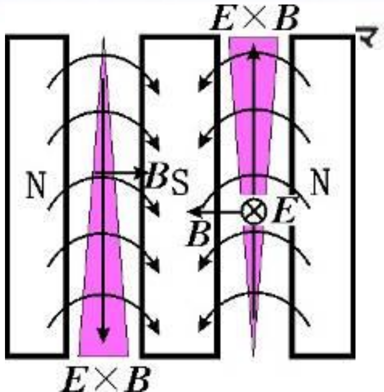

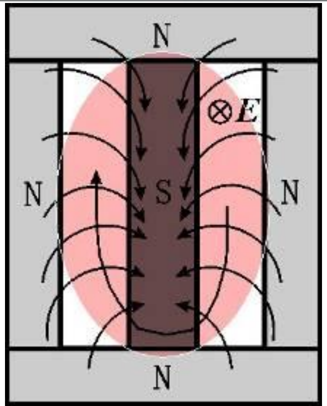

Design Aspects

Cylindrically Comb-Shaped Magnetic Field

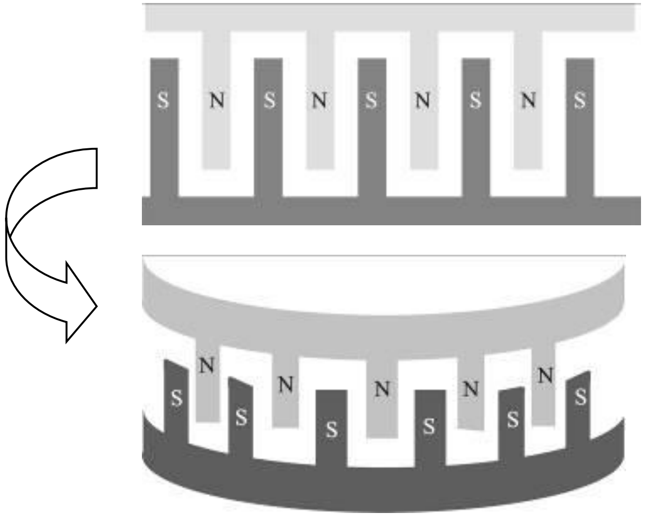

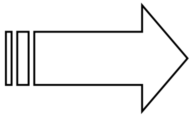

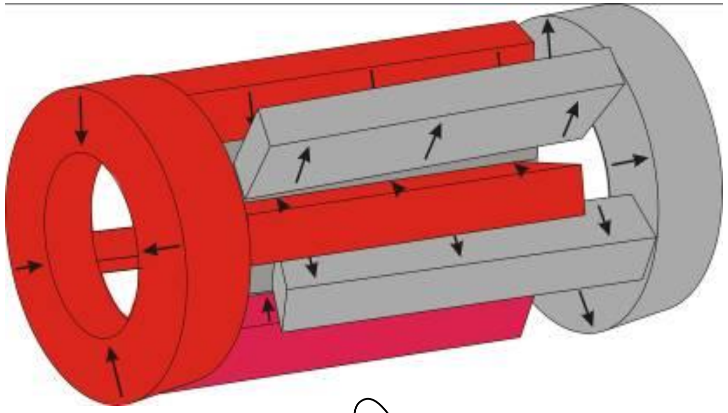

- New aspects against conventional ECRIS !

Multipole magnets

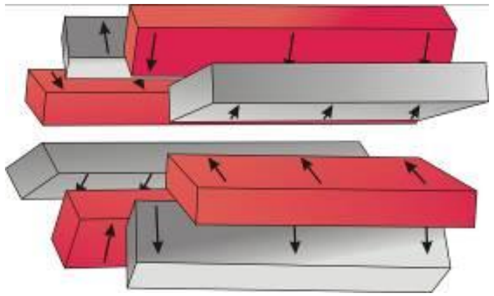

+

mirror field

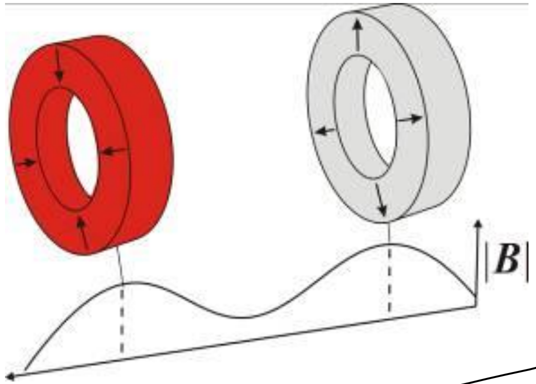

enough particle-confinement to produce multicharged ion→ feasibility of new application

Cylindrically comb-shaped magnetic field

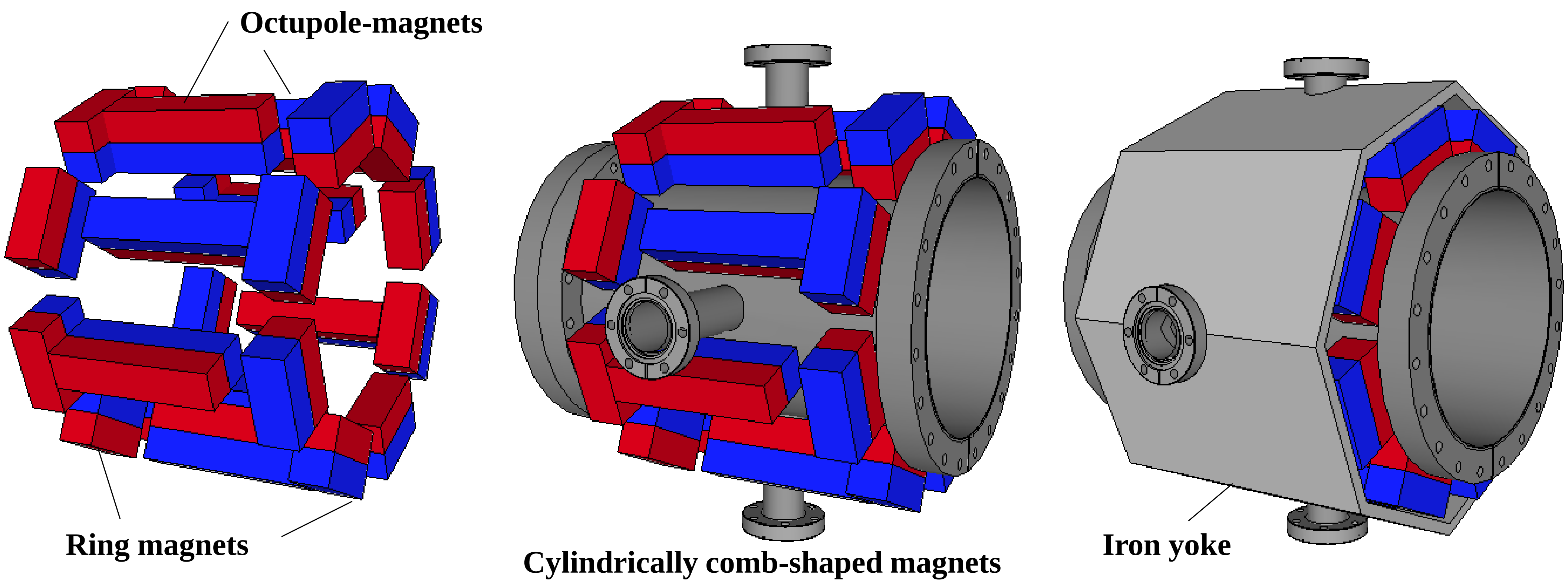

200mmϕ

図 3.4.2 円筒櫛状磁場の構造, 磁石外側は鉄ヨークにより磁気回路を形成している.

Tandem type ECRIS

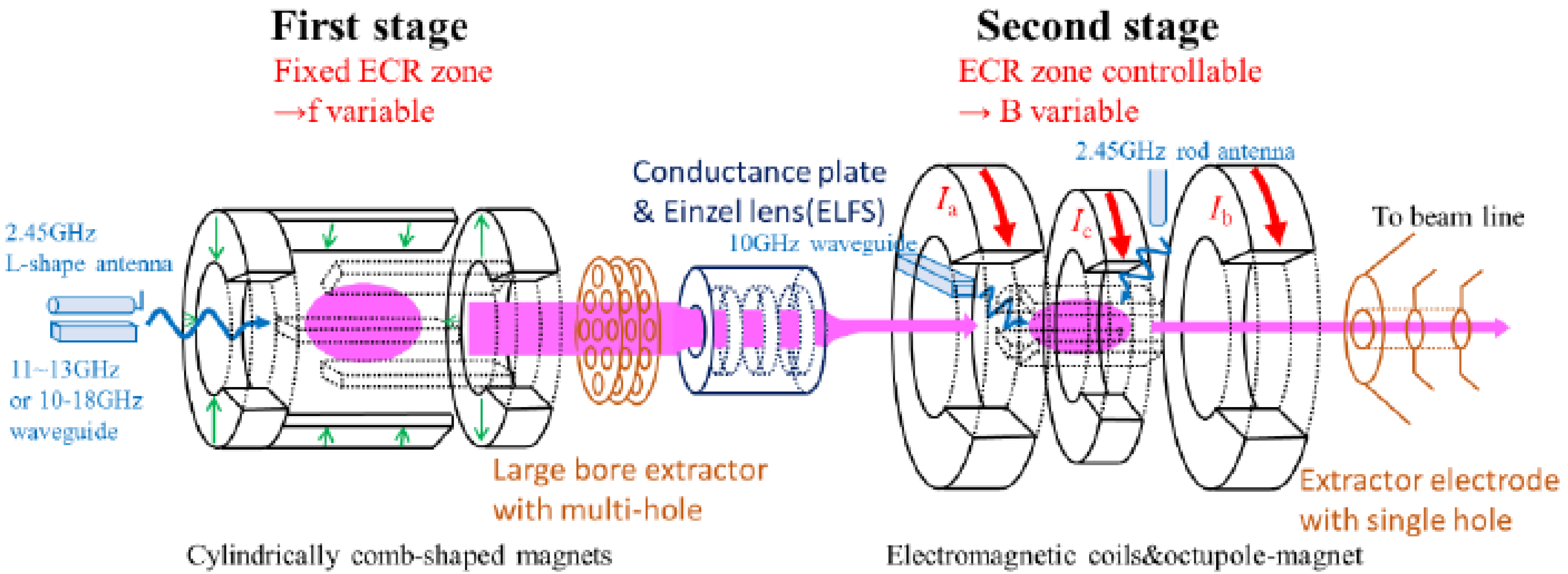

図 3.1.1 タンデム型 ECR イオン源の概略図

Production: *Microwave (μW) discharges* Electron Cyclotron Ion Sources
NIRS Kei3での2f waves exp
(2016.0615-17 & 1121-25)

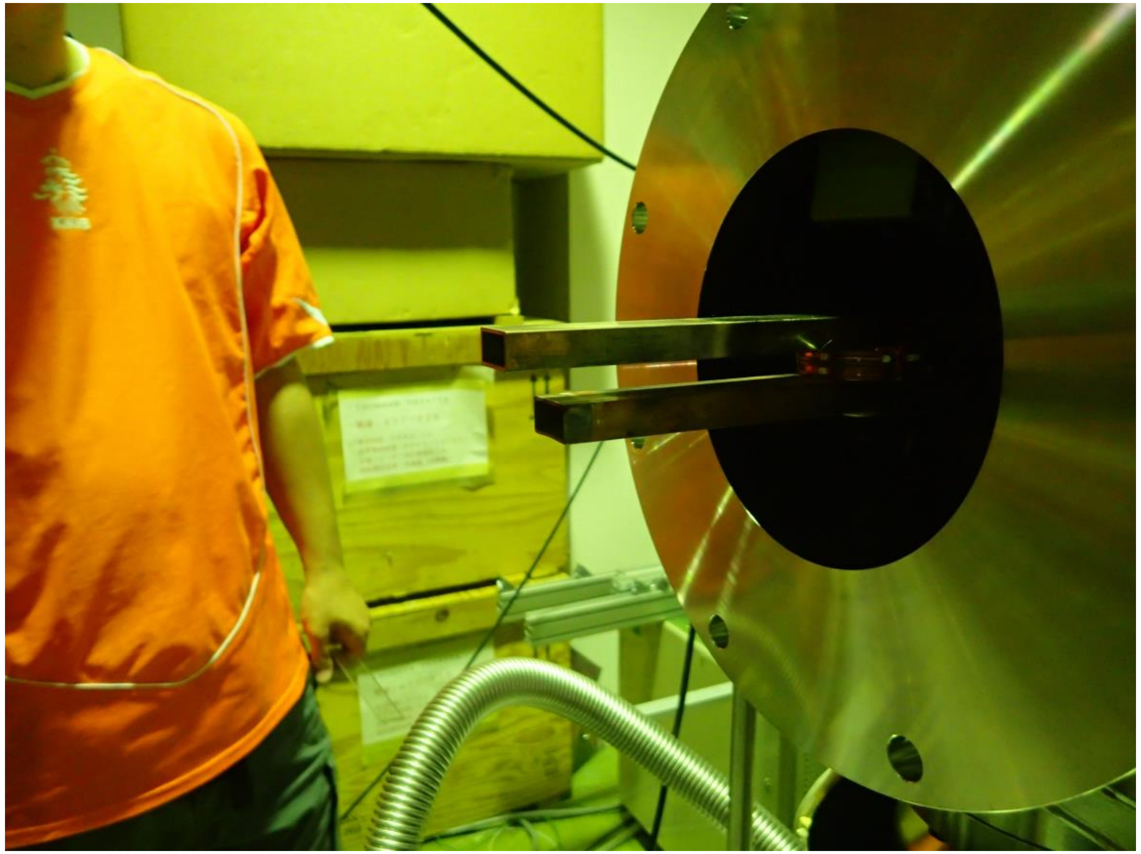

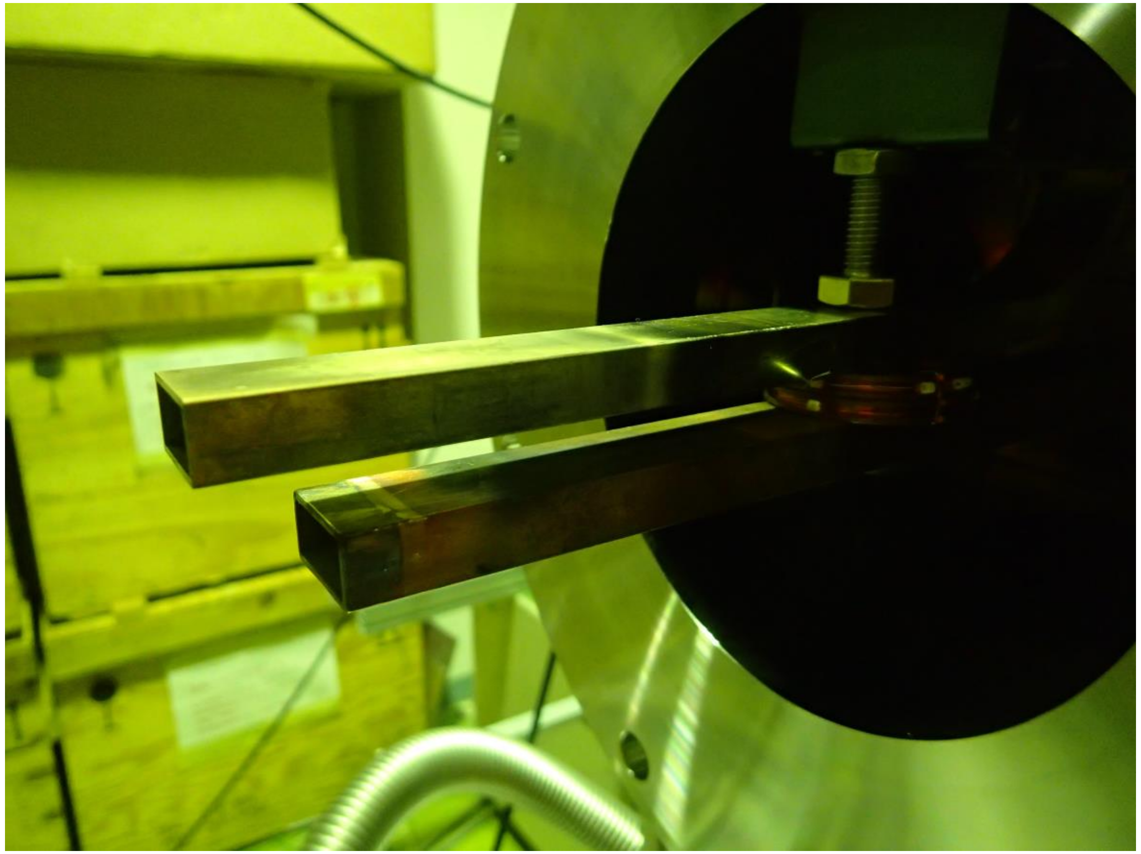

Panoramic view of our ECRIS(O.U.) 2025(R7)0218

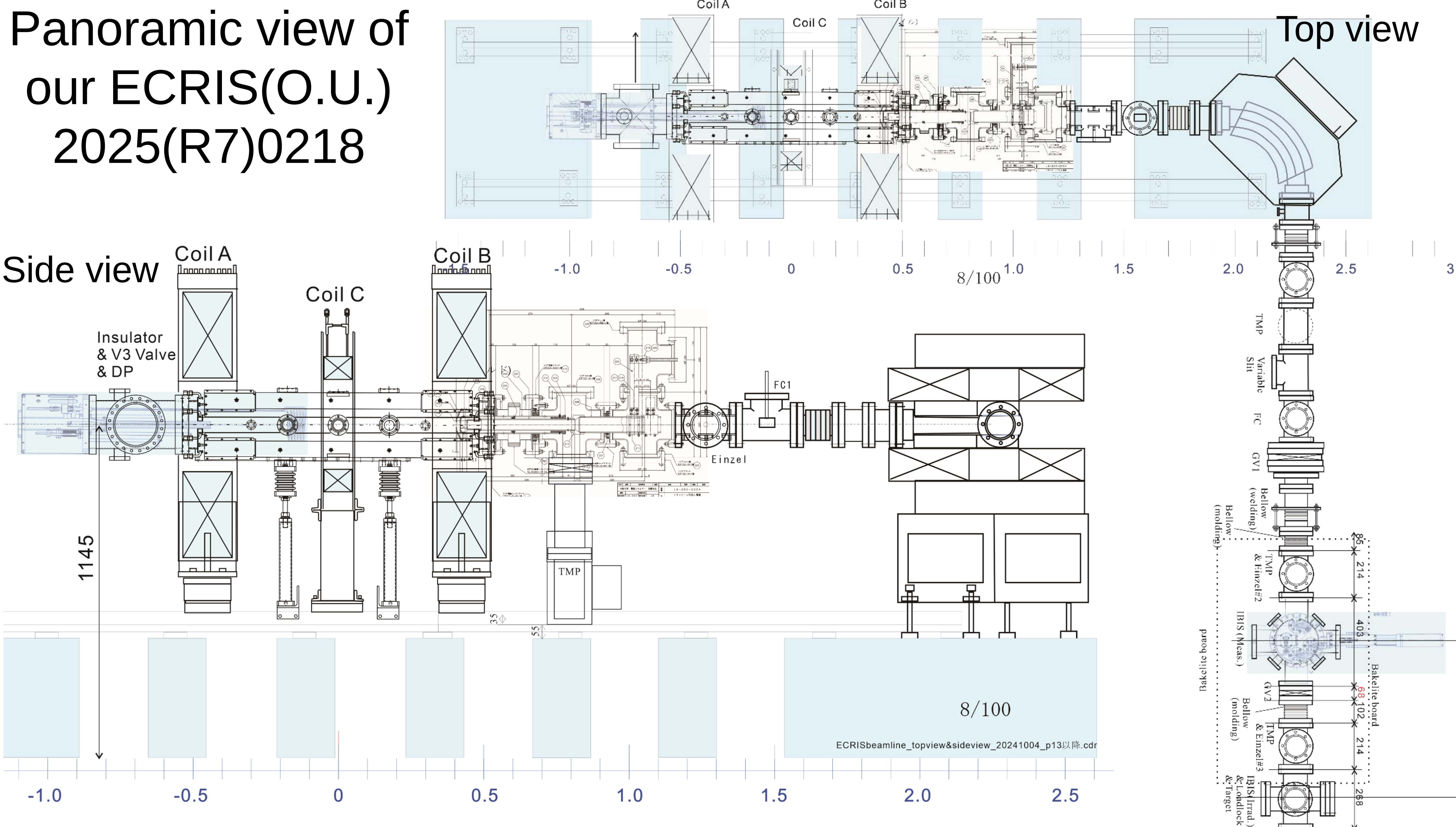

Panoramic view of our ECRIS(O.U.) I I

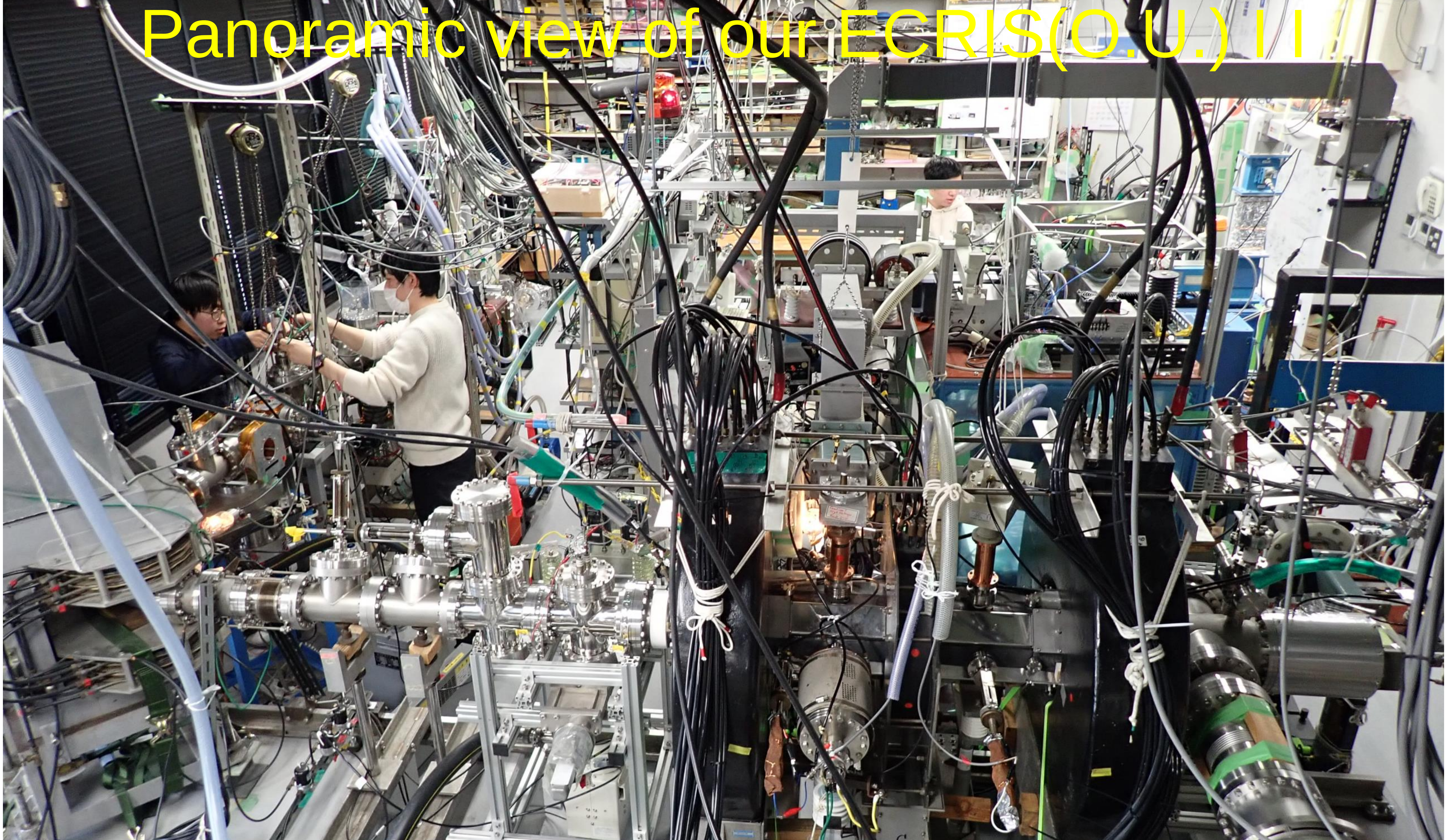

Panoramic view of our ECRIS(O.U.) II

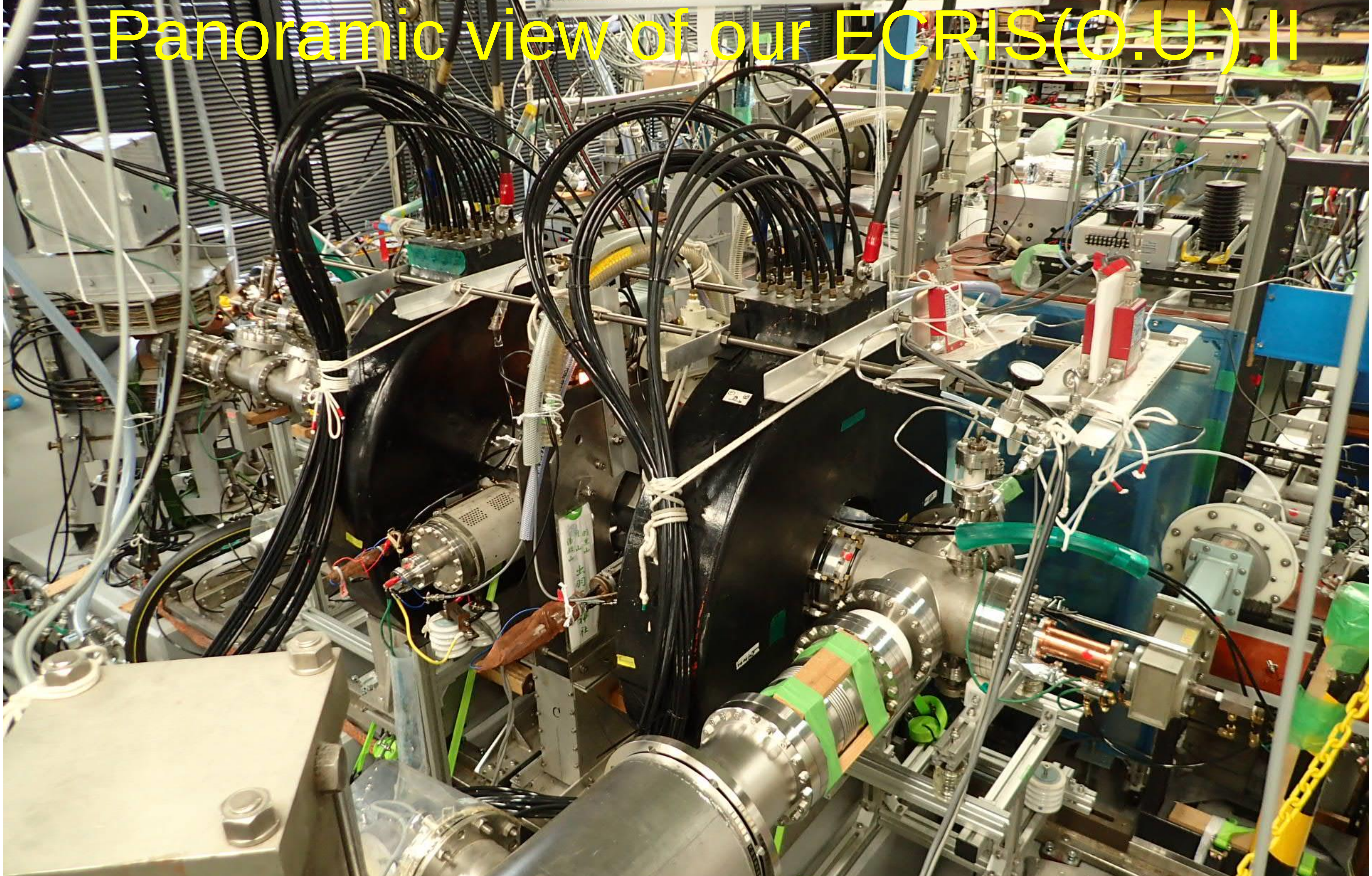

μW introduction system

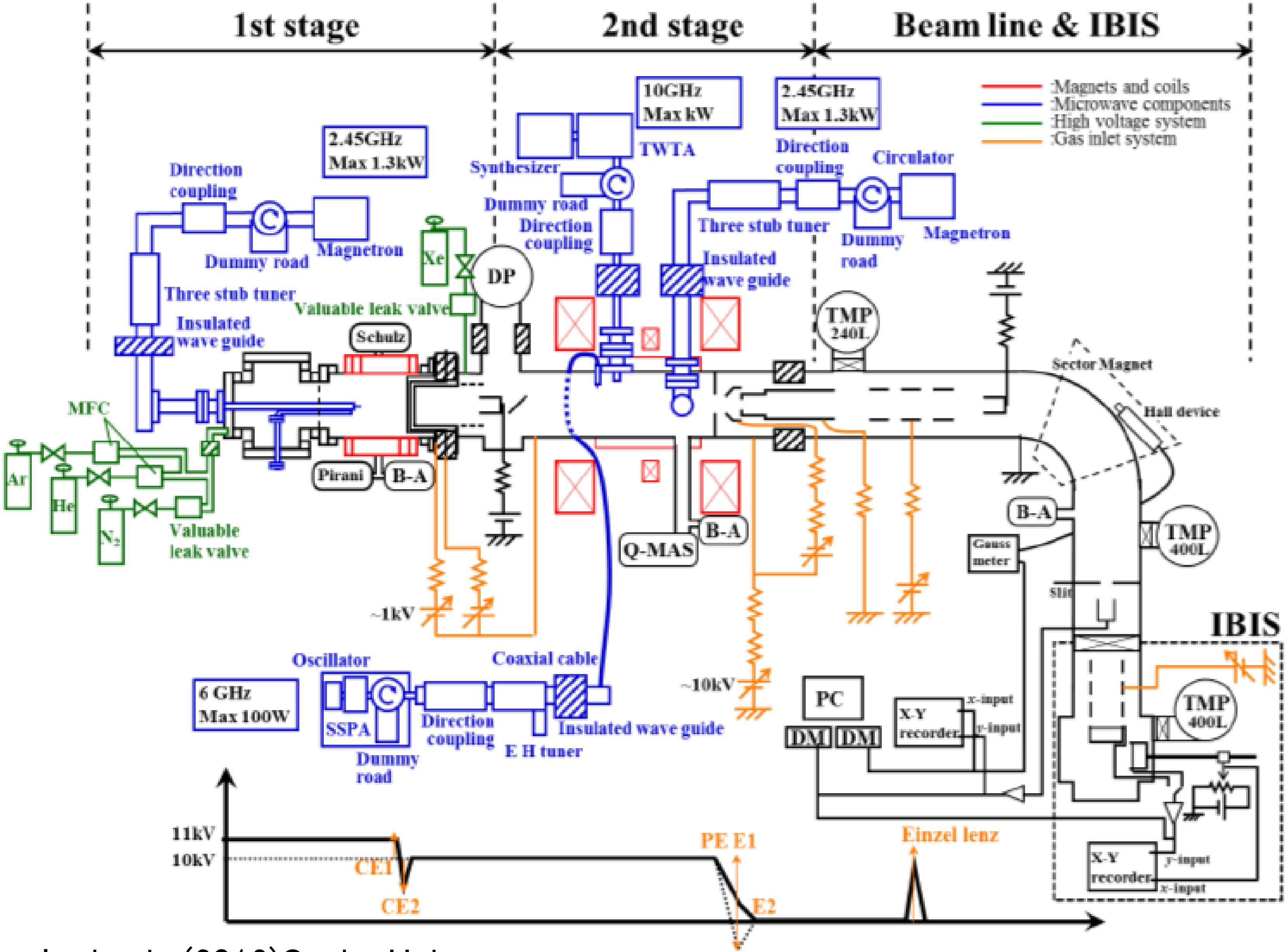

Nishiokada, T. master's thesis (2016)Osaka Univ.

µW Launcher / Antenna / Window

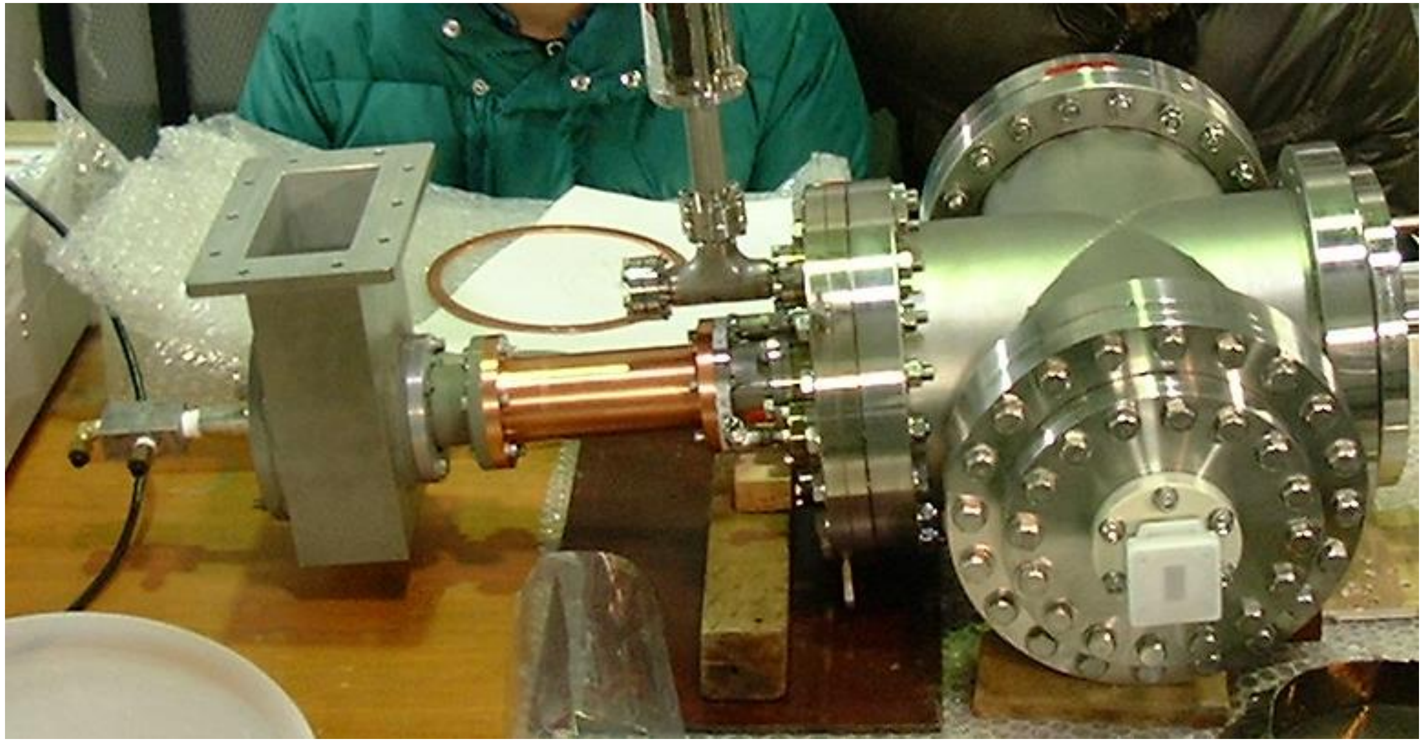

テーパー型同軸セミダイポールアンテナ

ヘイカルアンテナとアレー

同軸真空窓と各種アンテナ

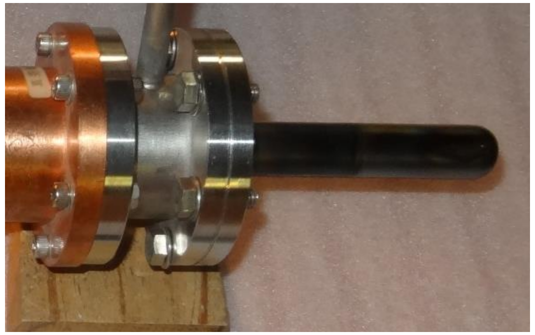

スロットアンテナ

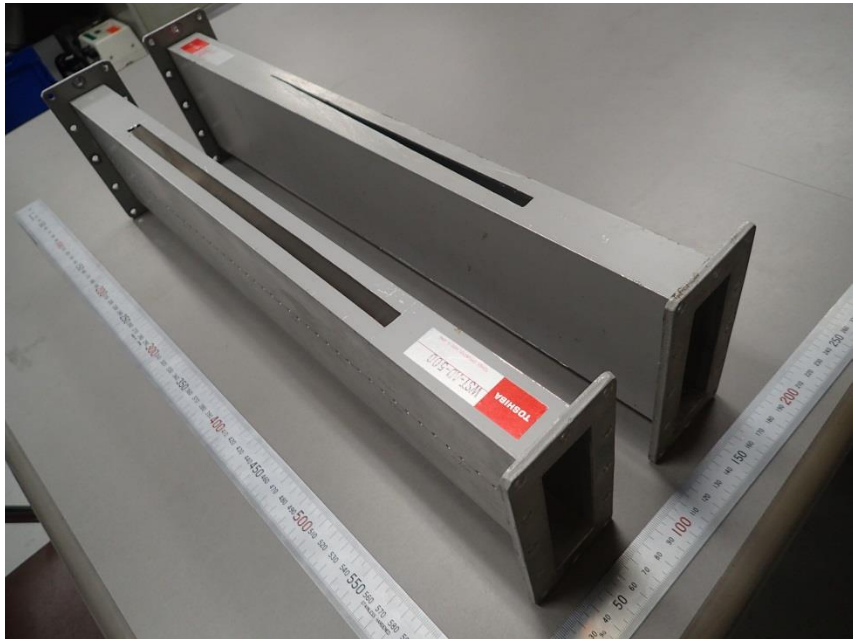

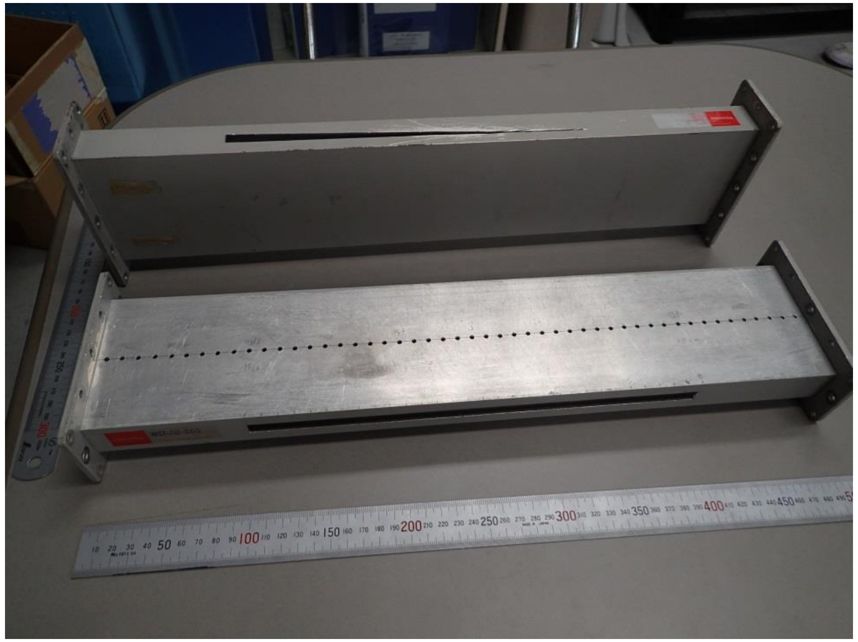

Guided wavelengths in circular cavity resonator

$$\frac{1}{\lambda^2} = \frac{1}{\lambda_g^2} + \frac{1}{\lambda_c^2} \qquad (1)$$

λ: The free-space wavelength

λ_c : The cut-off wavelength and is given by $\lambda_c = 2\pi a/\chi$. χ indicates the *n*-th eigen mode value of the differential *m*-th Bessel function for the circular transverse electric TE_{mn}, and one of the *m*-th Bessel function for the transverse magnetic TM_{mn} modes microwaves. Similar relationship stands up at various frequencies of the microwaves.

Mode 測定事例

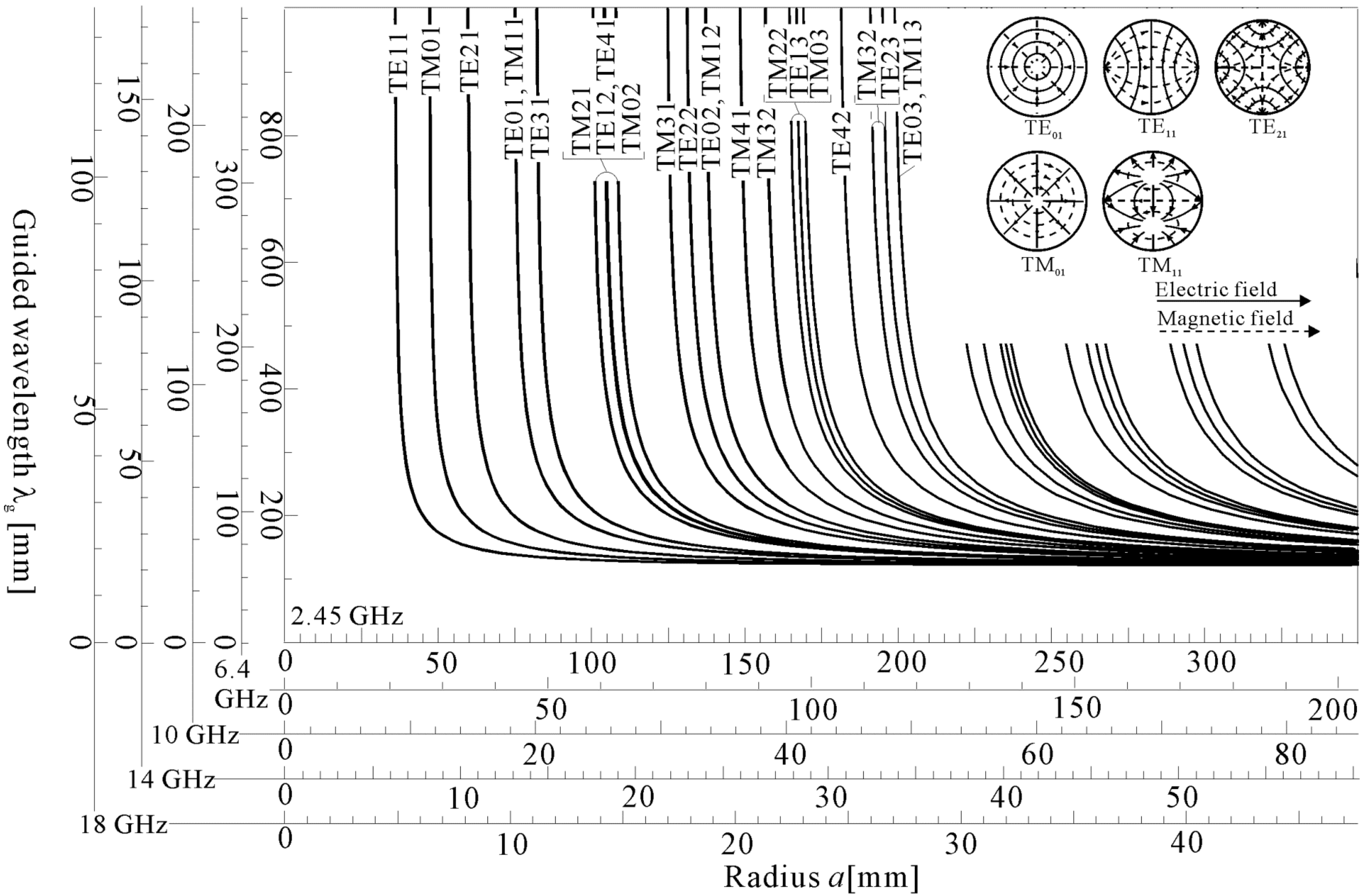

Yushi KATO, *et.al*, RSI. 77(2006)03A336-1-4

Charge state distributions (CSD) of extracted multicharged ion beams

- Typical CSD

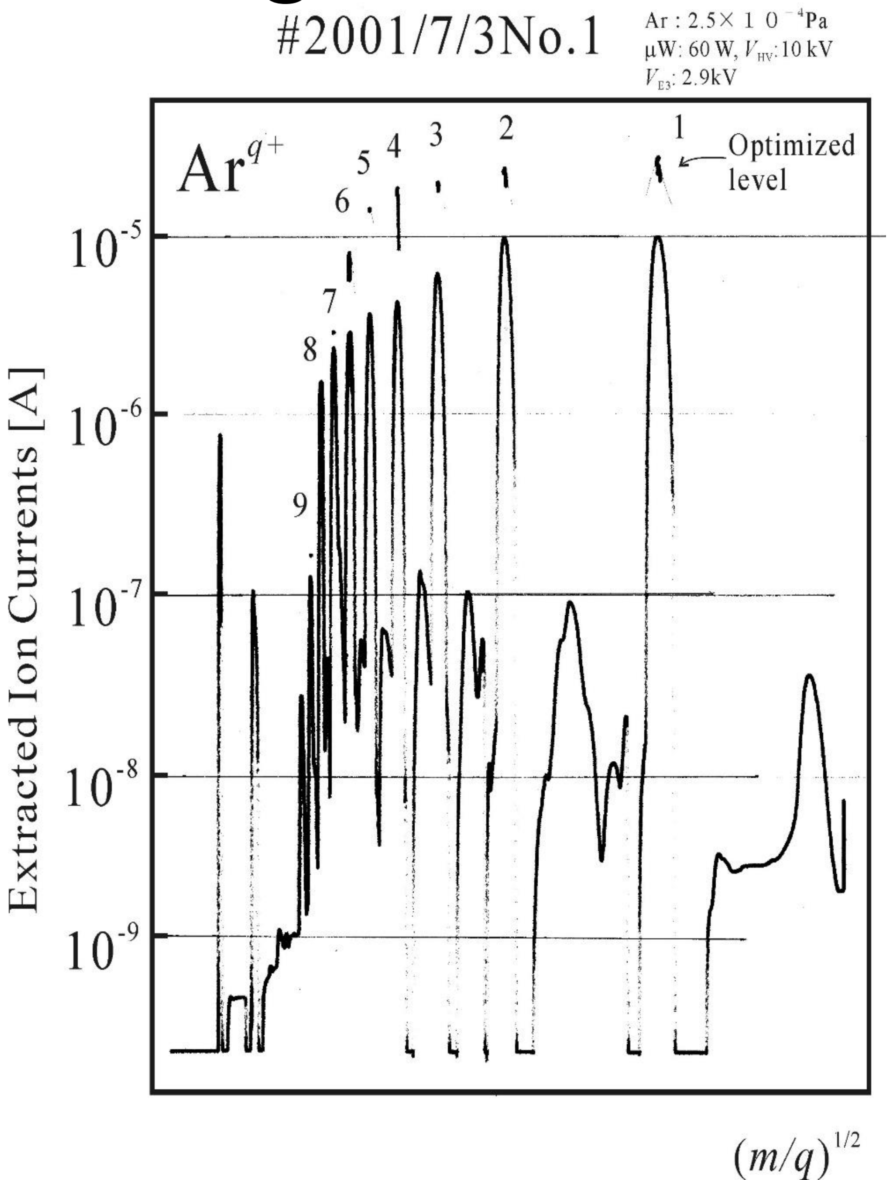

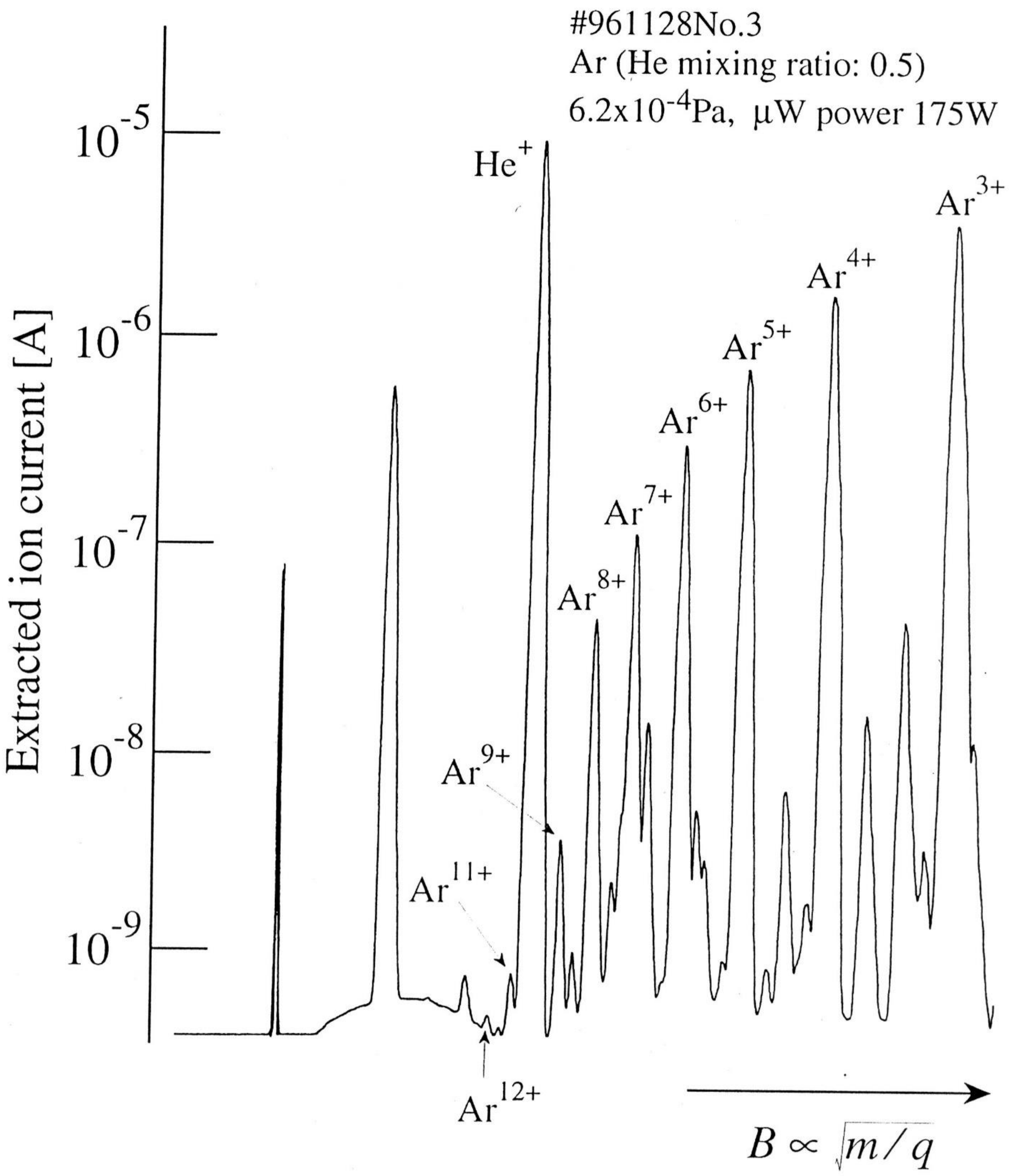

#961128No.3
Ar (He mixing ratio: 0.5)
6.2×10^{-4}Pa, μW power 175W
Extracted ion current [A]
10^{-5}
10^{-6}
10^{-7}
10^{-8}
10^{-9}
He^{+}
Ar^{3+}
Ar^{4+}
Ar^{5+}
Ar^{6+}
Ar^{7+}
Ar^{8+}
Ar^{9+}
Ar^{11+}
Ar^{12+}
$B \propto \sqrt{m/q}$

Typical plasma parameters

- Langmuir probe

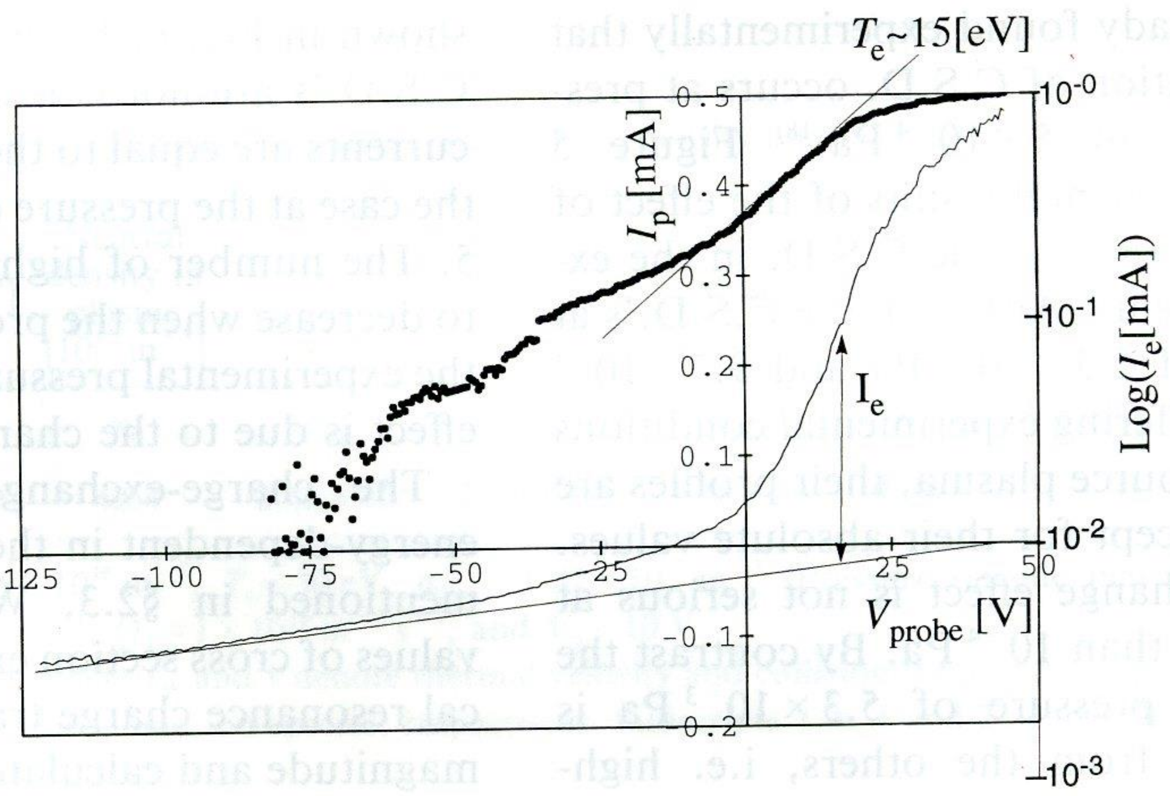

Fig. 4. Measurement of the electron temperature by means of the Langmuir probe. The probe is mounted at a distance of 0.2 m from the resonance point on the axis. The experimental conditions are nearly the same as in the experiment conducted in extremely low pressures with the source plasma (Fig. 3). The thin line and the bold dots represent the probe current (I_p) and the electron current (I_e), respectively. V_{probe} denotes the voltage applied to the probe. The electron temperature is deduced from the slope of the I_e-curve. It indicates that the electron temperature is about 15 eV and that a high component exists.

Y. Kato, *et.al*, Journal of the Physical Society of Japan, Vol.64(1993)p.1221-1232

Note:

n_e: n_{ee} (from I_{es} at V_{s1}), n_{ei} (from I_{is} at V_{s1})

T_e: T_e (from I_e fitting) & T_{eff} (from EEDF)

V_s: V_{s1}(cross point of I_{es} and I_e fitting),
V_{s2}(from V_f and T_e),
& V_{s3} (from ion beam)

$$V_{s2} = V_f - V_W = \frac{kT_e}{2e}\left\{1 + \ln\left(\frac{m_i}{2\pi m_e}\right)\right\}$$

The EEDF $g_e(V)$ is identified by

$$g_e(V) \equiv \frac{2m}{e^2 S}\left(\frac{2eV}{m}\right)^{1/2}\frac{d^2 I_e}{dV^2}, \qquad (1)$$

where m, S, V are the electron mass, the surface area of the probe, and $V = |V_p - V_s|$, respectively. The V_s is the plasma space potential. The method is available to any type EEDF of plasma. The $g_e(V)$ is calculated from by means of numerical differentiation with several smoothing by the method of moving average. The electron density N from the $g_e(V)$ and the effective temperature T_{eff} from the $g_e(V)$and the N can be written as

$$N \equiv \int_0^\infty g_e(V)dV, \qquad (2)$$

$$T_{eff} \equiv \frac{2}{3N}\int_0^\infty eV \cdot g_e(V)dV, \qquad (3)$$

In this study, the $g_e(V)$ is evaluated in term of correlation of the N, the T_{eff}, electron density n_{ee}, n_{ei}, electron temperature T_e from the probe. T_e, n_{ee}, n_{ei}, and V_s are estimated from the conventional probe analysis, where n_{ee} and n_{ei} are calculated from I_{es} and I_{is}, respectively. The $\widehat{g_e}(V)$ is also identified by normalized $g_e(V)$ by the maximum value.

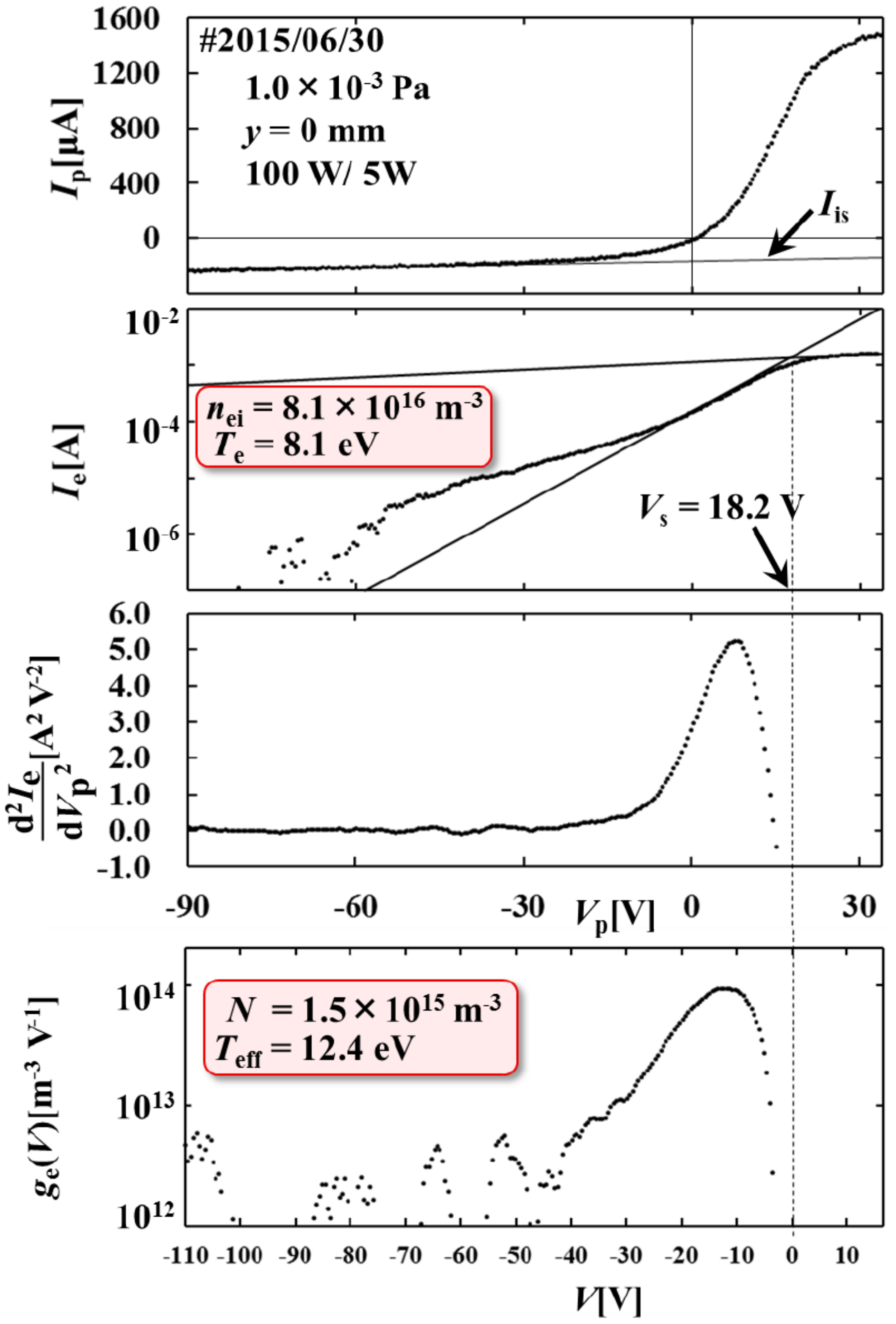

▪Sampling points: typicall 2000 points

Nishiokada T, master's thesis, 2016(Osaka Univ.)

Formation of *'potential well'*

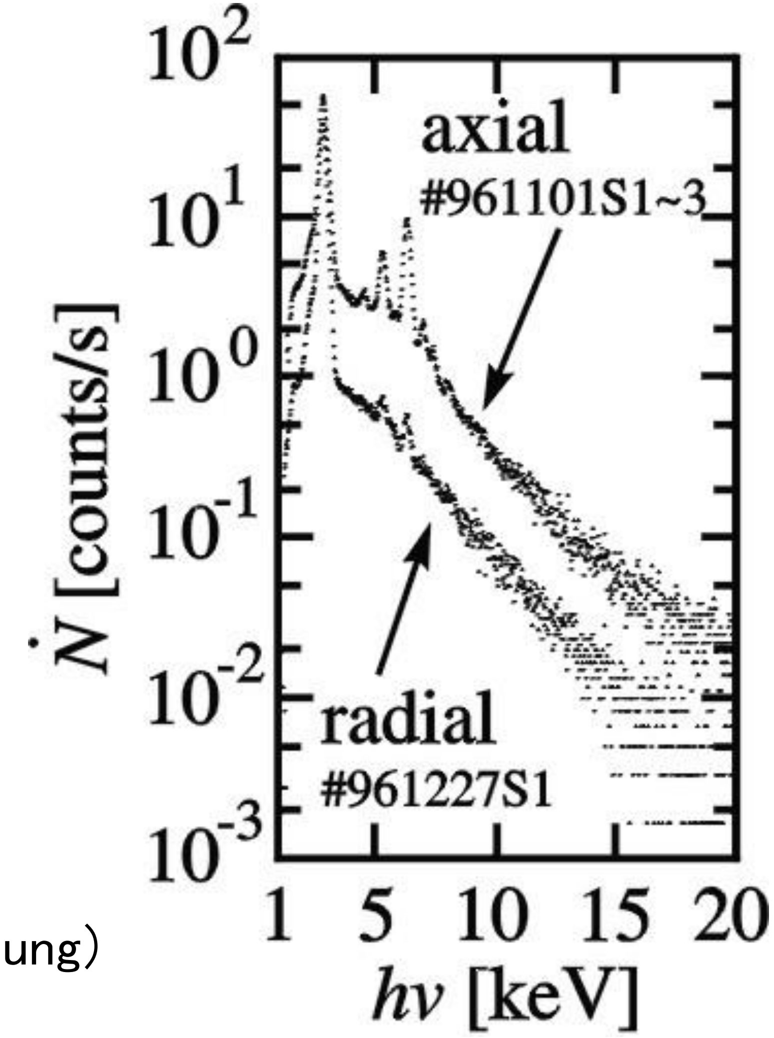

Kato, et.al., RSI, 69(1998)1179.

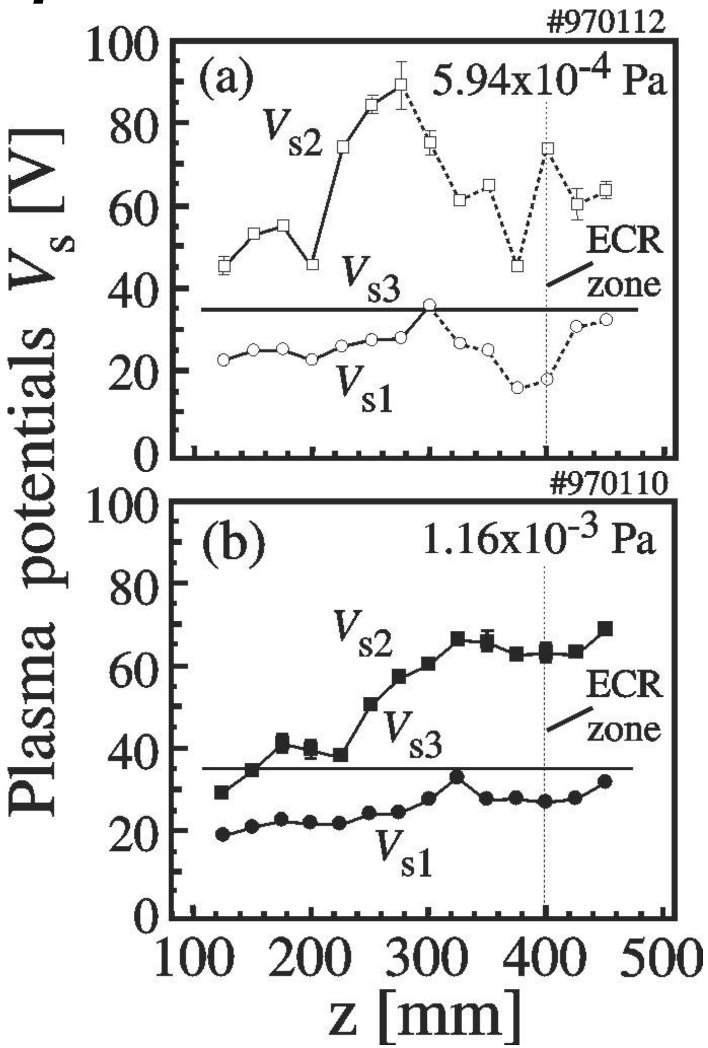

ibid, 69(1998)1176.

制動放射光
（Bremsstrahlung）

$$\dot{N} = \frac{\mathrm{d}P}{\mathrm{d}E} = \frac{2^5 e^6 \pi}{3\sqrt{3} m_e c^3 h}\left(\frac{2\pi m_e}{k_B T_e^h}\right)^{\frac{1}{2}} Z^2 n_e^h n_i \bar{g}_{ff} \exp\left(-\frac{E}{k_B T_e^h}\right) = \frac{9.53\times10^{-8}}{\sqrt{k_B T_e^h}} Z^2 n_e^h n_i \bar{g}_{ff} \exp\left(-\frac{E}{k_B T_e^h}\right)$$

Existence of resonance electrons
↓
Change of ambipolar diffusion in side *mirror field* by excess Δ (～$10^{-6\sim-7}$)of charge neutrality
↓
Formation of potential well
(Y. KATO et.al., Rev.Sci.Instrum., 69, 1998, 1176.)

CF1:divergent field
↓
Formation of potential hell:
Kaneko et.al, PRL, 80, 1998, 2602

CF2: 'After grow effects'（Potential confinements !）

- Ar Rate Equations;

$$\frac{dn_1}{dt} = n_0 S_0 - n_1\left[S_1 + S2_1 + S3_1 + \alpha_1 + \frac{1}{\tau_1}\right] + n_2[\alpha_2 + 2\cdot C1_2] + n_3 C2_3 + \sum_{j=3}^{18} n_j C1_j + Q_1$$

$$\frac{dn_2}{dt} = n_0 S2_0 + n_1 S_1 - n_2\left[S_2 + S2_2 + S3_2 + \alpha_2 + C1_2 + \frac{1}{\tau_2}\right] + n_3[\alpha_3 + C1_3 + C2_3] + 2n_4 C2_4 + \sum_{j=5}^{18} n_j C2_j + Q_2$$

$$\frac{dn_3}{dt} = n_0 S3_0 + n_1 S2_1 + n_2 S_2 - n_3\left[S_3 + S2_3 + \alpha_3 + C1_3 + C2_3 + \frac{1}{\tau_3}\right] + n_4[\alpha_4 + C1_4] + n_5 C2_5 + Q_3$$

$$\frac{dn_4}{dt} = n_0 S4_0 + n_1 S3_1 + n_2 S2_2 + n_3 S_3 - n_4\left[S_4 + S2_4 + \alpha_4 + C1_4 + C2_4 + \frac{1}{\tau_4}\right] + n_5[\alpha_5 + C1_5] + n_6 C2_6 + Q_4$$

$$\frac{dn_5}{dt} = n_0 S5_0 + n_2 S3_2 + n_3 S2_3 + n_4 S_4 - n_5\left[S_5 + \alpha_5 + C1_5 + C2_5 + \frac{1}{\tau_5}\right] + n_6[\alpha_6 + C1_6] + n_7 C2_7 + Q_5$$

$$\frac{dn_6}{dt} = n_0 S6_0 + n_4 S2_4 + n_5 S_5 - n_6\left[S_6 + \alpha_6 + C1_6 + C2_6 + \frac{1}{\tau_6}\right] + n_7[\alpha_7 + C1_7] + n_8 C2_8 + Q_6$$

$j = 7 \sim 18$

$$\frac{dn_j}{dt} = n_{j-1} S_{j-1} - n_j\left[S_j + \alpha_j + C1_j + C2_j + \frac{1}{\tau_j}\right] + n_{j+1}[\alpha_{j+1} + C1_{j+1}] + n_{j+2} C2_{j+2} + Q_j$$

- Charge Neutrality;

$$n_e = \sum_{j=1}^{18} Z_j n_j$$

- Neutral density balance;

$$\frac{dn_0}{dt} = \frac{S}{V}\frac{v_0}{3}(n_{0out} - n_0) - n_e\langle\sum_{j=1}^{6} {}_0\sigma_j^{i} v_e\rangle n_0 + n_e\langle {}_1\sigma_0^{r} v_e\rangle n_1 - n_0\langle v_i\rangle\left[\sum_{j=2}^{18} {}_j\sigma_{j-1}^{c} n_j + \sum_{j=3}^{18} {}_j\sigma_{j-2}^{c} n_j\right]$$

- Rate coefficients;

Single ionization

$$S_j \equiv n_e\langle {}_j\sigma_{j+1}^{i} v\rangle, j = 0 \sim 17$$

Radiative recombination

$$\alpha_j \equiv n_e\langle {}_j\sigma_{j+1}^{r} v\rangle, j = 1 \sim 18$$

Charge exchange

single electron capture

$$C1_j \equiv n_0\langle v_i\rangle {}_j\sigma_{j-1}^{c}, j = 1 \sim 18$$

double electron capture

$$C2_j \equiv n_0\langle v_i\rangle {}_j\sigma_{j-2}^{c}, j = 2 \sim 18$$

Multiply ionization

$$\begin{cases} S2_j \equiv n_e\langle {}_j\sigma_{j+2}^{i} v\rangle, j = 0 \sim 4 \\ S3_j \equiv n_e\langle {}_j\sigma_{j+3}^{i} v\rangle, j = 0 \sim 2 \\ S4_j \equiv n_e\langle {}_j\sigma_{j+4}^{i} v\rangle, j = 0 \\ S5_j \equiv n_e\langle {}_j\sigma_{j+5}^{i} v\rangle, j = 0 \\ S6_j \equiv n_e\langle {}_j\sigma_{j+6}^{i} v\rangle, j = 0 \end{cases}$$

Multiply Ionization Effect on C.S.D.

- Fitting Formula........Belfast Group

$$\sigma(E) = \frac{1}{IE}\left\{A\ln(E/I) + \sum_{i=1}^{N} B_i\left(1-\frac{I}{E}\right)^i\right\}$$

E: electron incident energy (eV), I: ionization potential (eV); summation of step by step ionization, A, B_i: fitting parameters by the least square methods (in units of 10^{-13} eV^{2}cm^2). N=5.

- Cross section data quoted from AMDIS database (NIFS)

$Ar \dashrightarrow Ar^{2+\sim6+}$, $Ar^{+} \dashrightarrow Ar^{3+\sim4+}$, $Ar^{2+} \dashrightarrow Ar^{4+\sim5+}$, $Ar^{3+} \dashrightarrow Ar^{5+}$, $Ar^{4+} \dashrightarrow Ar^{6+}$.

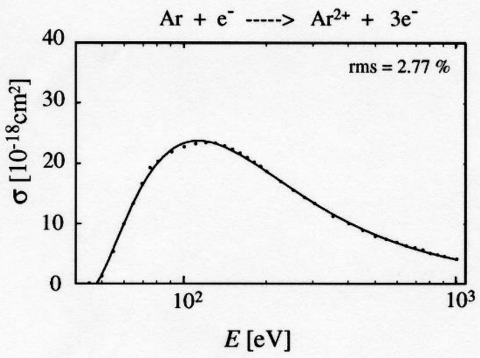

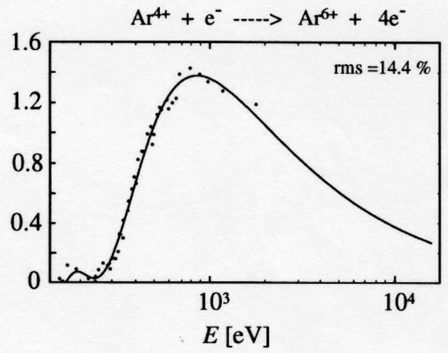

- Rate coefficients

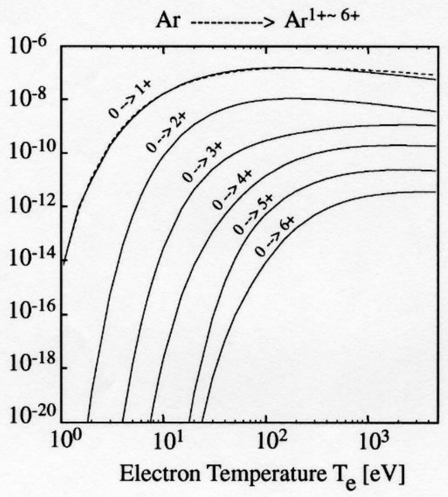

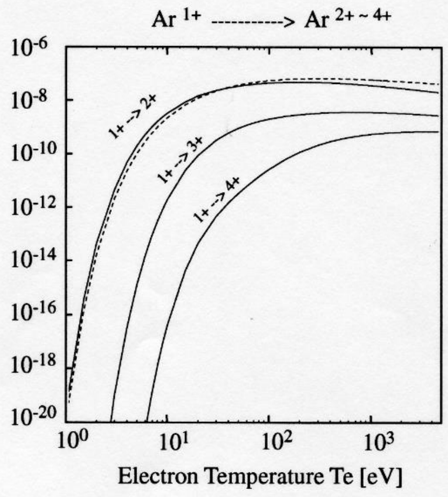

具体例

Outline of Modelling for Multicharged Ion Production

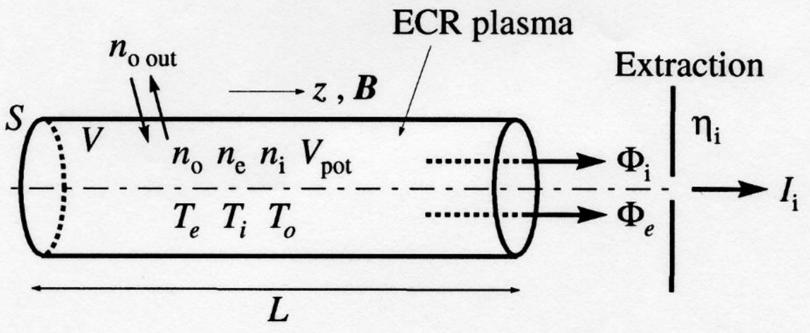

$$\Phi_i = \frac{N_i}{\tau_i} = \frac{Vn_i}{\tau_i}$$

$$I_i = \eta_i e Z_i \Phi_i = \eta_i e Z_i \frac{Vn_i}{\tau_i}$$

- Dominant collisional processes;

$$\lambda_{i-\Sigma i'} \ll \lambda_{e-e} \quad \lambda_{e-i} \quad \lambda_{e-N} \quad \lambda_{i-N} \quad L$$

- Ion diffusion along magnetic field (z-axis) with plasma potential (V_{pot})

- Simplicity; density gradient ∇n_i and electric field E are constant along z-axis using mean values of n_i and V_{pot} and characteristics length; l

- Ion confinement time; τ_i

$$\tau_i \propto l \cdot Z_i \cdot A^{1/2} \cdot T_i^{-3/2} \cdot \left(\frac{V_{pot}}{l}\right)^{-1} \cdot \sum_{i'} n_{i'} \cdot Z_{i'}^2 \cdot \ln\Lambda_{i-i'}$$

- Atomic processes
  - · Ionization: step-by-step; direct and E-A (Arnaud-Rothenflug formula)
    multiply; using analytical formula by fitting the experimental cross section data
  - · Recombination: radiative and dielectronic (Shull-Van Steenberg formula)
  - · Charge exchange: single and double electron capture

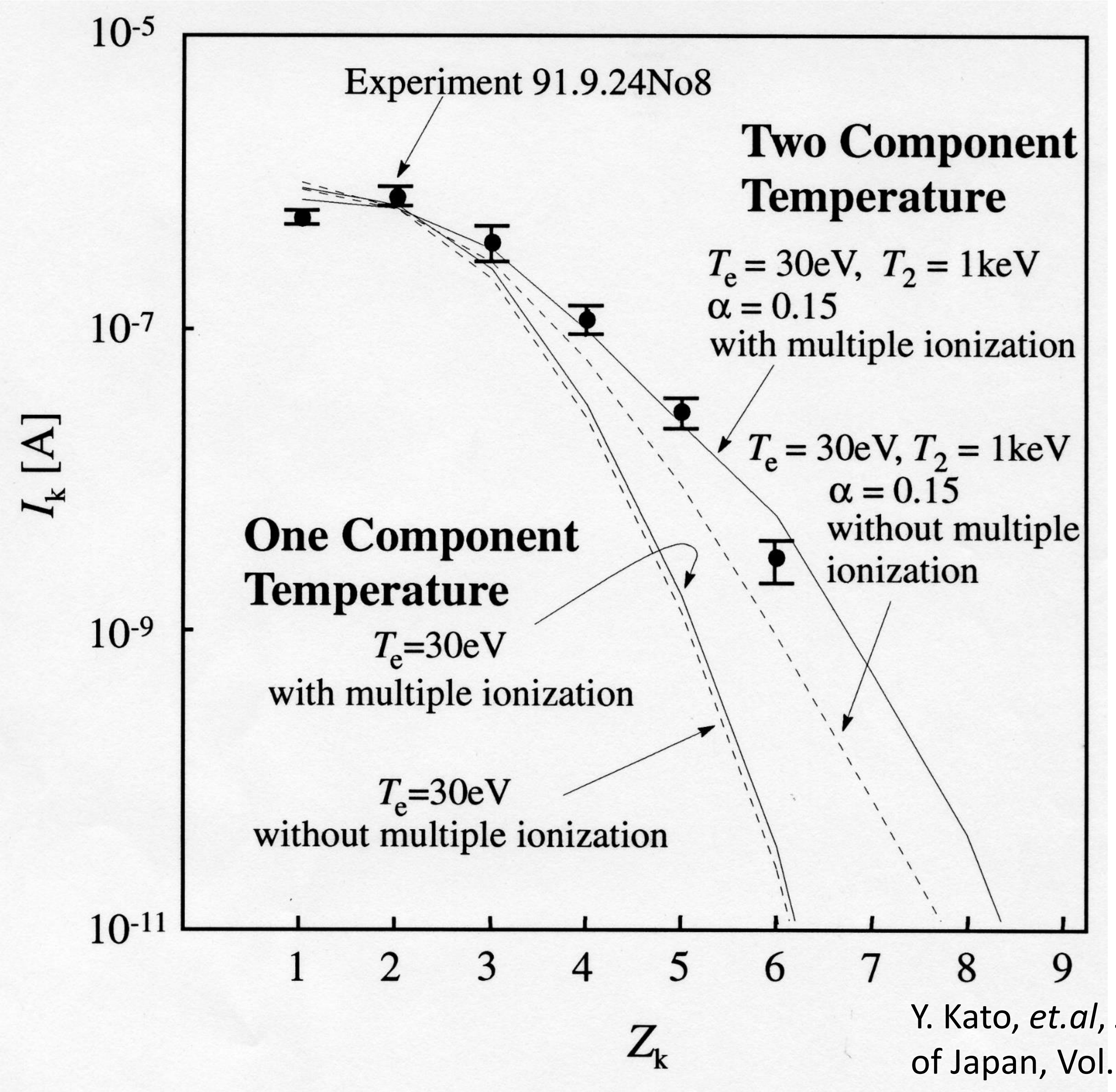

Y. Kato, *et.al*, Journal of the Physical Society of Japan, Vol.64(1993)p.1221-1232

Table I. Typical calculated results of ion density and mean free path.[a)]

Ar ion density n_k [10^{15} m^{-3}]					Neutral density in plasma [10^{15} m^{-3}]	Mean free path [m][b)]					
n_1	n_2	n_3	n_4	n_5	n_0	$\lambda_{\text{e-e}}$ [c)]	$\lambda_{\text{e-N}}$	$\lambda_{\text{i-N}}$	$\lambda_{\text{e}-\sum k}$ [d)]	$\lambda_{1-\sum k}$ [e)]	$\lambda_{2-\sum k}$ [e)]
17.6	10.8	3.18	0.32	0.01	42.4	2.46×10^{2}	2.26×10^{2}	3.68×10^{1}	9.74×10^{1}	3.35×10^{-2}	8.75×10^{-3}

a) Input parameters; $n_e=5\times10^{16}$ m^{-3}, $T_e=30$ eV, $n_{0\text{out}}=1.32\times10^{17}$ m^{-3} (Pressure outside plasma is 5.3×10^{-4} Pa), $T_i=0.5$ eV, $Q_1=2\times10^{18}$ m^{-3} s^{-1}, $Q_2=1\times10^{18}$ m^{-3} s^{-1}, and $V_p=10$ V.

b) Mean free path: $\lambda=v_{\text{th}}/\nu$, where v_{th} and ν denote thermal velocity and collision frequency, respectively. Subscripts e, N and i represent electron, neutral and ion species, respectively. Subscripts $\sum k$, 1 and 2 denote the summation over all ions, Ar^{1+} and Ar^{2+} species, respectively.

c) $\nu_{\text{e-e}}=3.01\times10^{-12}\dfrac{n_e \ln \Lambda_{\text{e-e}}}{T_e^{3/2}}$.

d) $\nu_{\text{e-}\sum k}=4.21\times10^{-12}\dfrac{\sum n_k Z_k^2 \ln \Lambda_{\text{e-}k}}{T_e^{3/2}}$.

e) Equation (6).

Y. Kato, *et.al*, Journal of the Physical Society of Japan, Vol.64(1993)p.1221-1232

Ref.
Transports:

B.A. Trubnikov, `Particle interactions in fully ionized plasma`, Review of Plasma Physics I

S.I. Braginskii, `Transport processes in a plasma`, *ibid*.

L. Spitzer, Jr, `Physics of fully ionized gases`, Chap. 5

Empirical improvement methods I

Biased dick methods

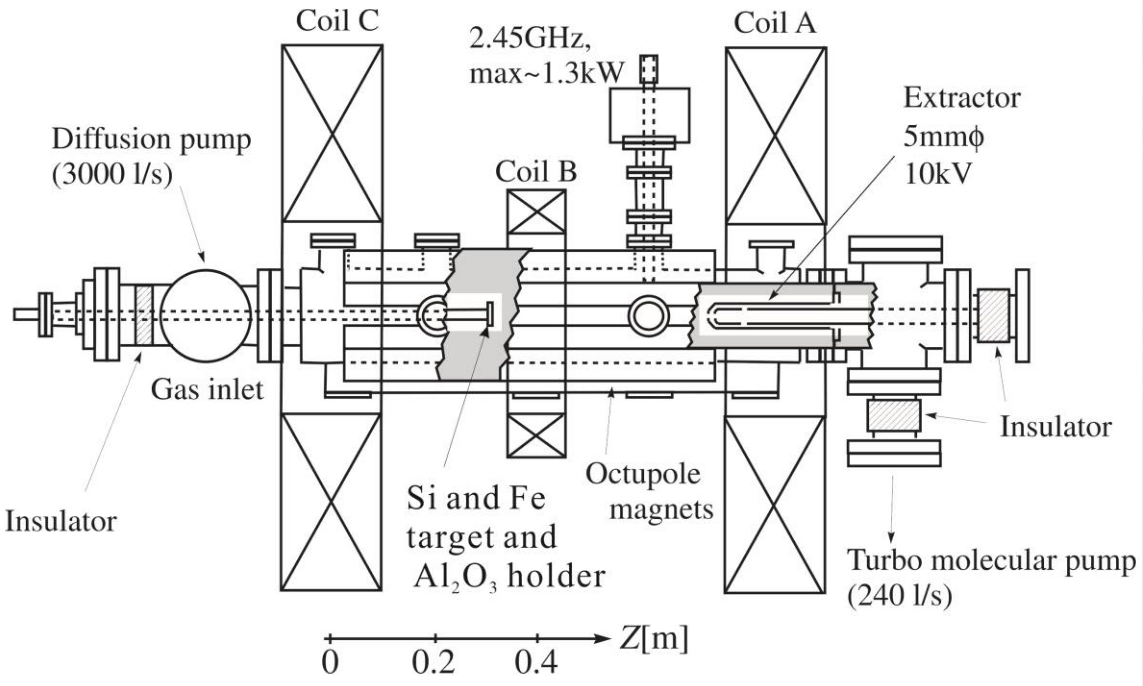

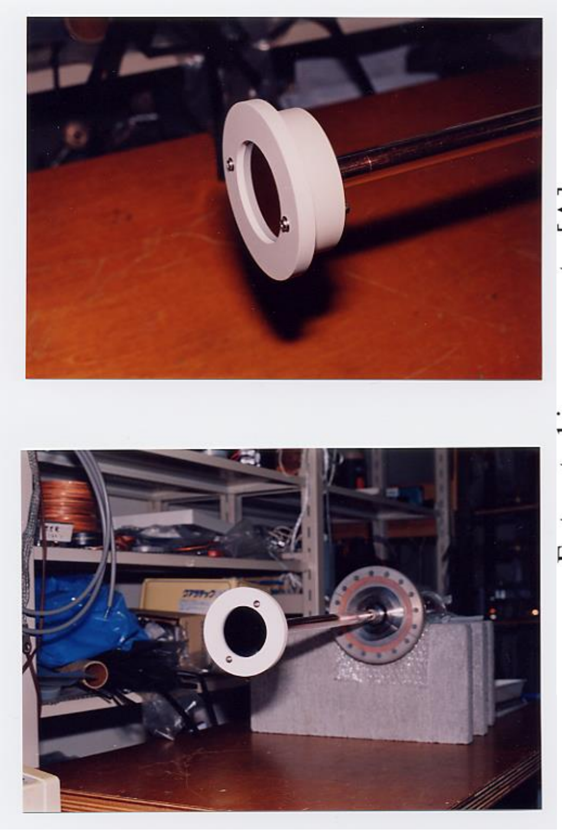

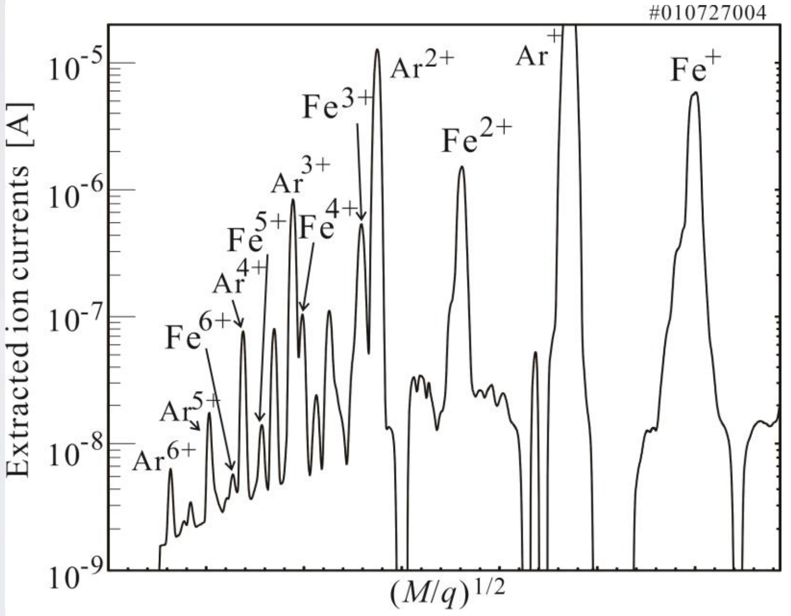

Empirical improvement methods II

Low Z gas mixing Ar/He

Ar: 0.192sccm

He: 0.035sccm #2021/06/08

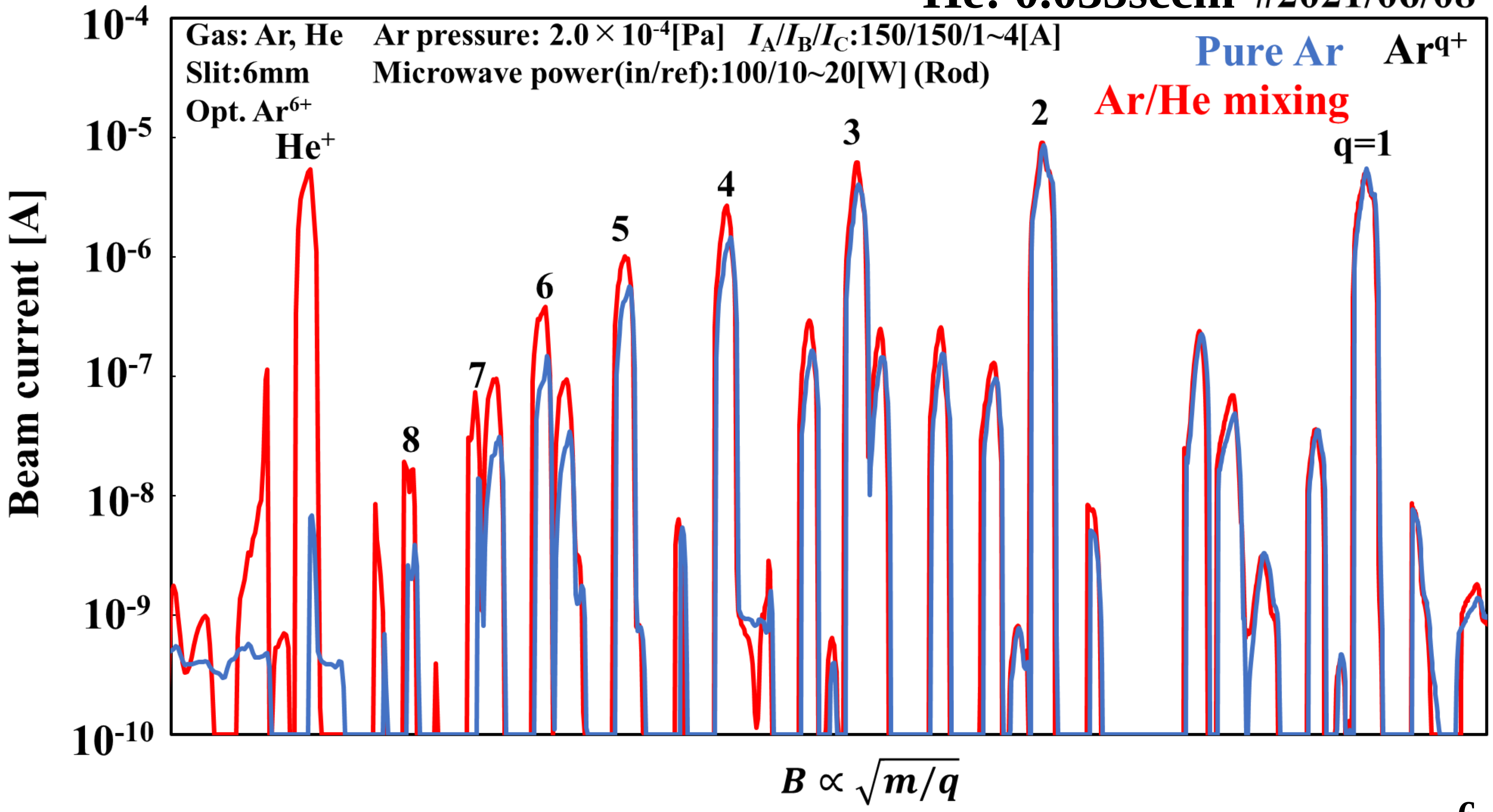

Empirical improvement methods III: After grow effects & μW moduration

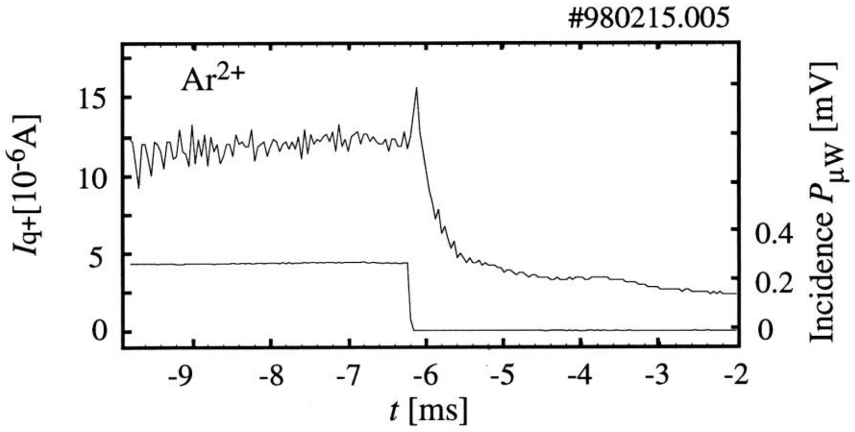

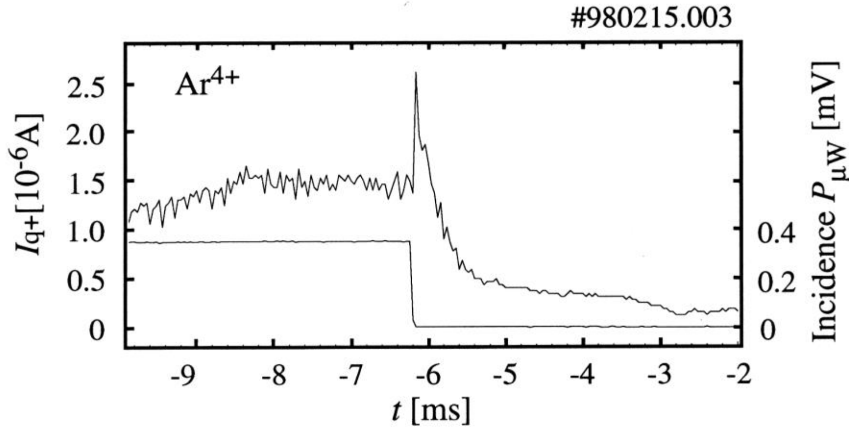

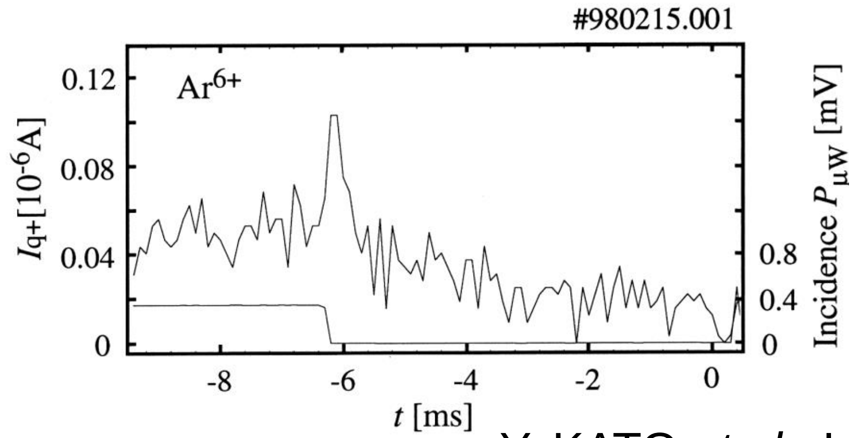

Generally τ_{ii} (ion-ion collision time) << τ_i (life time of a high charge-state ion) << τ_{ei} (equi-partition time between electrons and ions).

In a one-dimensional model, we can say that the pressure force balances the electrical one on an ionic species between the central plasma and the edge of this one.

$$\frac{\delta}{\delta z} n_q(z)\, kT_q = -n_q(z)\, qe \frac{\delta \phi(z)}{\delta z}$$

So

$$\frac{1}{n_q} \frac{\delta}{\delta z} n_q(z) = -\frac{qe}{kT_q} \frac{\delta}{\delta z} \phi(z)$$

where

$$n_q(z) = n_q(0) \exp\left(-\frac{qe\Delta\phi}{kT_q}\right)$$

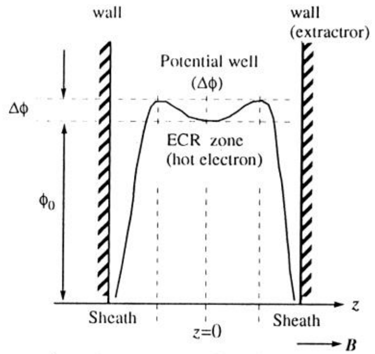

where $\phi(z)$ is the axial potential distribution, n_q and T_q are the density and temperature of q charge state ions, respectively.
During the steady-state operation the flux of ions coming to the edge of the central plasma is proportional to

$$\exp\left(-\frac{qe\Delta\phi}{kT_q}\right).$$

At the end of the microwave pulse, the electrical plugging effect disappears due to the cancelation of the potential well $\Delta\phi$, so at the beginning of the afterglow process the ion flux increases for a short while.
If we neglect the increasing volume effect we must verify that

$$\frac{I_{afterglow}}{I_{steady-stae}} \propto exp\left(\frac{qe\Delta\phi}{kT_q}\right).$$

If we have an homogeneous density and temperature for any ionic species, this ratio must be proportional to $\exp(q)$.

Is ICR available to increase multicharged ion currents by relaxing potential well?

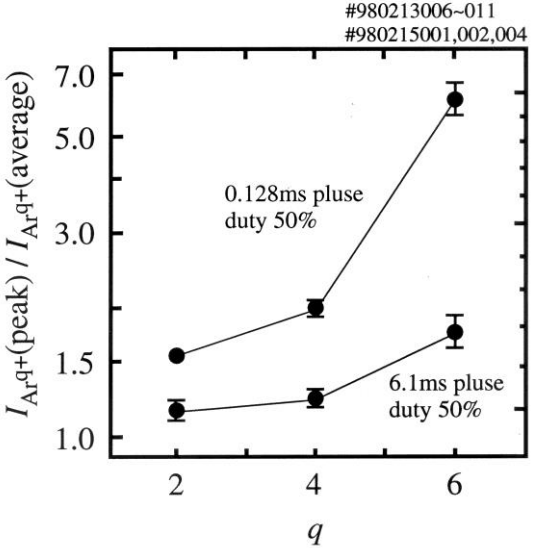

Y. KATO *et.al.*, Ion Implantation Technology-98, Vol. 1, 1999, pp. 448-451.

Ar μW Modulation

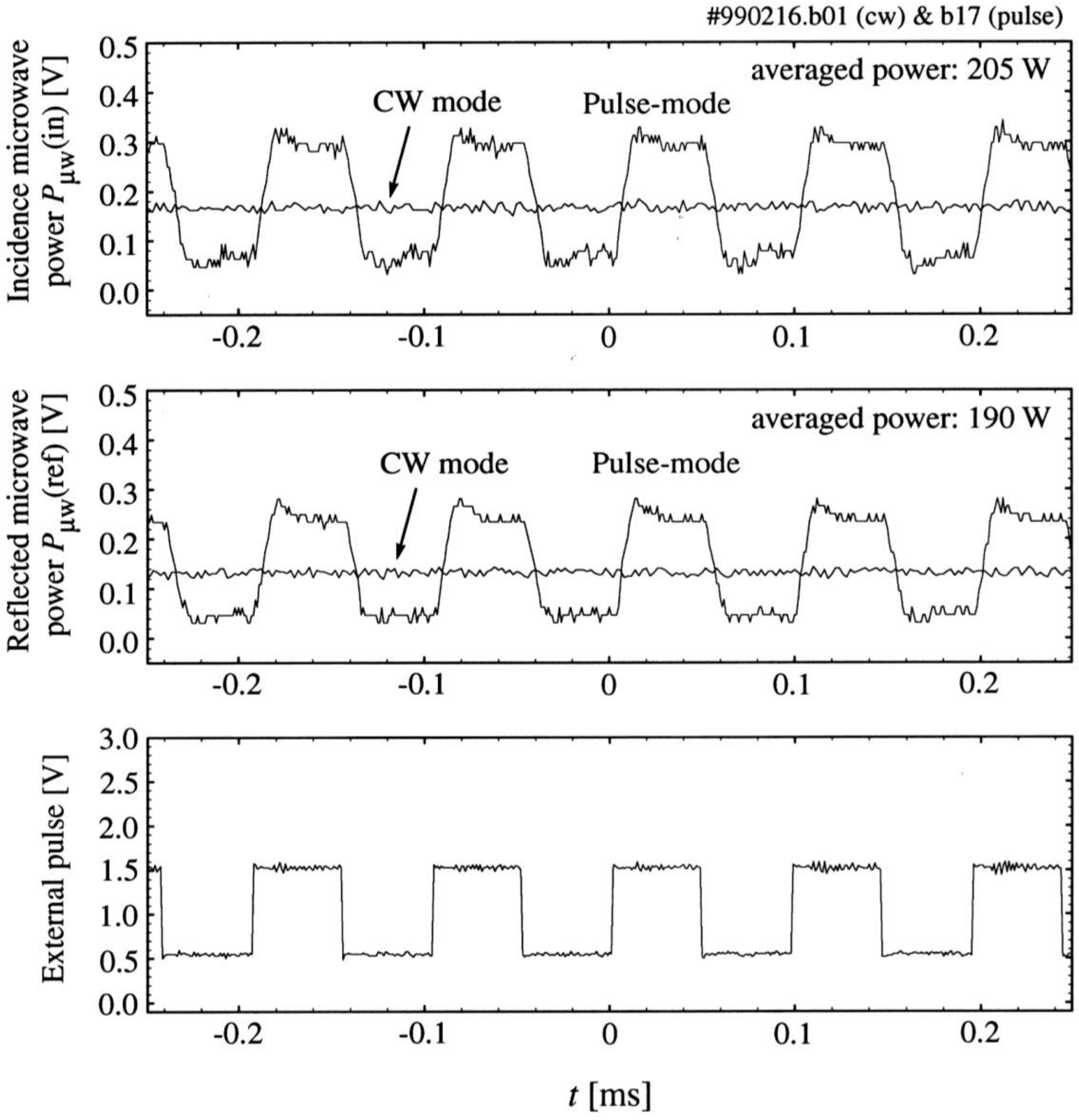

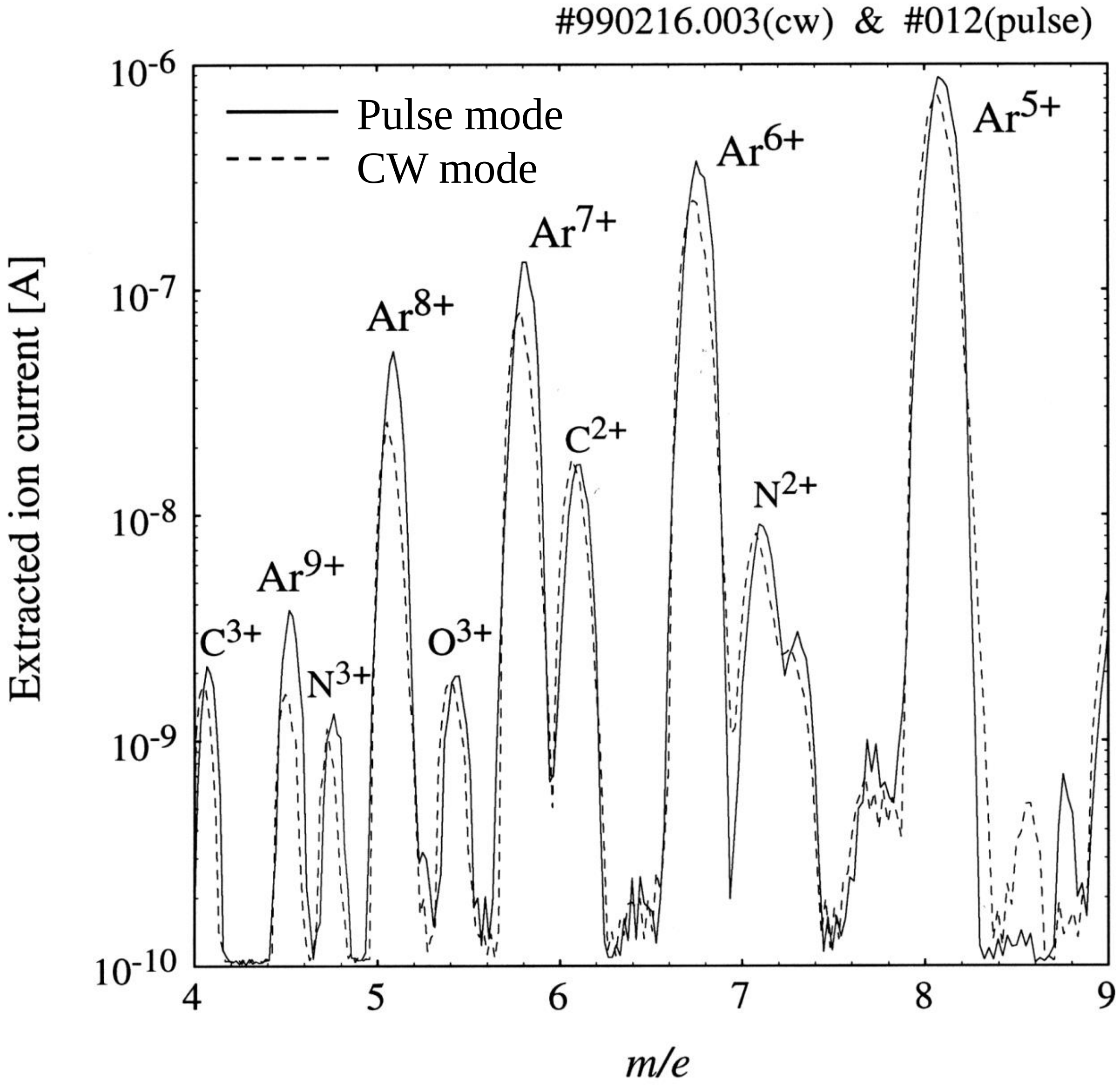

Y. KATO et.al., Rev.Sci.Instrum., 71, 2000, 657

Ar μW Modulation

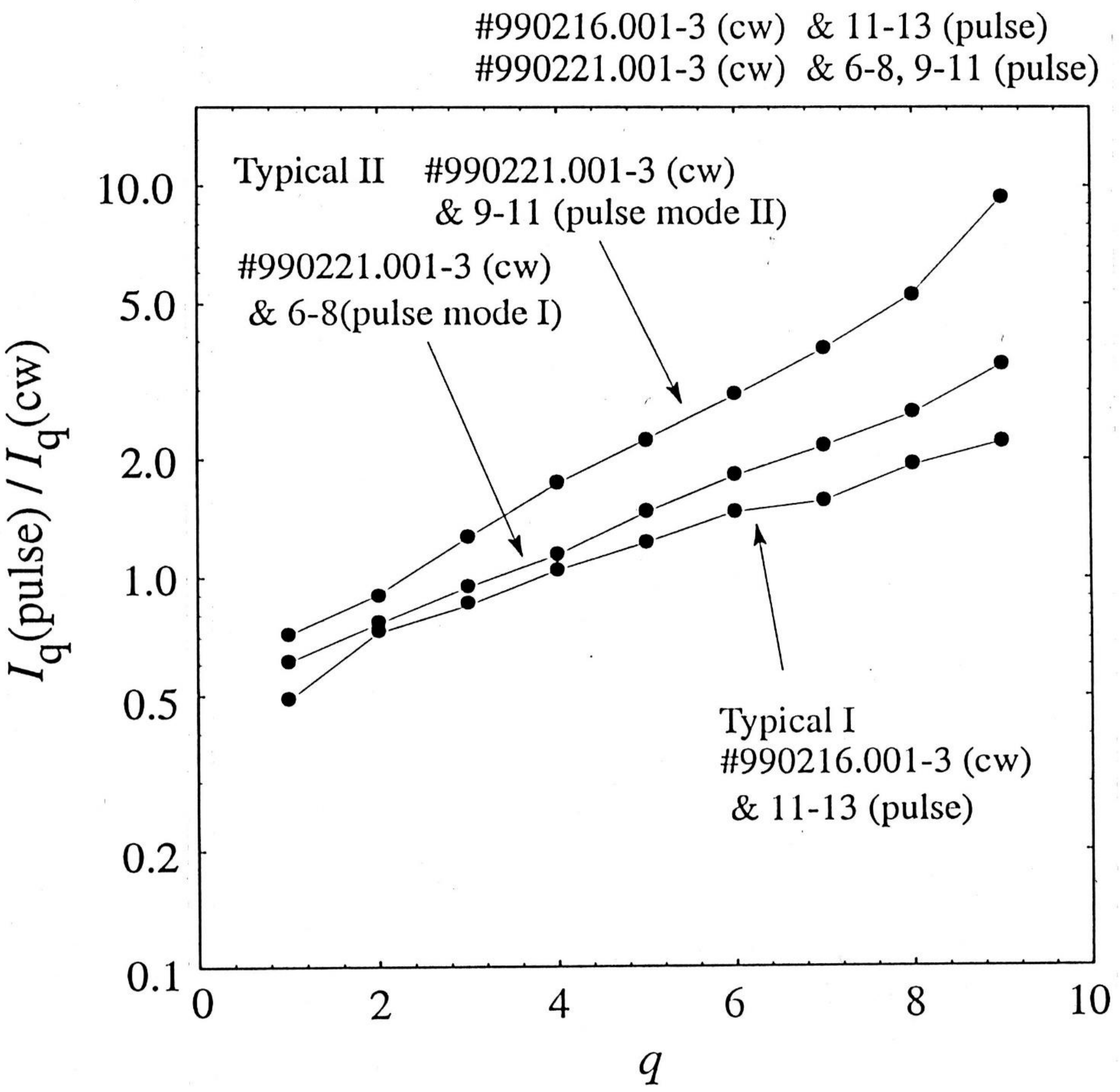

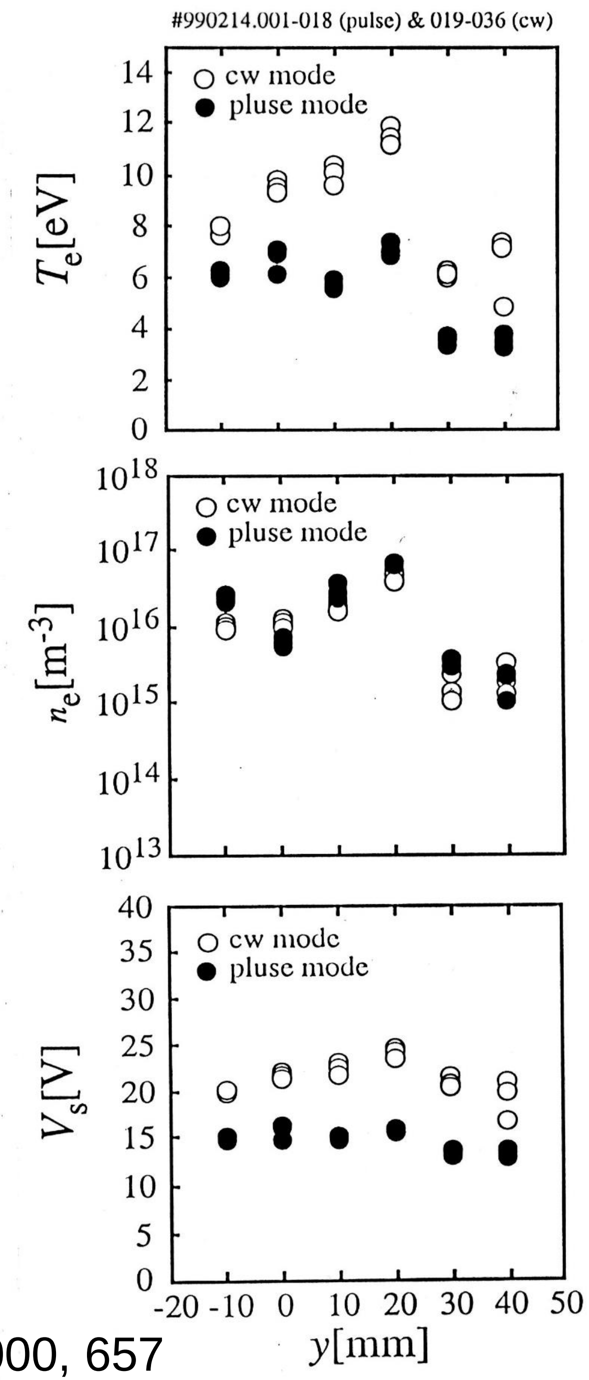

Ionizing plasma：<q>↓
⇕
Recombining plasma：<q>↑

Y. KATO et.al., Rev.Sci.Instrum., 71, 2000, 657

Xe

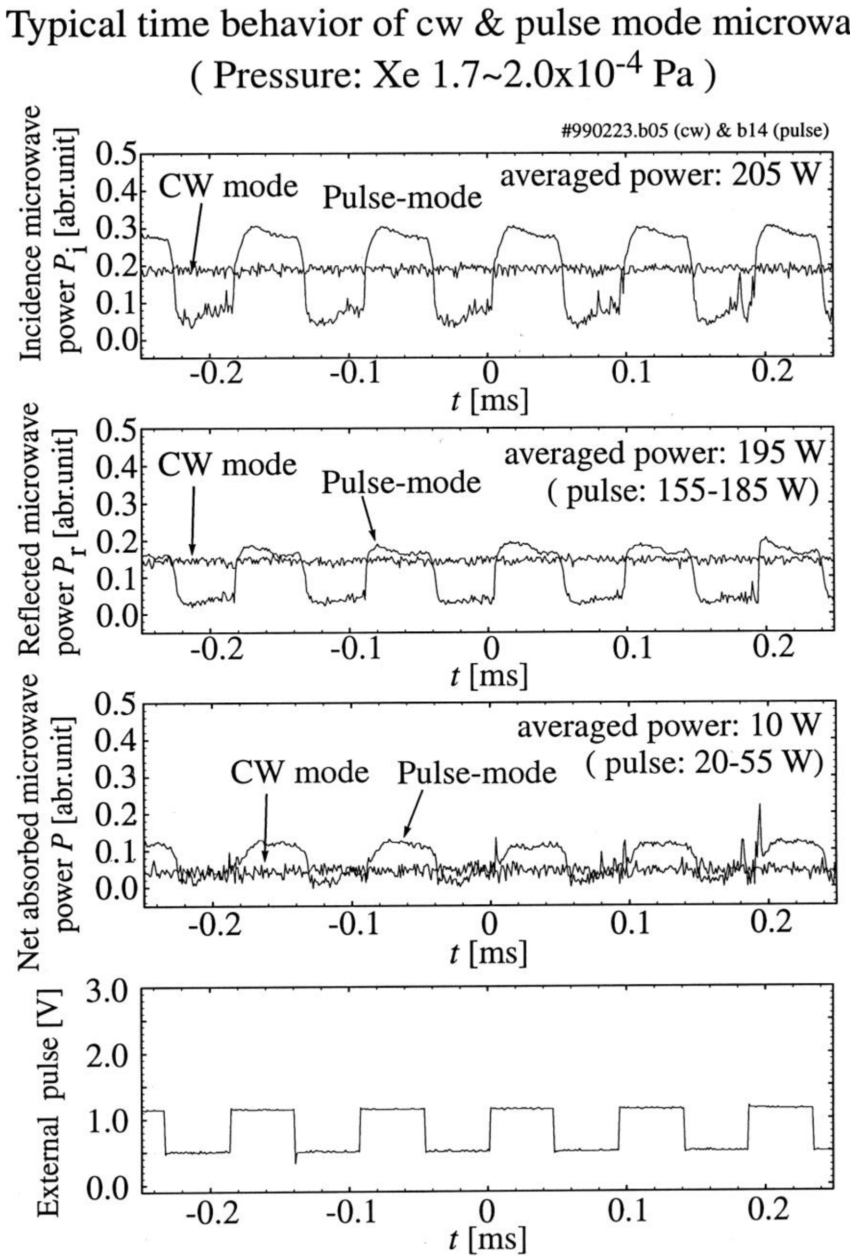
Typical time behavior of cw & pulse mode microwave
(Pressure: Xe 1.7~2.0x10-4 Pa)
#990223.b05 (cw) & b14 (pulse)
Incidence microwave power P_i [abr.unit]
CW mode
Pulse-mode
averaged power: 205 W
Reflected microwave power P_r [abr.unit]
averaged power: 195 W
(pulse: 155-185 W)
Net absorbed microwave power P [abr.unit]
averaged power: 10 W
(pulse: 20-55 W)
External pulse [V]
t [ms]

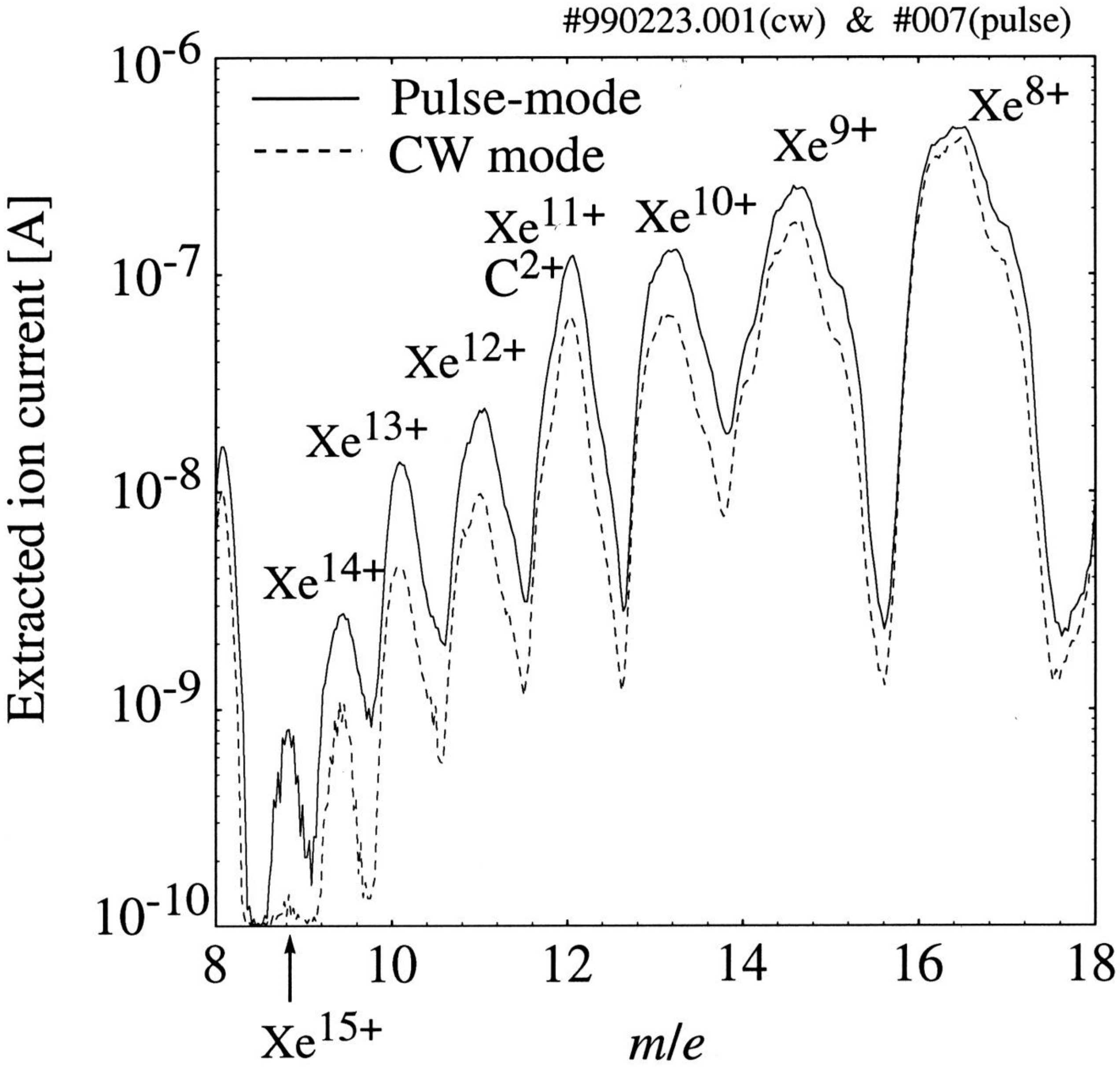
#990223.001(cw) & #007(pulse)
Pulse-mode
CW mode
Extracted ion current [A]
Xe^{8+}
Xe^{9+}
Xe^{10+}
Xe^{11+}
C^{2+}
Xe^{12+}
Xe^{13+}
Xe^{14+}
Xe^{15+}
m/e

Empirical improvement methods IV: Two (multi-) frequencies feeding

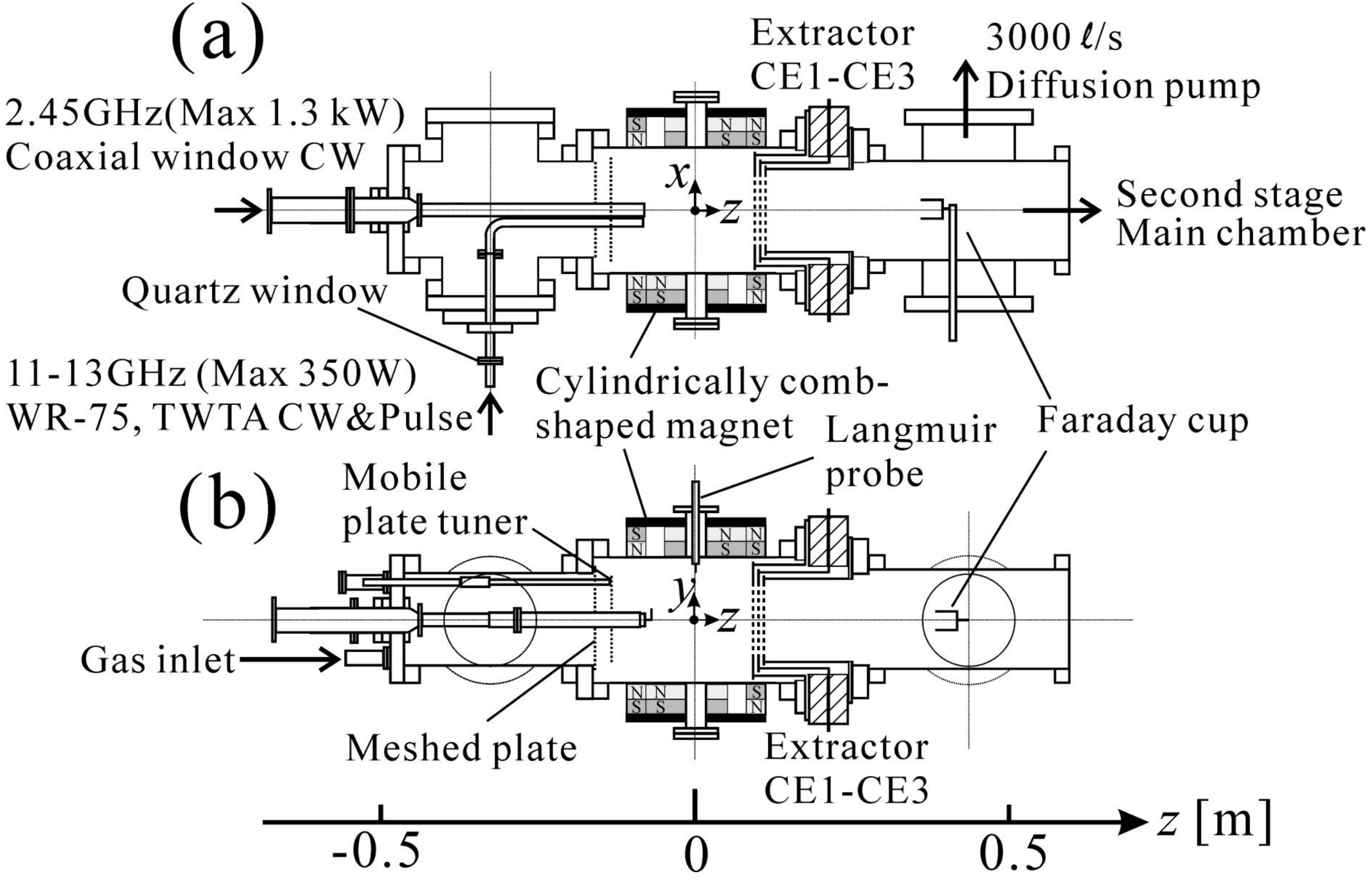

マイクロ波導入系と引き出し電極

Mobile plate tuner

Electrode CE1-CE3

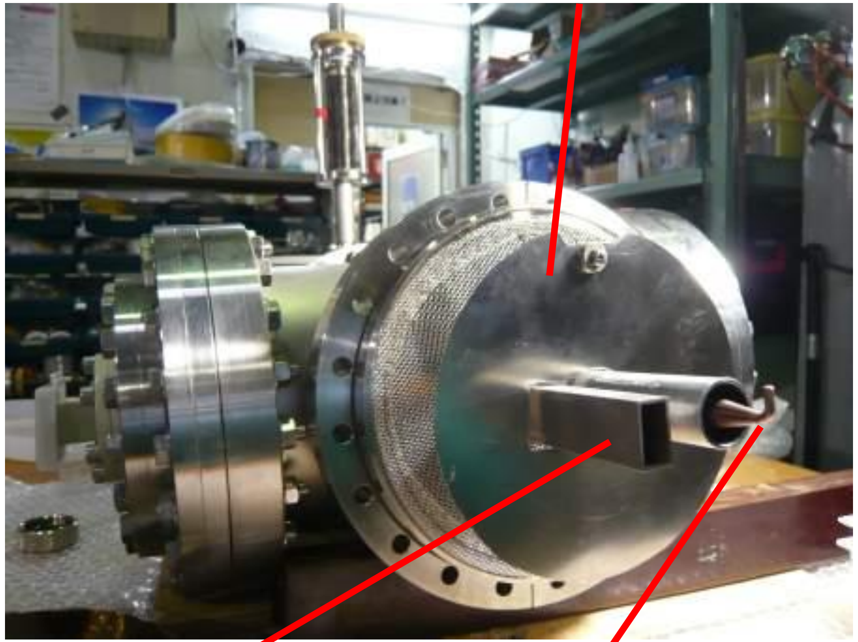

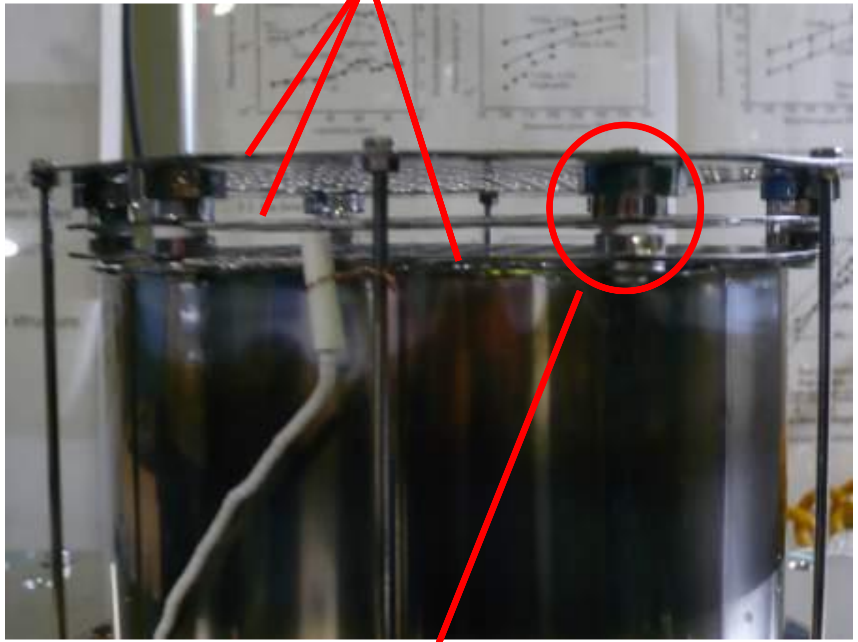

11~13 GHz wave guide
(WR - 75)

Cu semi-dipole antenna
(Coaxial mode 2.45GHz)

スパッタよけ

Overview of electromagnetic (EM) & electrostatic (ES) waves in magnetized plasma and ECR efficiency

Brief theoretical background I: Analysis scheme of EM waves in the ECRIS can be summarized very roughly (assuming ‘cold plasma approximation’)

- Equation of motion under $\boldsymbol{B}$

- Electrons
- for fast-time varying
- (ECR&UHR)

Including ions
for slow-time varying field
(ICR&LHR)

$\boldsymbol{v}_e$ $\boldsymbol{v}_i$

- Current density $\boldsymbol{J}$

- Maxwell’s curl Eqs.
- Dielectric constant $\varepsilon_0\overline{\overline{\boldsymbol{\kappa}_\mathrm{p}}}$ component

- det | left-hand side | =0

- $\widetilde{E_x}:\widetilde{E_y}:\widetilde{E_z}$ &
- Dispersion relation are decided.

$$\boldsymbol{k}\times\widetilde{\boldsymbol{E}}=\omega\mu_0\widetilde{\boldsymbol{H}}, \qquad \text{(o)}$$
$$\boldsymbol{k}\times\widetilde{\boldsymbol{H}}=-\omega\varepsilon_0\overline{\overline{\boldsymbol{\kappa}_\mathrm{p}}}\cdot\widetilde{\boldsymbol{E}}, \qquad \text{(p)}$$
$$\downarrow$$
$$\boldsymbol{k}\times\left(\boldsymbol{k}\times\widetilde{\boldsymbol{E}}\right)+k_0^2\overline{\overline{\boldsymbol{\kappa}_\mathrm{p}}}\cdot\widetilde{\boldsymbol{E}}=0, \quad \text{(q)}$$

where $k_0={}^{\omega}/_{c}$, $\overline{\overline{\epsilon_\mathrm{p}}}=\varepsilon_0\overline{\overline{\kappa_\mathrm{p}}}=\varepsilon_0\begin{pmatrix}\kappa_\perp & -j\kappa_\times & 0\\ j\kappa_\times & \kappa_\perp & 0\\ 0 & 0 & \kappa_{/\!/}\end{pmatrix}$, (j)

and $\kappa_r=1-\sum_j\frac{\omega_{pj}^2}{\omega(\omega+\epsilon_j\omega_{cj})}$, $\kappa_l=1-\sum_j\frac{\omega_{pj}^2}{\omega(\omega-\epsilon_j\omega_{cj})}$, $\kappa_{/\!/}=1-\sum_j\frac{\omega_{pj}^2}{\omega^2}$, $\kappa_\perp=\frac{1}{2}(\kappa_r+\kappa_l)$, $\kappa_\times=\frac{1}{2}(\kappa_r-\kappa_l)$, $\epsilon_j=\left(\frac{q_j}{|q_j|}\right)$, j =e (for electron), i(for ion), ω_{ci} (ω_{pi}) and ω_{ce}(ω_{pe}) represent the ion and electron cyclotron (plasma) frequencies, respectively, q_i represents charge of electron (j=e) and j charge state ion species, and i is the imaginary unit. $\kappa_\perp$, $\kappa_\times$, $\kappa_{/\!/}$, κ_r and κ_l are the dielectric tensor elements.

$$\begin{bmatrix}\kappa_z^2 & 0 & -\kappa_x\kappa_z\\ 0 & \kappa_x^2+\kappa_z^2 & 0\\ -\kappa_x\kappa_z & 0 & \kappa_x^2\end{bmatrix}\begin{bmatrix}\widetilde{E_x}\\ \widetilde{E_y}\\ \widetilde{E_z}\end{bmatrix}=\kappa_0^2\begin{bmatrix}\kappa_\perp & -j\kappa_\times & 0\\ j\kappa_\times & \kappa_\perp & 0\\ 0 & 0 & \kappa_{/\!/}\end{bmatrix}\begin{bmatrix}\widetilde{E_x}\\ \widetilde{E_y}\\ \widetilde{E_z}\end{bmatrix}$$

$$\det\begin{bmatrix}N^2\cos^2\theta-\kappa_\perp & -j\kappa_\times & -N^2\cos\theta\sin\theta\\ -j\kappa_\times & N^2-\kappa_\perp & 0\\ -N^2\cos\theta\sin\theta & 0 & N^2\sin^2\theta-\kappa_{/\!/}\end{bmatrix}=0 \qquad \text{(r)}$$

Eq.(r) is the dispersion equation, which relates $k\equiv k_0N$, ω, and θ.

$\widetilde{E_x}:\widetilde{E_y}:\widetilde{E_z}::(\kappa_\perp-N^2)(\kappa_{/\!/}-N^2\sin^2\theta):j\kappa_\times(N^2\sin^2\theta-\kappa_{/\!/}):(N^2-\kappa_\perp)N^2\cos\theta\sin\theta$ (t2)

$$\tan^2\theta=-\frac{\kappa_{/\!/}(N^2-\kappa_r)(N^2-\kappa_\ell)}{(N^2-\kappa_{/\!/})(\kappa_\perp N^2-\kappa_r\kappa_\ell)} \qquad \text{(v)}$$

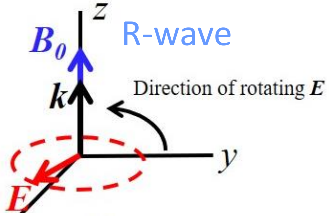

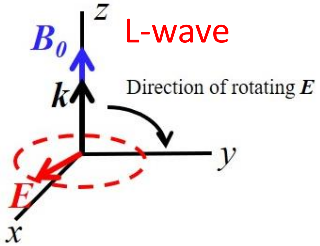

- $\theta=0$ ($\boldsymbol{B}/\!/\boldsymbol{k}$):
- PO, R-wave(ECR), L-wave(ICR);
- R-& L- cutoffs

Summeraized to CMA daiagram

$\theta=\pi/2$($\boldsymbol{B}\perp\boldsymbol{k}$):
O-wave(interferometer)
& X-waves(UHR&LHR)
R-& L- cutoffs

Summeraized to CMA daiagram

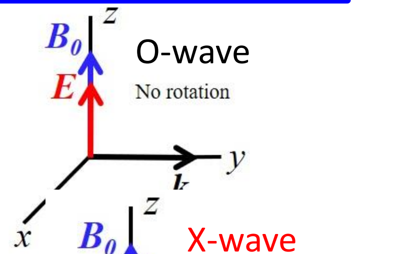

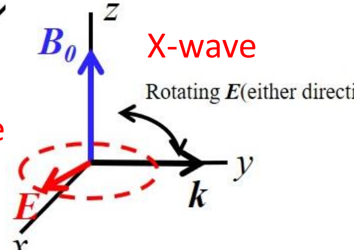

- Arbitrary θ & $\nabla\cdot\widetilde{\boldsymbol{E}}\approx 0$ & $\nabla\times\widetilde{\boldsymbol{E}}\approx\boldsymbol{0}$
- Helicon waves*

*a superimposed wave of multiple low-frequency Whistler waves propagating at a constant angle θ.

ECR & ICR & LHR theoretical background

Dispersion relations, resonances and cutoffs

The dispersion relation of electromagnetic (EM) waves in a homogeneously magnetized plasma with a z-axis magnetic field in a Cartesian coordinate system is given by the dielectric tensor in the cold plasma approximation including the ion contribution as follows.

$$\overline{\overline{\epsilon_p}} = \epsilon_0 \overline{\overline{\kappa_p}} = \epsilon_0 \begin{pmatrix} \kappa_\perp & -i\kappa_\times & 0 \\ i\kappa_\times & \kappa_\perp & 0 \\ 0 & 0 & \kappa_{/\!/} \end{pmatrix}, \qquad (1)$$

where $\kappa_r = 1 - \sum_j \frac{\omega_{pj}^2}{\omega(\omega+\epsilon_j\omega_{cj})}$, $\kappa_l = 1 - \sum_j \frac{\omega_{pj}^2}{\omega(\omega-\epsilon_j\omega_{cj})}$, $\kappa_{/\!/} = 1 - \sum_j \frac{\omega_{pj}^2}{\omega^2}$, $\kappa_\perp = \frac{1}{2}(\kappa_r + \kappa_l)$, $\kappa_\times = \frac{1}{2}(\kappa_r - \kappa_l)$, $\epsilon_j = \left(\frac{q_j}{|q_j|}\right)$, j =e (for electron), i(for ion), ω_{ci} (ω_{pi}) and ω_{ce}(ω_{pe}) represent the ion and electron cyclotron (plasma) frequencies, respectively, and i is the imaginary unit. $\kappa_\perp$, $\kappa_\times$, $\kappa_{/\!/}$, κ_r and κ_l are the dielectric tensor elements. Here we use an expression similar to that of Lieberman.[3] $\epsilon_0$is the permittivity in vacuum, and $\overline{\overline{\kappa_p}}$ is the relative permittivity tensor.

When the wave vector ***k*** (magnitude $|\boldsymbol{k}|= k$) of the electromagnetic wave propagates in the direction forming an angle of q with respect to the magnetic field ***B***, the dispersion relation of electromagnetic waves in magnetized plasma in cold uniform plasma is given by the following relation.

$$(\kappa_\perp \sin^2\theta + \kappa_{/\!/}\cos^2\theta)N^4 - \{(\kappa_\perp{}^2 - \kappa_\times{}^2)\sin^2\theta + \kappa_{/\!/}\kappa_\perp(1+\cos^2\theta)\}N^2 + (\kappa_\perp{}^2 - \kappa_\times{}^2)\kappa_{/\!/} = 0, \quad (2)$$

where N (=k/k_0=ck/ω, k_0 is the wavenumber in vacuum) is the refractive index.

The magnitude of the wave vector ***k*** in directions perpendicular and parallel to the magnetic field, respectively, and c and ω represent the speed of light in vacuum and the angular frequency of the electromagnetic wave, respectively.

The following relational expression is derived from Eq.(2).

$$\tan^2\theta = -\frac{\kappa_{/\!/}(N^2-\kappa_r)(N^2-\kappa_l)}{(N^2-\kappa_{/\!/})(\kappa_\perp N^2-\kappa_r\kappa_l)}. \qquad (3)$$

Assuming that $\theta = 0$, the numerator on the right side of Eq. (3), the dispersion relations of right-hand circularly polarized waves (R-wave) and left-hand circularly polarized waves (L-wave) are derived as follows.

$$N_r^2 = \kappa_r = 1 - \sum_j \frac{\omega_{pj}^2}{\omega(\omega+\epsilon_j\omega_{cj})}, \ (4) \quad N_l^2 = \kappa_l = 1 - \sum_j \frac{\omega_{pj}^2}{\omega(\omega-\epsilon_j\omega_{cj})}. \qquad (5)$$

It is shown that electron cyclotron resonance (ECR) and ion cyclotron resonance (ICR) exist in the former and latter, respectively.

Also, from $N_r^2 = 0$, $N_l^2 = 0$, there are cutoff frequencies ω_R (R-cutoff) and ω_L (L-cutoff) for each wave propagation mode, considering the contribution of only electrons for ECR-related high frequencies, it is derived as follows.

$$\omega_R = \frac{\omega_{ce} + \sqrt{\omega_{ce}^2 + 4\omega_{pe}^2}}{2}, \ (6) \qquad \omega_L = \frac{-\omega_{ce} + \sqrt{\omega_{ce}^2 + 4\omega_{pe}^2}}{2}. \qquad (7)$$

Considering the density dependence of electromagnetic waves at specific frequencies from the low-density region to the high-density region in the plasma, we encounter the cutoff density limits of O-cutoff, R-cutoff, and L-cutoff, respectively. When the microwave frequency is 2.45GHz, the O-cutoff limit density is about 7.5×10^{16}m^{-3}, and the L-cutoff limit density formed near the center of the mirror in Osaka University ECRIS at the same frequency is about 2.5-3.5$\times 10^{17}$m^{-3}, and these values are in good agreement with the measurement results.

2-1. X-mode resonances

As a resonance phenomenon related to X-wave, there is upper hybrid resonance (UHR),

$$\omega_{UH}^2 = \omega_{ce}^2 + \omega_{pe}^2 \qquad (4)$$

in the high frequency region.

In addition to ω_{UH}, a lower hybrid resonance (LHR) appears at the frequency ω_{LH}($\omega_{LH} \ll \omega_{ce}$) in the low-frequency region because $\kappa_\perp = 0$ when $\omega_{pi}^2 \gg \omega_{ci}^2$.

By using $\omega_{ci} \ll \omega \ll \omega_{ce}$, $\omega_{pe} \sim \omega_{ce}$, $\omega_{pi} \sim (M/m)^{1/2}\omega_{ci}$,

$$\frac{1}{\omega_{LH}^2} = \frac{1}{\omega_{pi}^2} + \frac{1}{\omega_{ce}\omega_{ci}} \qquad (5)$$

is derived.

Cut off & Resonance (for common understanding)

- $N = \frac{k}{k_0} = \frac{k}{\omega/c}\left(= \frac{ck}{\omega}\right) = \frac{c}{\omega/k} = \frac{c}{v_p}\left(= \sqrt{\frac{\varepsilon\mu}{\varepsilon_0\mu_0}} = \sqrt{\frac{\varepsilon_r\varepsilon_0\mu_r\mu_0}{\varepsilon_0\mu_0}} \sim \sqrt{\varepsilon_r\mu_r} \sim \sqrt{\varepsilon_r}\right),$
- $k_0 = \omega/c,\ k = \omega/v_p\left(= \frac{\omega}{\omega/k}\right) = \frac{\omega}{c}\frac{c}{v_p} = \frac{\omega}{c}N = \frac{2\pi}{\lambda}$
- $v_p = \frac{\omega}{k} = \frac{c}{N} = \frac{c}{c/v_p} \approx \frac{c}{\sqrt{\varepsilon_r}}$ $\quad N^2 = \varepsilon/\varepsilon_0,\ \varepsilon = \varepsilon_0\varepsilon_r$

cf. F.F.Chen:
$\frac{v_p^2}{c^2}\left(= \frac{\omega^2}{c^2k^2}\right) = \frac{1}{N^2}$
v.s. ω

- **Resonance:** $N \rightarrow \boxed{\infty}$ i.e. $k \rightarrow \boxed{\infty}$, $\varepsilon \rightarrow \boxed{\infty}$ $\left(v_\varphi \rightarrow \boxed{0},\ \lambda \rightarrow \boxed{0}\right)$
- **Cut off & refraction/evanescent (skin effect)**

  $N \rightarrow \boxed{0}$ i.e. $k \rightarrow \boxed{0}$, $\varepsilon \rightarrow \boxed{0}$ $\left(v_\varphi \rightarrow \boxed{\infty},\ \lambda \rightarrow \boxed{\infty}\right)$

The four principle wave modes (O, X, L, R) & their dispersion relations

- ***Left-hand circularly polarized wave*** (L)
- (θ=0)

ICR: $\omega_{ci} = \omega_{RF}$

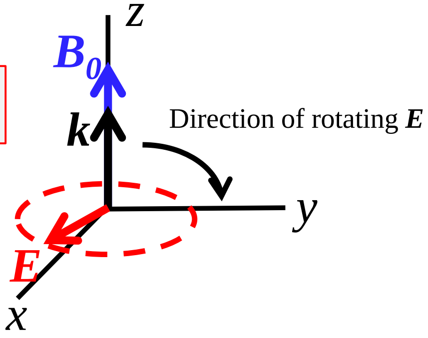

- ***Right-hand circularly polarized wave*** (R)
- (θ=0)

ECR: $\omega_{ce} = \omega_{RF}$

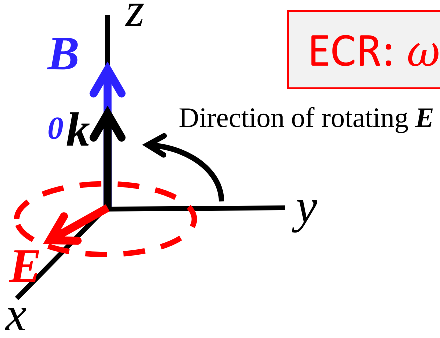

- ***Ordinary wave*** (O)
- (θ=π/2)

Interferometry

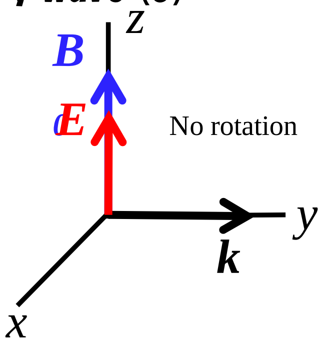

- ***Extraordinary wave*** (X)
- (θ=π/2)

UHR: $\omega_{UH}^2 \equiv \omega_{ce}^2 + \omega_{pe}^2 = \omega_{RF}^2$

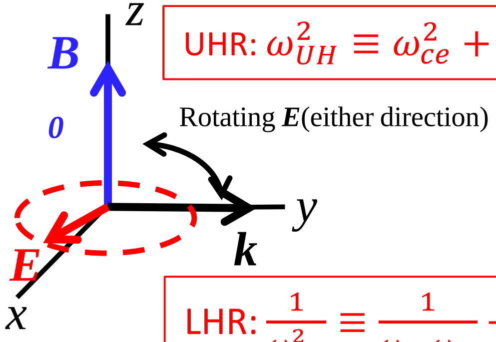

LHR: $\frac{1}{\omega_{LH}^2} \equiv \frac{1}{\omega_{ce}\omega_{ci}} + \frac{1}{\omega_{pi}^2} = \frac{1}{\omega_{RF}^2}$

Wave launched towards a magnetoplama

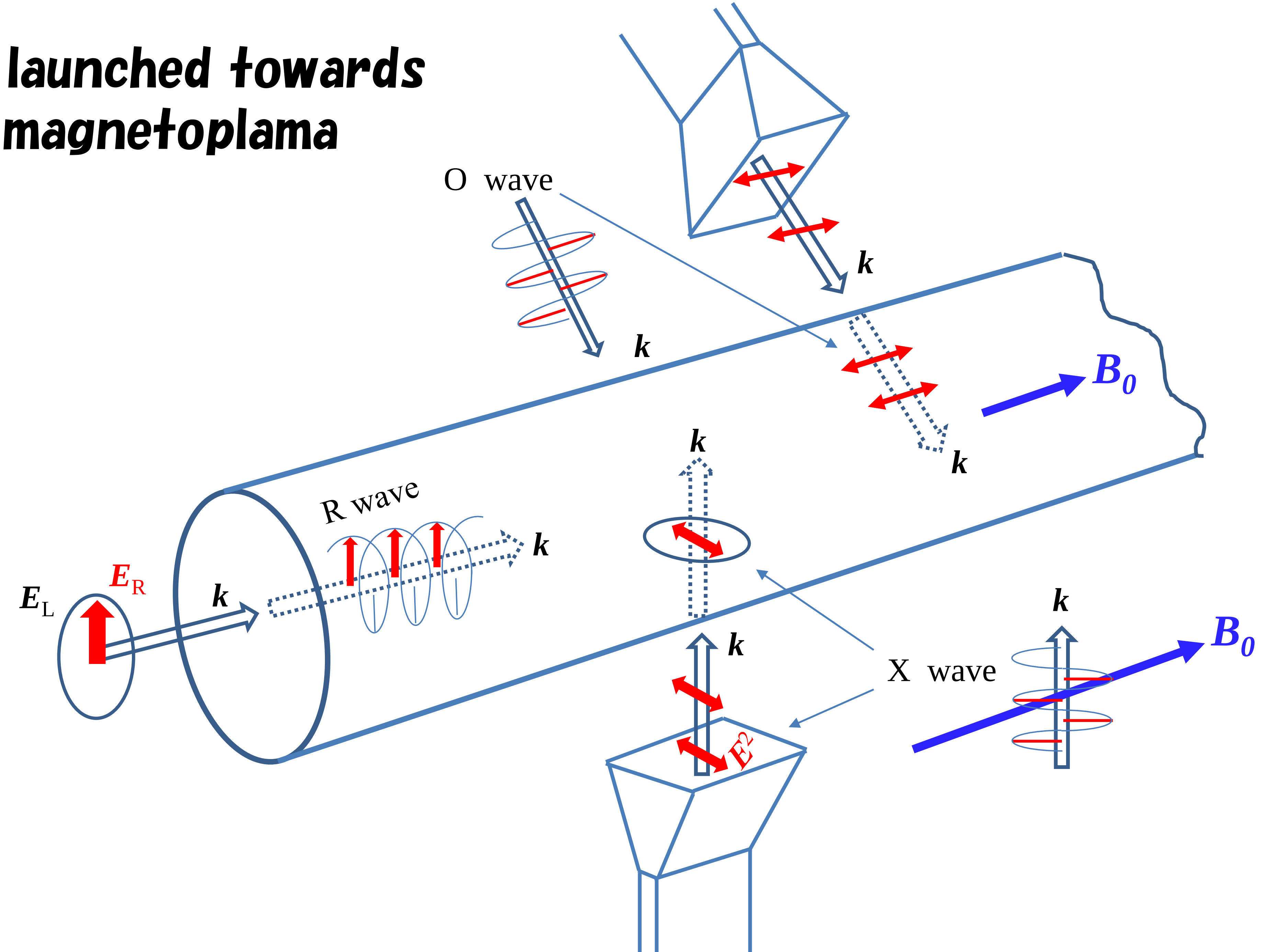

波動加熱プロセス

- **ElectroMagnetic(EM) ⇒ mode converting & enhancing Internal Electrostatic(ES) waves**
  - **Langmuir mode (Lm)**
    - $\omega_{\mathrm{Lm}}{}^2 = \omega_p{}^2 + k^2 v_{th}{}^2$
  - **Bernstain mode (Bm)**
    - $\omega_{Bm}{}^2 = m^2 \omega_c{}^2 \left[1 + \left(\frac{\omega_p}{\omega_c}\right)^2 F_m \left(k_{Bn}{}^2 \rho_L{}^2\right)\right]$ -->**m=0:UHR**

      Bessel function
    - **Cut-off free, as well as Whistler mode (R-wave)**
    - $\frac{\partial\omega}{\partial k} \sim v_{th}\ (very\ slow) \&\ Cyclotron\ damping\ efficiency\ (high)$
  - **Parametric decay:**
    - **Plasmons, Phonons, Cavitons,…**
- **Optimum conditions:** $\omega_{UH}{}^2 \sim \omega_{Bm}{}^2 \sim \omega_p{}^2 + \omega_{ce}{}^2$
  - **Dense plasmas:** $\omega_p/\omega_{RF} \sim 1$
  - $v\phi_{RF}/\omega_{RF} = v_{th}/m\omega_{internal}$ $(\omega_{RF} = m\omega_{interna\cdot}\ \lambda_{RF} = \lambda_{internal})$
  - $\omega_{UH} \sim 2\omega_{ce}$ **(from simulation results by Lin et al)**
- **Accessibilities**

CF:
Geller R 1996 Electron Cyclotron Resonance Ion Sources and ECR Plasmas, first ed.; Institute of Physics, Bristol and Philadelphia, IOP Publishing Ltd., UK, *Chapter 2, p.162*

Chen F F, *Introduction to Plasma Physics and Controlled Fusion*,
2nd Edit., Volume 1: Plasma Physics, Plenum Press.,1984, *Chap.7.10.3, p.278.*

Accessibility conditions of EM wave propagation to understand resonance & cutoff limitation

ECR efficiency & μW modes applications

Behavior of Microwave modes in an ECRIS

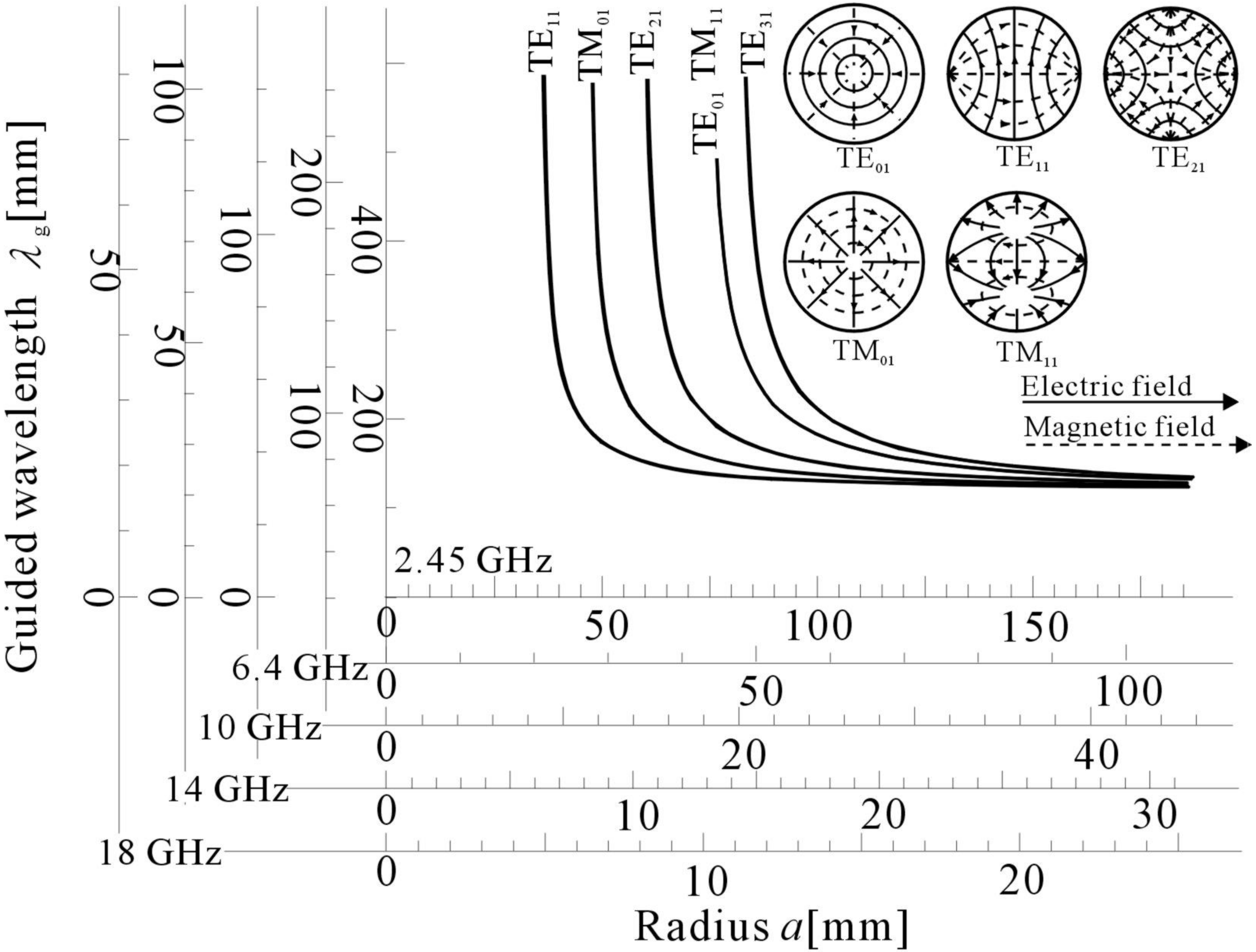

Yushi KATO, et.al., Nuclear Instruments and Methods in Physics Research B 237, 2005, pp. 256-261.

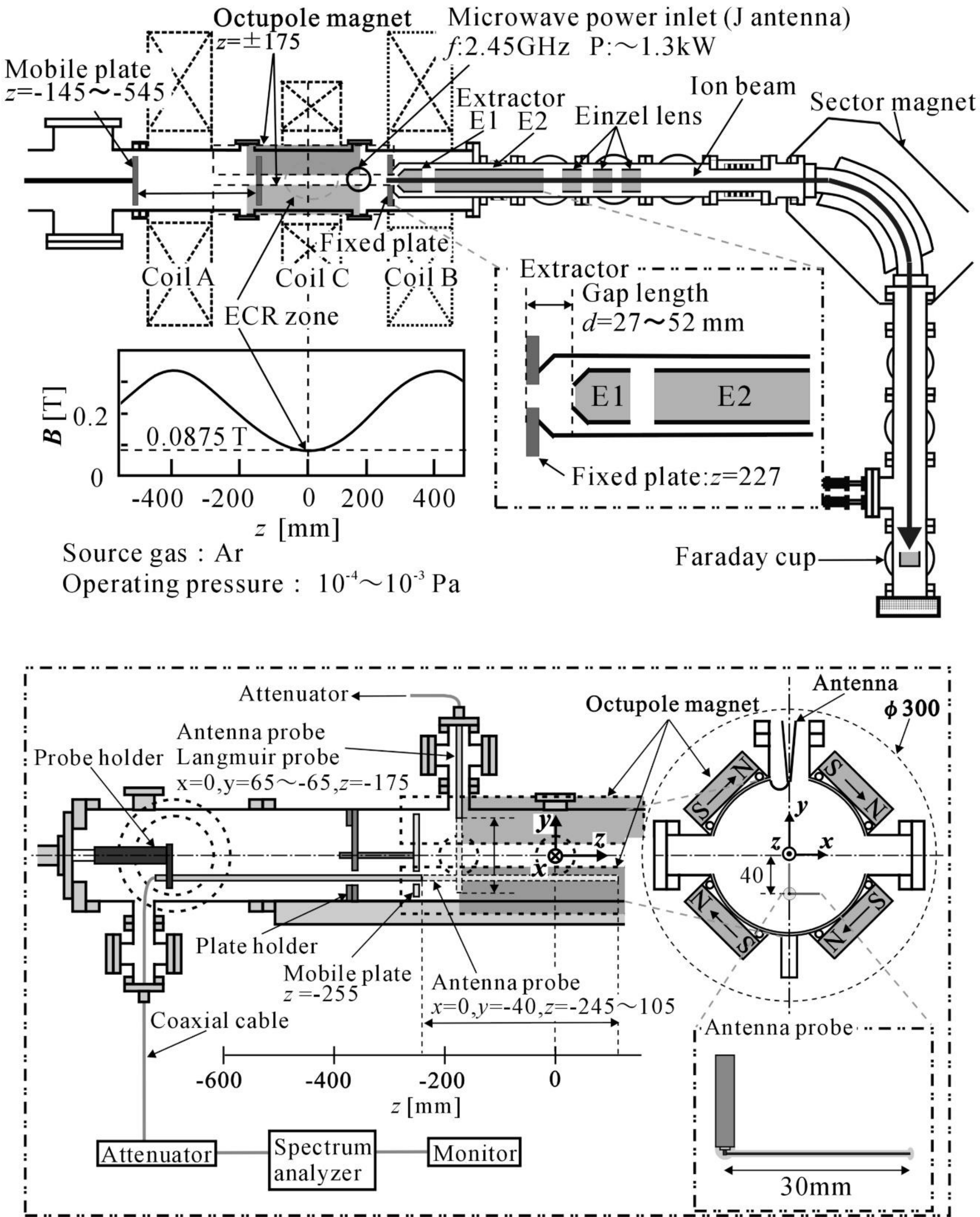

Yushi KATO, *et.al*, RSI. 77(2006)03A336-1-4

Recalling mode analysis

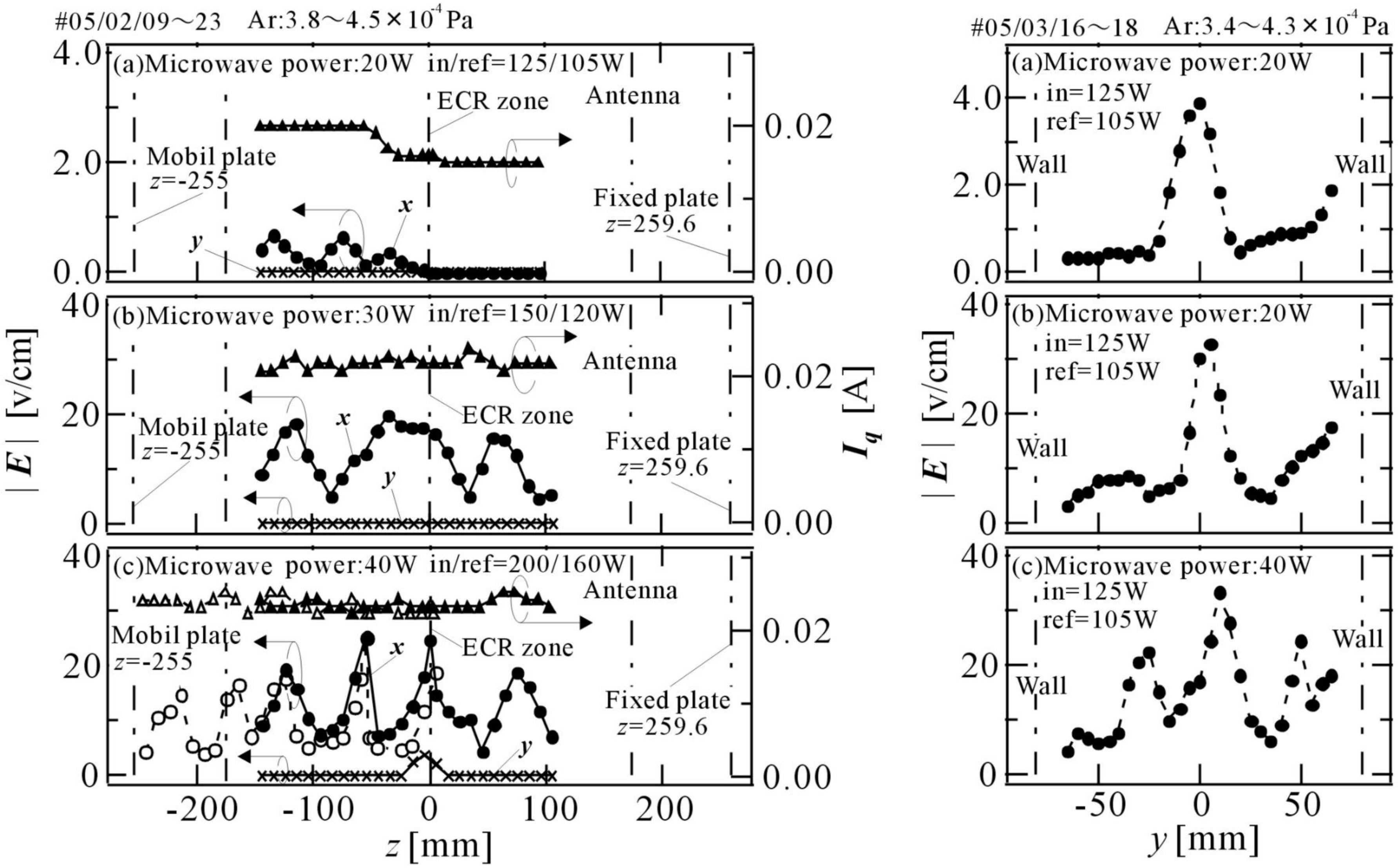

Yushi KATO, *et.al*, RSI. 77(2006)03A336-1-4

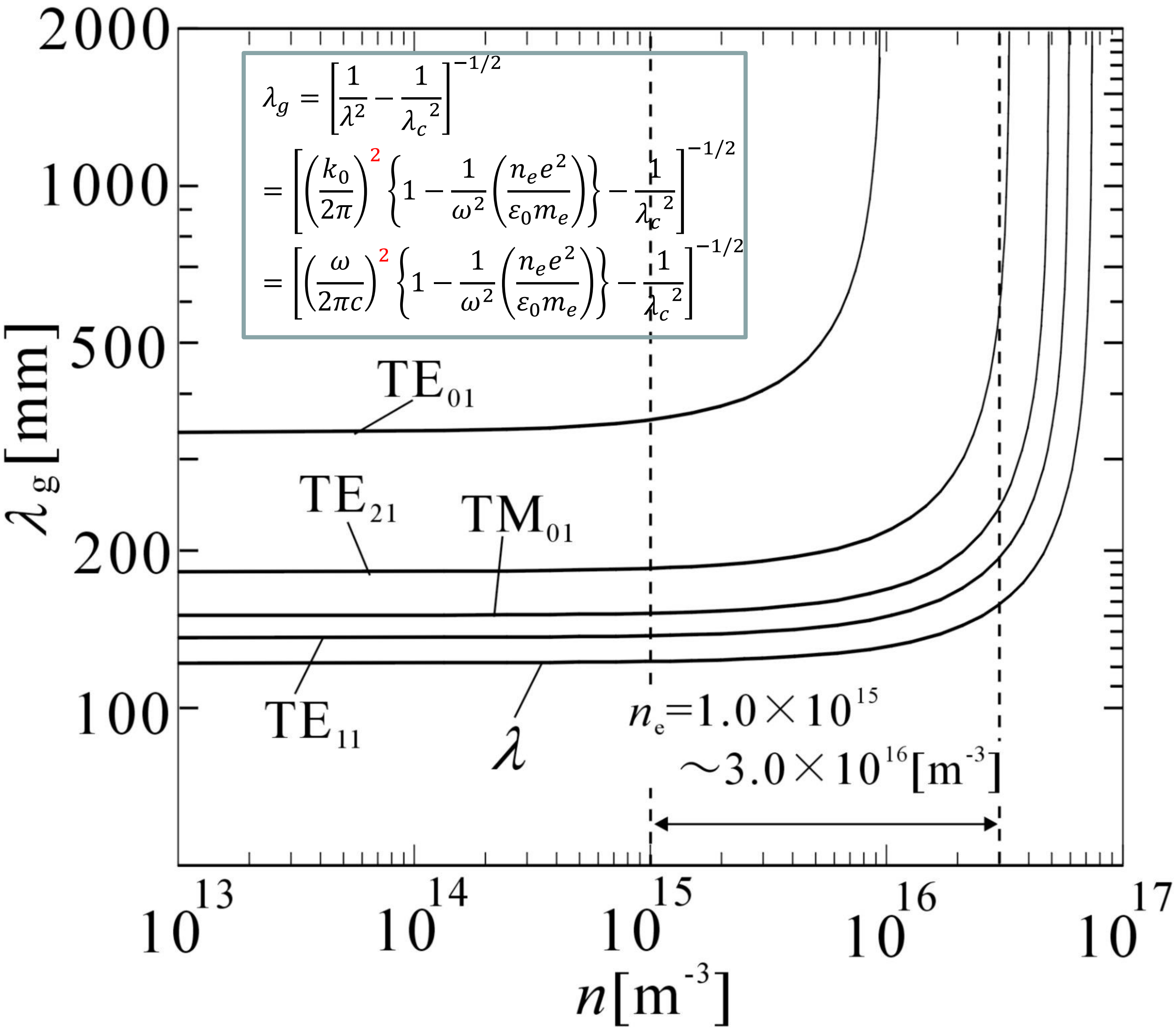

$$\lambda_g = \left[\frac{1}{\lambda^2} - \frac{1}{{\lambda_c}^2}\right]^{-1/2}$$
$$= \left[\left(\frac{k_0}{2\pi}\right)^2 \left\{1 - \frac{1}{\omega^2}\left(\frac{n_e e^2}{\varepsilon_0 m_e}\right)\right\} - \frac{1}{{\lambda_c}^2}\right]^{-1/2}$$
$$= \left[\left(\frac{\omega}{2\pi c}\right)^2 \left\{1 - \frac{1}{\omega^2}\left(\frac{n_e e^2}{\varepsilon_0 m_e}\right)\right\} - \frac{1}{{\lambda_c}^2}\right]^{-1/2}$$

Typical plasma parameters on the 2nd stages

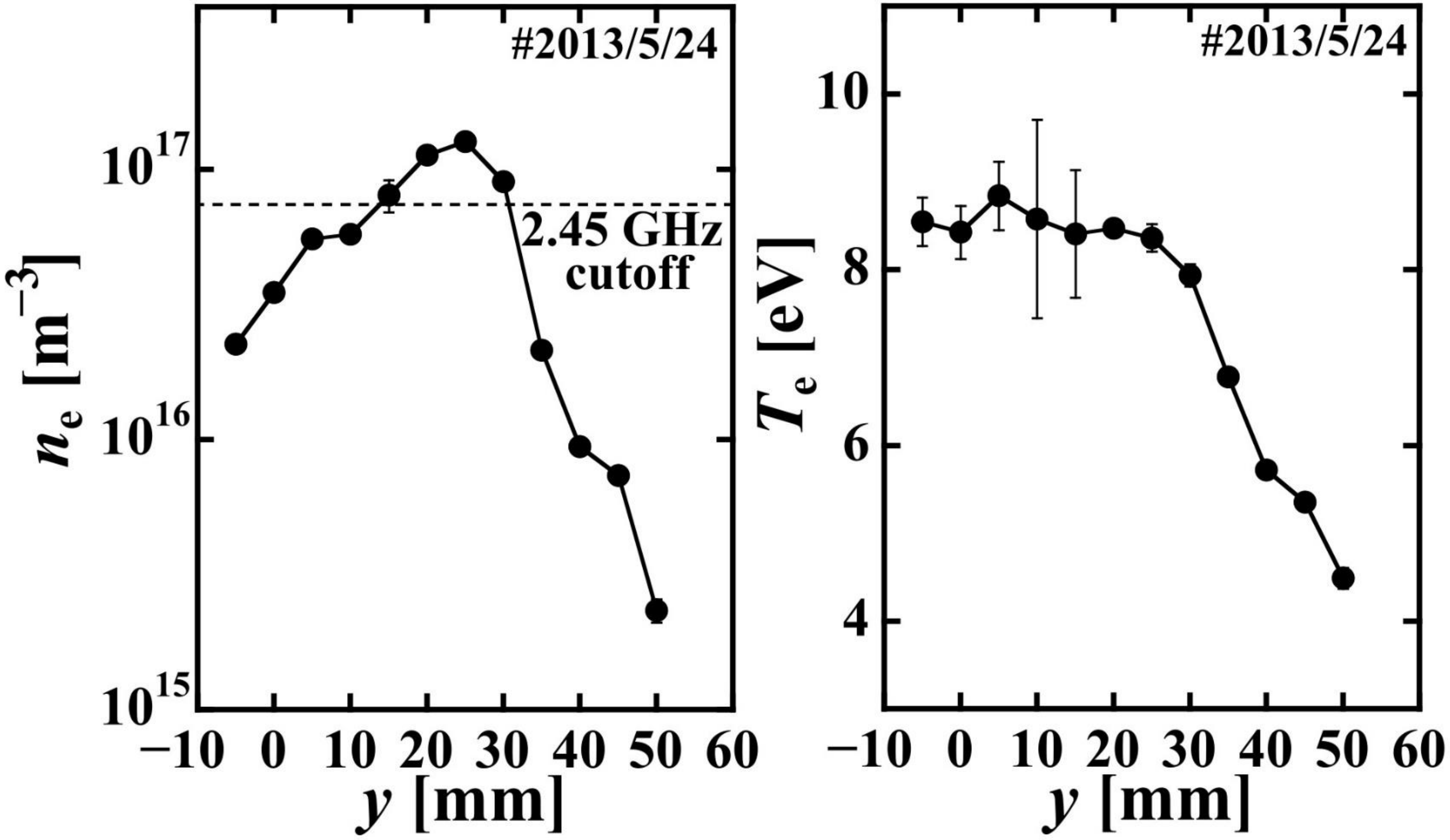

第2ステージ装置構成

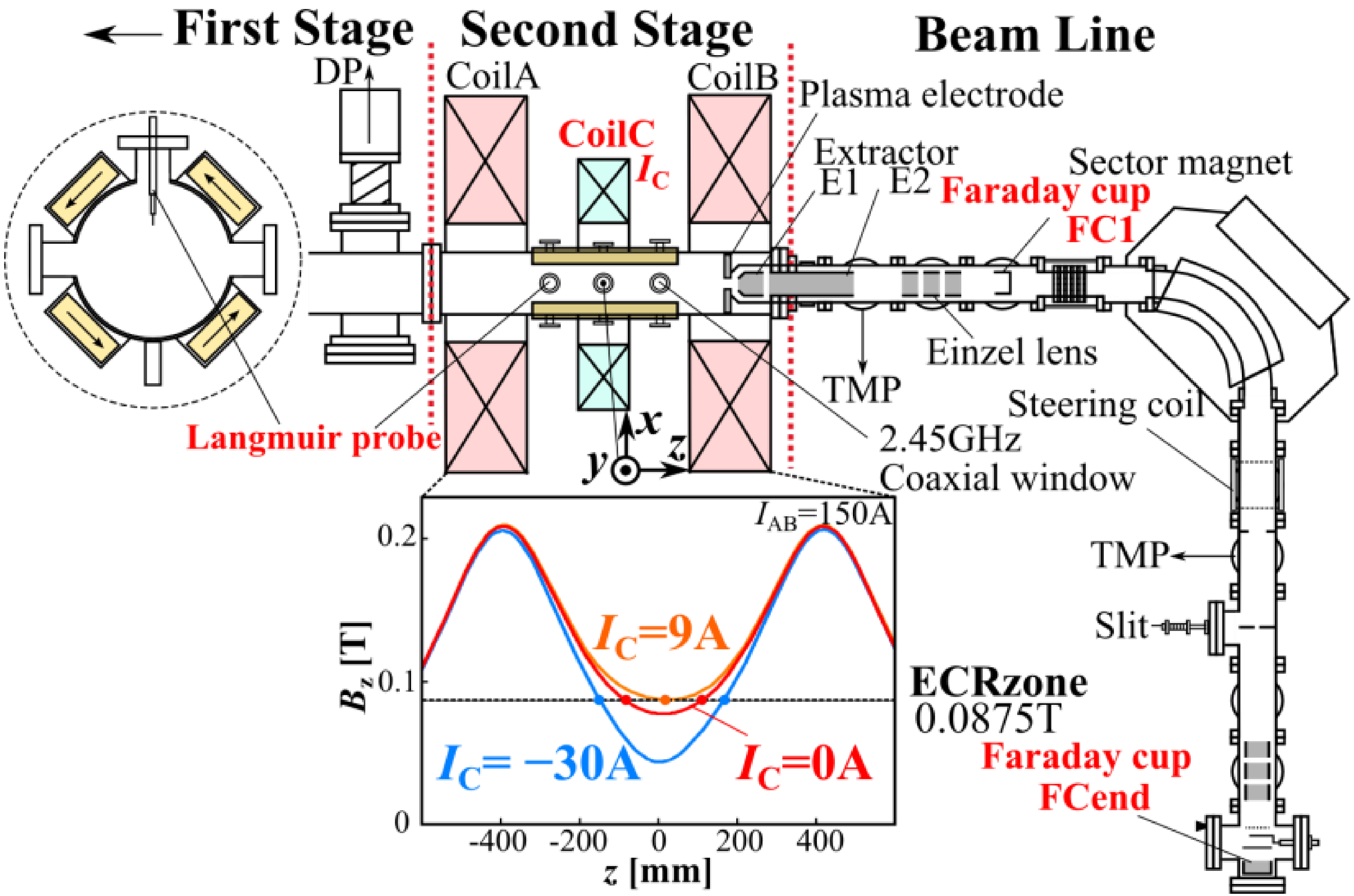

First beam in Osaka Univ. 2013.11.21

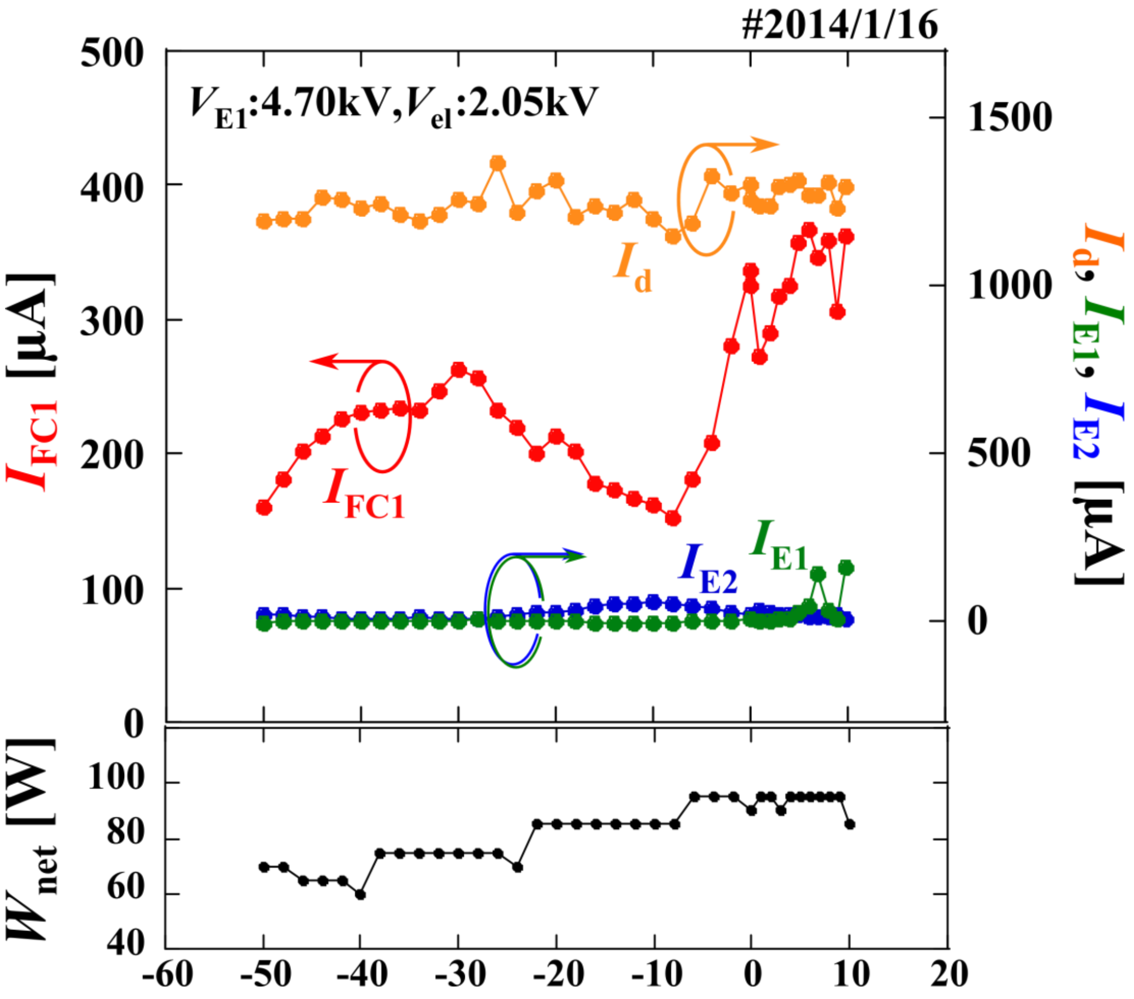

#2014/1/16
V_{E1}:4.70kV,V_{el}:2.05kV
I_{FC1} [μA]
I_d, I_{E1}, I_{E2} [μA]
I_d
I_{FC1}
I_{E2}
I_{E1}
W_{net} [W]
500
400
300
200
100
0
1500
1000
500
0
100
80
60
40
-60
-50
-40
-30
-20
-10
0
10
20

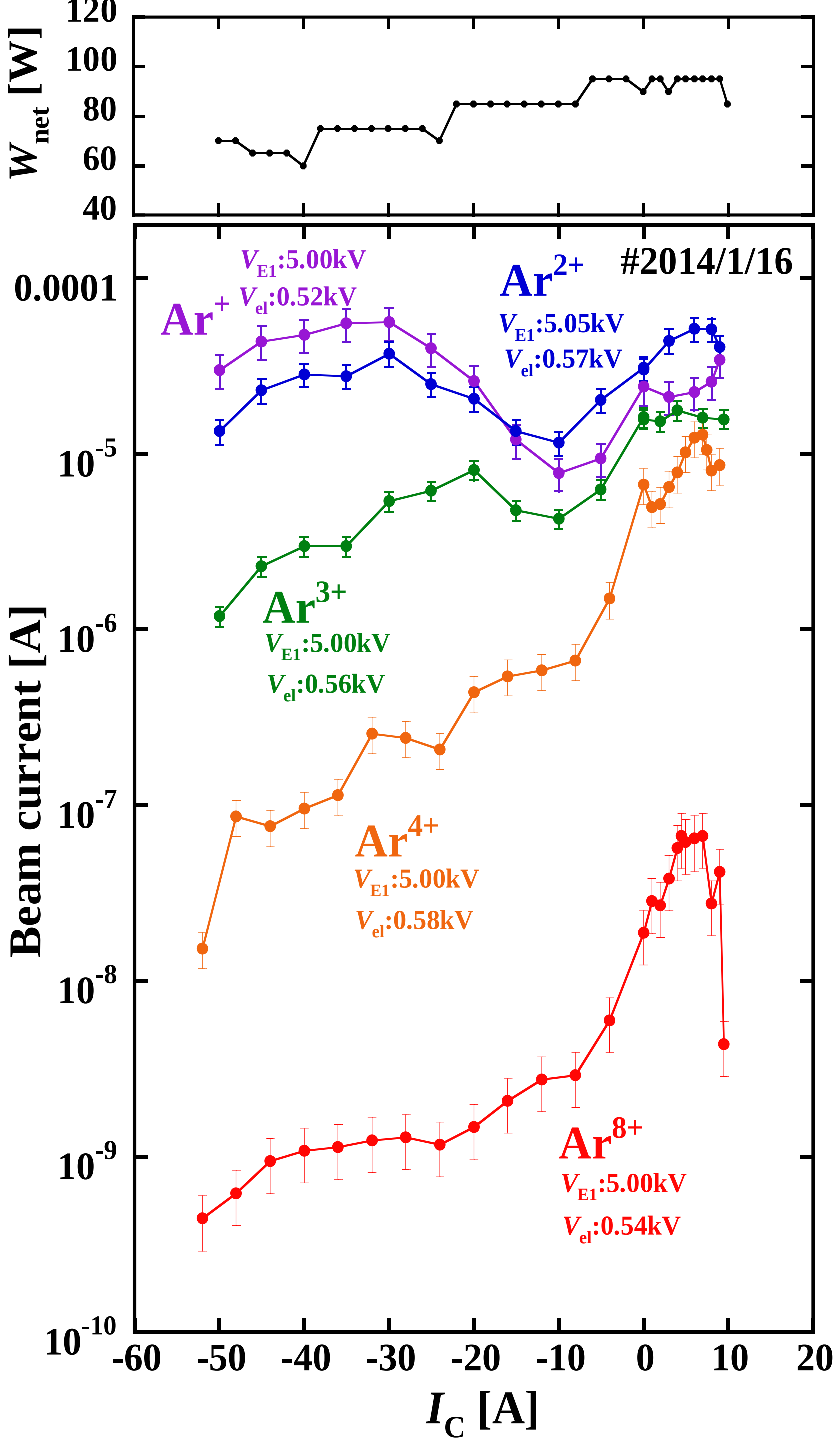

W_{net} [W]
120
100
80
60
40
Beam current [A]
0.0001
10^{-5}
10^{-6}
10^{-7}
10^{-8}
10^{-9}
10^{-10}
-60
-50
-40
-30
-20
-10
0
10
20
I_C [A]
#2014/1/16
Ar^{+}
V_{E1}:5.00kV
V_{el}:0.52kV
Ar^{2+}
V_{E1}:5.05kV
V_{el}:0.57kV
Ar^{3+}
V_{E1}:5.00kV
V_{el}:0.56kV
Ar^{4+}
V_{E1}:5.00kV
V_{el}:0.58kV
Ar^{8+}
V_{E1}:5.00kV
V_{el}:0.54kV

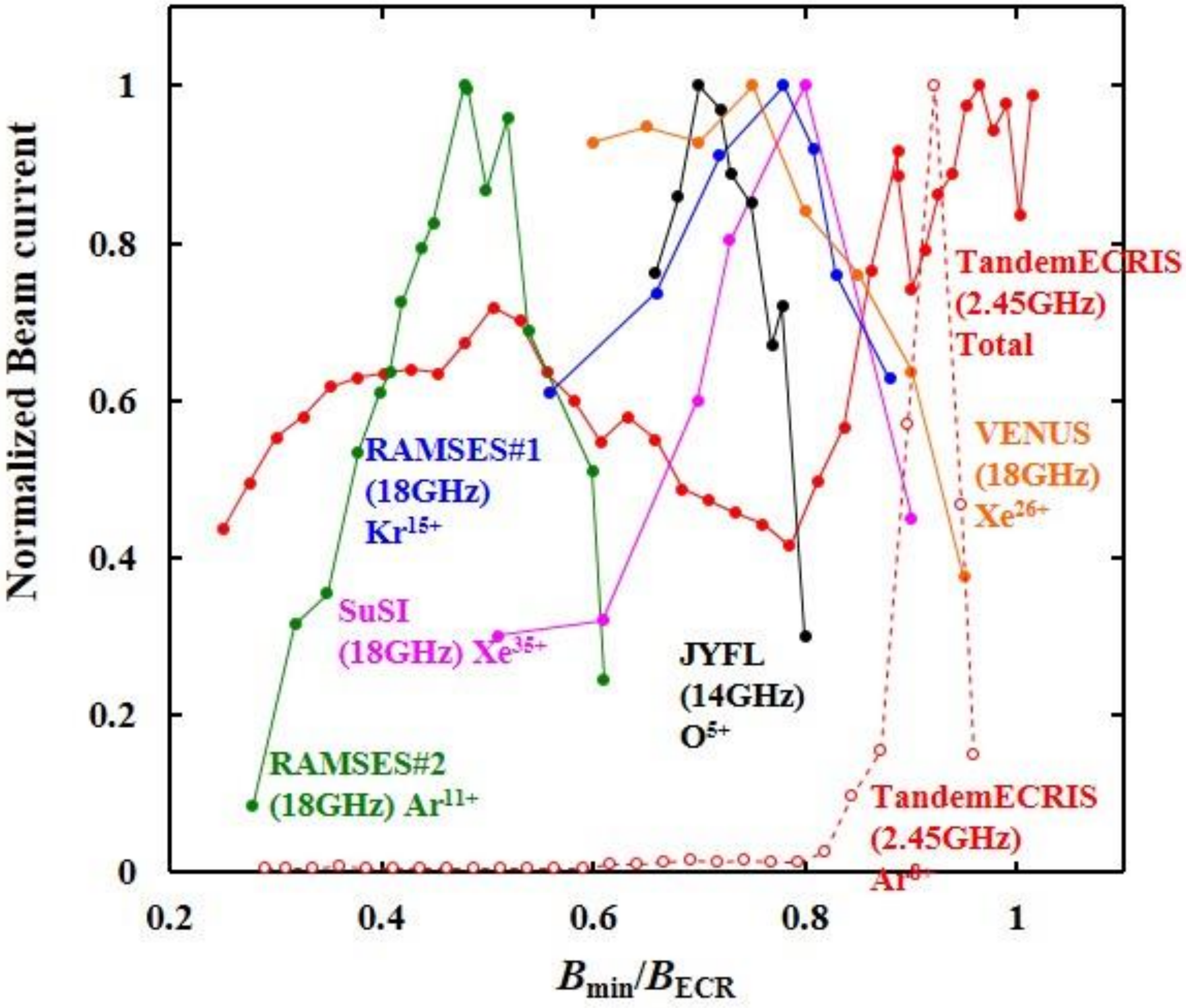

Normalized Beam current
B_{min}/B_{ECR}
0
0.2
0.4
0.6
0.8
1
0.2
0.4
0.6
0.8
1
RAMSES#1
(18GHz)
Kr^{15+}
SuSI
(18GHz) Xe^{35+}
RAMSES#2
(18GHz) Ar^{11+}
JYFL
(14GHz)
O^{5+}
TandemECRIS
(2.45GHz)
Total
VENUS
(18GHz)
Xe^{26+}
TandemECRIS
(2.45GHz)

Efficiency of ECR I

($\underline{E_r}$ & λ within the resonance zone is constant !)

- The average energy gain per pass is

$$W_{ecr} = \frac{\pi e^2 E_r^2}{m\omega|\alpha| v_{res}}$$

- The absorbed power per unit area, or energy flux

$$S_{ecr} = \frac{\pi n e^2 E_r^2}{m\omega|\alpha|} \quad (collisionless)$$

$$\bar{S}_{ecr} = \frac{2e^2 E_r^2 n}{m\omega|\alpha|} \tan^{-1}\left(\frac{\omega|\alpha| z_0}{v_m}\right) \quad (collisional)$$

Cf: $f \uparrow \rightarrow \lambda \downarrow$ $\varepsilon_e = \varepsilon E^2/2 \uparrow$

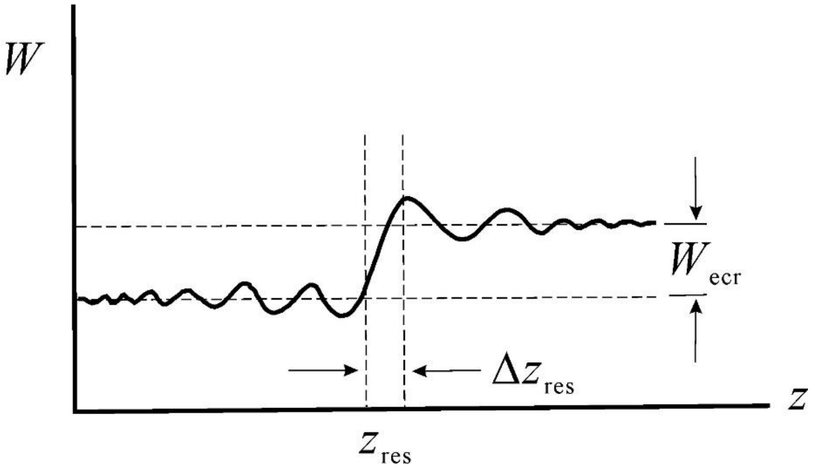

$$\Delta t_{res} = \left(\frac{2\pi}{\omega|\alpha| v_{res}}\right)^{1/2}$$

$$\Delta z_{res} \equiv v_{res}\Delta t_{res} = \left(\frac{2\pi v_{res}}{\omega|\alpha|}\right)^{1/2}$$

Refs: E_r & λ is not constant;
II. Wentzel-Kramers-Brillouin (WKB) wave expansion ($d\lambda/dz \ll 1$)
III. Budden (1966, Radio waves in the ionosphere)

Ref: Lieberman M A and Lichtenberg A J, *Principle of Plasma Discharges and Materials Processing*, 2nd Edit., A John Wiley & Son, Inc Publications, 2005, Chap.4, pp.110; ibid, Chap.13, pp.514.

マイクロ波モード

ECR zone

(0.0875T)

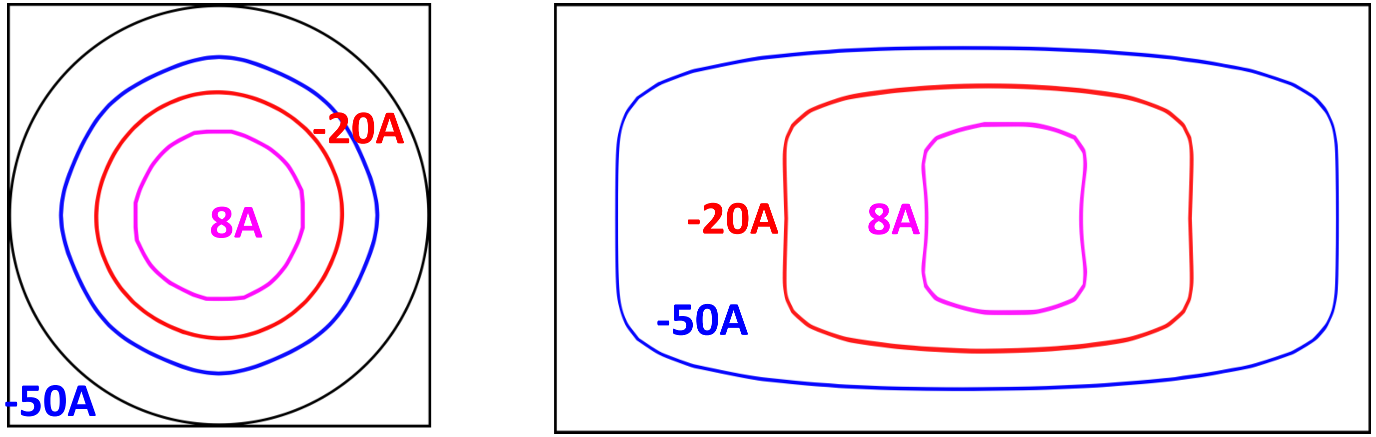

電界強度分布

TE$_{01}$

TE$_{11}$

TE$_{21}$

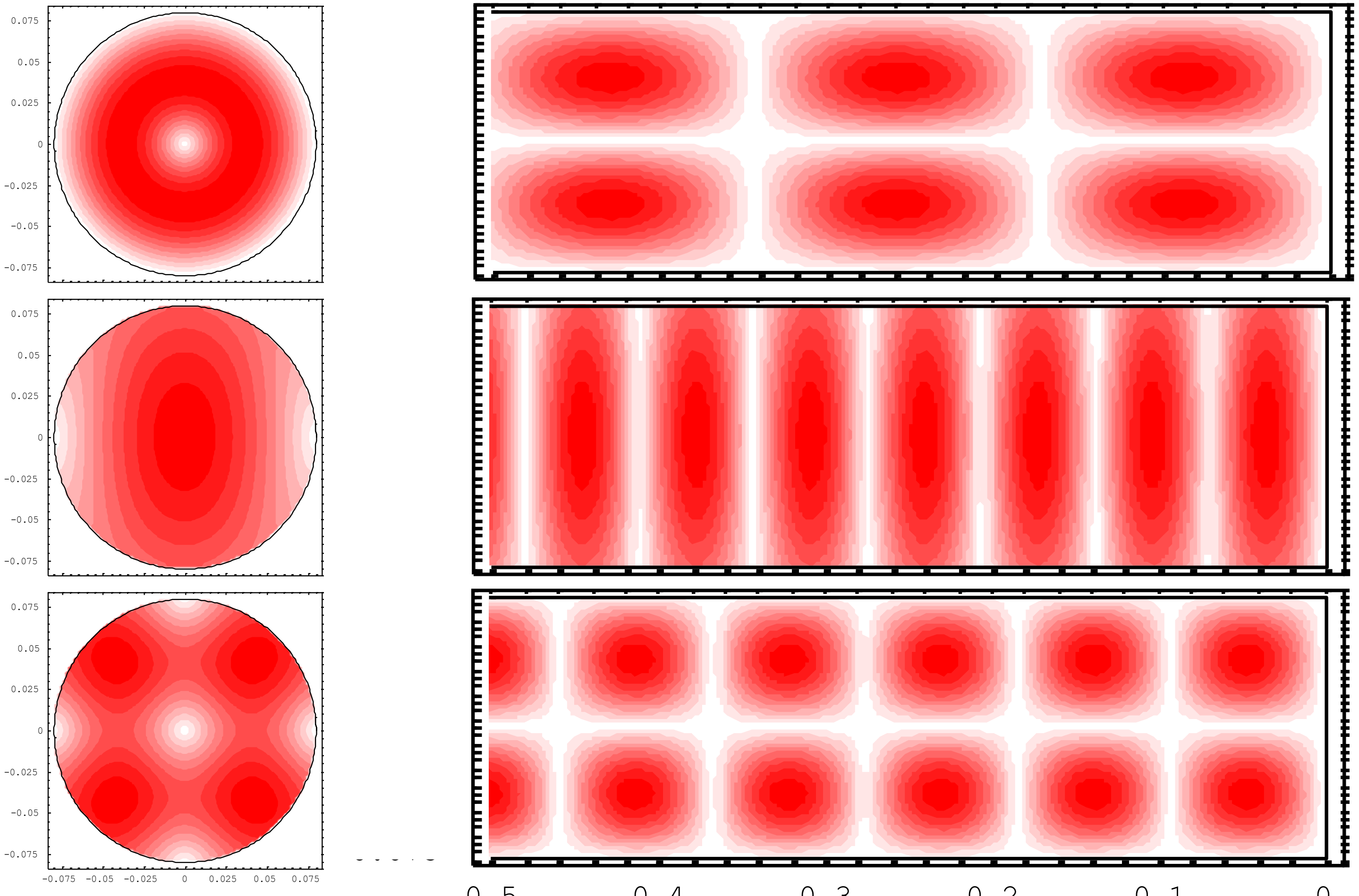

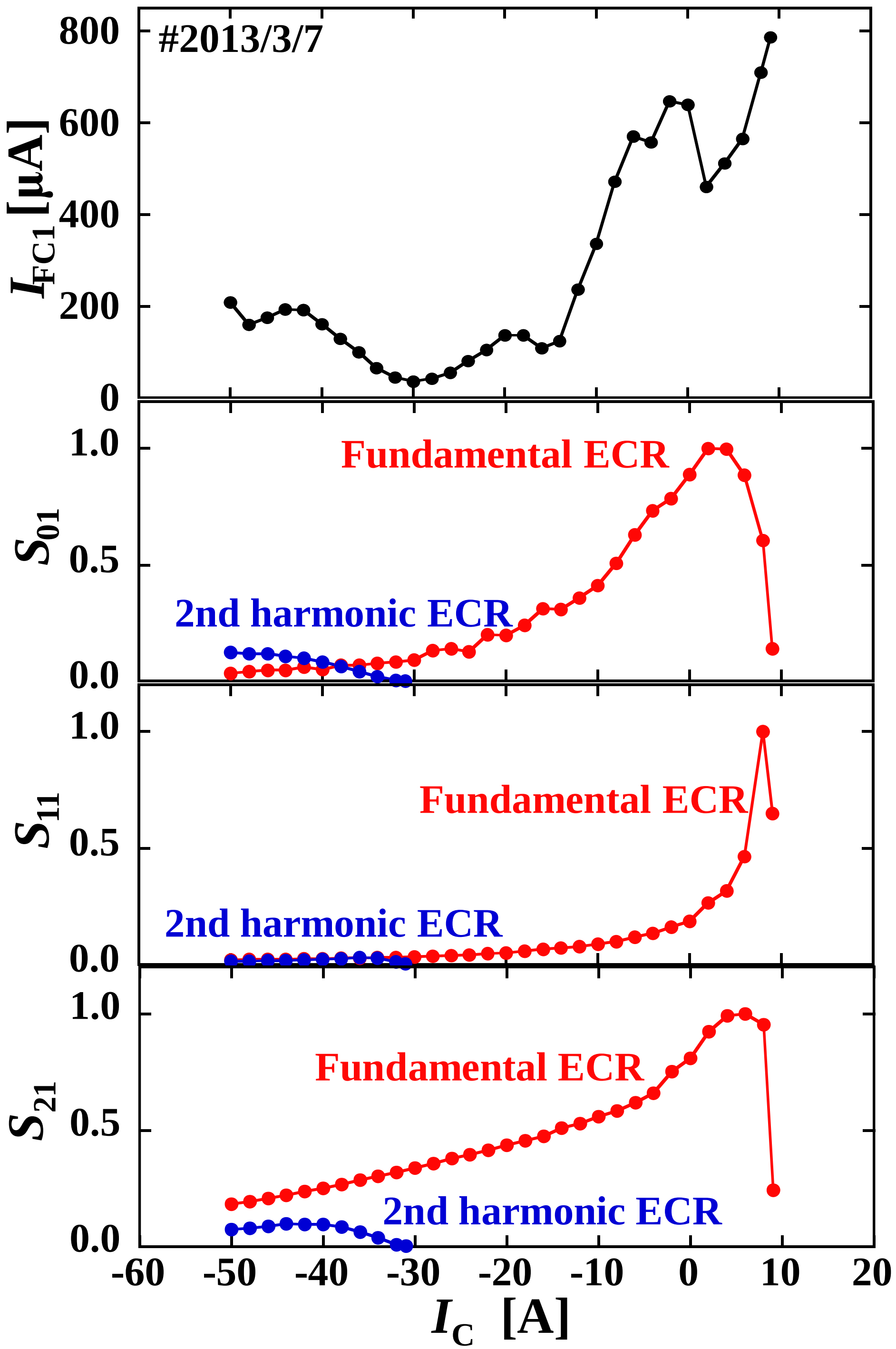

マイクロ波吸収効率とビーム電流の比較

TE$_{mn}$に対する積分値：S_{mn} (規格化)

各モードごとの積分値は
異なる位置でピークをとる

0.0875Tの1/2の磁場強度の位置
(2nd harmonic ECR zone)についても
同様に計算

高密度のプラズマ中で
導波管モードの適用が可能か？
→プラズマ中での波動伝搬
に対する考察が課題に

Upper Hybrid Resonance Heating Experiments on Electron Cyclotron Resonance Ion Source

Yushi Kato, Takuya Nishiokada, Kouta Hamada, Koji Onishi, Tatsuto Takeda, Kazuki Okumura, Takayuki Omori, Wataru Kubo, Masaki Ishihara, and Shuhei Harisaki

Graduate School of Engineering, Osaka Univ., Suita, Osaka, Japan

Contents

ICIS2019, Lanzhou, China,

Experimental apparatus

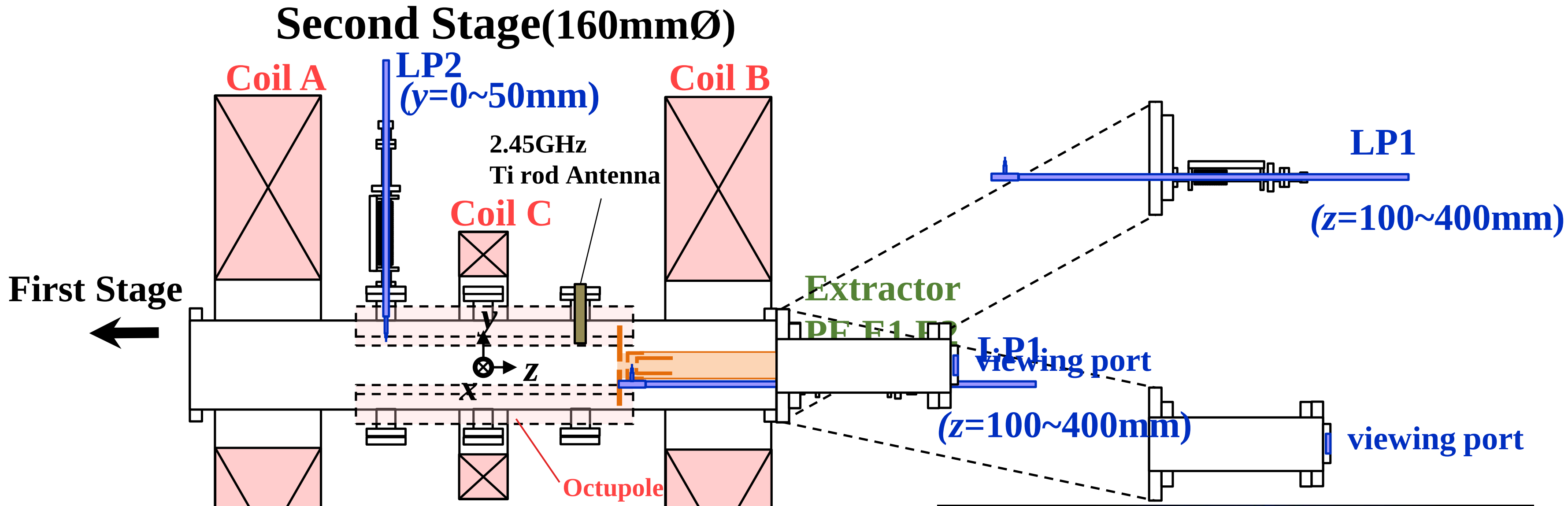

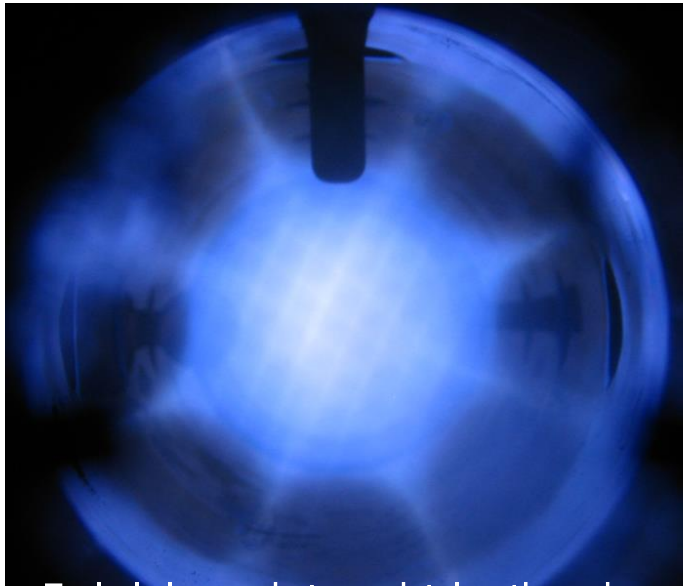

Typical plasma photograph taken through viewing port

◆Behavior of plasma image depending on Coil C current

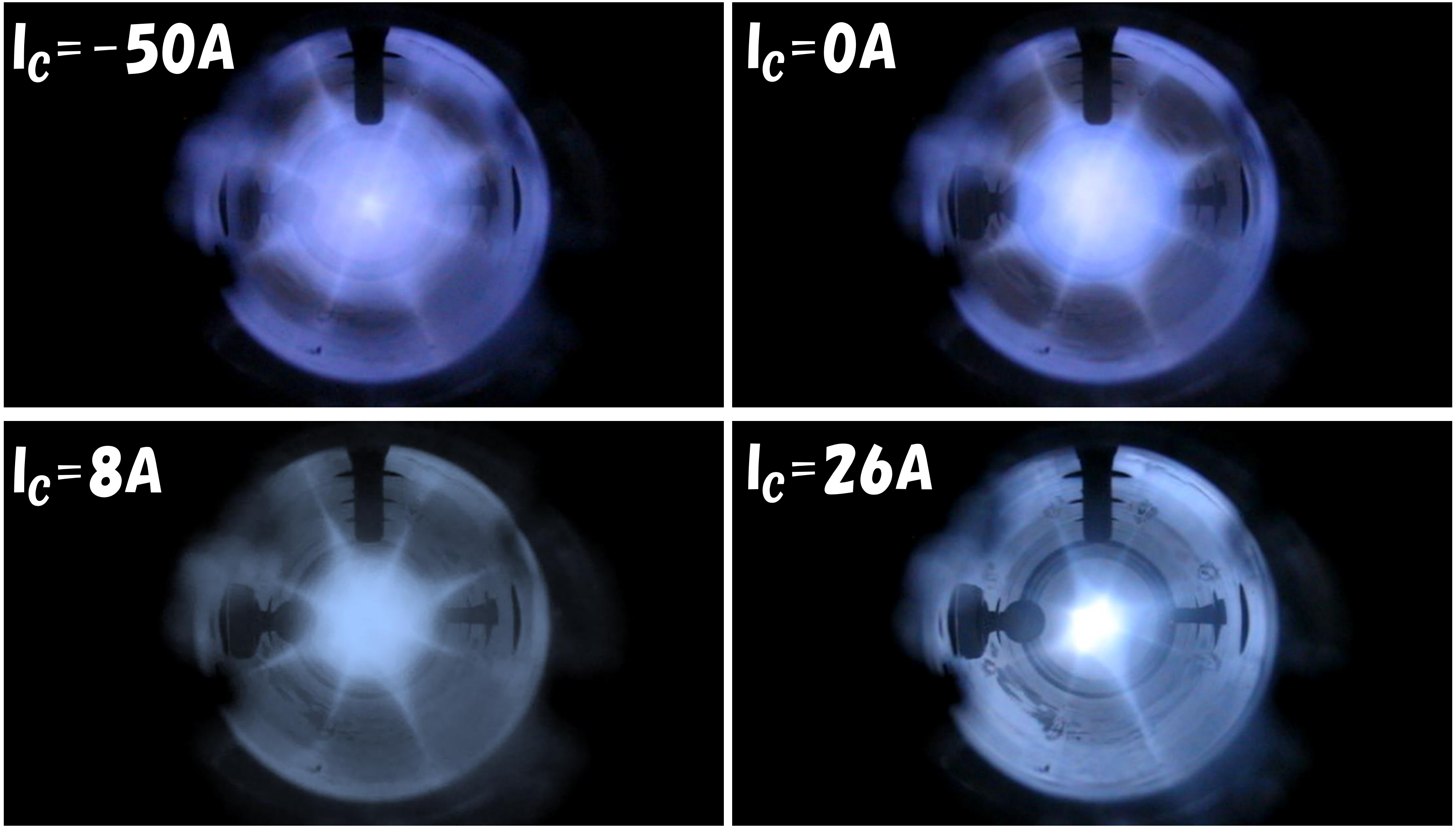

プラズマ中での波動伝搬を考慮して実験結果を考察する

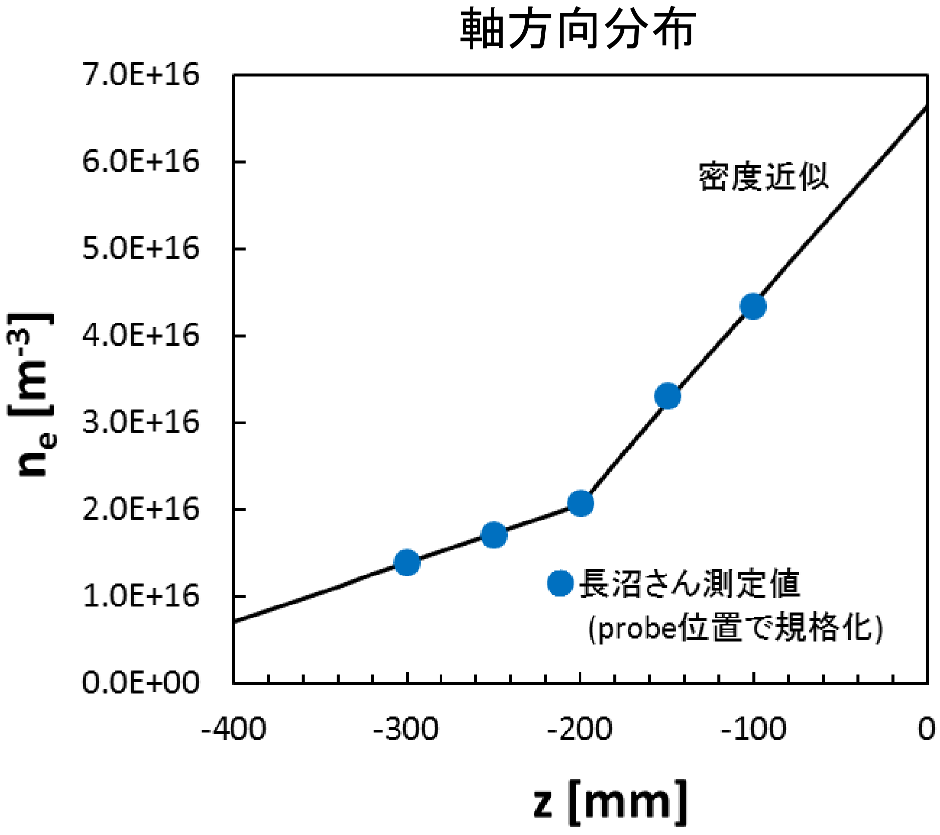

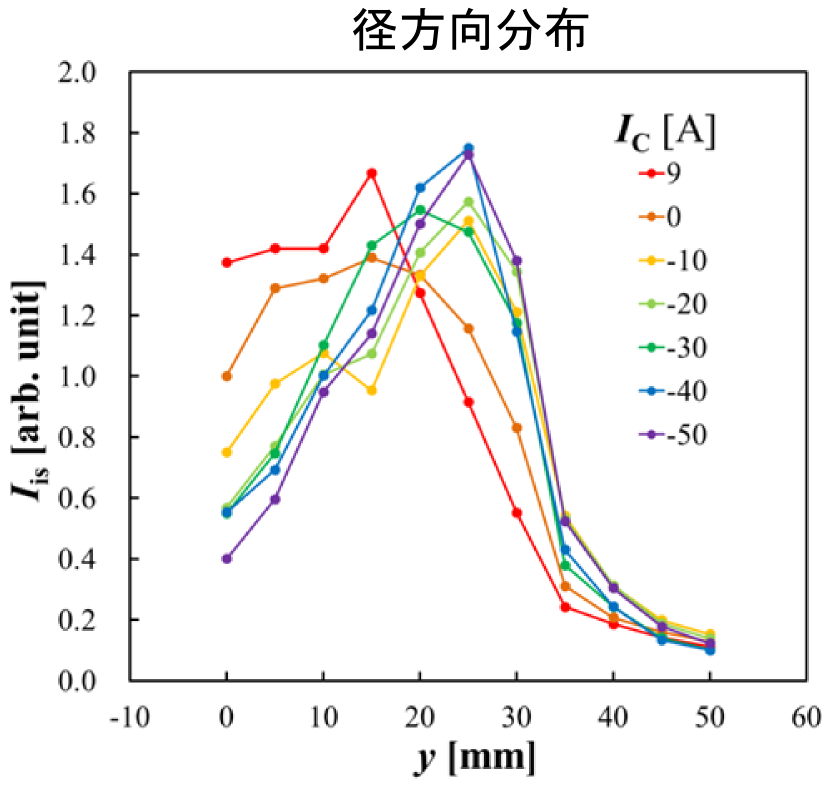

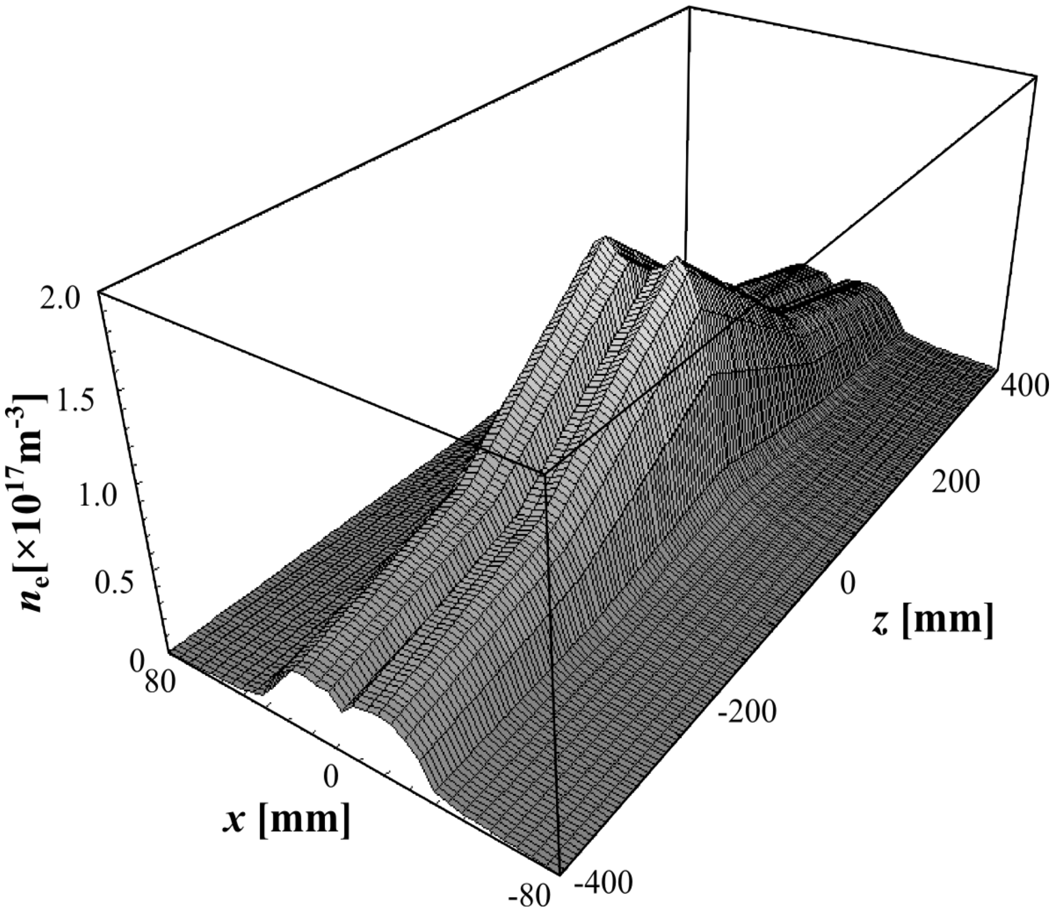

2.0
1.5
1.0
0.5
0
$n_e[\times 10^{17}m^{-3}]$
80
0
-80
x [mm]
400
200
0
-200
-400
z [mm]

●Accessibility condition of 2.45GHz microwave propagation

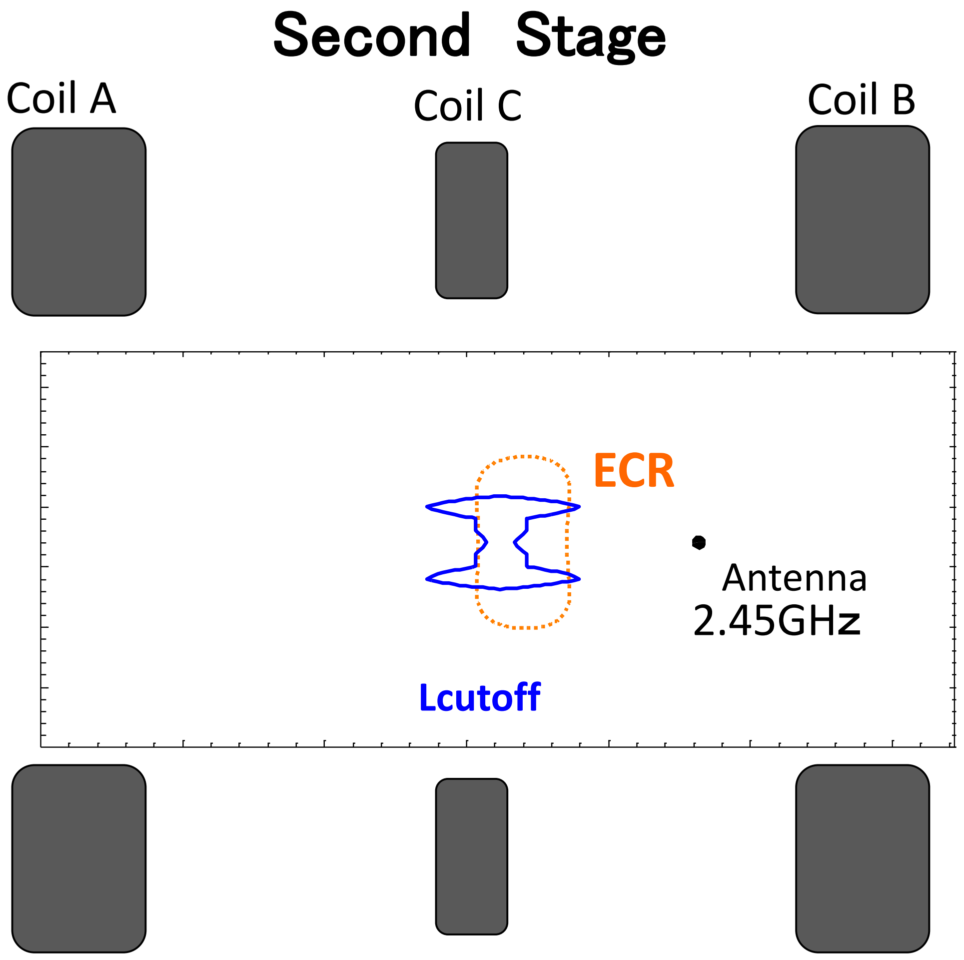

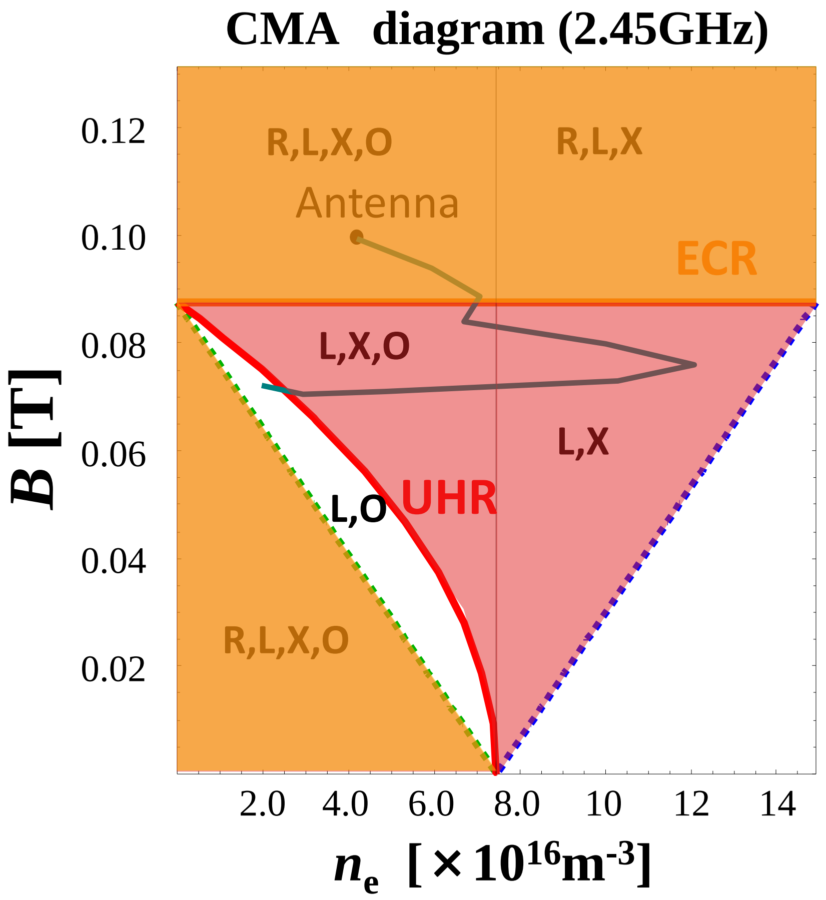

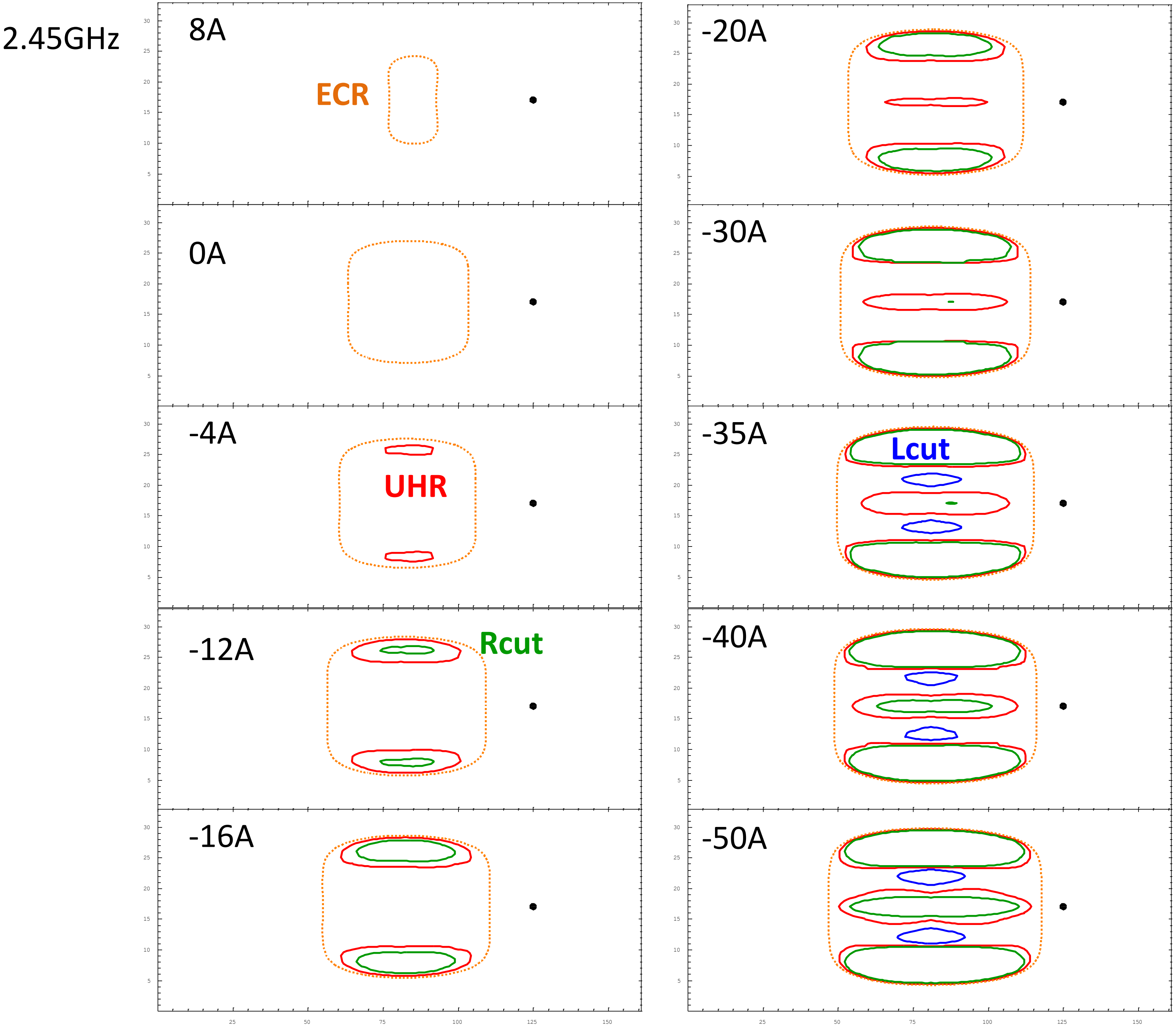

2.45GHz
8A
ECR
0A
-4A
UHR
-12A
Rcut
-16A
-20A
-30A
-35A
Lcut
-40A
-50A

Our trials for improving performance I

Upper hybrid resonance (UHR)

Upper hybrid resonance experiments by using two frequencies

- the 1st try: 9-10GHz (twice)
- the 2nd try: 4-6GHz

Schematic diagram of ion beam current enhancement experiment with X-mode UHR heating (2nd Exp)

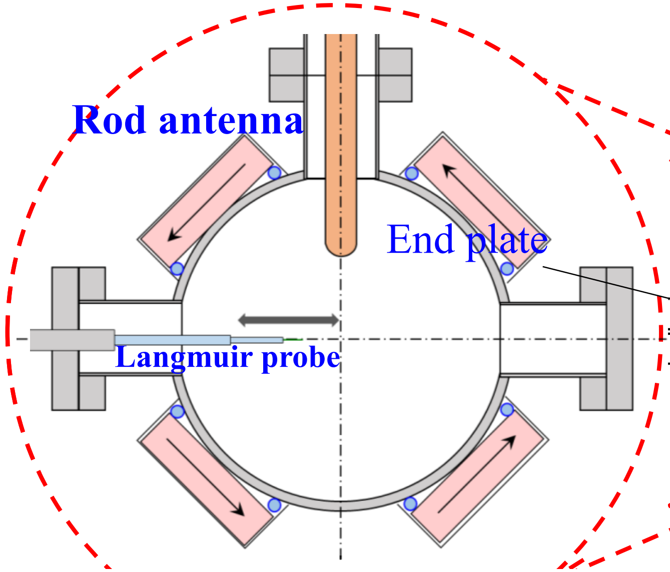

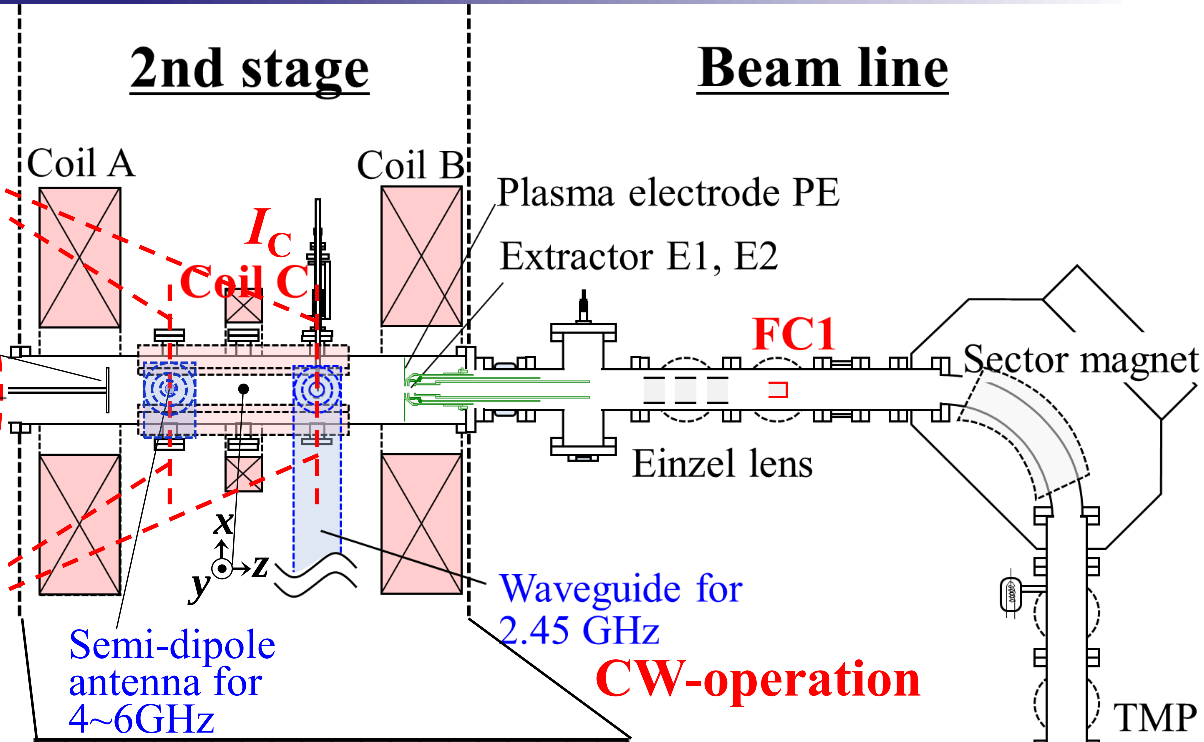

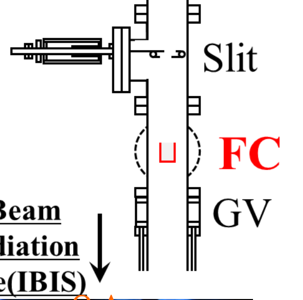

Electron density and temperature by general probe method

$$T_e \equiv \frac{k_B}{e}\frac{d \ln I_e}{dV_p}$$

$$n_{ei} \equiv \frac{I_{is}}{0.61eS}\sqrt{\frac{m_i}{k_B T_e}}$$

Electron energy distribution function EEDF

$$g_e(V) \equiv \frac{2m}{e^2 S}\left(\frac{2eV}{m}\right)\frac{d^2 I_e}{dV_p{}^2}$$

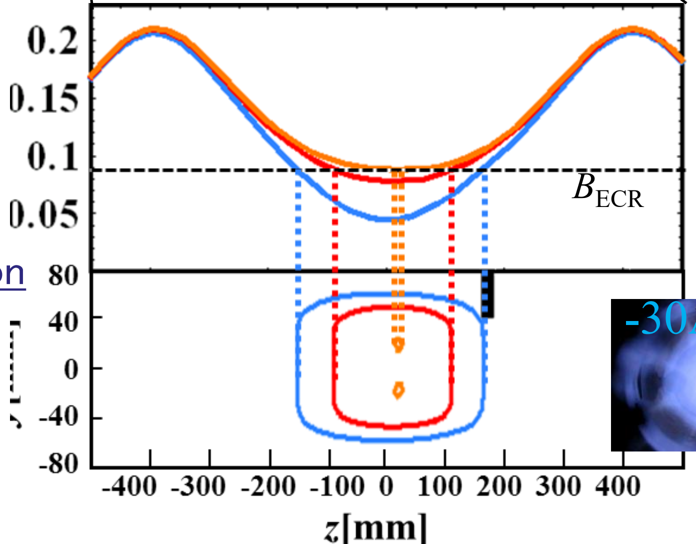

(※)Kumakura, et al.,Rev. Sci. Instrum., 2014, 85, 02A925-1-3

Photograph of ion beam current enhancement experiment with X-mode UHR heating

- February 17, 2016 : First beam extracted after relocation of device & Lab. (Jan. 27 – Feb. 2, 2016)
- March 18, 2016 : Ion beam current enhancement experiment by UHR heating superposition

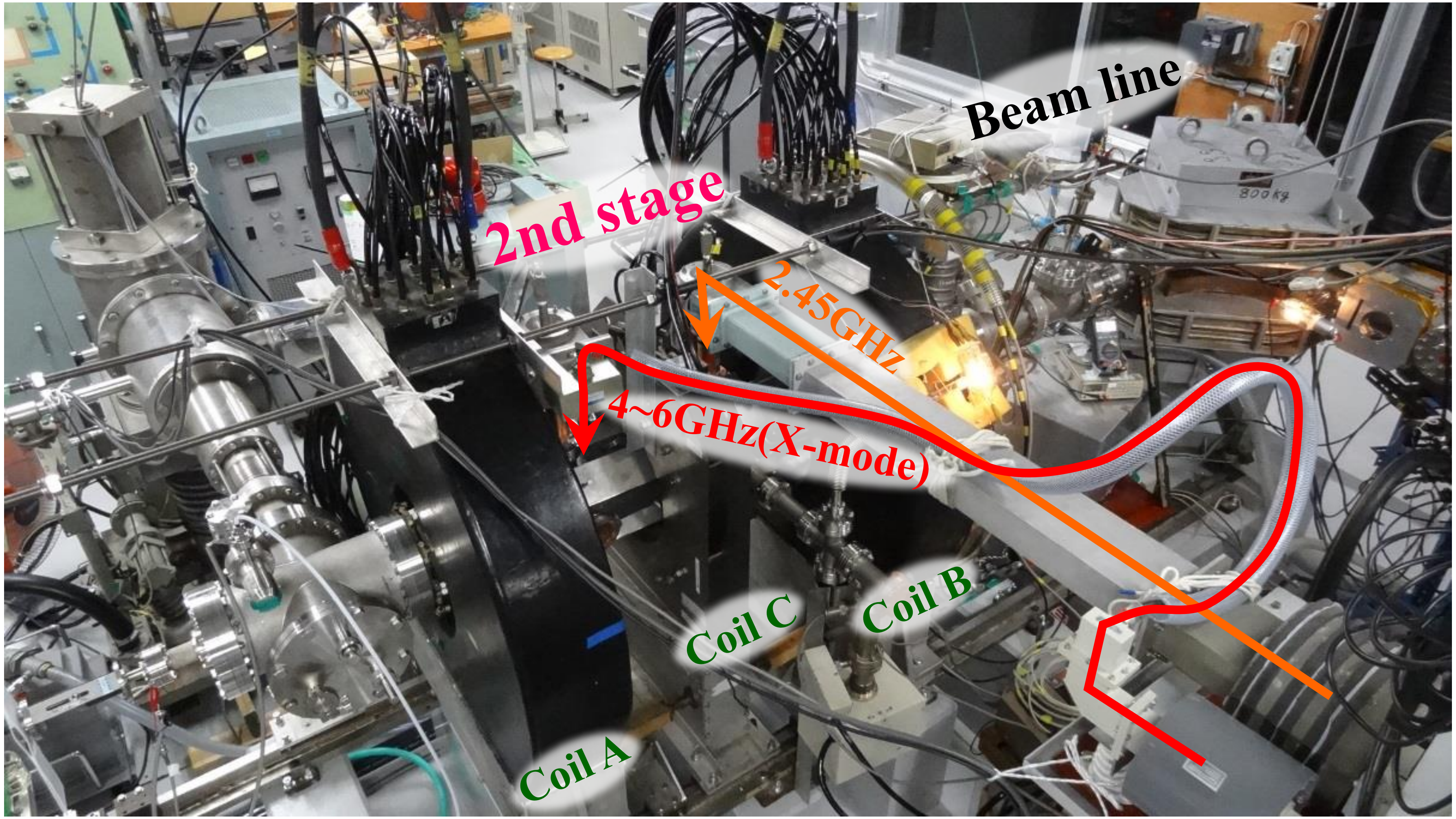

4-6GHz X-mode microwave accessibility

In real space (Longitudinal section)

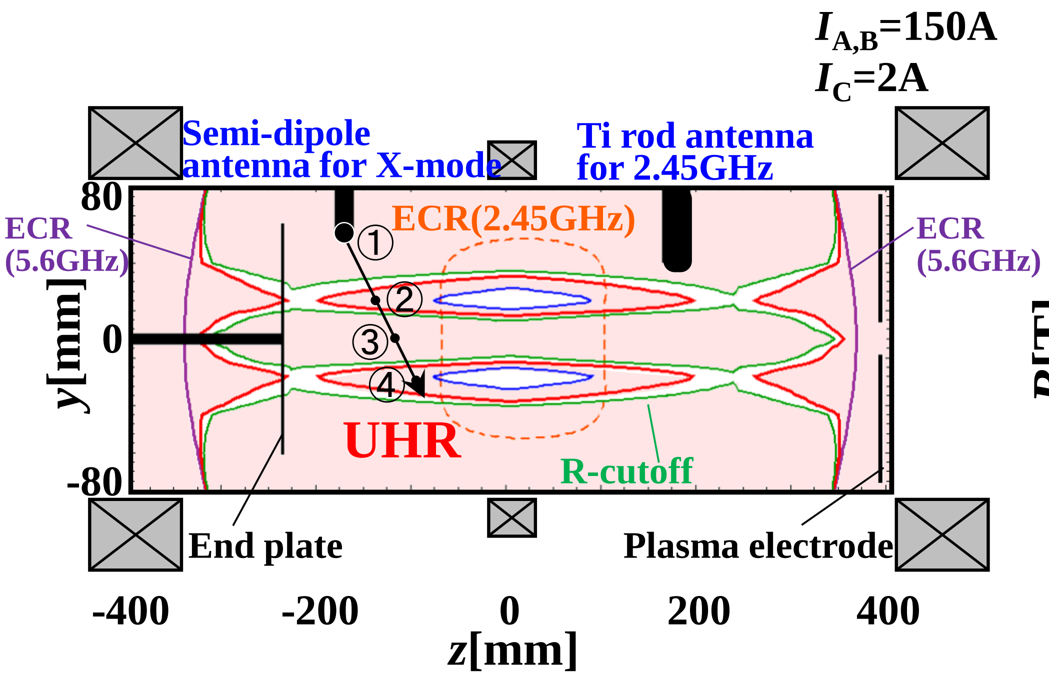

On the CMA diagram

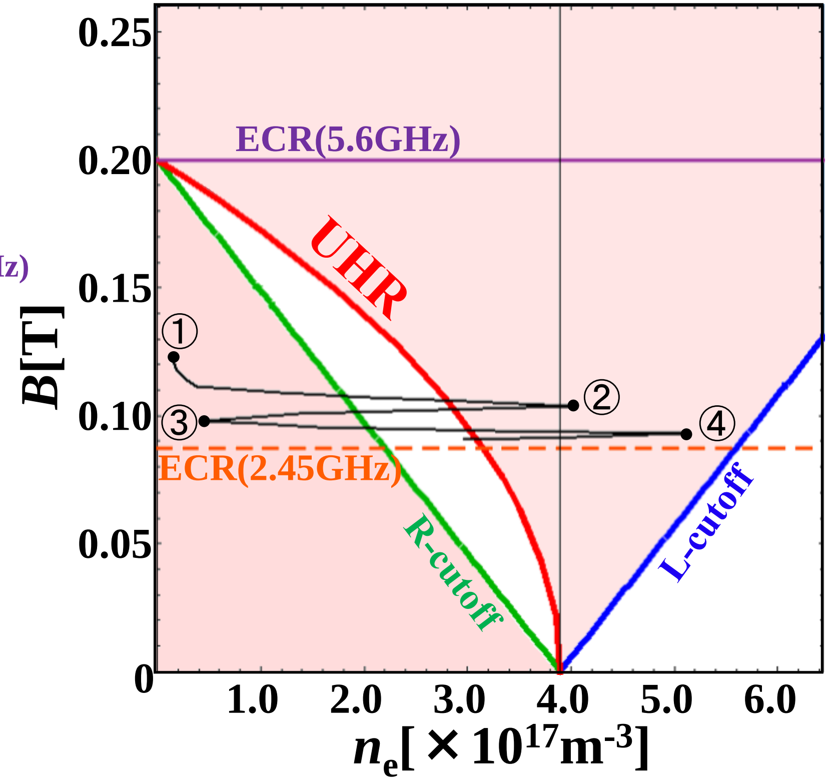

- These accessibilities are evaluated using actual measurement results.
- The correspondence on the CMA diagram is also confirmed.
- Though waves become evanescent in the region between R-cutoff (green lines) and UHR layer, they can penetrate this region and reach the UHR because the thickness of the region is estimated a few millimeters in real space.

4-6GHz X-mode microwave experiment results

Typical CSD (CW-operation)

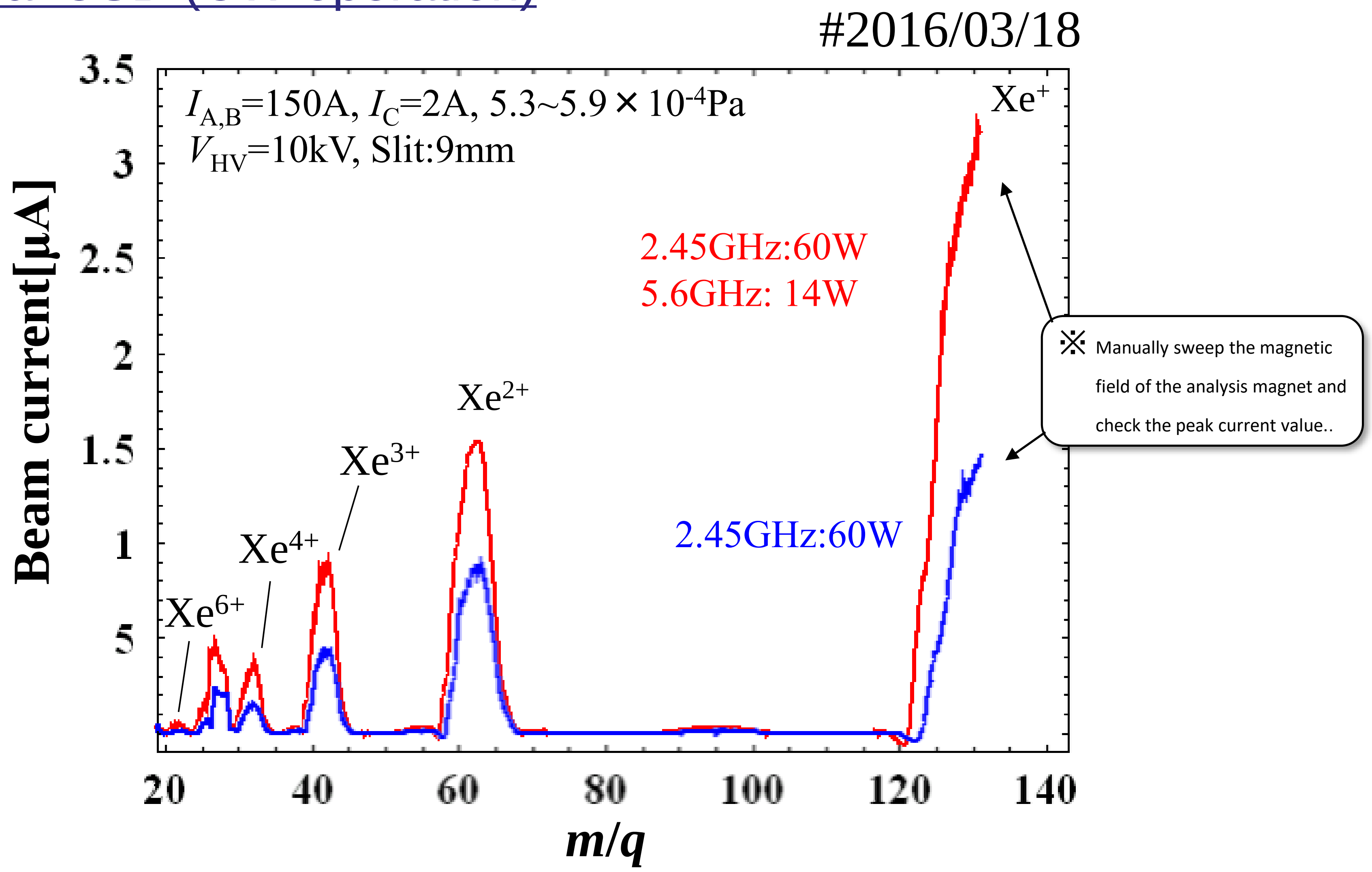

Increased ion beam current by introducing X-mode microwave are confirmed

4-6GHz X-mode microwave experiment results

Typical CSD (CW-operation)

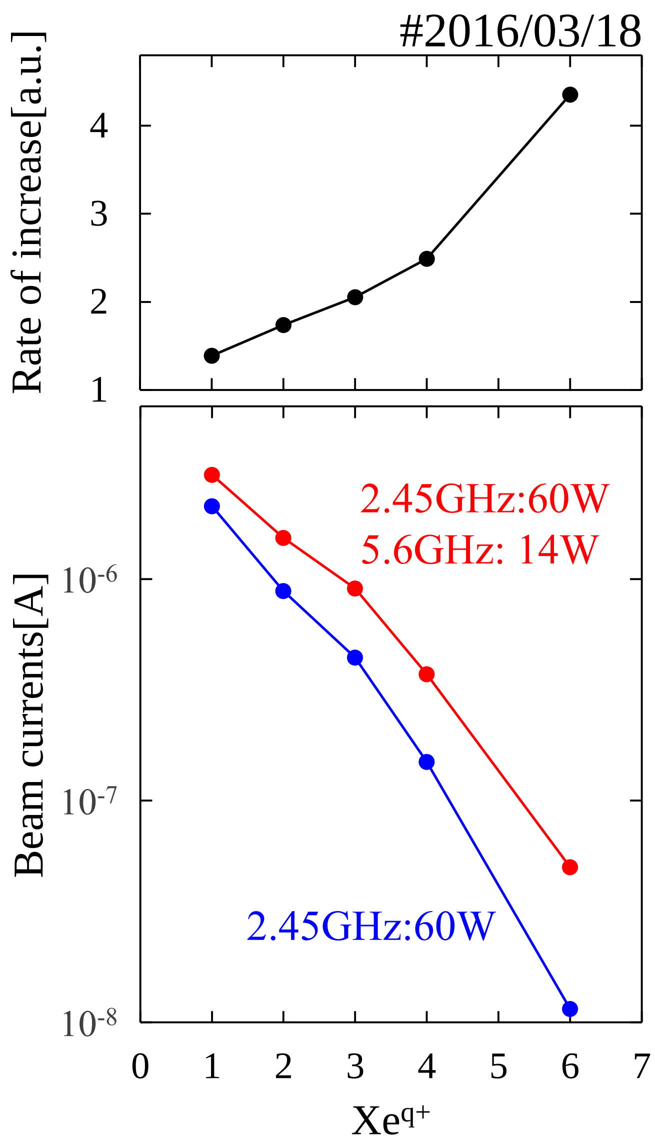

Higher charge states tend to increase significantly
→Confirmed with good reproducibility.
Increased about 4.5 times with 6th charge state

Measurement condition

$I_{A,B}$=150A, I_C=2A, 5.3~5.9 × 10^{-4}Pa
V_{HV}=10kV, Slit:9mm

4-6GHz X-mode microwave experiment results

Electron energy distribution function (EEDF) measurements

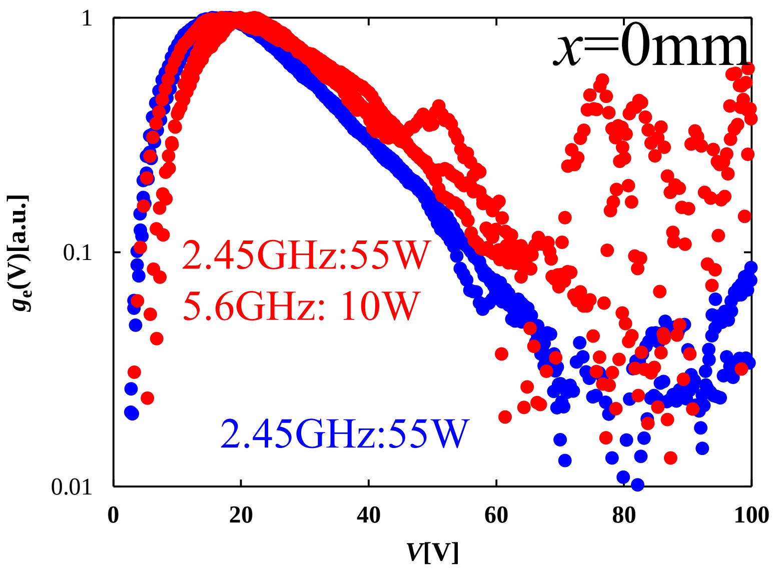

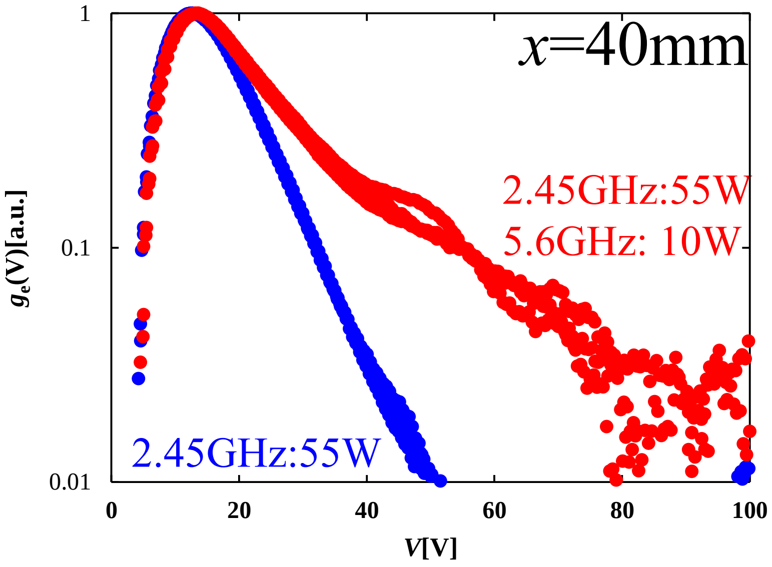

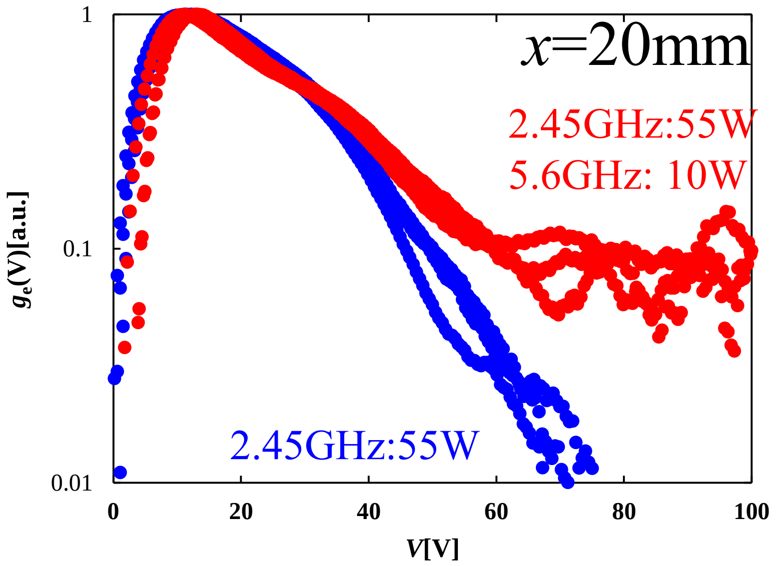

- The energy region after 20 ~ 60eV is particularly affected.
- → especially increased at tail regions.

Measurement condition

$I_{A,B}$=150A, I_C=2A, 4.8 × 10^{-4}Pa

Earthquake occurrence at 7:58am on June 18th, 2018)

- An earthquake of magnitude 6.1 with epicenter of North Osaka at 7:58 on June 18, 2018 occurred.
- The laboratory was on the 6th floor, so the damage was enormous.

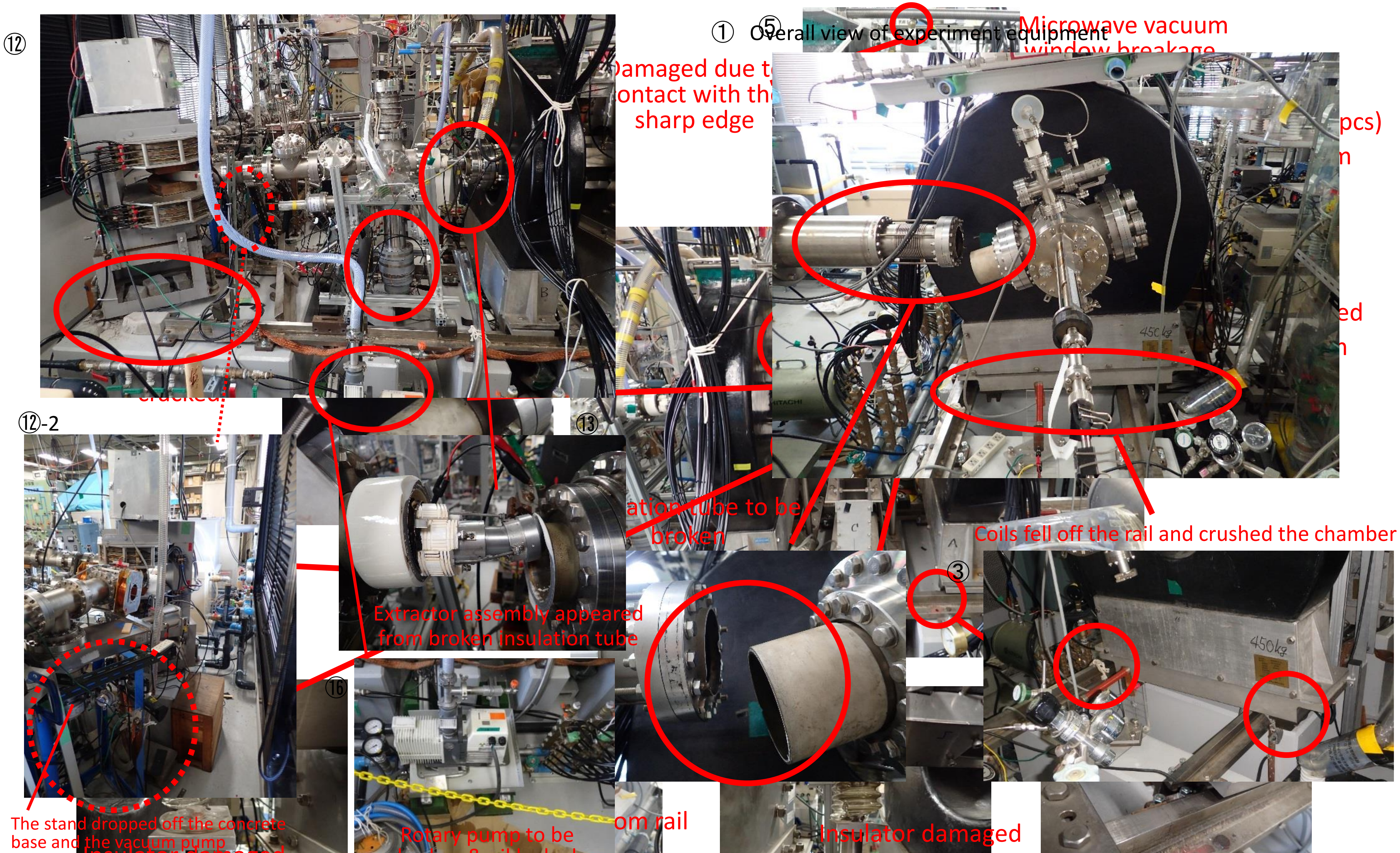

X-mode Exp. in ECR high power region: Typical Xe^{q+} CSD

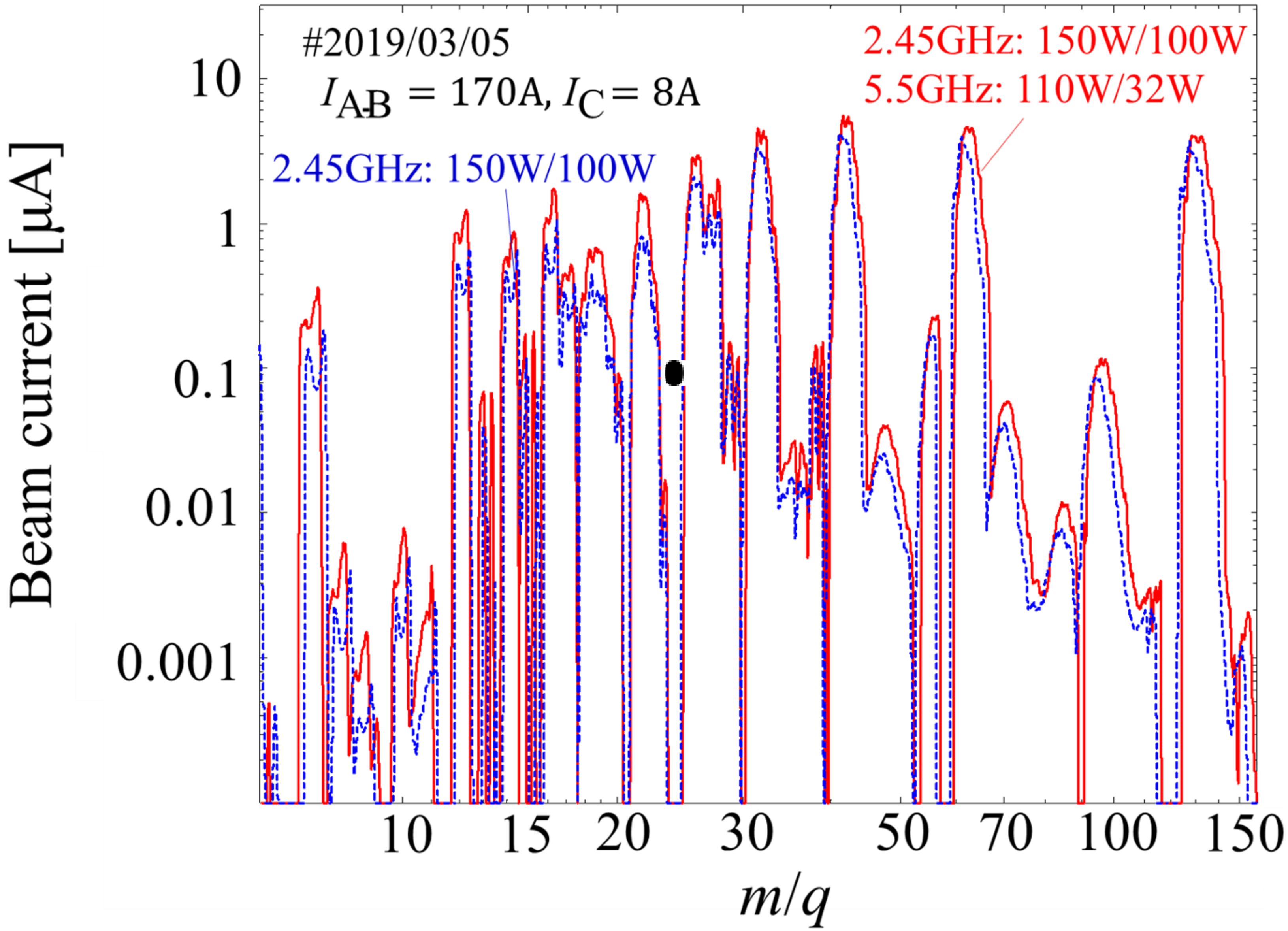

X-mode Exp. in ECR high power regions: Xe^{q+} currents & normalized CSD

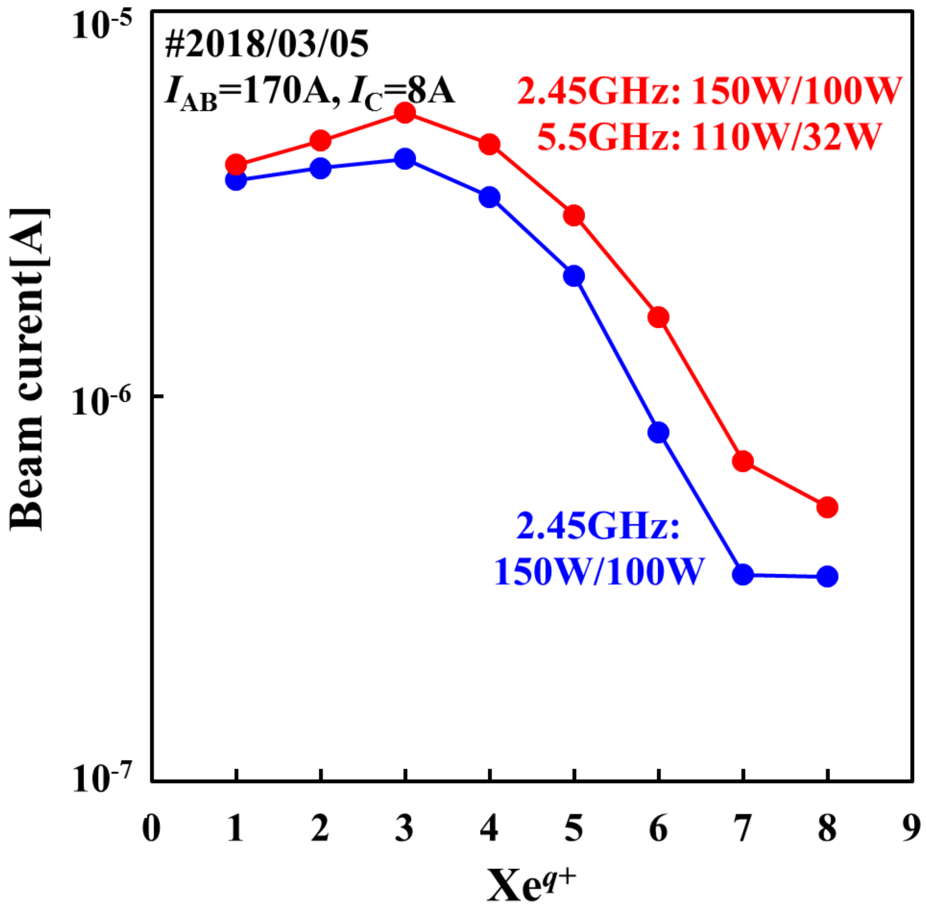

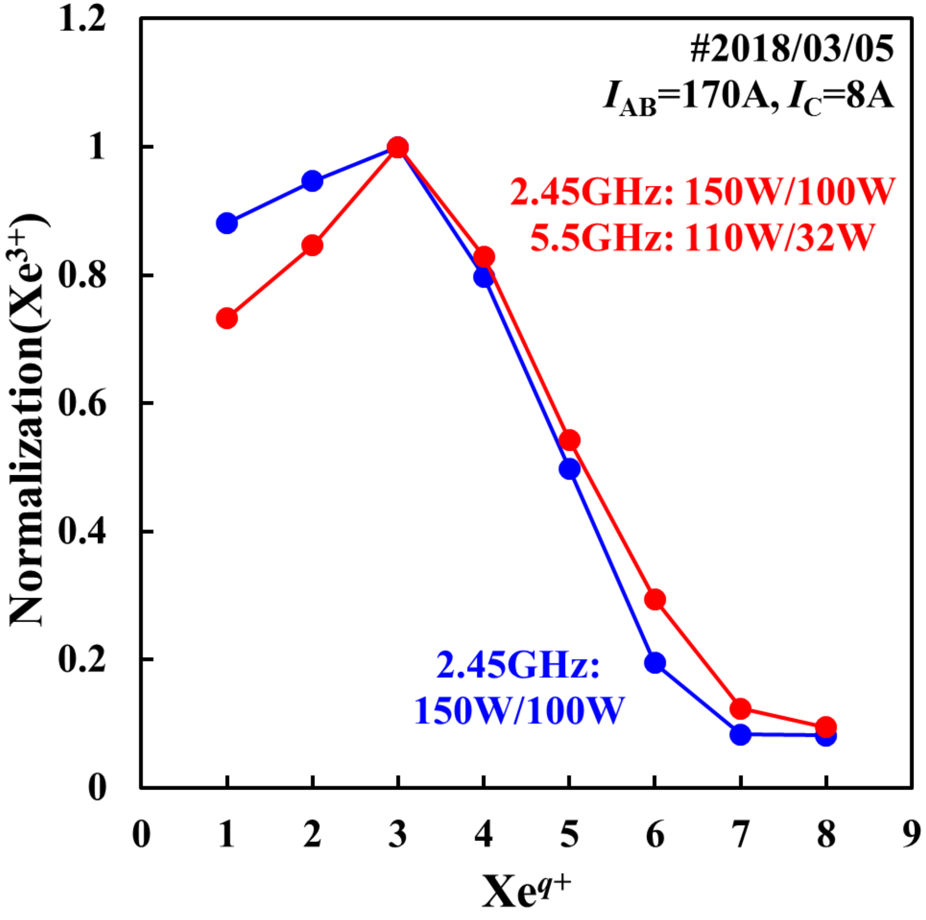

X-mode Exp. in ECR high power regions: T_e & n_e profiles

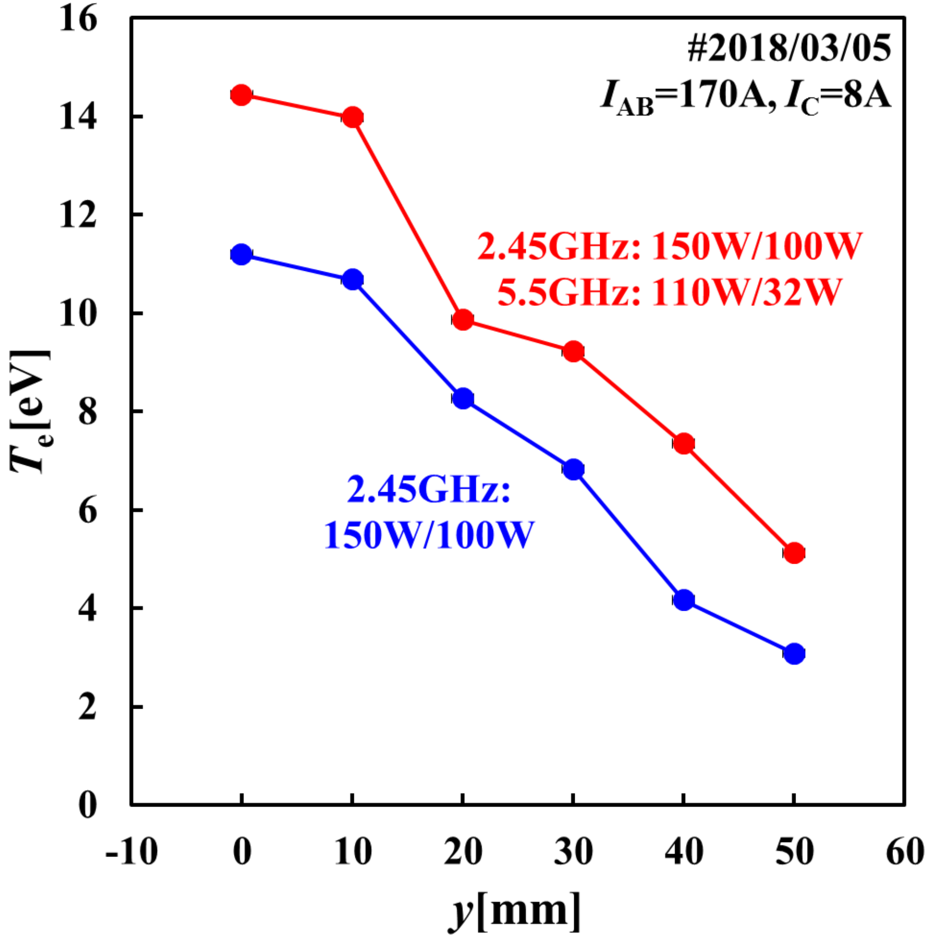

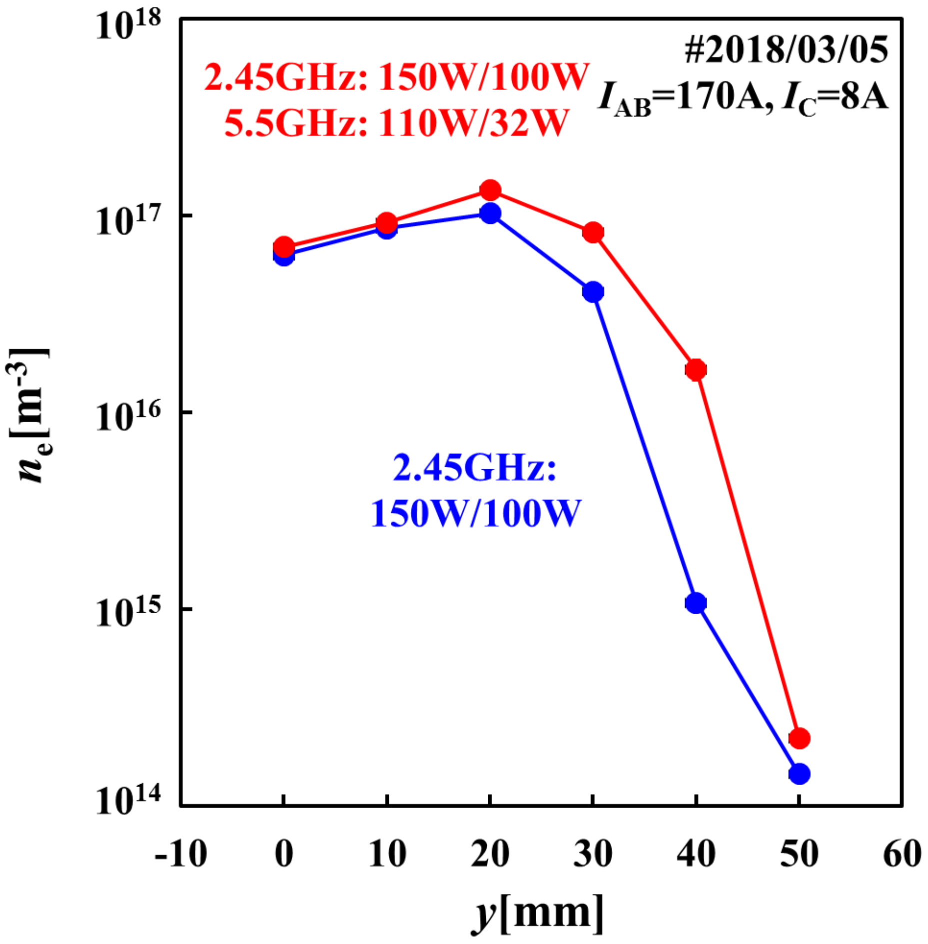

X-mode frequency dependence in ECR high power region

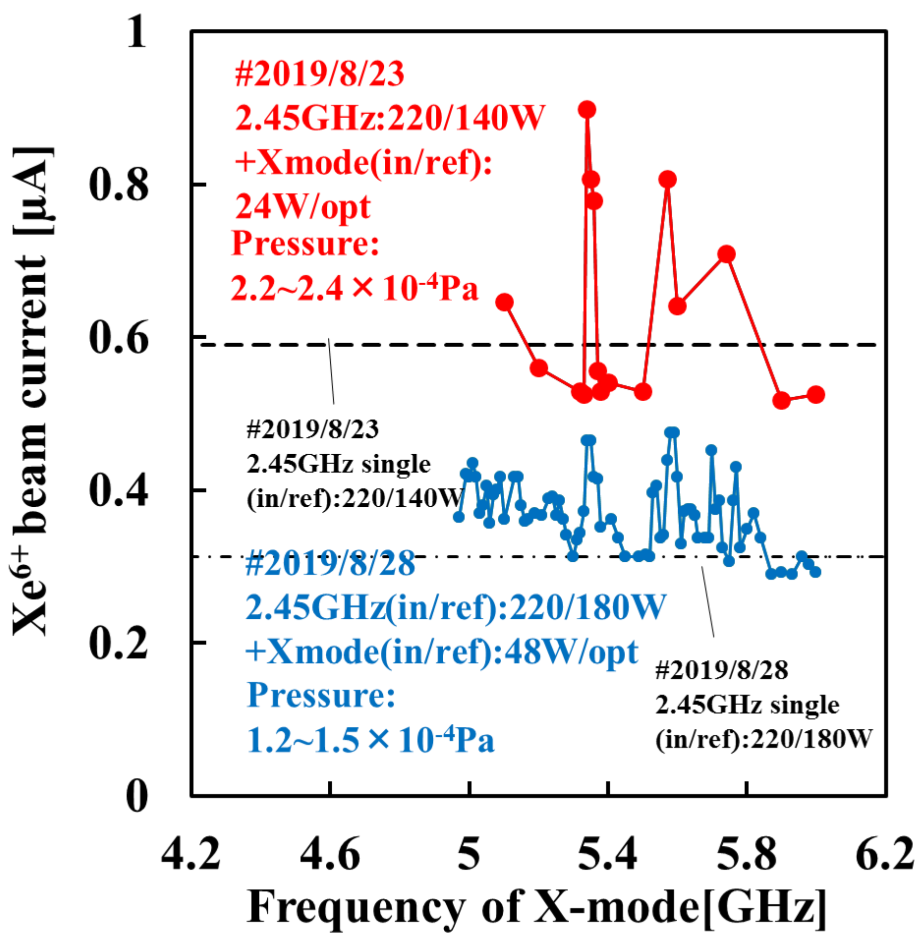

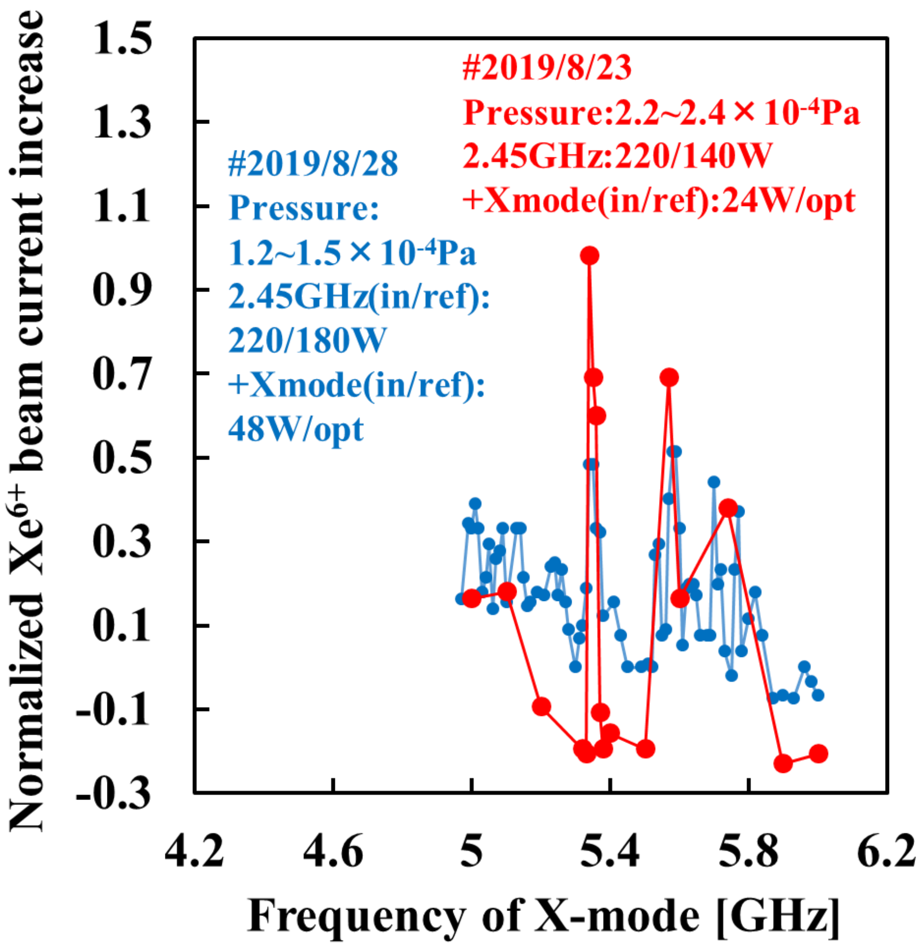

Our trials for improving performance II

Single frequencies Dual ECR

Review of Scientific Instruments | ARTICLE | scitation.org/journal/rsi

Microwave-accessibility conditions estimated by plasma parameters obtained experimentally on electron cyclotron resonance ion source

Cite as: Rev. Sci. Instrum. 92, 043514 (2021); doi: 10.1063/5.0035631
Submitted: 30 October 2020 • Accepted: 17 March 2021 •
Published Online: 2 April 2021

View Online Export Citation CrossMark

Wataru Kubo,[a] Shuhei Harisaki, Issei Owada, Koichi Sato, Kazuki Tsuda, and Yushi Kato

AFFILIATIONS

Division of Electrical, Electronic and Infocommunications Engineering, Graduate School of Engineering, Osaka University, 2-1 Yamada-oka, Suita-shi, Osaka 565-0871, Japan

[a]Author to whom correspondence should be addressed: w.kubo@nf.eie.eng.osaka-u.ac.jp

ABSTRACT

We insert two probes in the upstream and the downstream regions with respect to the electron cyclotron resonance (ECR) zone which is formed at the center of mirror fields. We measure simultaneously plasma parameters in those regions by each of them under the same operating condition. We measure ion saturation currents I_{is} and electron energy distribution functions at two positions. We obtain measurement results that suggest the more efficient ECR on the side closer to the microwave-launchings than those on the other side. It is consistent with the accessibility condition of the right-hand polarization wave. We also compare the charge state distributions of Ar ion beams extracted in the case of launching microwaves from the coaxial semi-dipole antenna and those from the rod antenna. We observe the higher multicharged ion beam currents at the low microwave powers in the case of the rod antenna than those in the case of the coaxial semi-dipole antenna. We also confirm stable increasements of ion beam currents at considerably high microwave powers in the case of the coaxial semi-dipole antenna. Based on the experimental results, we propose a new microwave-launching method, "dual-ECR heating" and report its preferable preliminary experimental results in this paper.

measurement by them. We measure plasma parameters, i.e., ion saturation currents I_{is} and electron energy distribution functions (EEDF) in two cases of the microwave-launchings from the coaxial semi-dipole antenna and the rod antenna. We obtain the experimental results which indicate the occurrence of the more efficient ECR on the side closer to the microwave-launchings than that on the other side. We compare charge state distributions (CSD) of extracted ion beams in both cases. The multicharged ion beam currents are higher at the low microwave powers in the case of the rod antenna than those in the case of the coaxial semi-dipole antenna. We also observe instability of ion beam currents and their decrease at high microwave powers. On the other hand, we observe stable increasements of ion beam currents at considerably high microwave powers in the case of the coaxial semi-dipole antenna. In this paper, we propose a new microwave launching method, which we have named "dual-ECR heating," based on experimental results and some estimations. In near future, we are going to conduct UHR, and other waves heating experiments under the condition that ECR will be optimized.

II. THEORICAL BACKGROUND AND EXPERIMENTAL APPARATUS

On the basis of the RHP wave dispersion relationship for the case of no collisions and infinite mass ions, the RHP wave refraction index N_r can be written using the electron plasma frequency f_{pe} and the electron cyclotron frequency f_{ce} as (1),

$$N_r^2 = \left(v_\varphi^2/c^2\right)^{-1} = 1 - \frac{f_{pe}^2}{f(f - f_{ce})} \tag{1}$$

where f is the frequency of the microwave (fixed at 2.45 GHz), v_φ is the phase velocity of the RHP wave, and c is the velocity of light.[8] The ECR occurs when the f is the f_{ce} ($N_r = \infty$). The cutoff frequency of the RHP wave f_R ($N_r = 0$) is defined as (2),

$$f_R = \frac{f_{ce} + \sqrt{f_{ce}^2 + 4 f_{pe}^2}}{2} \tag{2}$$

Figure 1(a) shows the typical mirror field in the ECRIS. The vertical and horizontal axes show the magnetic field strength B and

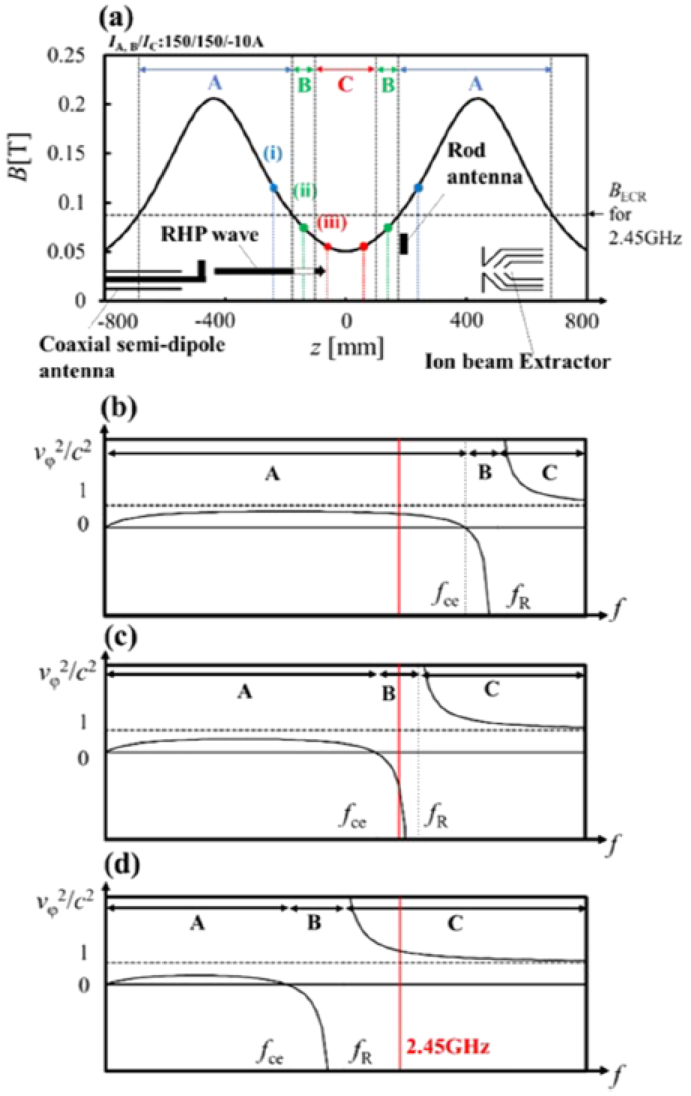

FIG. 1. The typical mirror field in the ECRIS (a). Diagrams showing typical dispersion relationships of the RHP wave at (i) in the mirror field (b) that at (ii) (c), and that at (iii) (d).

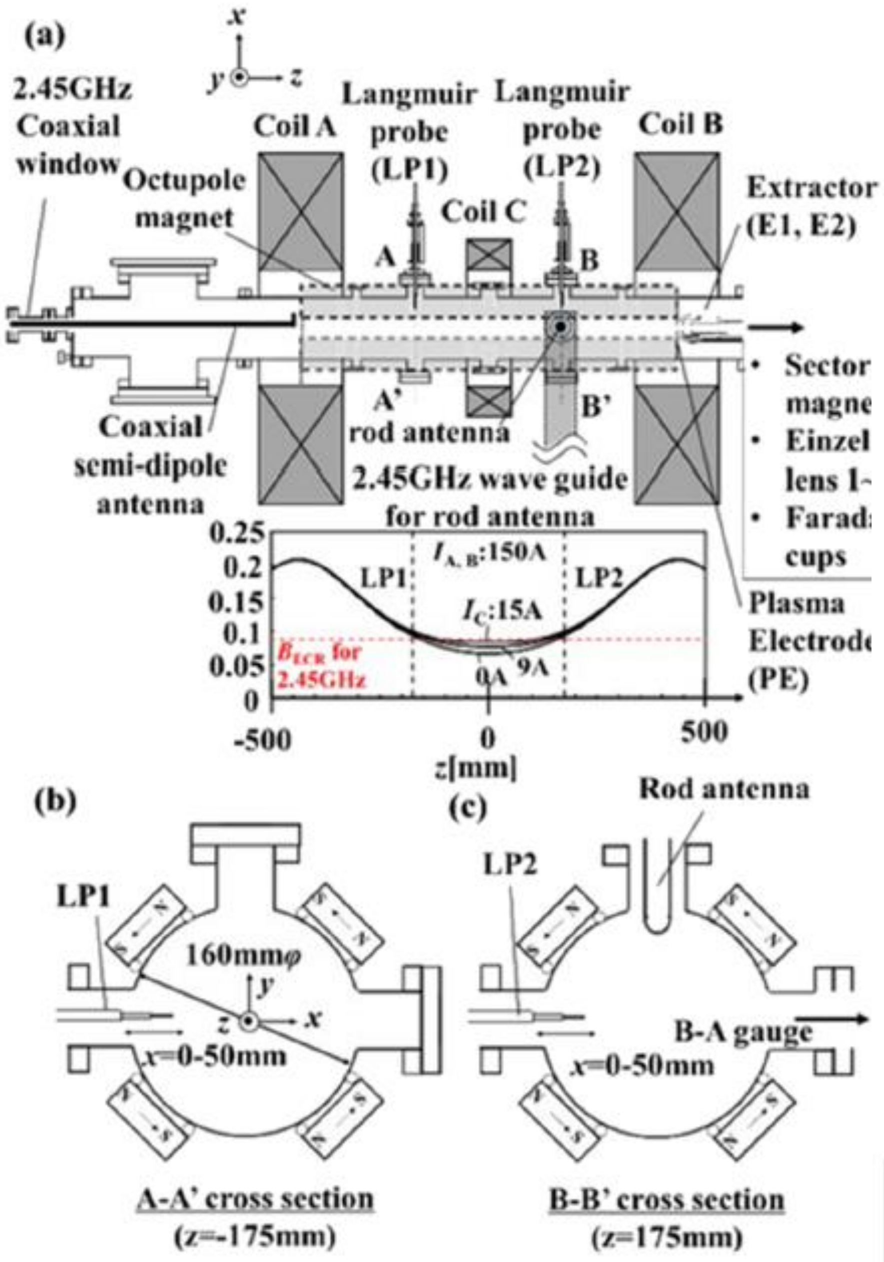

FIG. 2. Schematic drawing of ECRIS (the top view) (a). *x*-*y* plane cross-section (A–A′) at $z = -175$ mm (b). That (B–B′) at $z = 175$ mm (c).

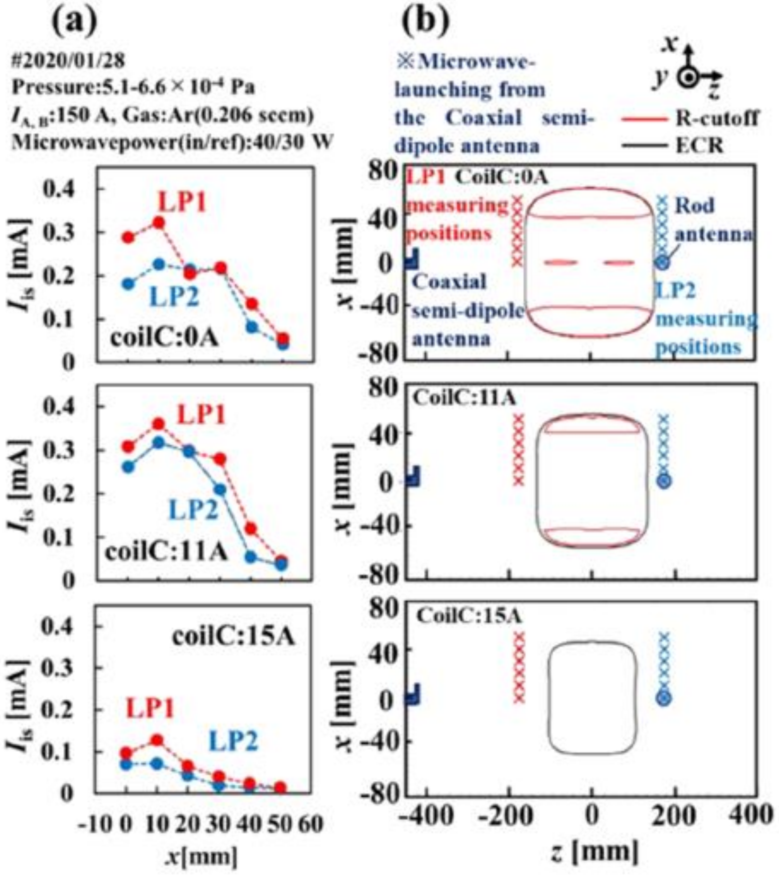

FIG. 7. The comparison of I_{is} profiles in *x*-direction measured by LP1 and LP2 at typical I_c values in the case of the coaxial semi-dipole antenna (a). The accessibility conditions of the RHP wave, i.e., the ECR-zone (the black line) and the R-cutoff (the red line) in the *x*-*z* plane of the vacuum chamber at typical I_c values (b).

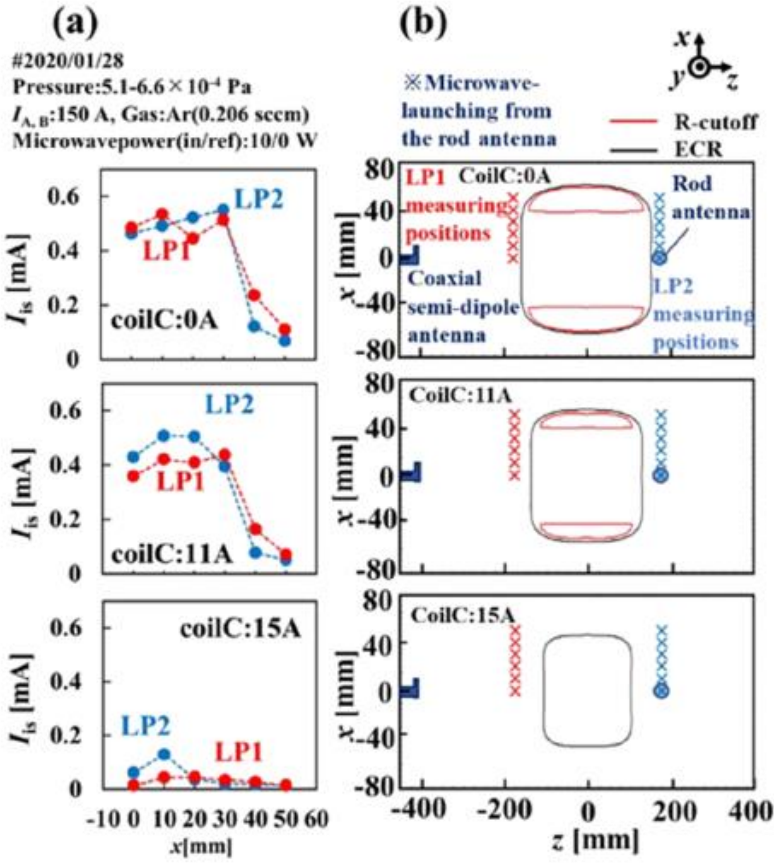

FIG. 8. The comparison of I_{is} profiles in *x*-direction measured by LP1 and LP2 at typical I_c values in the case of the rod antenna (a). The accessibility conditions of the RHP wave, i.e., the ECR-zone (the black line) and the Rcutoff (the red line) in the *x*-*z* plane of the vacuum chamber at typical I_c values (b).

Single-frequency dual ECR

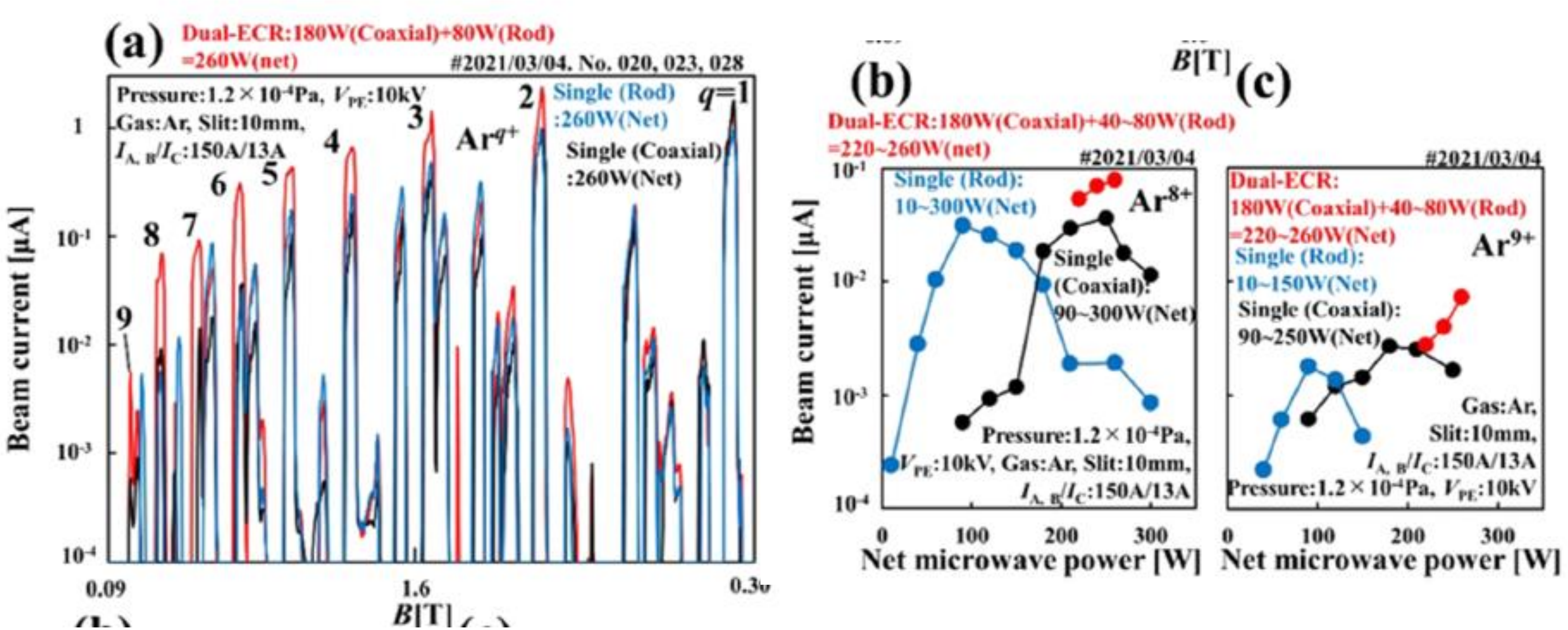

Ref: Example of Simulation study of other group

PHYSICAL REVIEW ACCELERATORS AND BEAMS **22,** 043402 (2019)

Resonance surface, microwave power absorption, and plasma density distribution in an electron cyclotron resonance ion source

M. Salahshoor and M. Aslaninejad*

Institute for Research in Fundamental Sciences (IPM), School of Particles and Accelerators, P.O. Box 19395-5531, Tehran, Iran

(Received 28 September 2018; published 12 April 2019)

Resonance surfaces for a 2.45 GHz electron cyclotron resonance ion source are investigated. In addition to the typical flat-B and minimum-B profiles, we have investigated on two new magnetic field structures, namely the torus zone and the double zone configurations. The impacts of such surfaces on the microwave power absorption are discussed. Furthermore, the uniformity of the ion emissive surfaces in connection with the resonance surfaces is examined. Different configurations for absorbing microwave power and simultaneously for producing uniform ion density distribution near the extraction wall of the source are discussed.

DOI: 10.1103/PhysRevAccelBeams.22.043402

Our trials for improving performance III

Efficient R-wave excitation with 4 pillars helical antenna

7 Dual-ECR加熱法の効果検証

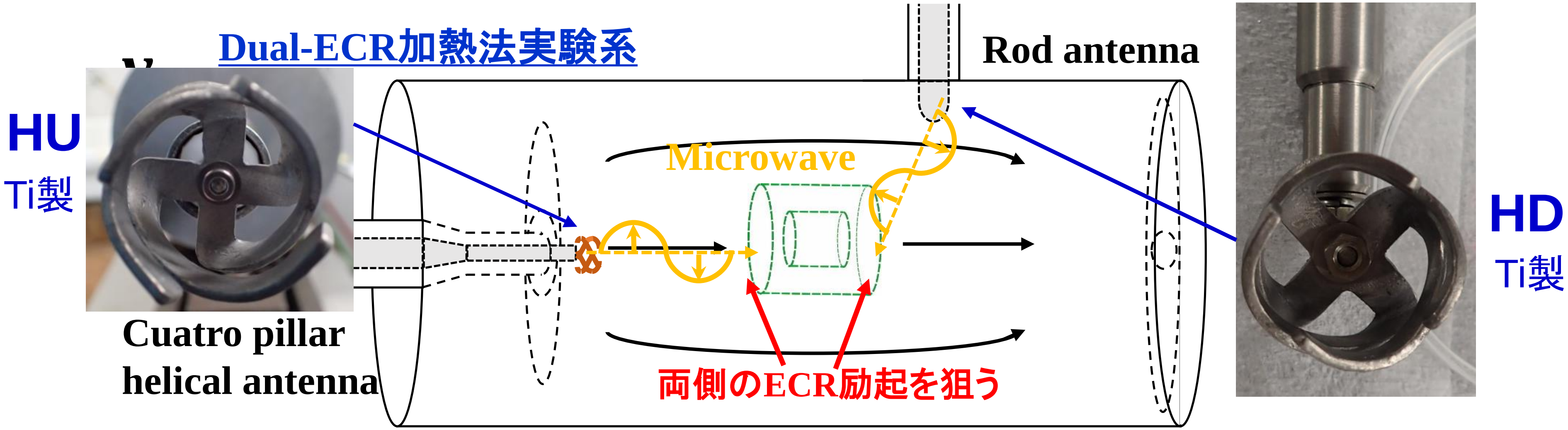

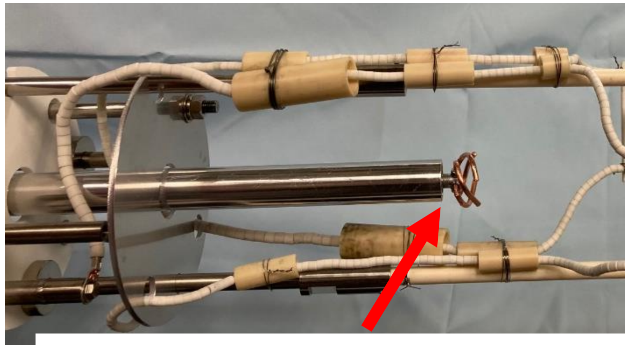

Cuatro pillar helical Antenna

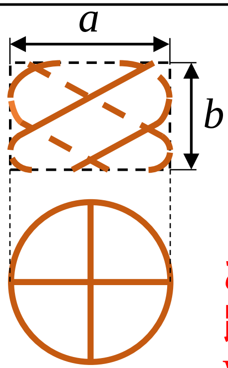

a=2×0.1λ=24mm(for 2.45GHz)

b=0.1λ=12mm(for 2.45GHz)

おおむね2.45GHzで自己共振回路となるように設計できる (H A. Wheeler, et.al, Proceedings of the I.R.E, 35, 1484-1487 (1947))

- 4本巻き(Cuatro Pillar Helical)ヘリカルアンテナを設計および自作し, よりRモードが励起された系で実験を行った.
- 自作したアンテナは本体装置を模擬した系でマイクロ波導入が試験され, 従来の同軸セミダイポールアンテナより伝送系の反射が低く, 電界強度も高いことが確認されている

Photographs of ICR antenna （2024.02.03）

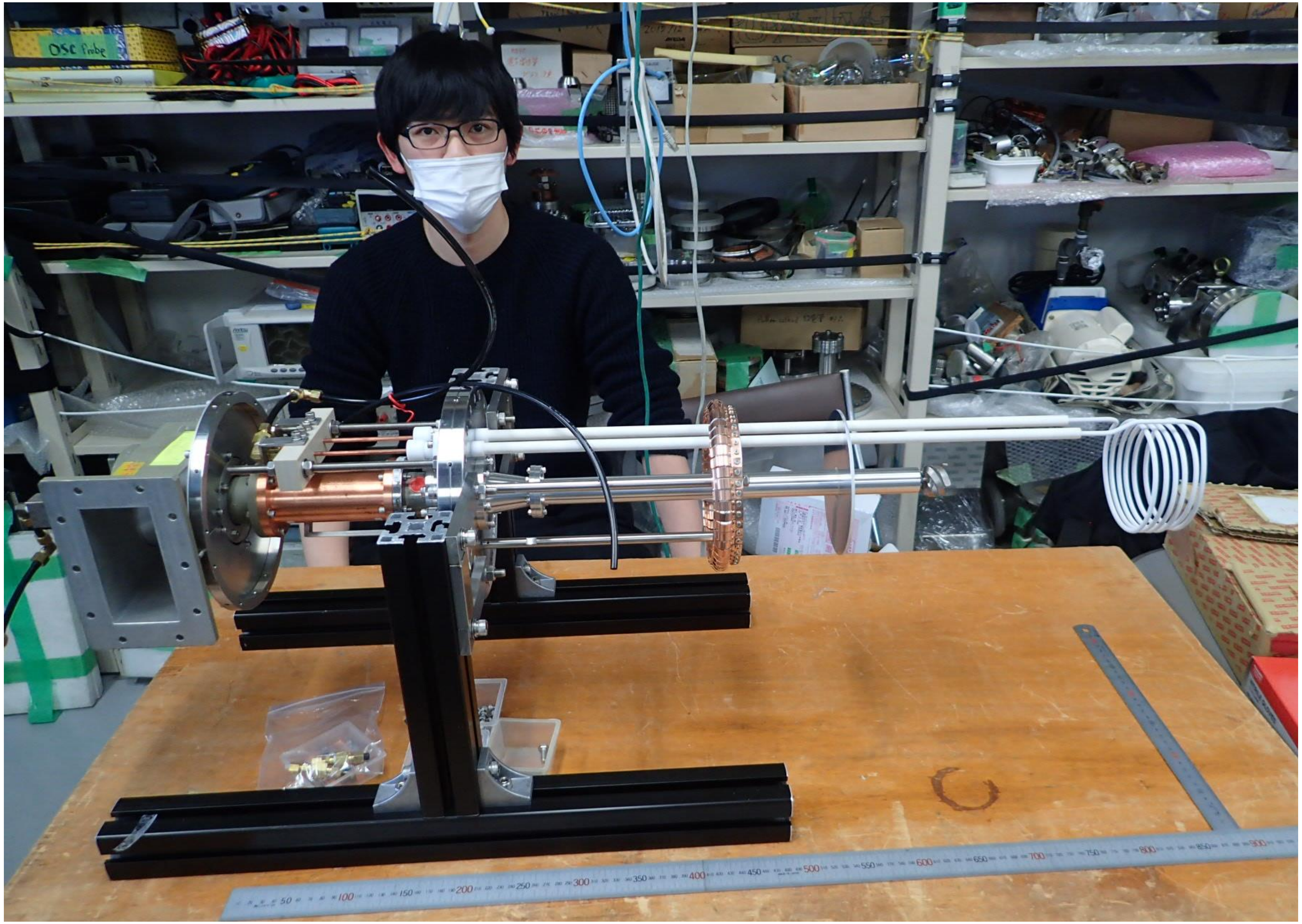

Photographs of setting situation (2024.02.03)

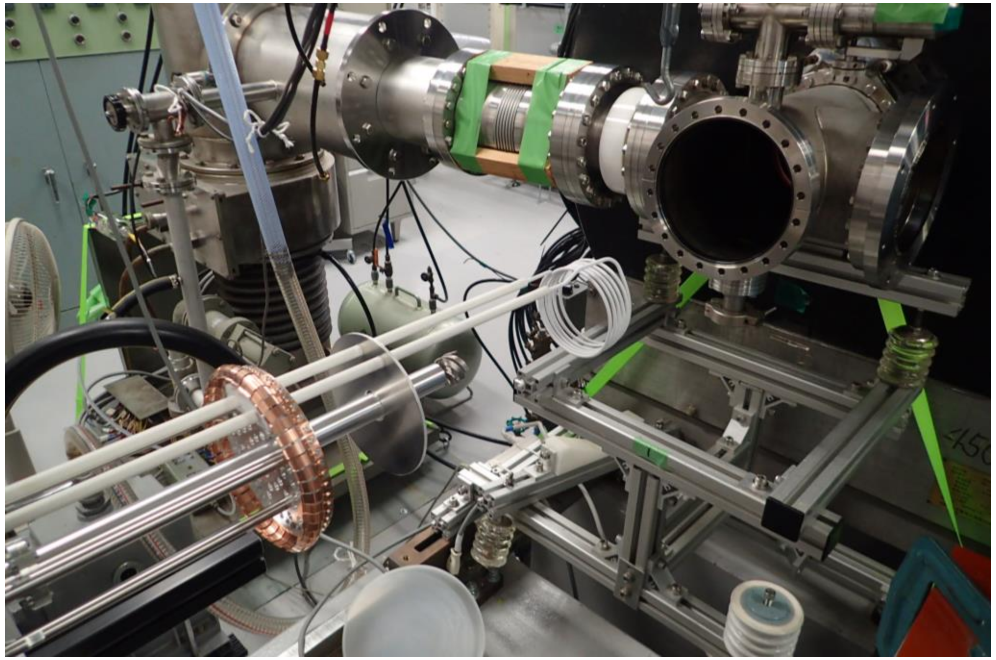

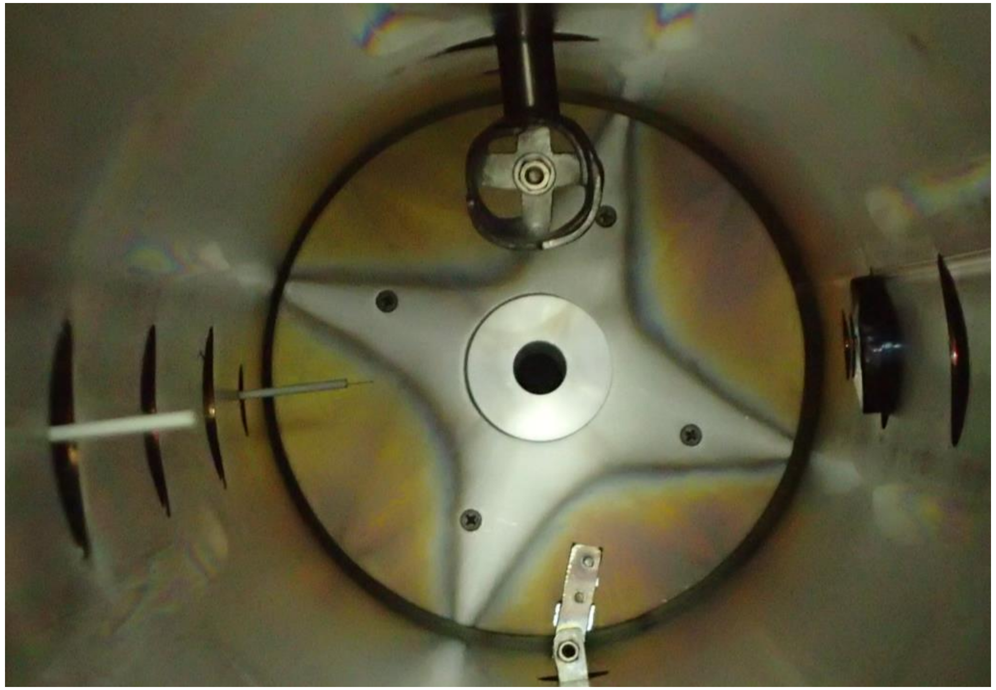

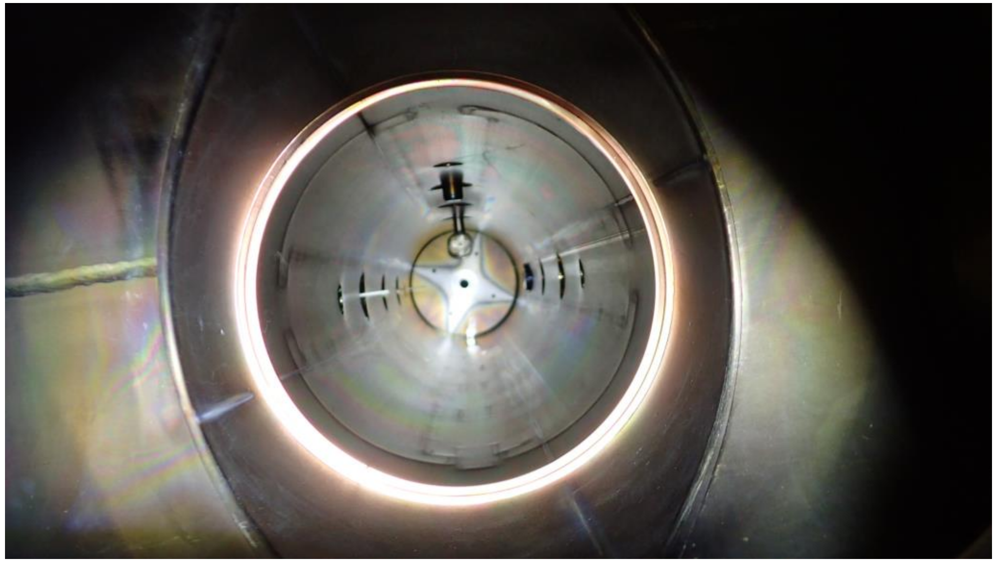

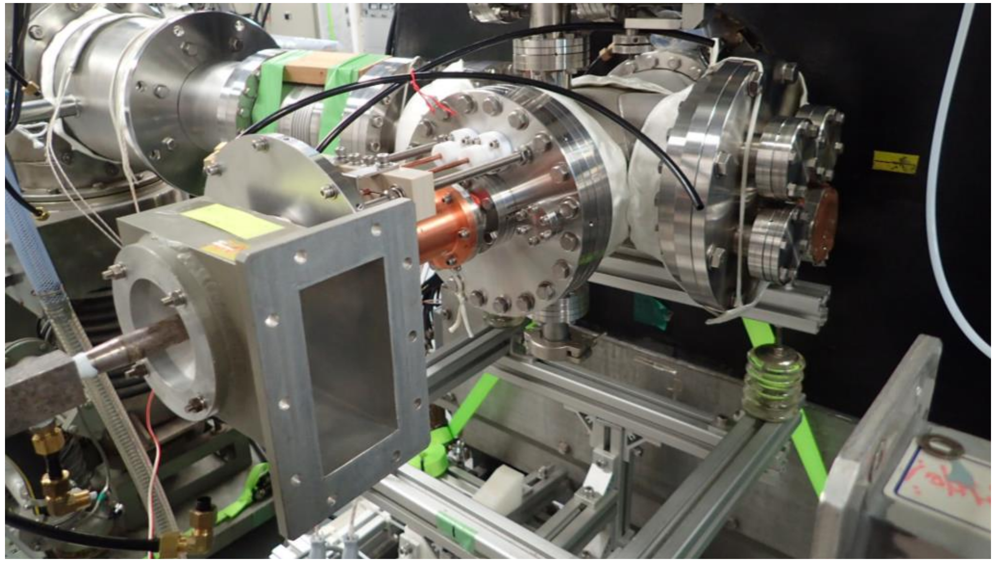

Photographs of setting situation (2024.02.06)

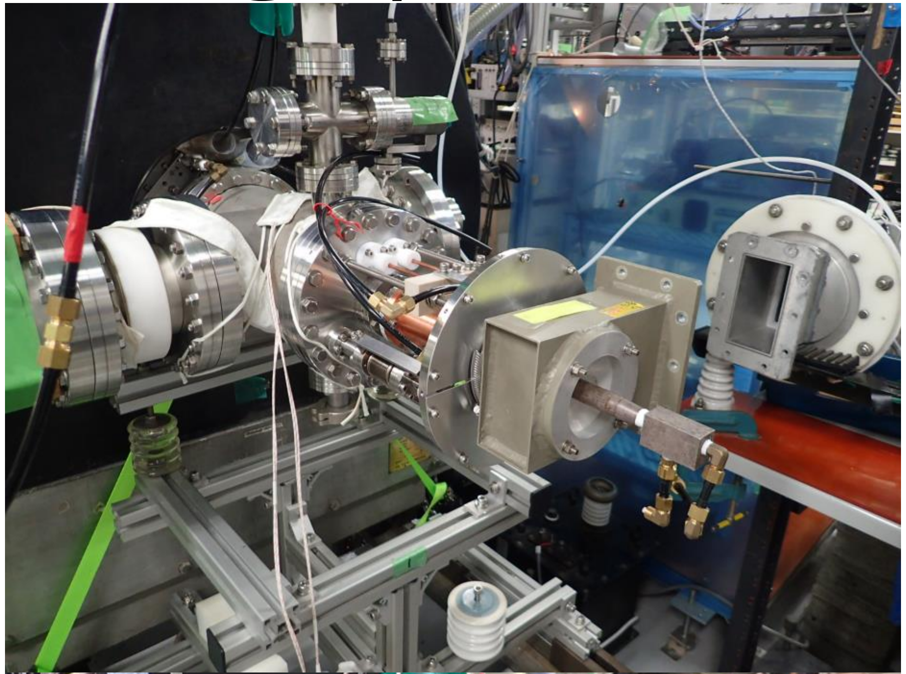

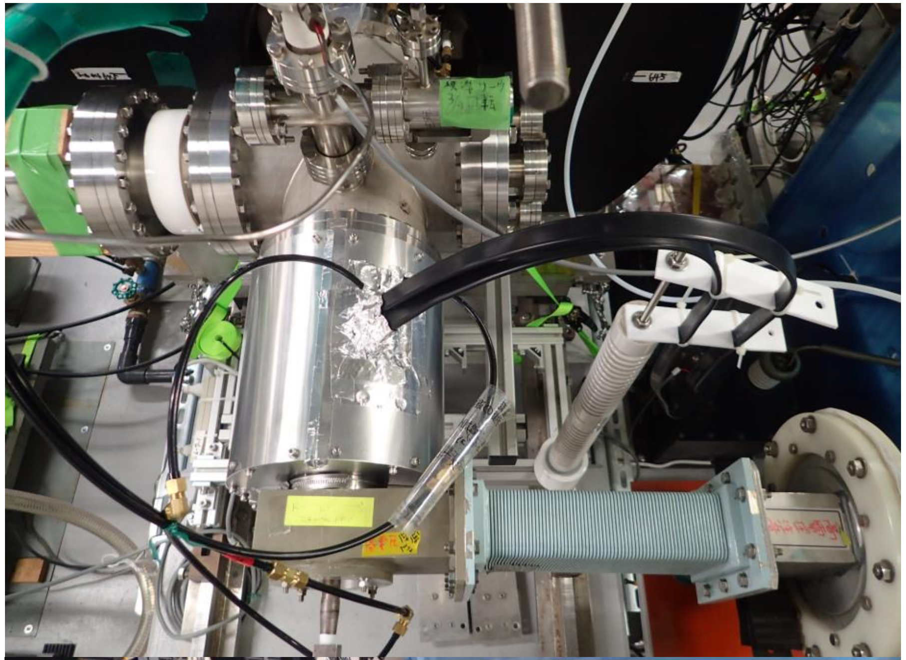

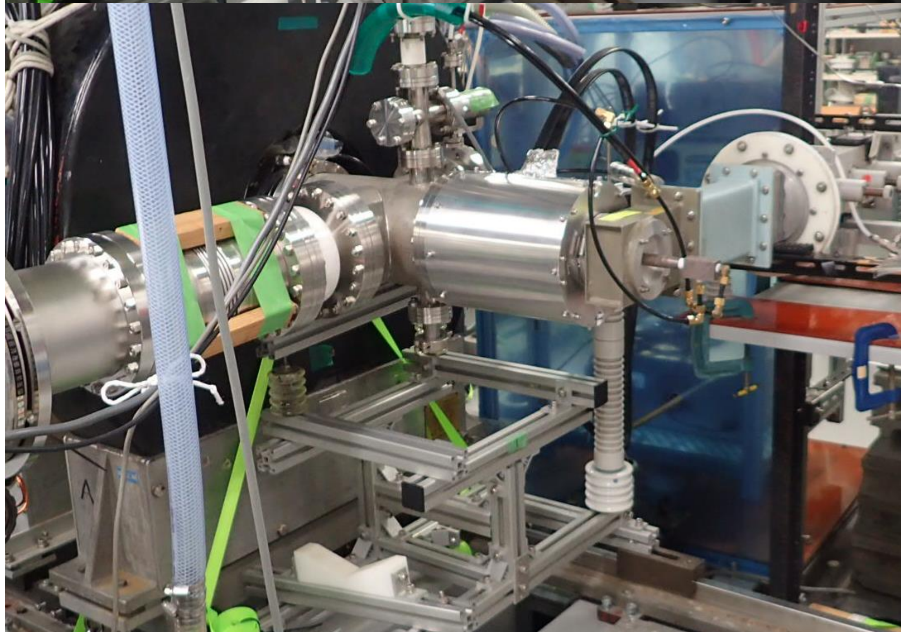

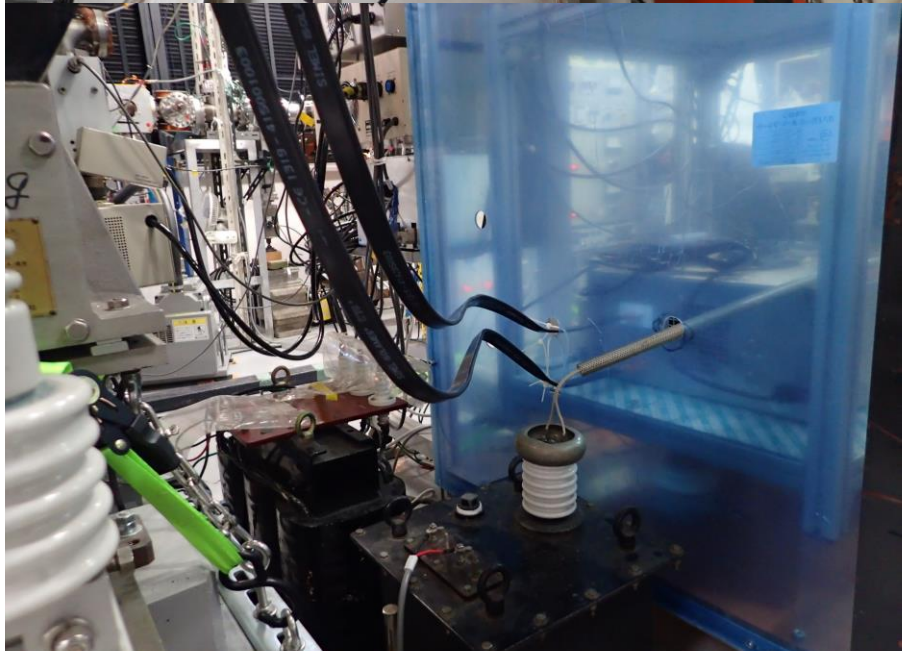

Our trials for improving performance IV

Electron energy distribution functions (EEDF) &
~~potential measurements~~

§ 3. Experimental Setup

- The 2nd stage of the tandem type of ECRIS (Osaka Univ.) (has just moved it's site & reconstructed)

- Measurement Apparatus

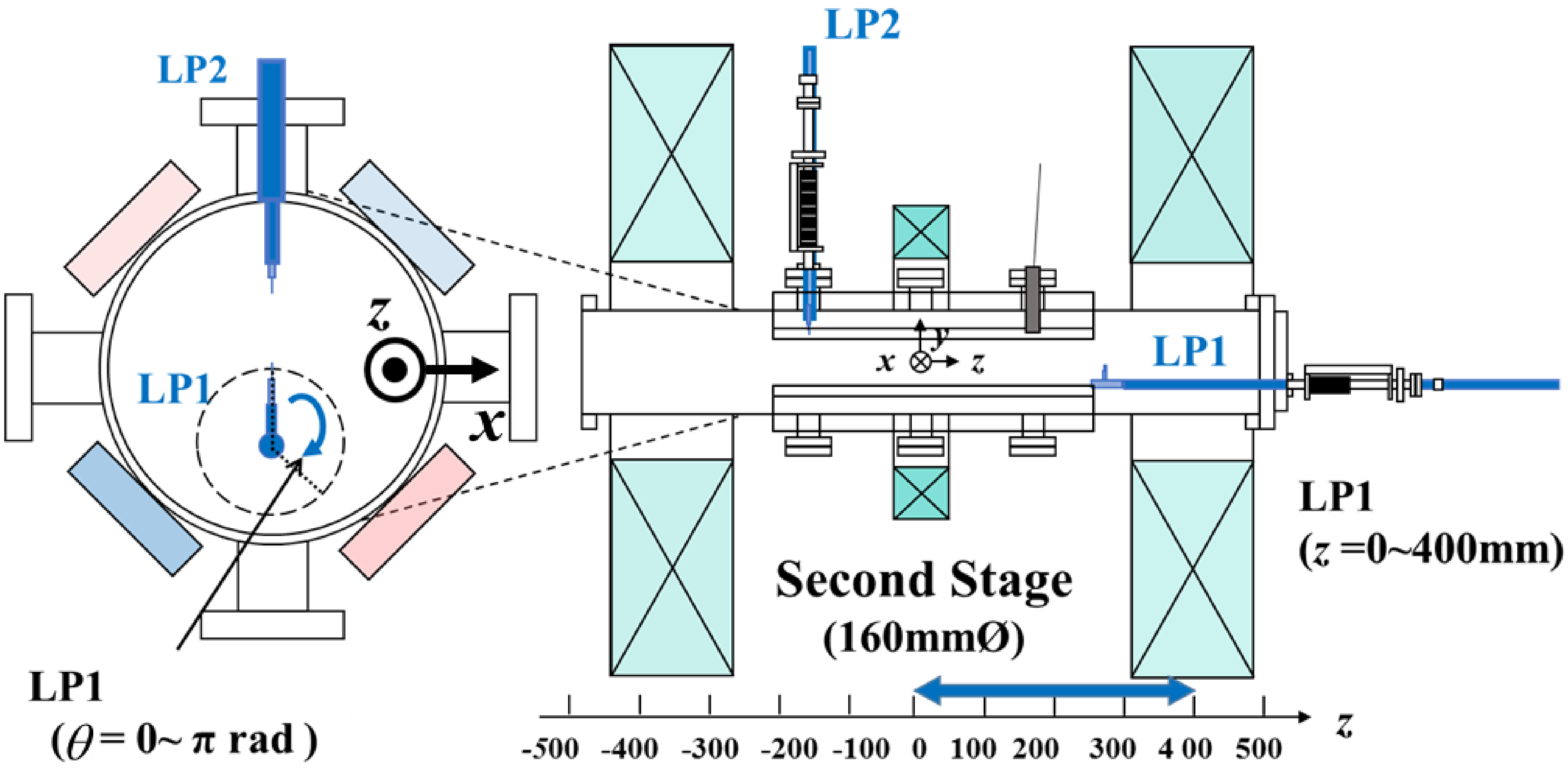

Magnetic field lines flowing to each z cut-surface through ECR zone on the 2nd stage

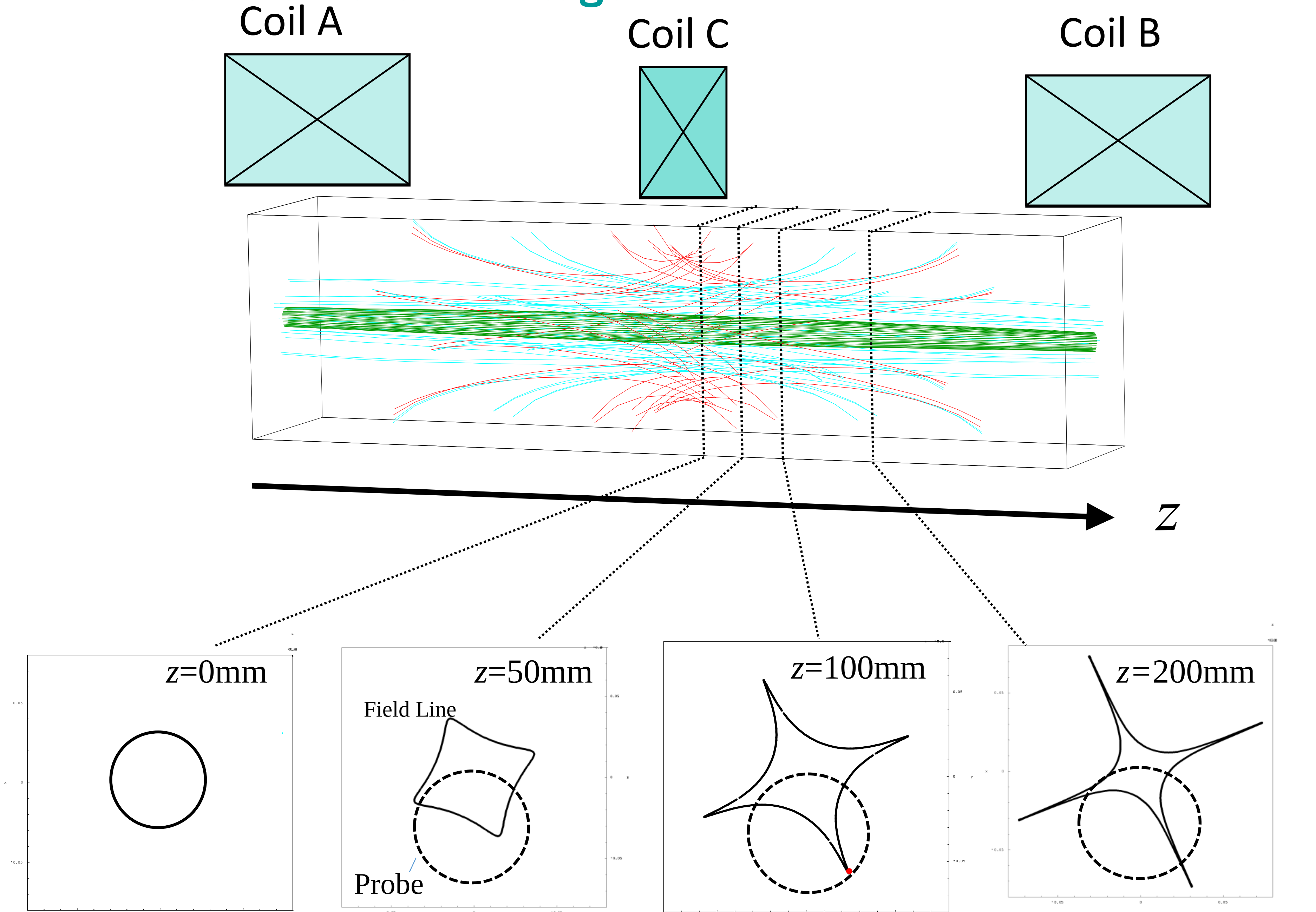

B. Typical Z-Profile's Survey of Plasma Parameters

Microwave power：30W　$I_{A,B}$=150A , I_C=0A

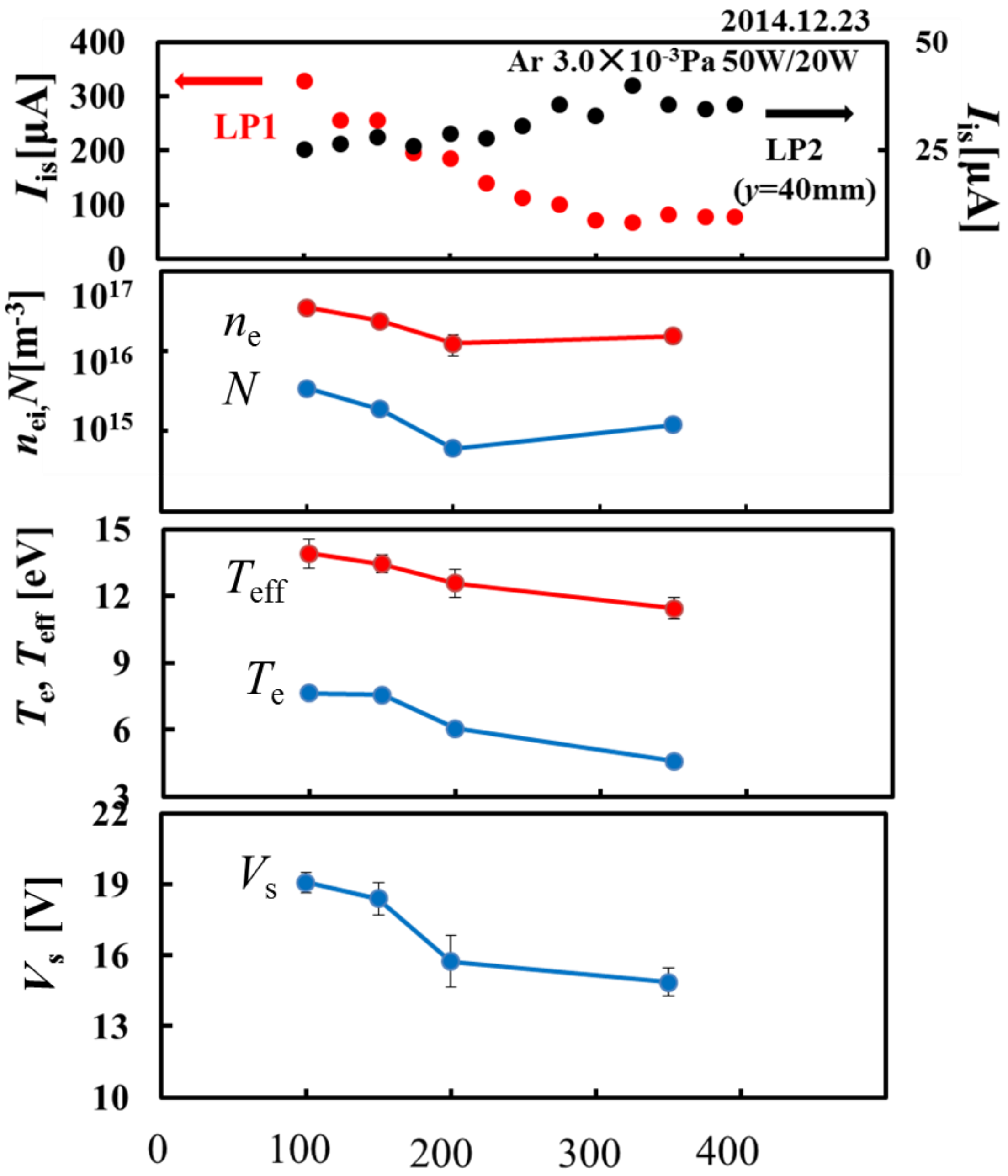

Typical z-profile's survey of plasma parameters along to the geometrical axis.

D. Dependences of EEDF's against θ Typically at Several Z-Profiles.

Microwave power : 30W $I_{A,B}$=150A , I_C=0A

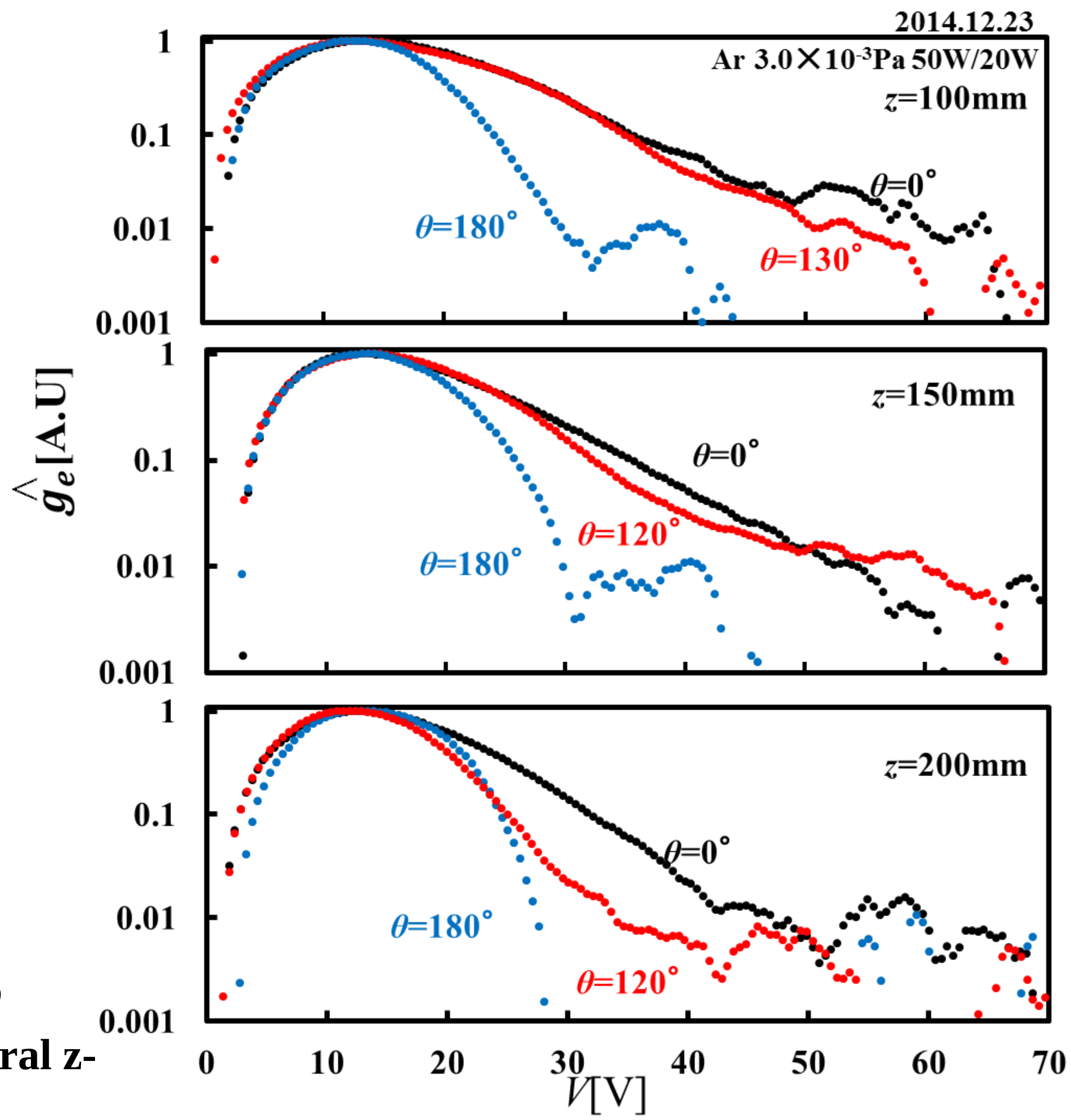

Dependences of EEDF against θ typically at several z-profiles.

F. Magnetic Flux Density and Mirror Ratios along to Field Lines.

$I_{A,B}$=150A , I_C=0A

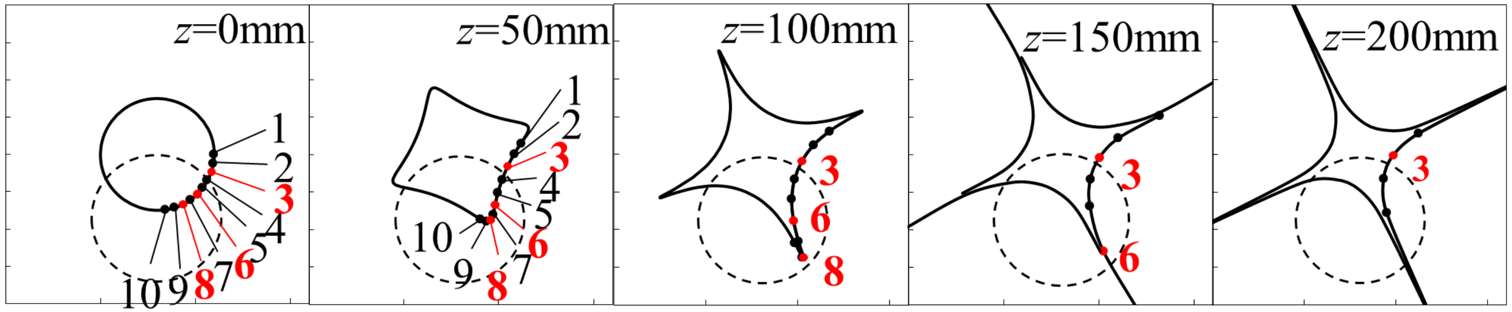

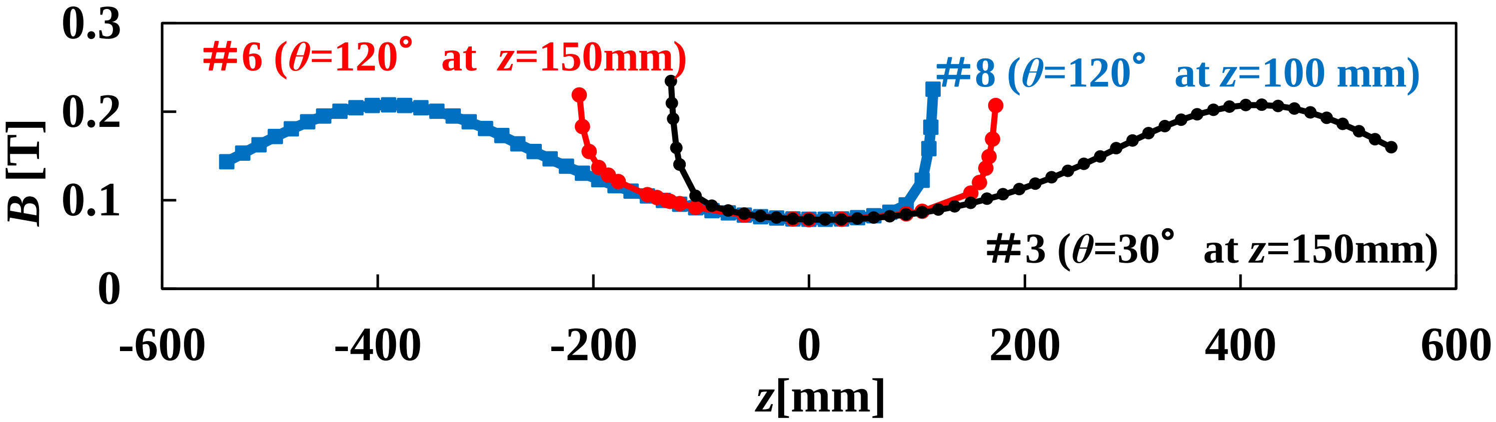

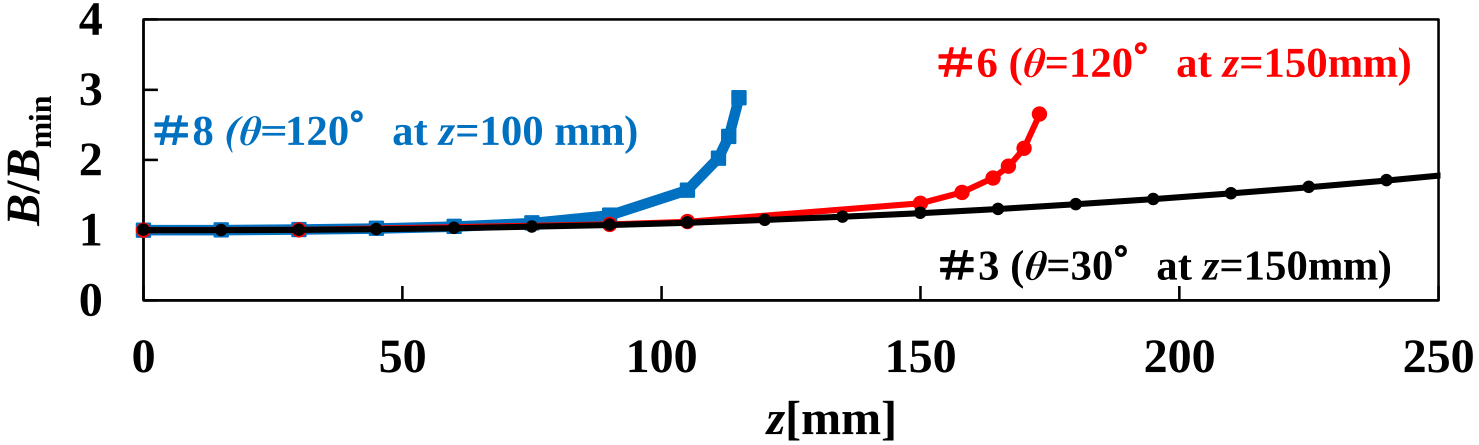

F. Magnetic Flux Density and Mirror Ratios along to Field Lines.

$I_{A,B}$=150A , I_C=0A

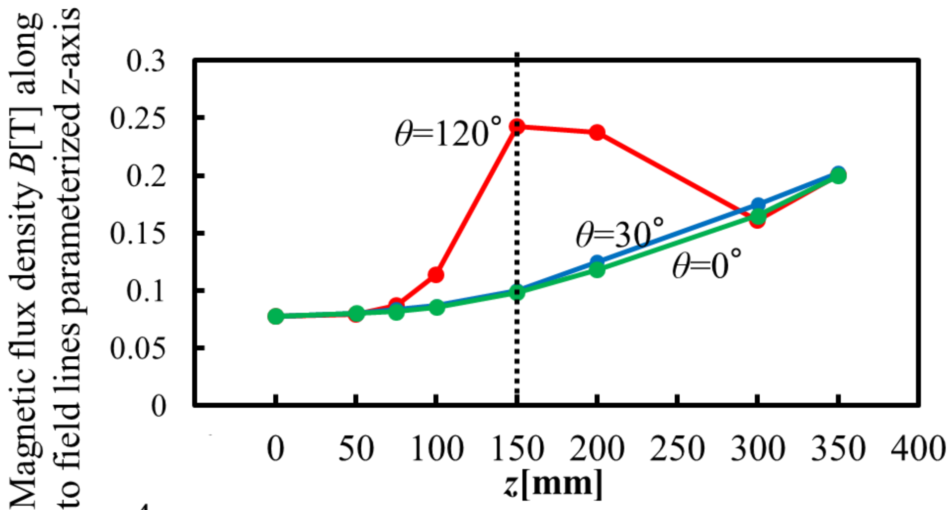

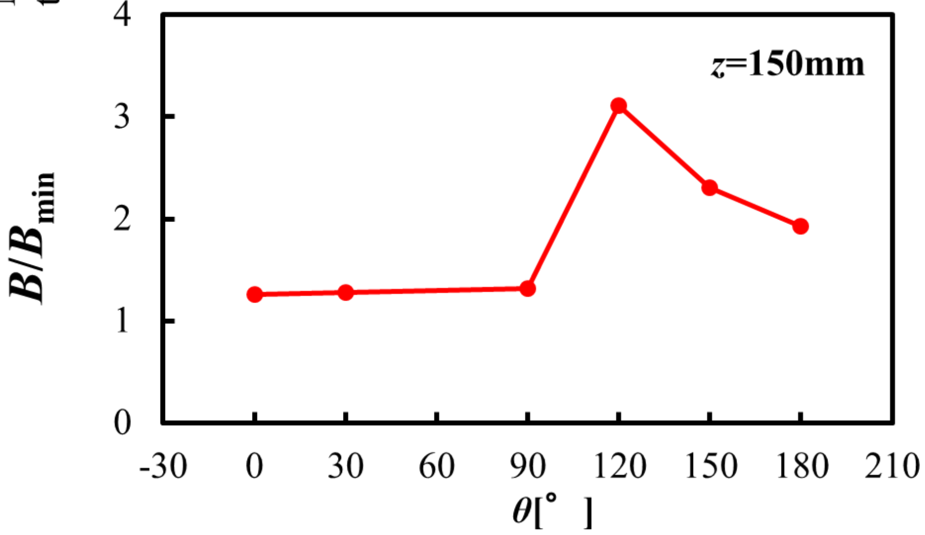

Magnetic flux density (upper figure) and mirror ratios along to field lines (lower figure).

A. Typical CSD of Mulicharged Ion Beam and Correlation between T_e and T_{eff} with Average Charge

Microwave power：100W　$I_{A,B}$=150A , I_C=7.5A

(a) CSD

#2014/02/04Ar 7.8×10^{-4}Pa

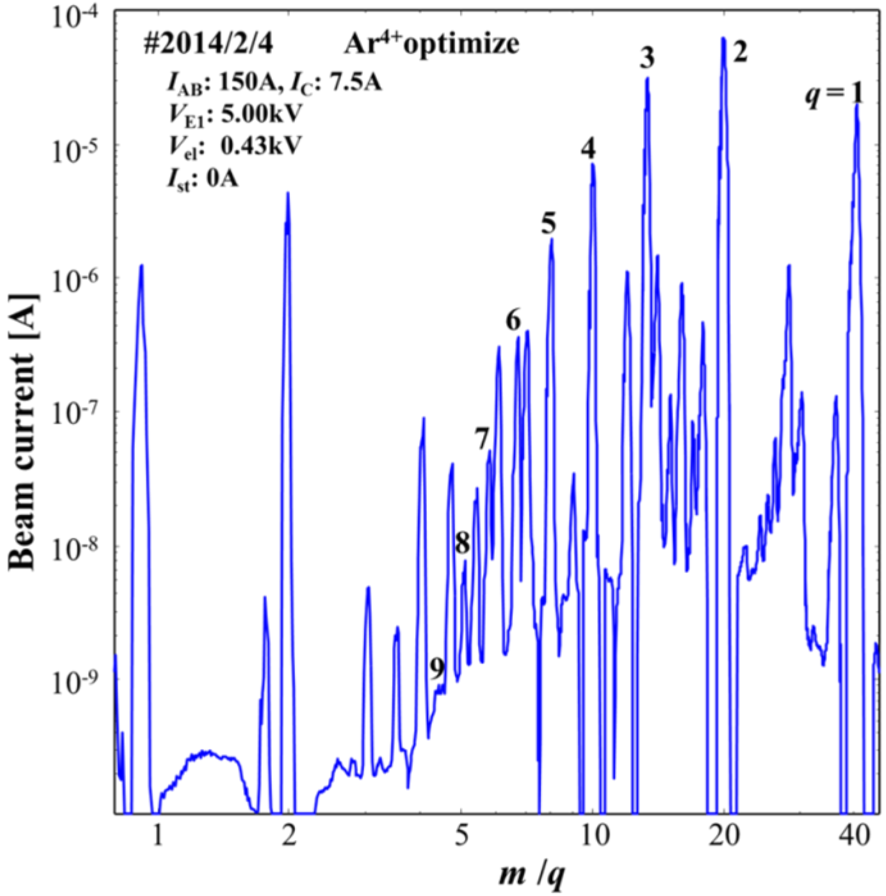

(b) T_e &T_{eff}

#2014/02/04Ar 7.8×10^{-4}Pa

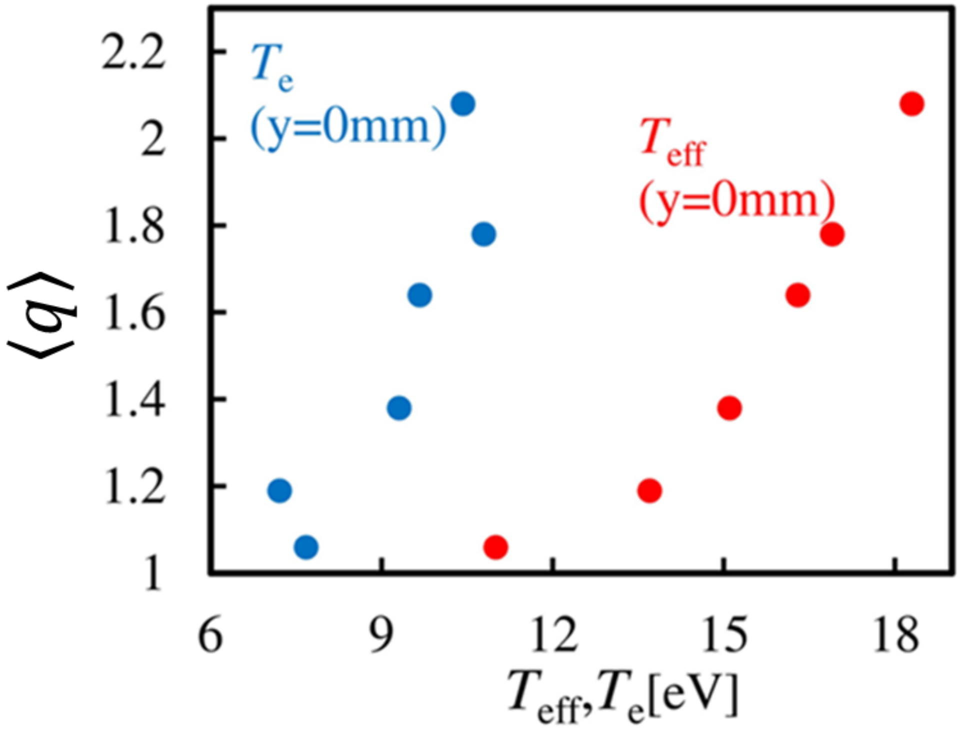

Typical charge state distribution (CSD) of the extracted multicharged ion beams from the 2nd stage of tandem-type ECRIS in Ar gas case (a). The correlation between with T_e and T_{eff} with averaged charge of ion beams (b).

Previous ECRIS for Fe@C_{60} (Case II)

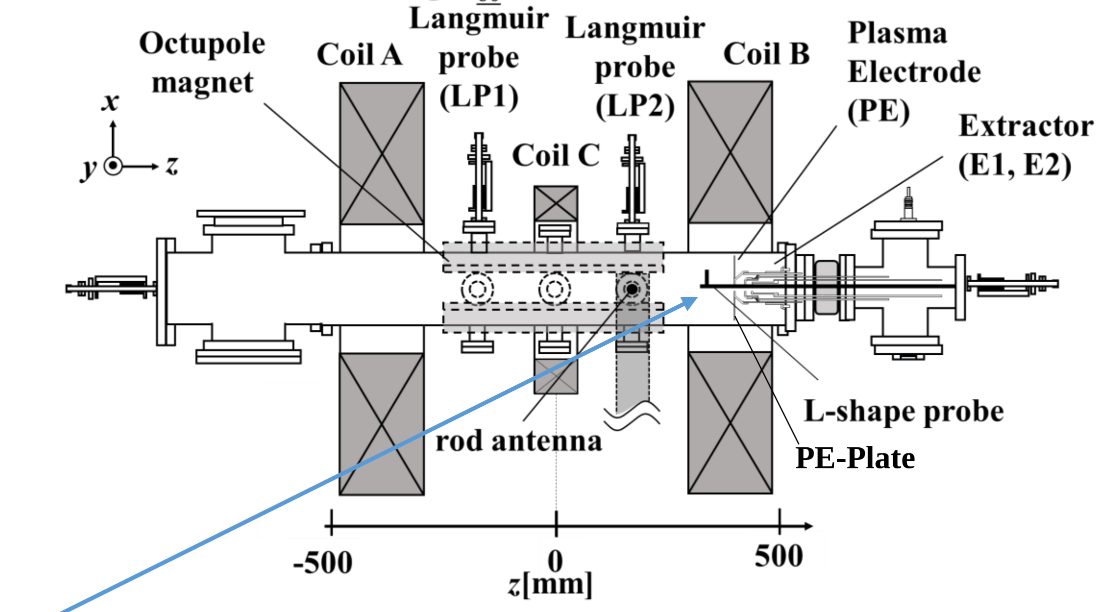

15Dec. 2018(H30) L-shaped probes

(c)PE-plate

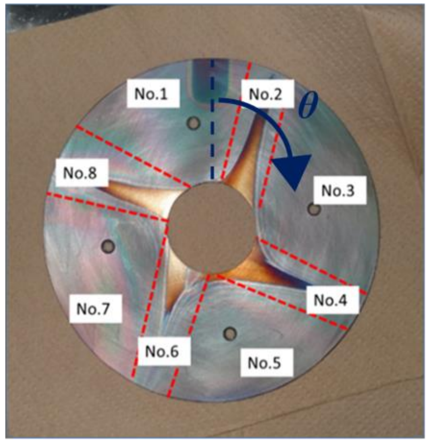

(d)Spectrum in No. 5

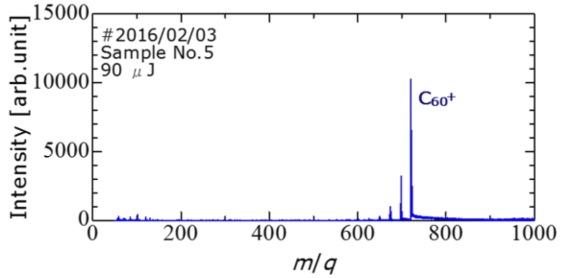

(e)Spectrum in No. 6

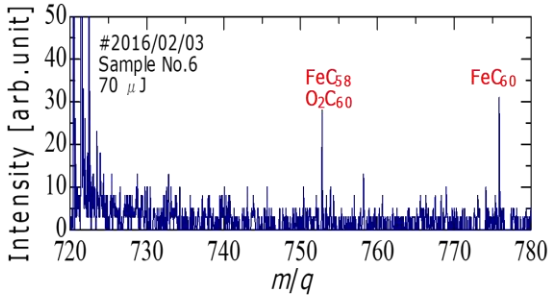

✓ **Results of TOFMS analysis[4]**

- **No. 5⇒C_{60} spectrum is confirmed**
- **No. 6⇒Productions of Fe@C_{58} and Fe@C_{60} are suggested**

[4] Y. Kato, et al., IIT2018, IEEE Conf. Publ., 2019, pp172-175.

Kubo W, ECRIS2020 (online)

Case II Experimental Results

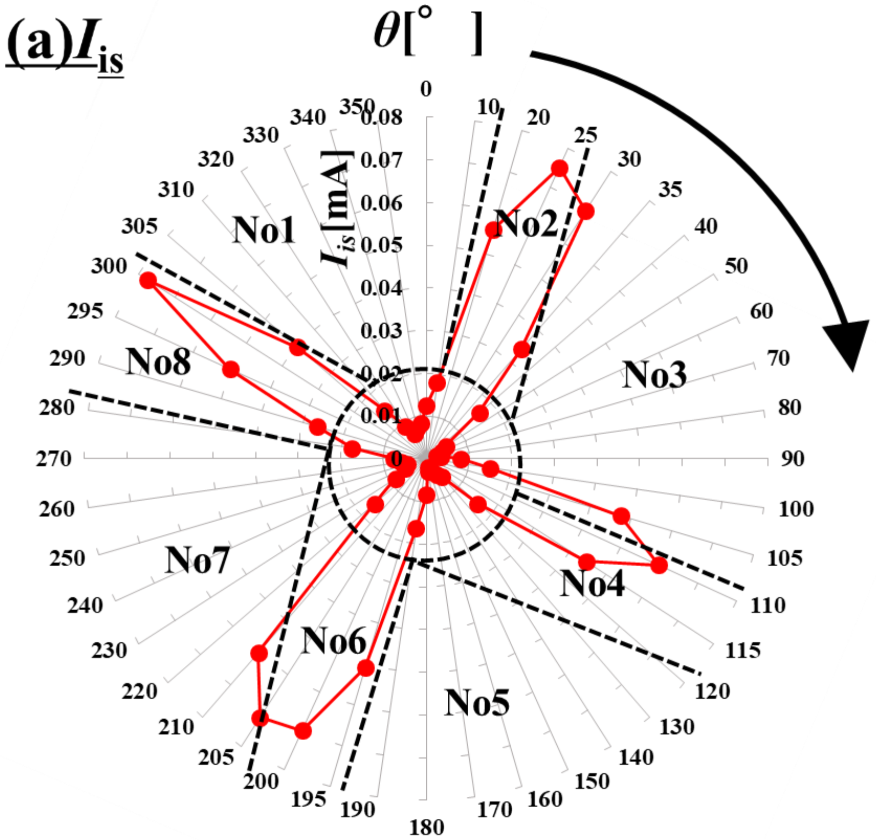

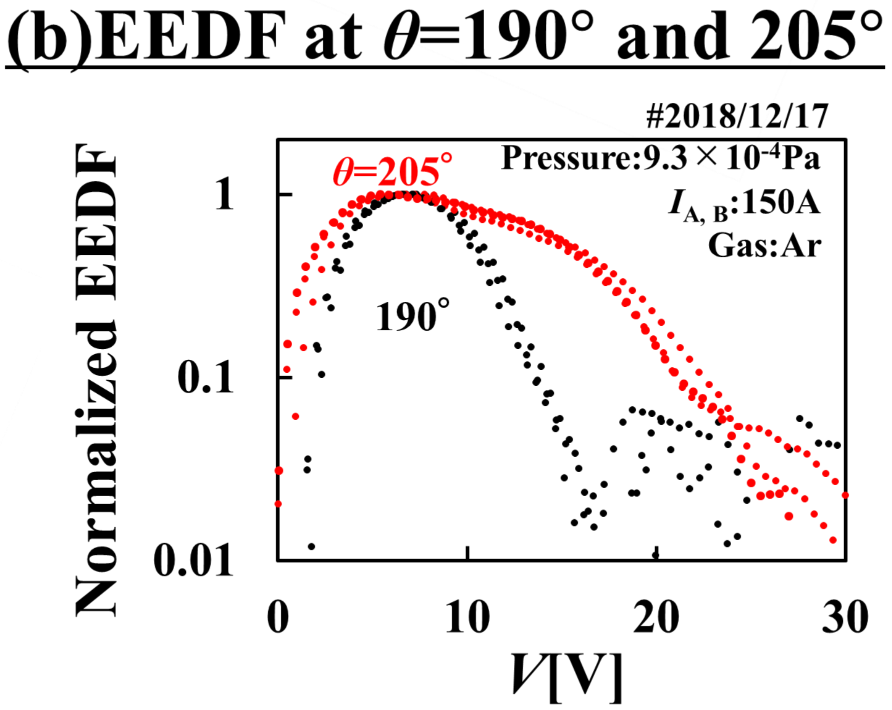

Reconsidering the shape of the extraction hole

- The I_{is} peaks are observed in even number regions (No. 2, 4, 6, 8).
- EEDF at θ=205° which is in the No.6 has the higher tail than that at θ=190° which is in the boundary region of No.5 and No. 6.

Kubo W,ECRIS2020 (online)

Our trials for improving performance V

L-cutoff limitation

Cutoff limitation of left-hand polarization wave and candidates for further enhanced producing multicharged ions on ECRIS

Yushi Kato, Wataru Kubo, Shuhei Harisaki, Masahiro Anan, Kazuki Tsuda, Koichi Sato, Issei Owada, and Takumu Maenaka

Graduate School of Engineering, Osaka Univ., Suita, Osaka, Japan

Focus: μW power & n_e ⇔ Accessibility of waves
(B config.(Last conf.))

Contents: Brief theory, Experimental results,
Discussions (L-cutoff, I_{q+}) & New candidates, Summary & perspective

ICIS2021, Online

Brief theoretical background

- In the electromagnetic waves propagating along the magnetic field lines, there exist right-hand polarization wave (R-wave) and left-hand polarization wave (L-wave). There are cutoff frequencies ω_r (R-cutoff) and ω_l (L-cutoff) for each wave propagation mode, and they are derived as follows:

$$\omega_{\mathrm{r}} = \frac{\omega_{\mathrm{ce}} + \sqrt{\omega_{\mathrm{ce}}^2 + 4\omega_{\mathrm{pe}}^2}}{2} \quad , \quad \omega_{\mathrm{l}} = \frac{-\omega_{\mathrm{ce}} + \sqrt{\omega_{\mathrm{ce}}^2 + 4\omega_{\mathrm{pe}}^2}}{2} \; .$$

- Resonance phenomena related to X-wave include high-frequency hybrid resonance (UHR) and low-frequency hybrid resonance (LHR) as follows:

$$\omega_{\mathrm{UH}}^2 = \omega_{\mathrm{ce}}^2 + \omega_{\mathrm{pe}}^2 \; , \qquad \frac{1}{\omega_{\mathrm{LH}}^2} = \frac{1}{\omega_{\mathrm{pi}}^2} + \frac{1}{\omega_{\mathrm{ce}}\omega_{\mathrm{ci}}} \; ,$$

where, $\omega_{\mathrm{ce(ci)}}$ and $\omega_{\mathrm{pe(pi)}}$ indicate the electron (ion) cyclotron frequency and the electron (ion) plasma frequency, $\omega_{\mathrm{ce}} = \frac{eB}{m_e}$, $\omega_{\mathrm{ci}} = \frac{qeB}{M}$, $\omega_{\mathrm{pe}} = \left(\frac{en}{\varepsilon_0 m_e}\right)^{1/2}$, and $\omega_{\mathrm{pi}} = \left(\frac{q^2 e^2 n}{\varepsilon_0 M}\right)^{1/2}$.

- In the wave propagation of the frequency ω microwaves in the magnetized ECRIS plasma, when O-cutoff density is n_c and the magnetic field strength corresponding ECR is B_{ECR}, R-, L-, and UH-cutoff densities n_{cr}, n_{cl}, and n_{cu} are expressed by the following equations:

$$n_{\mathrm{cr}} = n_c\left(1 - \frac{B}{B_{ECR}}\right)(*) \; , \qquad n_{\mathrm{cl}} = n_c\left(1 + \frac{B}{B_{ECR}}\right) , \qquad n_{\mathrm{cu}} = n_c\left(1 - \left(\frac{B}{B_{ECR}}\right)^2\right) .$$

(*) for R-wave coming from $B/B_{\mathrm{ECR}} < 1$)

Axial distribution measurement of plasma parameters in ECRIS by LP3 (z-direction)

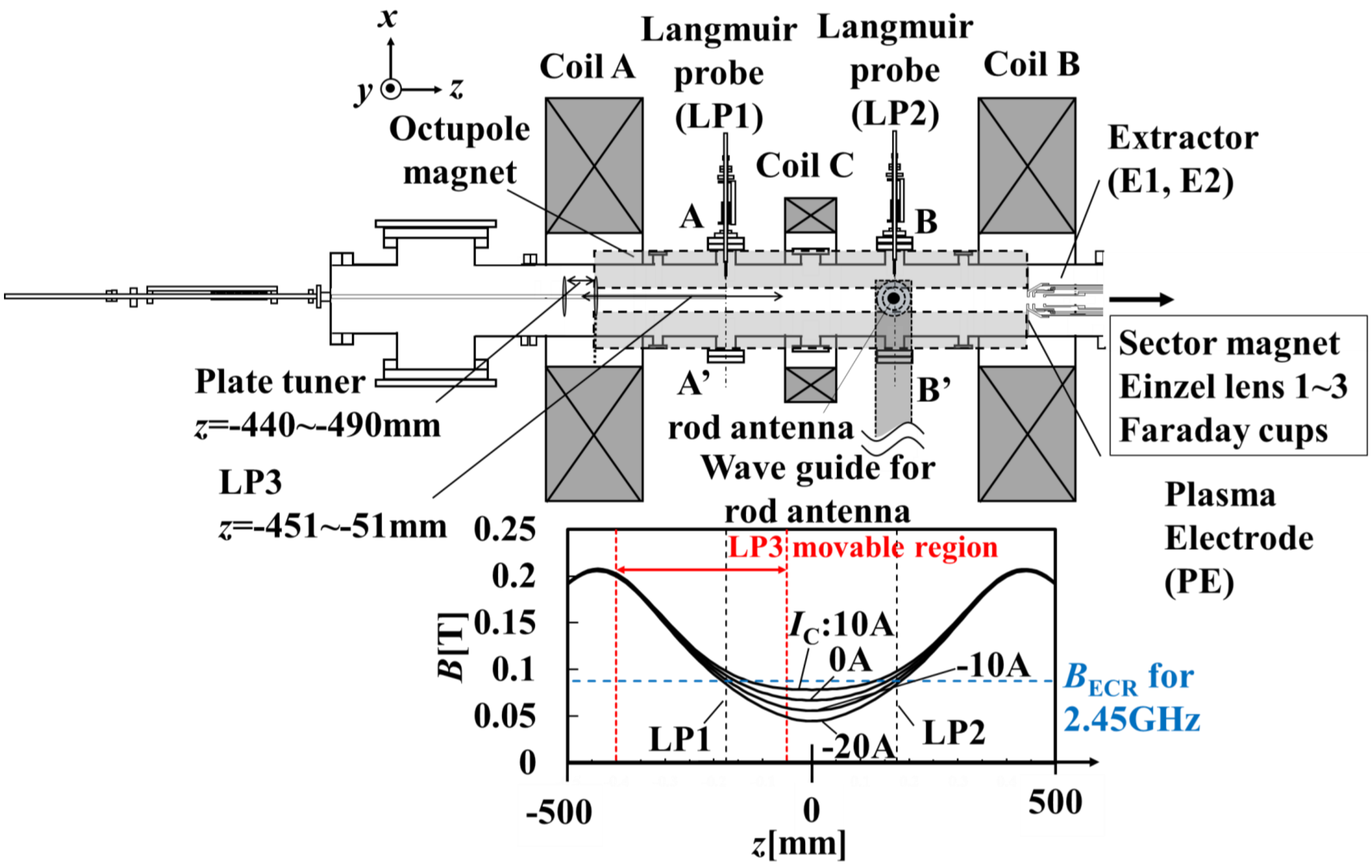

Figure 4. Top view of ECRIS(Osaka Univ.) with LP1, LP2 and LP3.

Axial distribution measurements of plasma parameters in ECRIS by LP3 (z-direction)

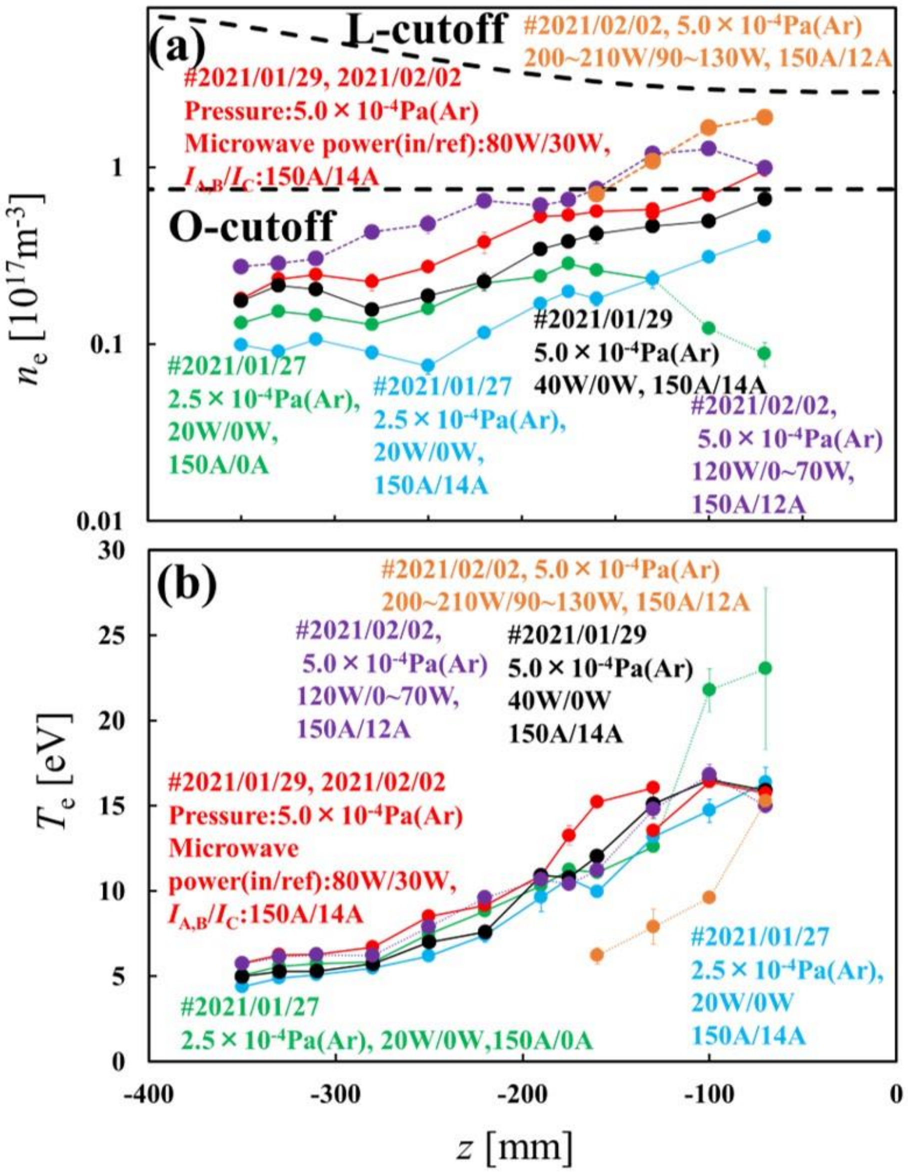

Figure 5. Measured axial (z) profiles of n_e(a) and T_e(b).

P9

Appearance/ disappearance of resonances & cutoffs according to microwave powers & n_e

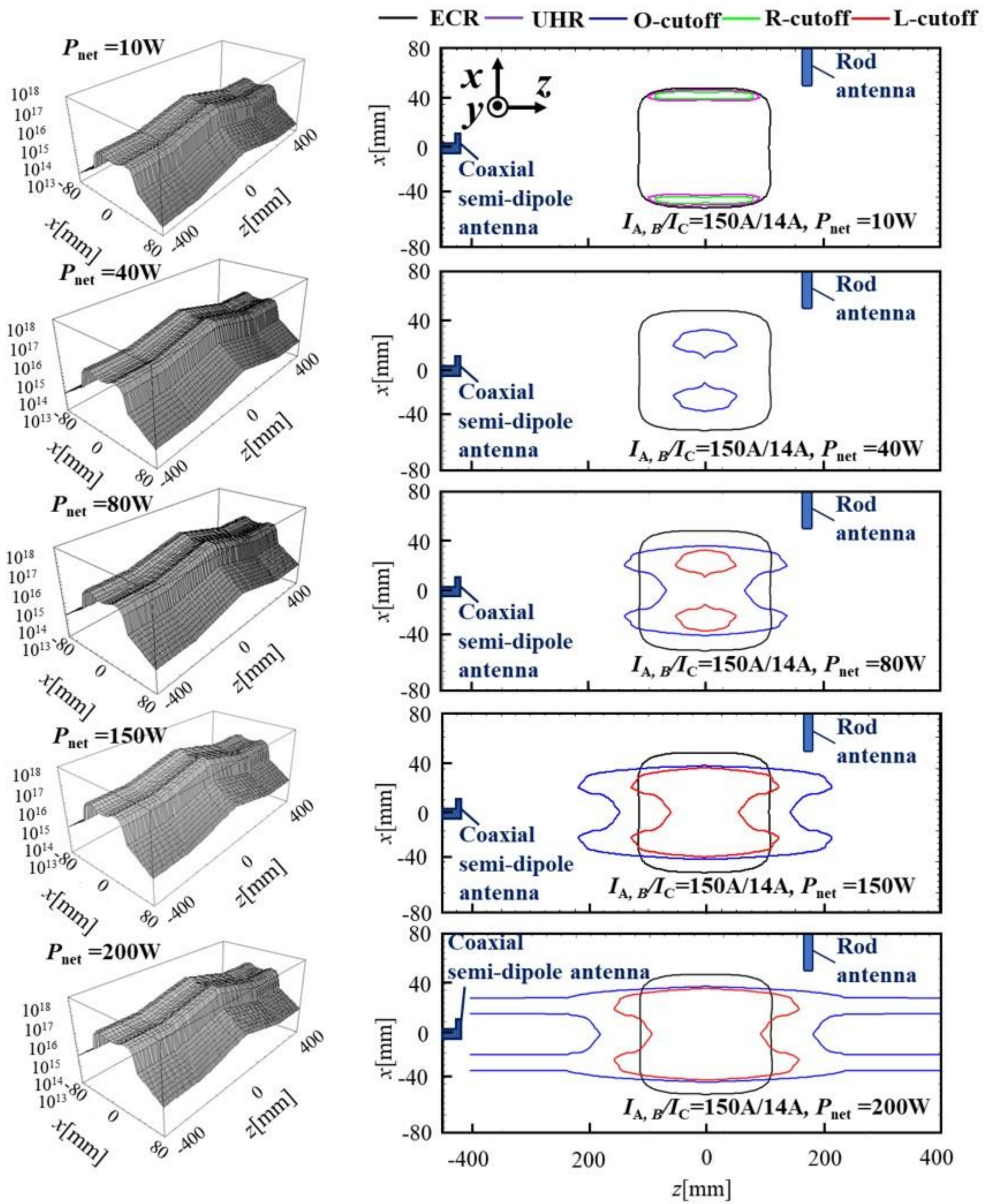

Figure 8. The *x*-*z* profiles of n_e (left side) and the contour plots of the corresponding various resonances and cutoff (right side) on various microwave powers.

Accessibility condition on real space & CMA diagram

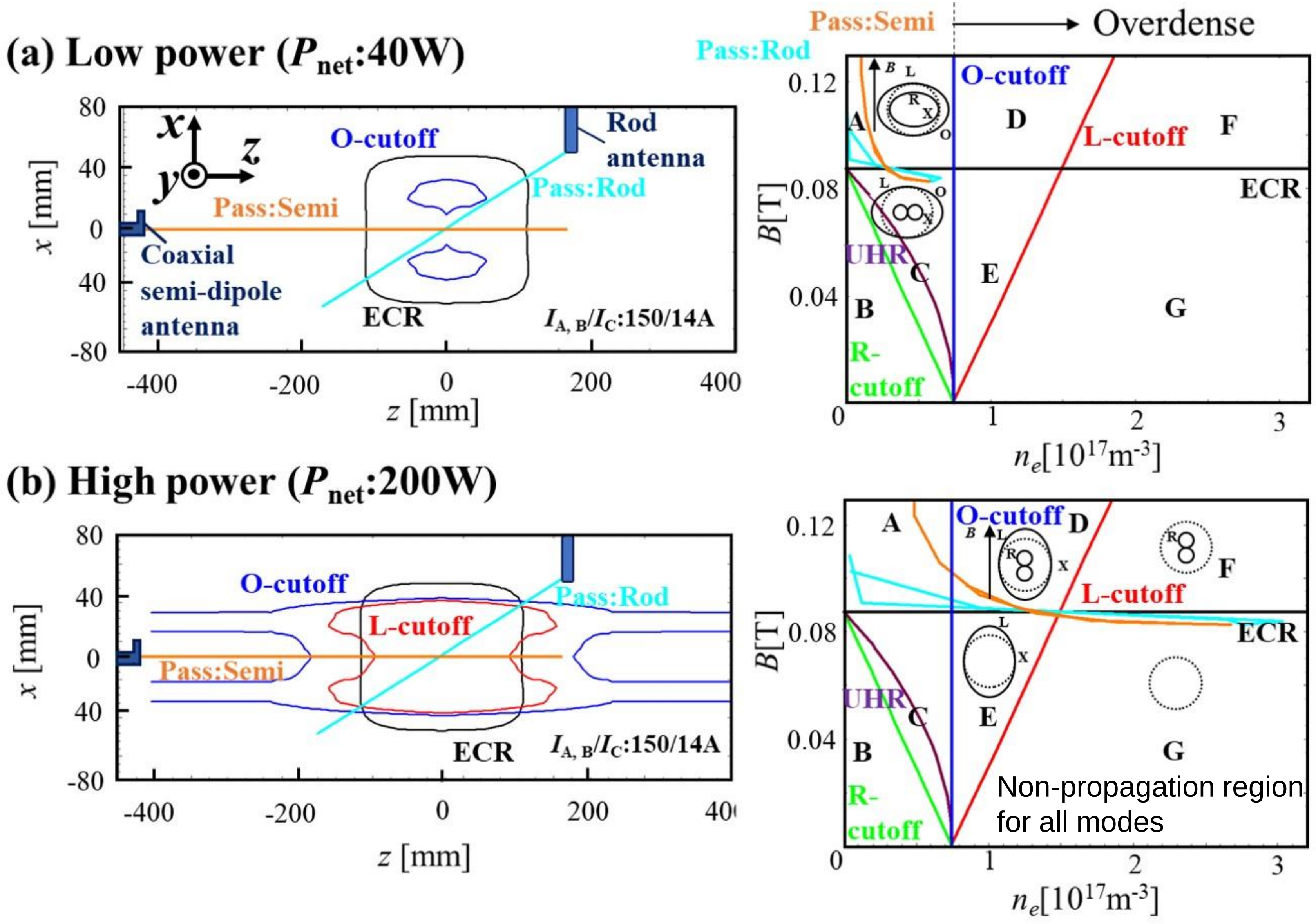

Figure 9. The accessibility condition in the real space of ECRIS (left figure) and in CMA diagram (right figures) at the microwave power 40 W (a) and 200 W (b), respectively.

Avoiding the existence of the "G region": What should we do?

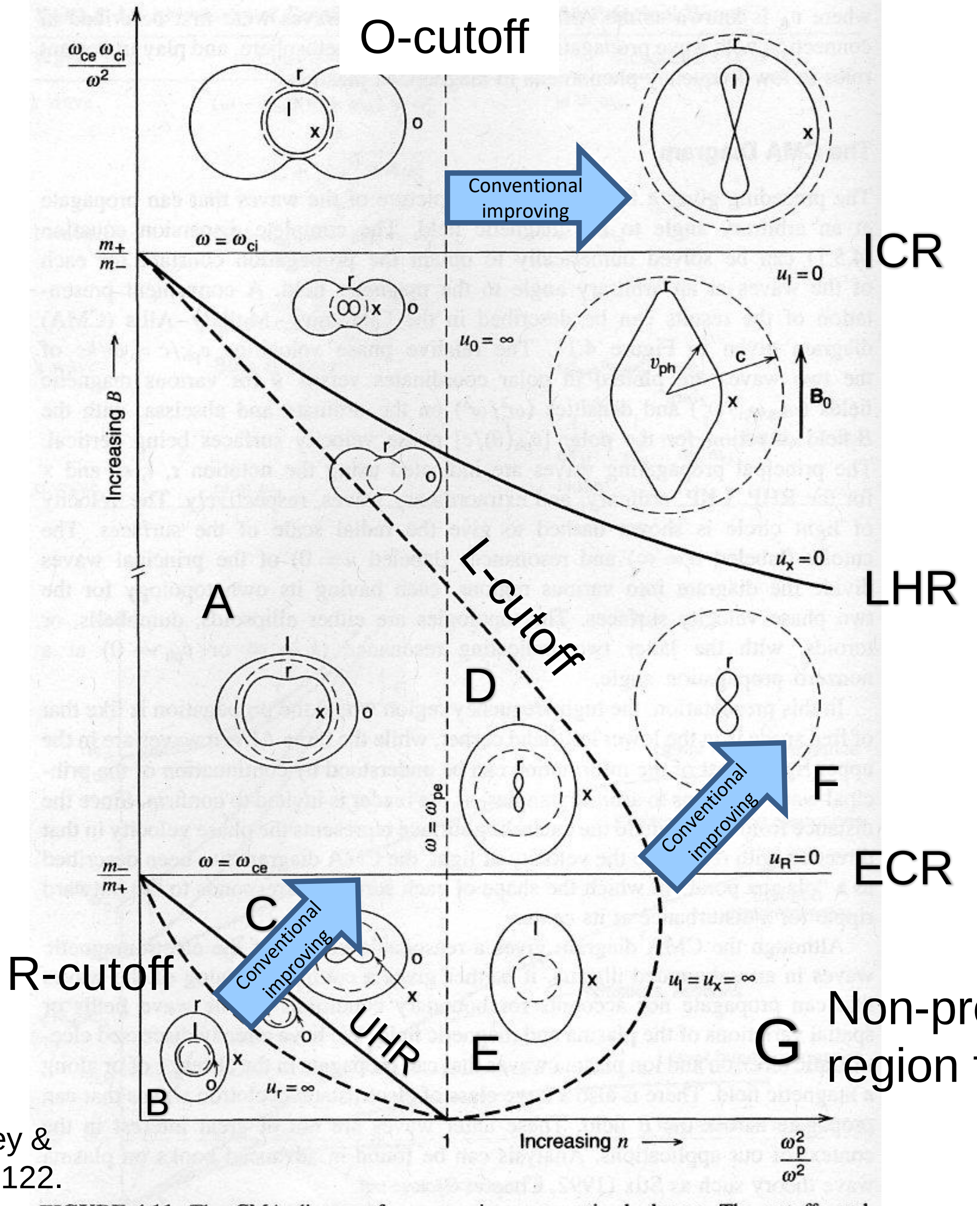

Simulation researchers also began to issue CMA on ICIS2023, via our oral presentations on ICIS 2019&2021 conferences

Quarted from Lieberman A M and Lichtenberg J A 2005 Principle of Plasma Discharges and Materials Processing, 2nd Edit., A John Wiley & Son, Inc Publications, Chap.4, pp.122.

New candidates for further enhanced producing multicharged ions on ECRIS

- Advanced high-frequency resonance via conversion from electromagnetic to electrostatic waves:
  – Upper hybrid resonance (UHR) heating
- Applications of new low-frequency resonances without density limit:
  – Lower hybrid resonance (LHR) heating
  – Ion cyclotron resonance (ICR) heating
- New microwave feeding methods:
  – For example: Dual-ECR heating (bidirectional)

+ α : EBEP (el. Beam)

Current limitation by instabilities

Trends of European ECRIS’s society

IOP Publishing

Plasma Sources Science and Technology

Plasma Sources Sci. Technol. **23** (2014) 025020 (8pp)

doi:10.1088/0963-0252/23/2/025020

Beam current oscillations driven by cyclotron instabilities in a minimum-*B* electron cyclotron resonance ion source plasma

O Tarvainen[1], I Izotov[2], D Mansfeld[2], V Skalyga[2,3], S Golubev[2,3], T Kalvas[1], H Koivisto[1], J Komppula[1], R Kronholm[1], J Laulainen[1] and V Toivanen[4]

[1] University of Jyväskylä, Department of Physics, PO Box 35 (YFL), 40500 Jyväskylä, Finland

[2] Institute of Applied Physics, RAS, 46, Ul‘yanova St., 603950 Nizhny Novgorod, Russian Federation

[3] Lobachevsky State University of Nizhny Novgorod (UNN), 23 Gagarina St., 603950 Nizhny Novgorod, Russian Federation

[4] CERN, 1211 Geneva 23, Switzerland

E-mail: olli.tarvainen@jyu.fi

Our trials for improving performance VI

Low frequencies resonances :

Ion cyclotron resonance (ICR) :

Please refer to Fujimura-san's oral presentation!

Lower hybrid resonance (LHR)

新たな試み

従来の2.45GHz ECRに以下の共鳴加熱を重畳する.

イオンサイクロトロン共鳴(ICR)

$$f_{\mathrm{ci}} = \frac{\omega_{\mathrm{ci}}}{2\pi} = \frac{1}{2\pi}\frac{q_{\mathrm{i}}B}{m_{\mathrm{i}}}\,[\mathrm{Hz}]$$

ガス混合時の選択的な

イオン加熱(L-wave)

本研究室の磁場強度では<u>Ar/He, Xe/Ar</u>等

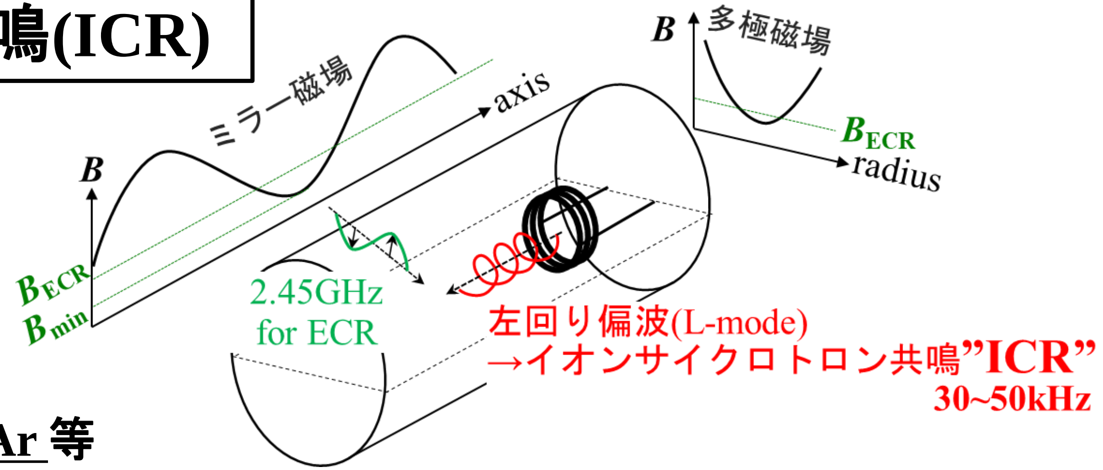

低域混成周波数共鳴(LHR)

$$f_{\mathrm{LHR}} = \frac{1}{2\pi}\sqrt{\frac{1}{\frac{1}{\omega_{\mathrm{pi}}^2}+\frac{1}{\omega_{\mathrm{ci}}\omega_{\mathrm{ce}}}}}\,[\mathrm{Hz}]$$

X-mode($E \perp B_0, k \perp B_0$)の共鳴

ヘリコン波による発生を狙う(電子加熱)

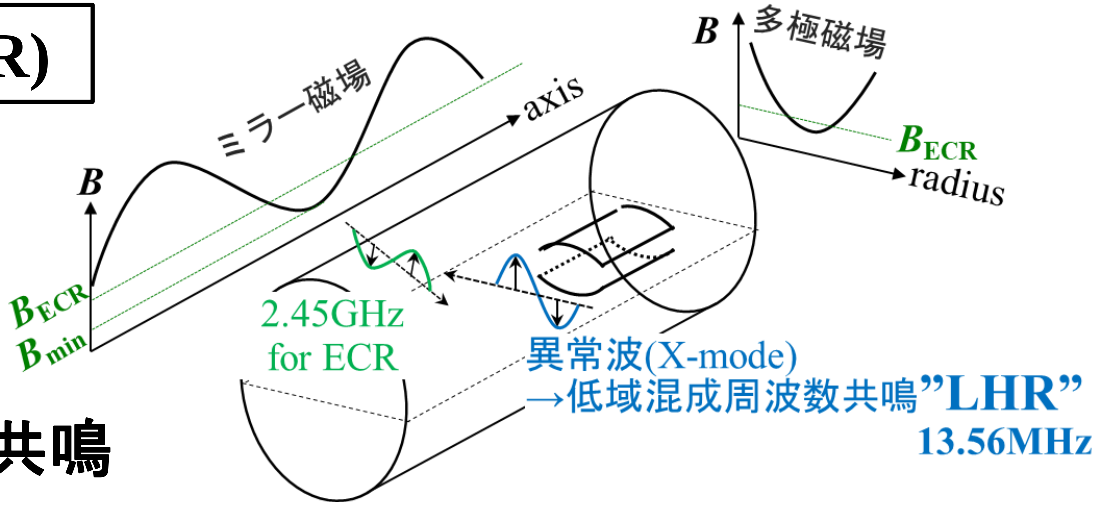

Mo IH coils coverd Al_2O_3 beads & Home appliance IH power supply

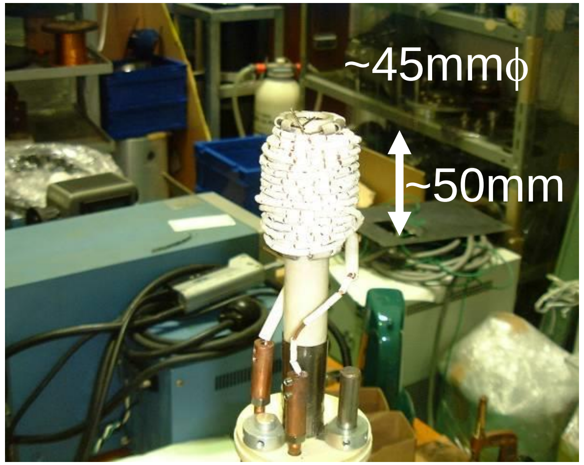

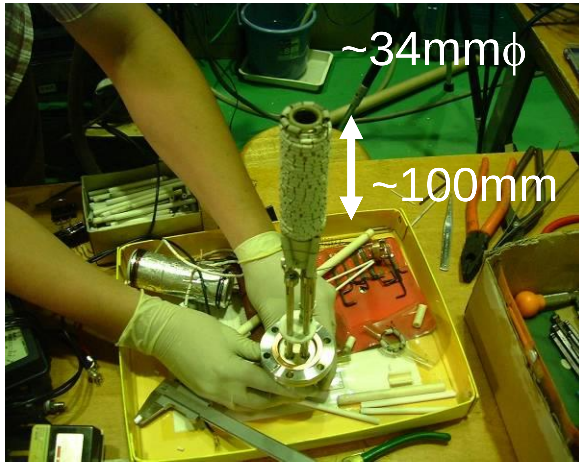

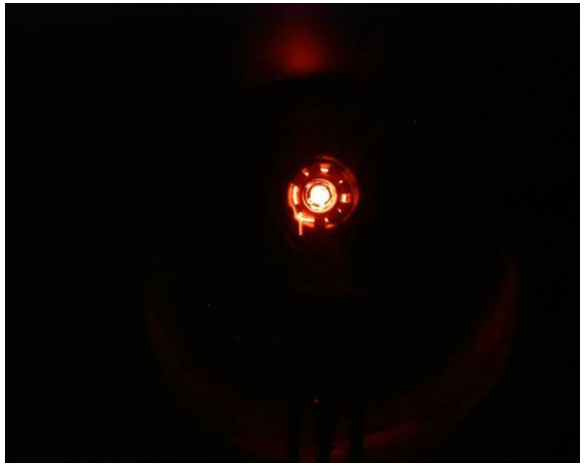

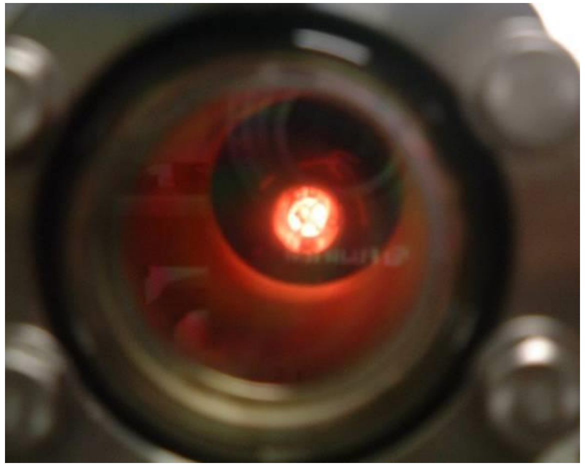

Induction heating vapor source (vacuum coil type) in Osaka univ.(2005 Summer)

We have achieved the heating temperature up to 2068 K.

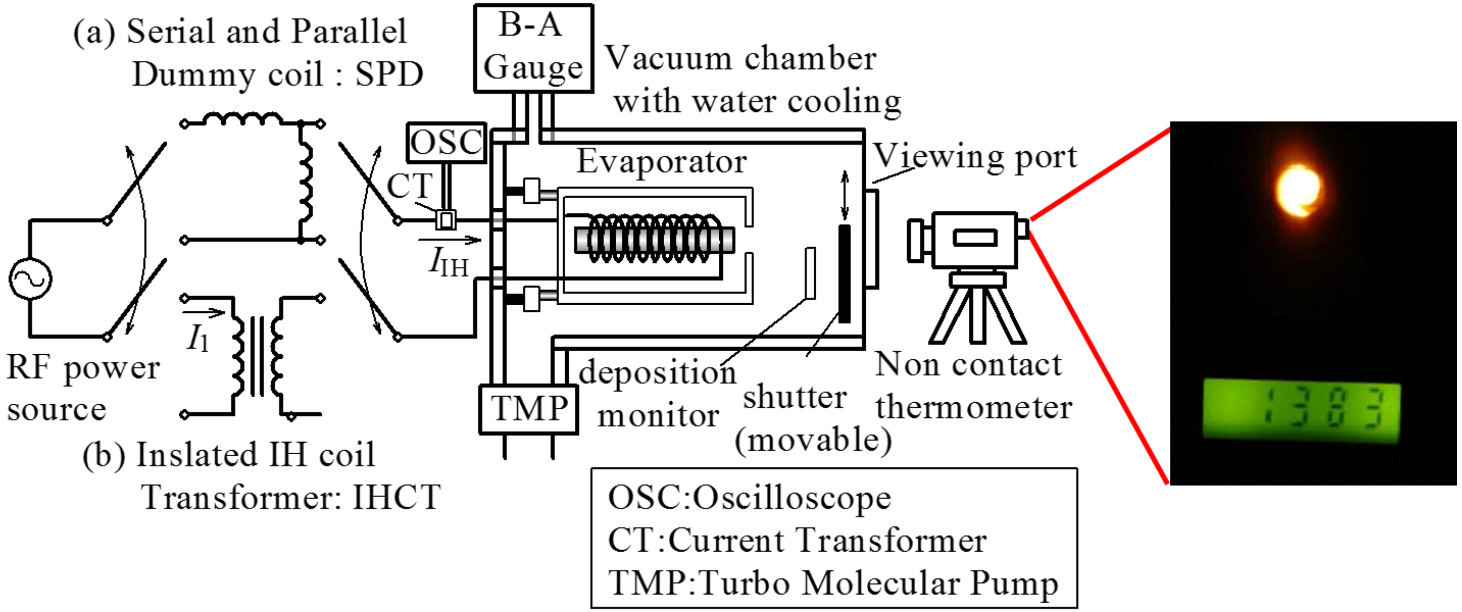

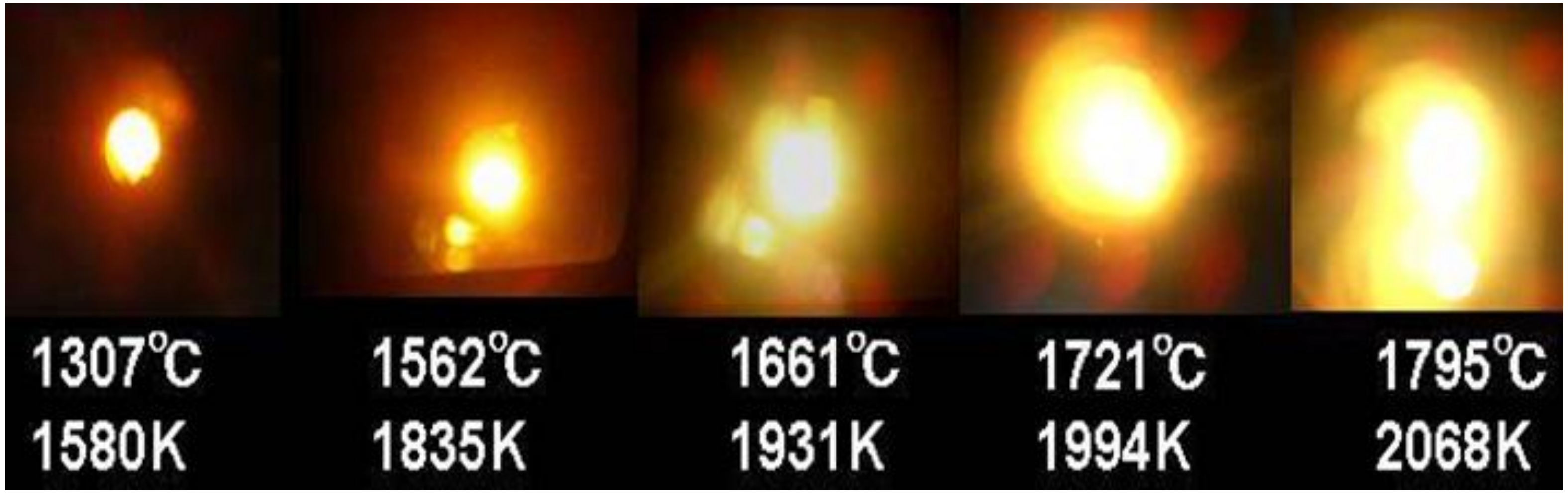

What is new in 2020-2023 under COVID-19 Pandemic ? No.2

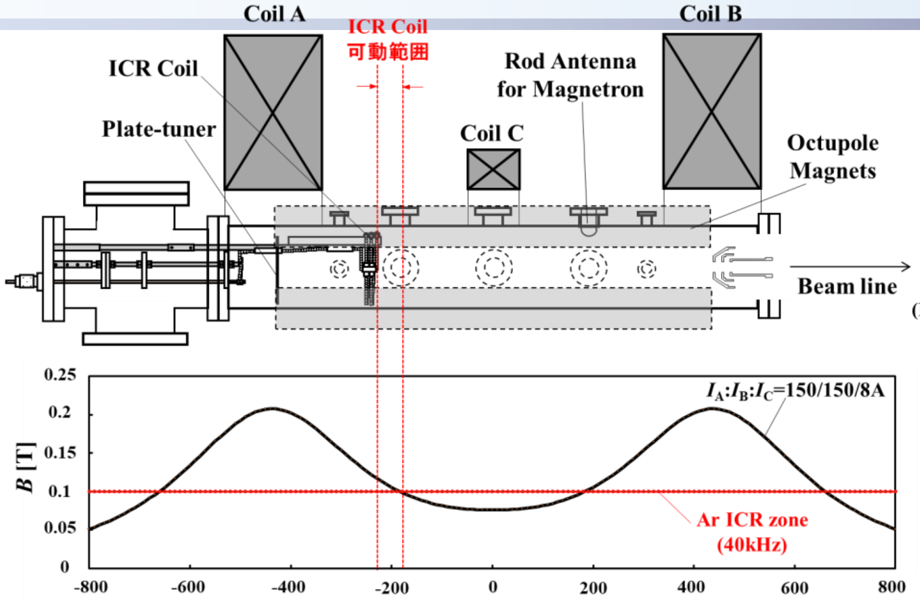

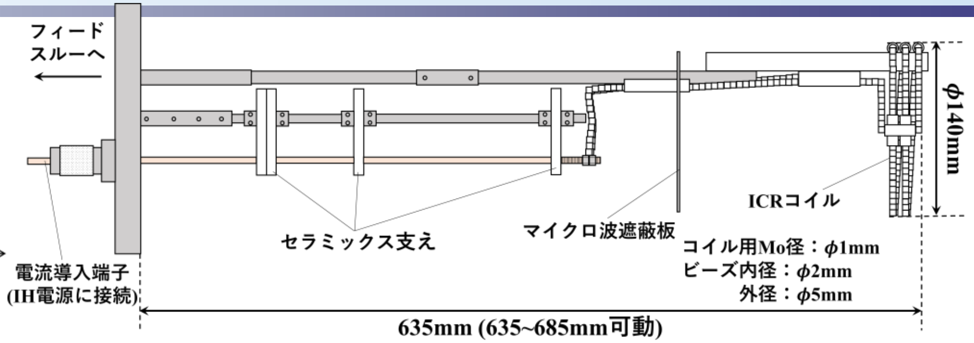

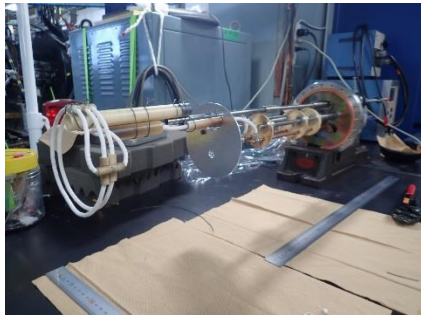

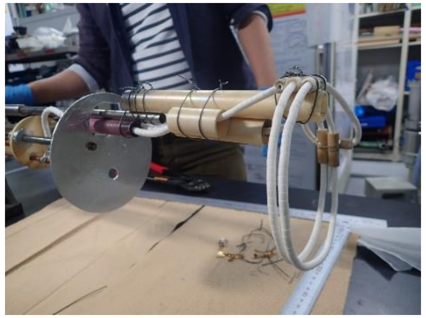

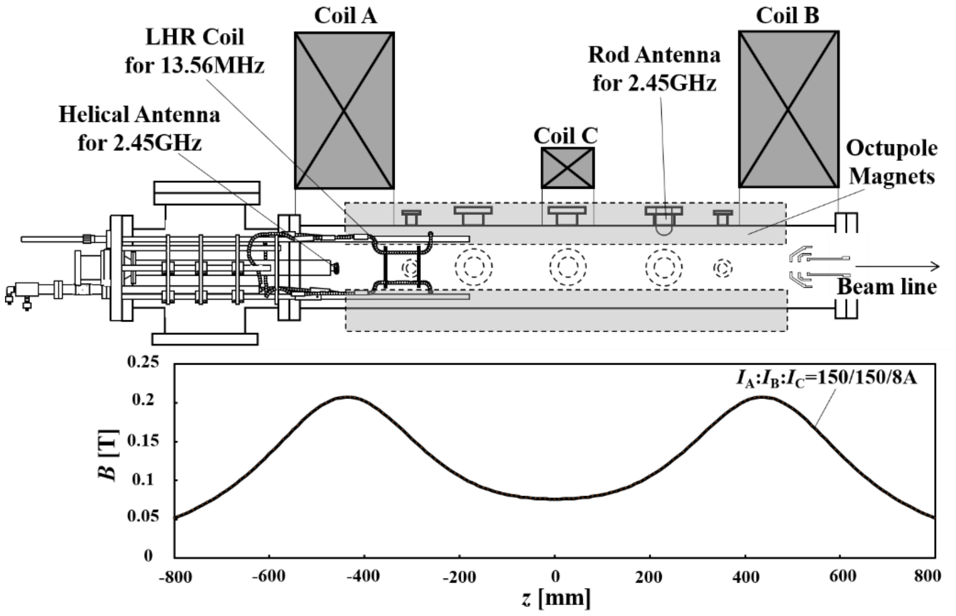

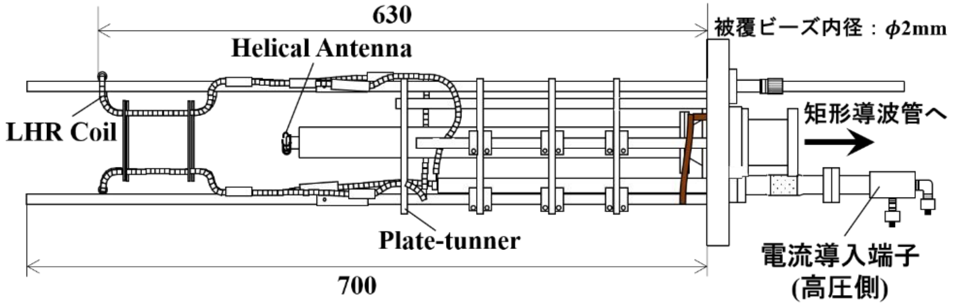

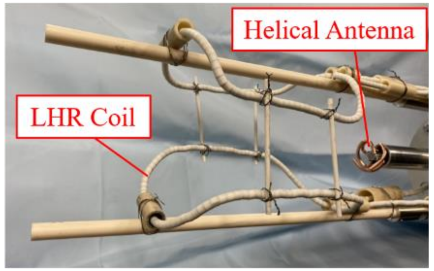

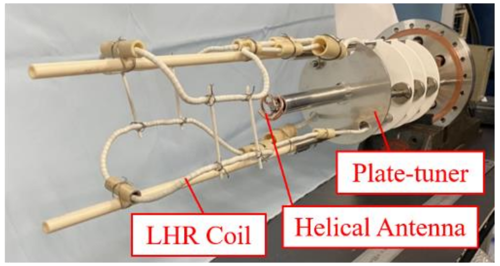

Xe^{7+} vs pulse duration in pure Xe & Xe+Ar

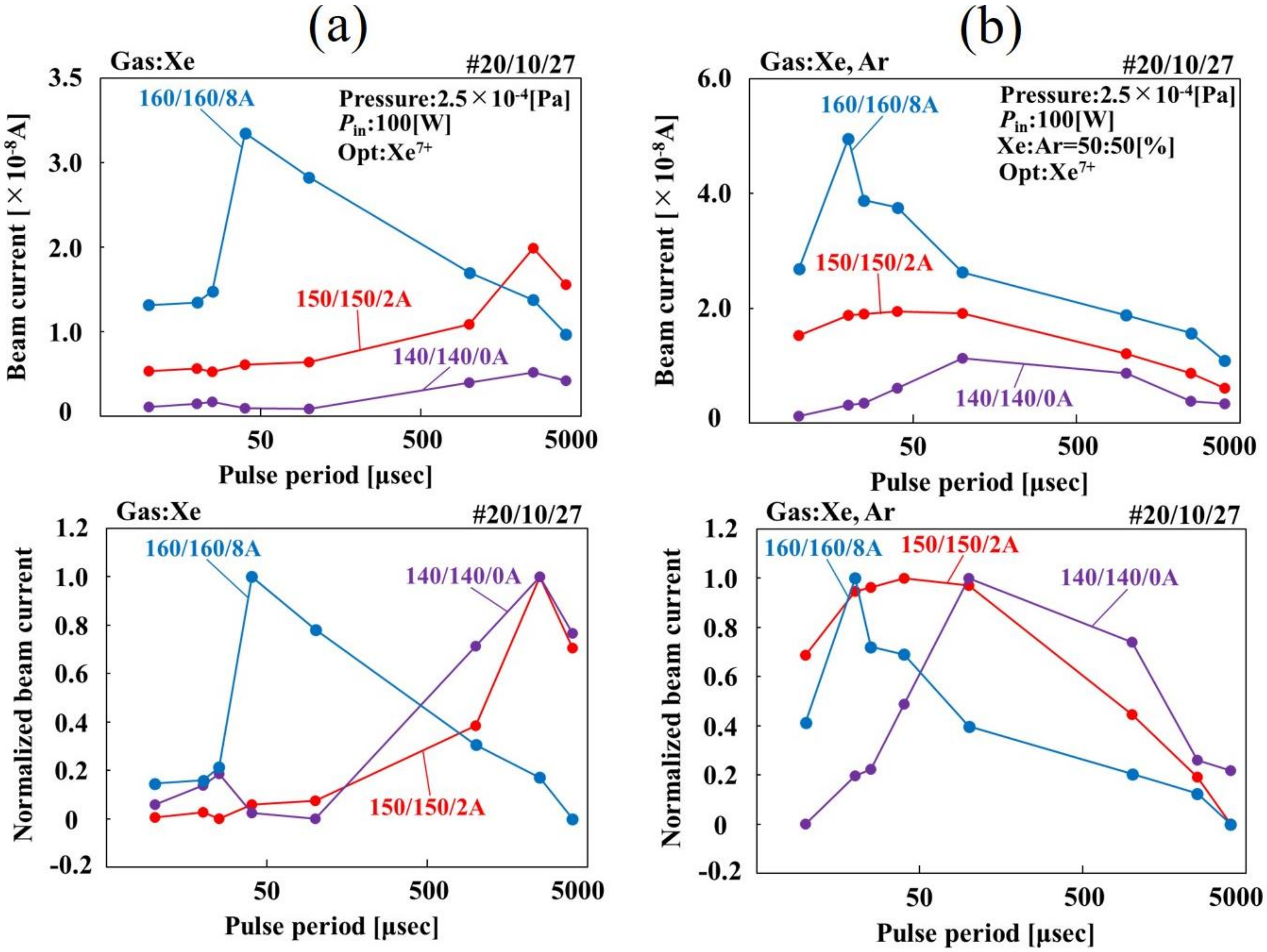

Fig. 4. Xe^{7+} *vs* pulse duration in pure Xe & Xe+Ar

Setting of ICR antenna to ECRIS & mirror field distribution

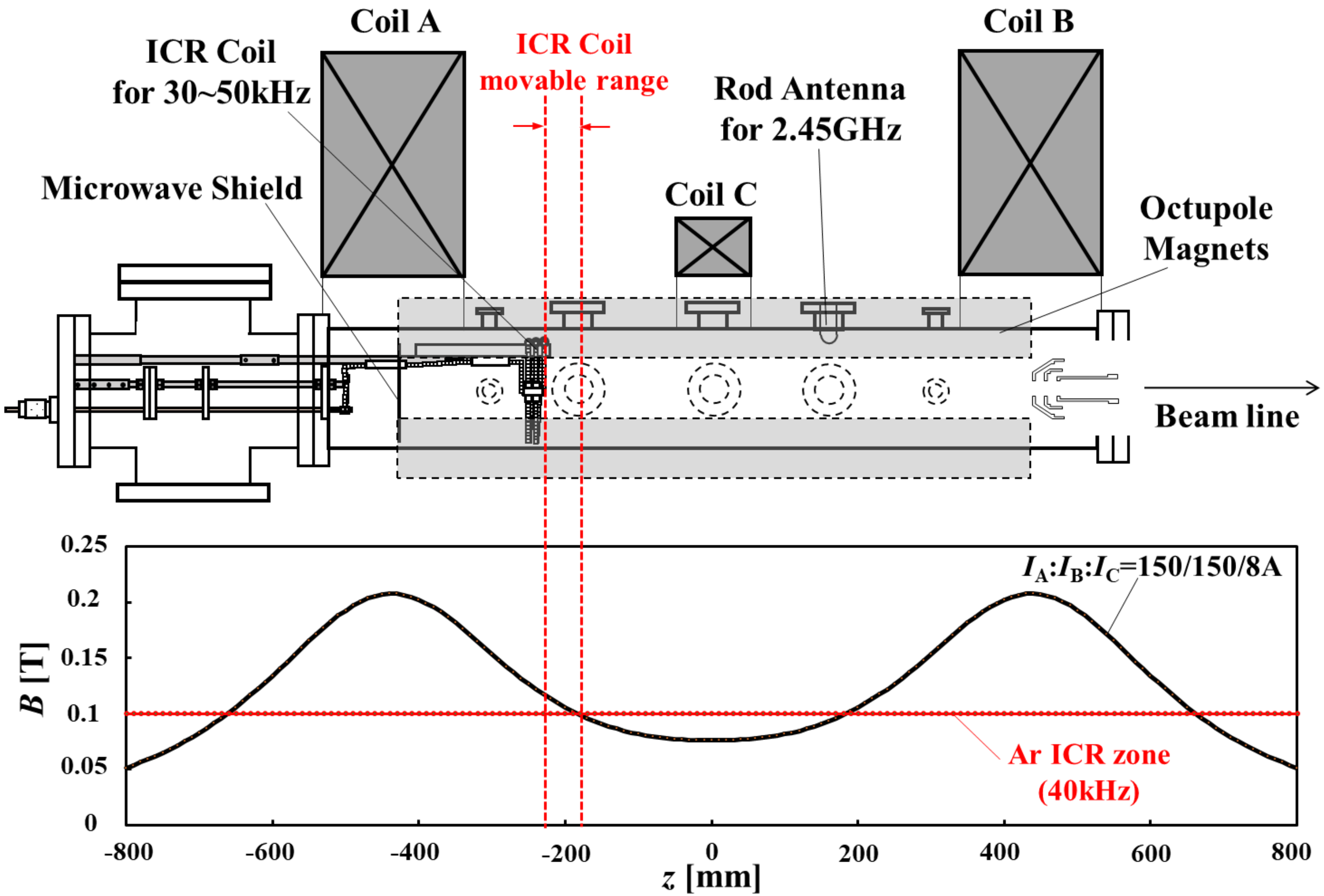

Fig. 6. Installation of ICR antenna at ECRIS (Osaka Univ.).

ICR Coil detail figure & photographs

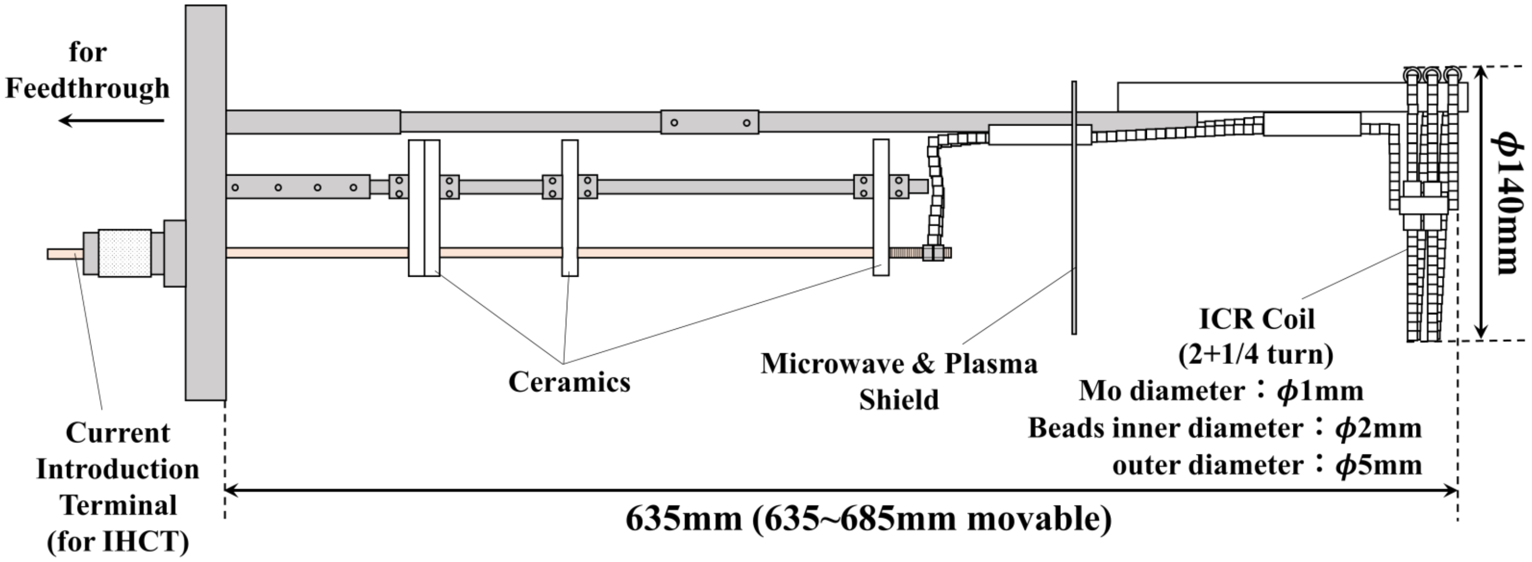

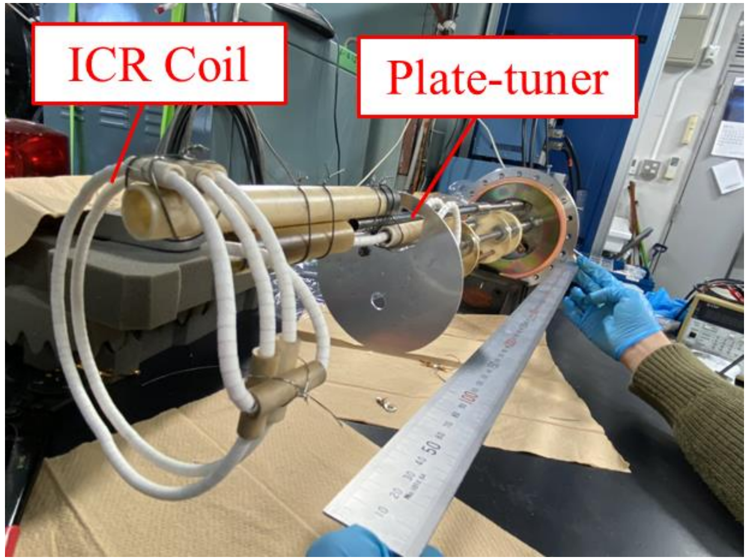

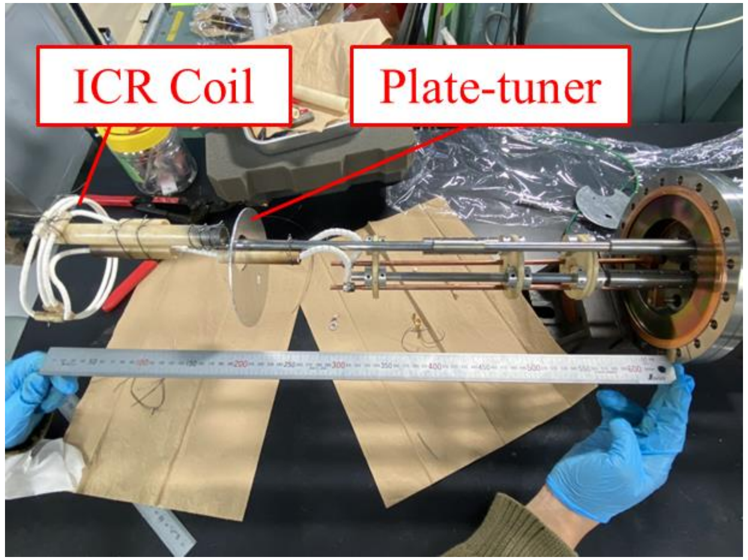

Fig. 7. ICR Coil detail figure & photographs

Low frequency RF power supply & RF introducing part into ECRIS

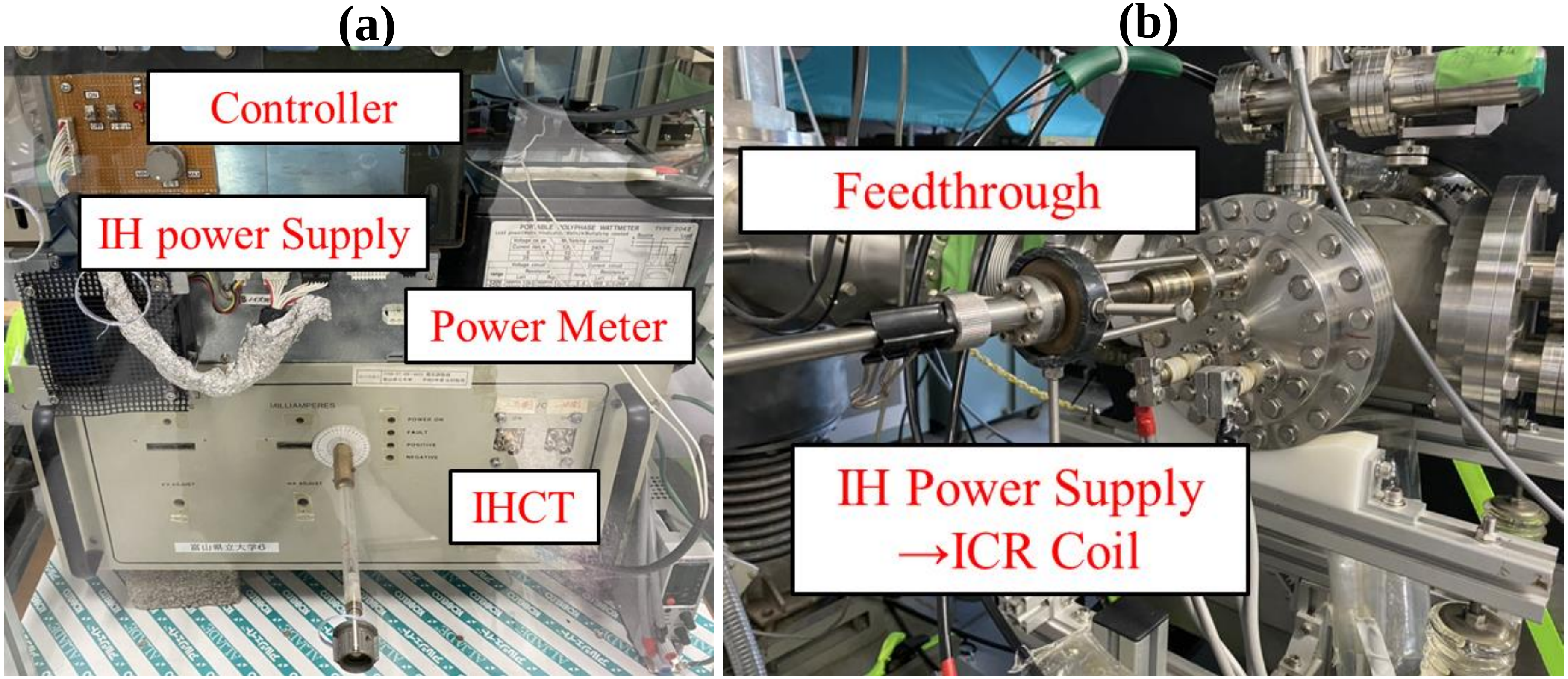

Fig. 8. Low frequency RF power supply & RF introducing part into ECRIS

■ Xe^{7+} & ⟨q⟩ in case A ($I_A/I_B/I_C$=150/150/8A)

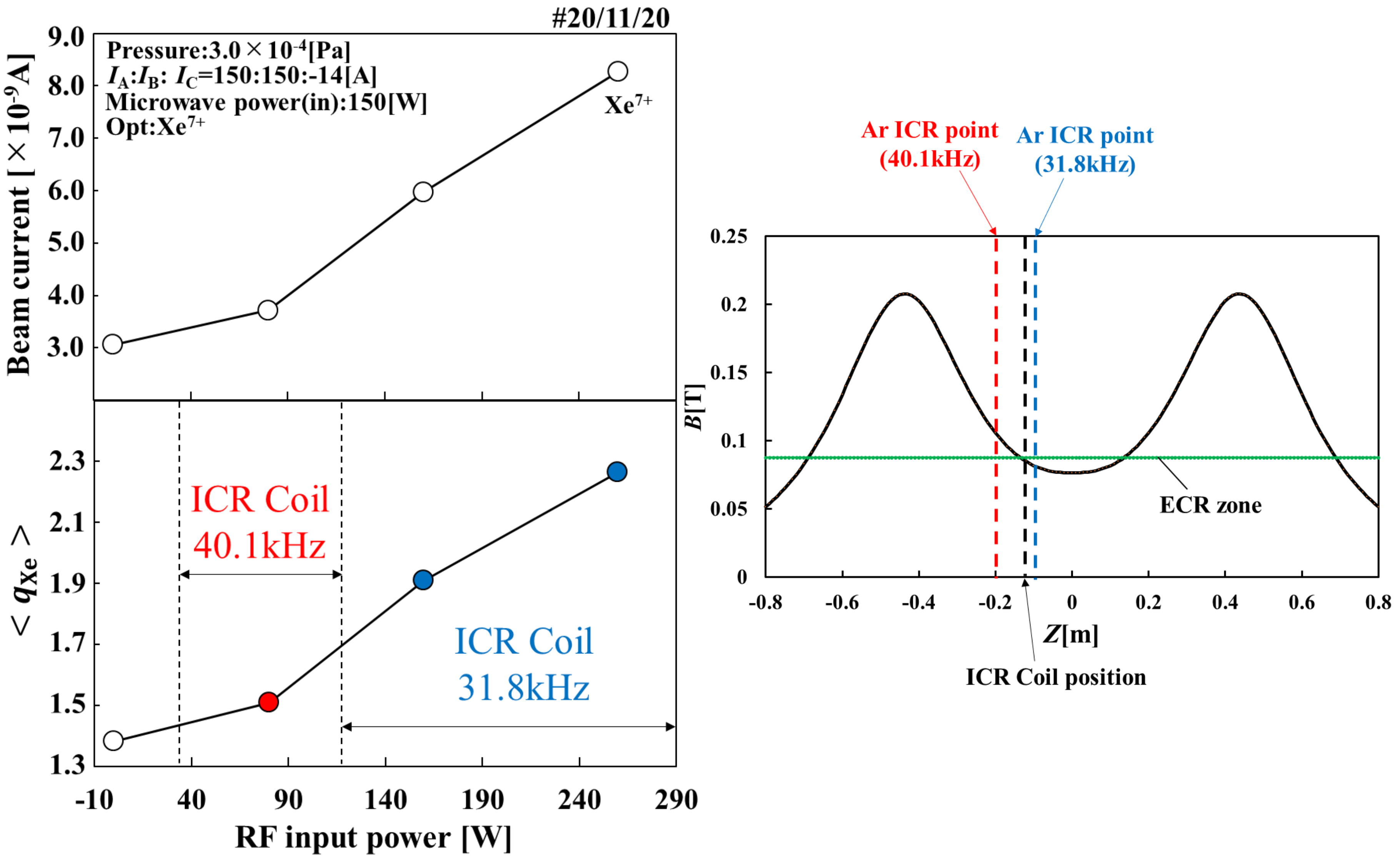

Fig. 10. Xe^{7+} & average charge state <q> in case A ($I_A/I_B/I_C$=150/150/8A)

ICR Exp. preparation status

- RF AMP・Matching box・Isolation transform (20kHz–1MHz, 300W, (Opt.40kHz&400kHz)):
  - Ordered 23 Dec. 2022(R4), delivered 14 July 2023(R5)
  - Adjustment according to load 21 Feb. 2024(R6)
- ICR antenna (108 ϕ 6turn 4 ϕ Cu pipe covered by ceramic spraying):
  - Ordered 28 Sept. 2023(R5), delivered 14 Jan. 2024(R6)
  - Installed to ECRIS 3 Feb. 2024(R6), two Helical antennas at the same time.
- Currently in progress:
  - Ar+He+RF(400kHz) with ε_{rms} & LP1&2: Serious contamination with impurities
    - Confirm the heating effect of He+ , Changes in plasma parameters are not obvious
  - Ar(40kHz): relaxations of potential well are not clear.
  - Xe+Ar+RF(40kHz): slightly effective & confirming Ar+ heating & parameters' changes not clear
  - Xe+He+RF(40kHz): drastic effects

Please refer to Fujimura-san's oral presentation!

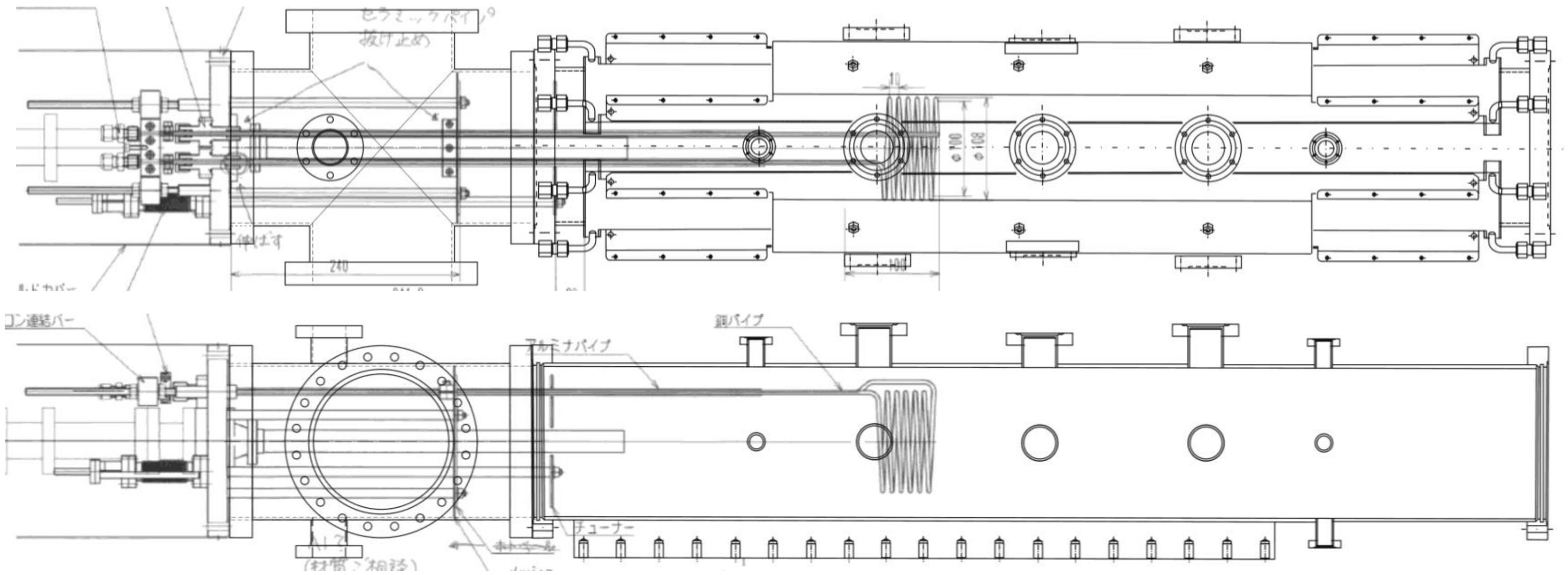

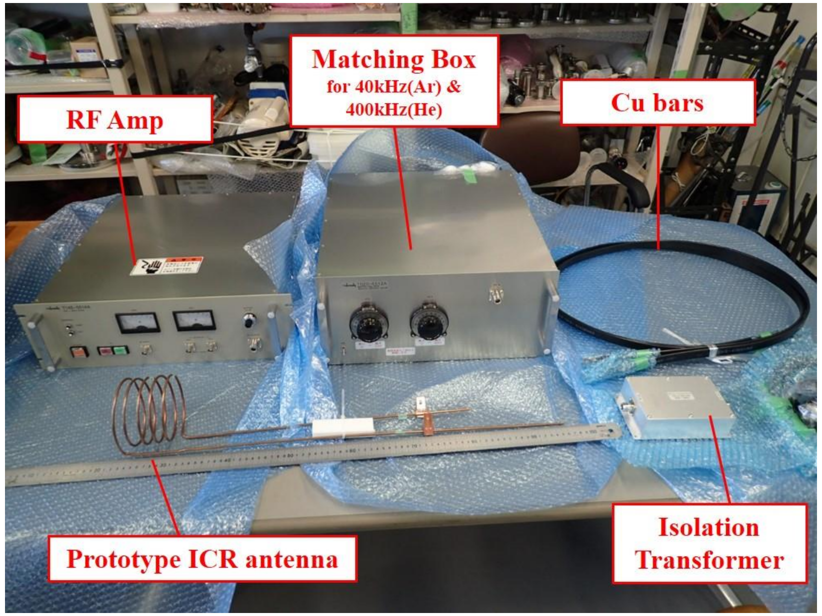

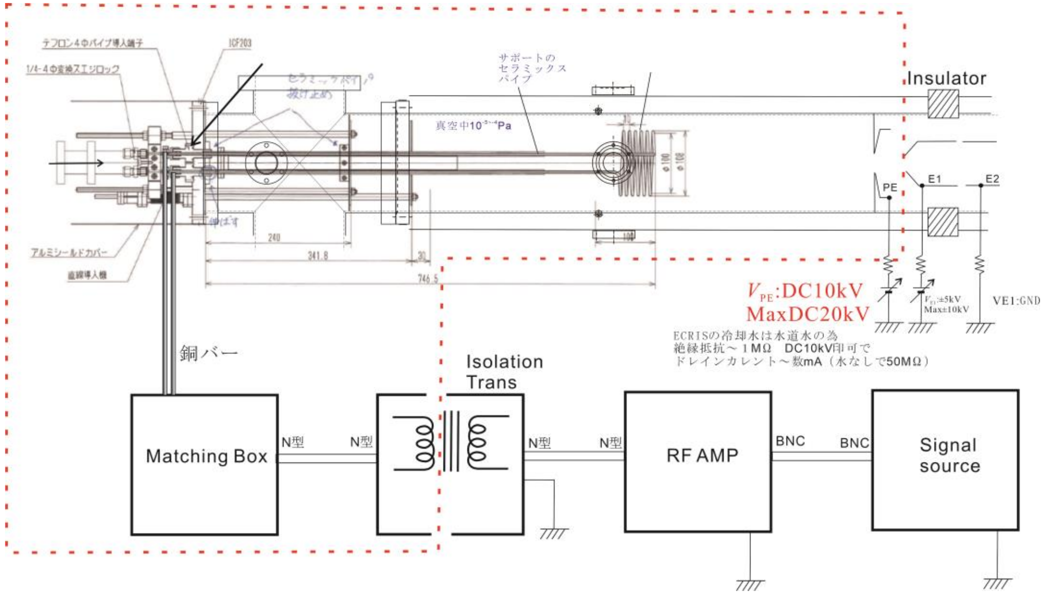

Please refer to Fujimura-san's oral presentation!

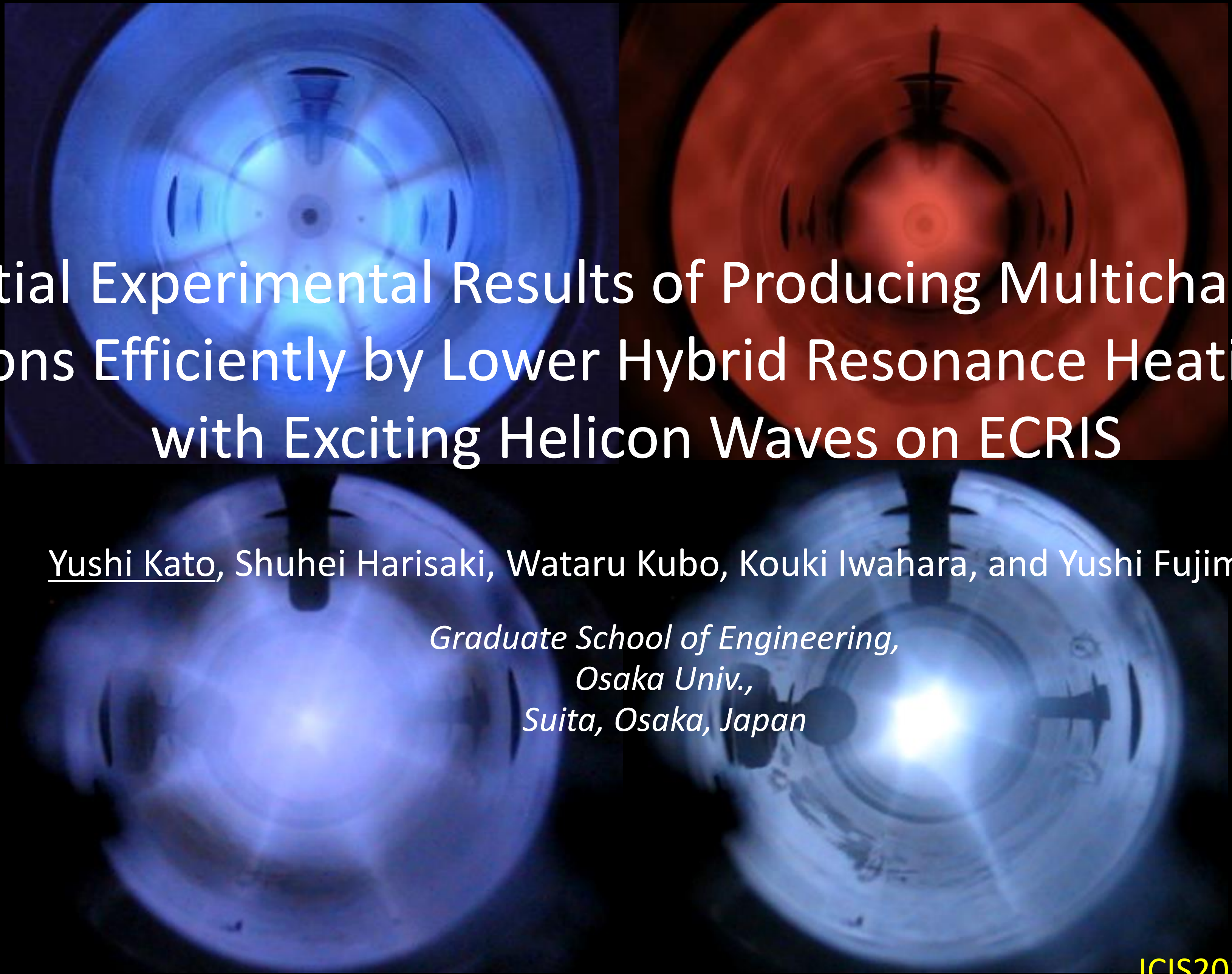

Initial Experimental Results of Producing Multicharged Ions Efficiently by Lower Hybrid Resonance Heating with Exciting Helicon Waves on ECRIS

Yushi Kato, Shuhei Harisaki, Wataru Kubo, Kouki Iwahara, and Yushi Fujimura

Graduate School of Engineering,
Osaka Univ.,
Suita, Osaka, Japan

ICIS2023, Victoria, BC, Canada

Brief theoretical background II:

- ***Dispersion relation of lower hybrid resonance (LHR):***

- $$\frac{1}{\omega_{\mathrm{LH}}^2} = \frac{1}{\omega_{\mathrm{pi}}^2} + \frac{1}{\omega_{ce}\omega_{ci}}$$

$\because \omega_{\mathrm{pi}}^2 \gg \omega_{\mathrm{ci}}^2$ & $\omega_{ci} \ll \omega_{\mathrm{LH}} \ll \omega_{ce}$,
$\omega_{\mathrm{pe}} \sim \omega_{\mathrm{ce}}$, $\omega_{\mathrm{pi}} \sim (M/m)^{1/2}\omega_{\mathrm{ci}}$,

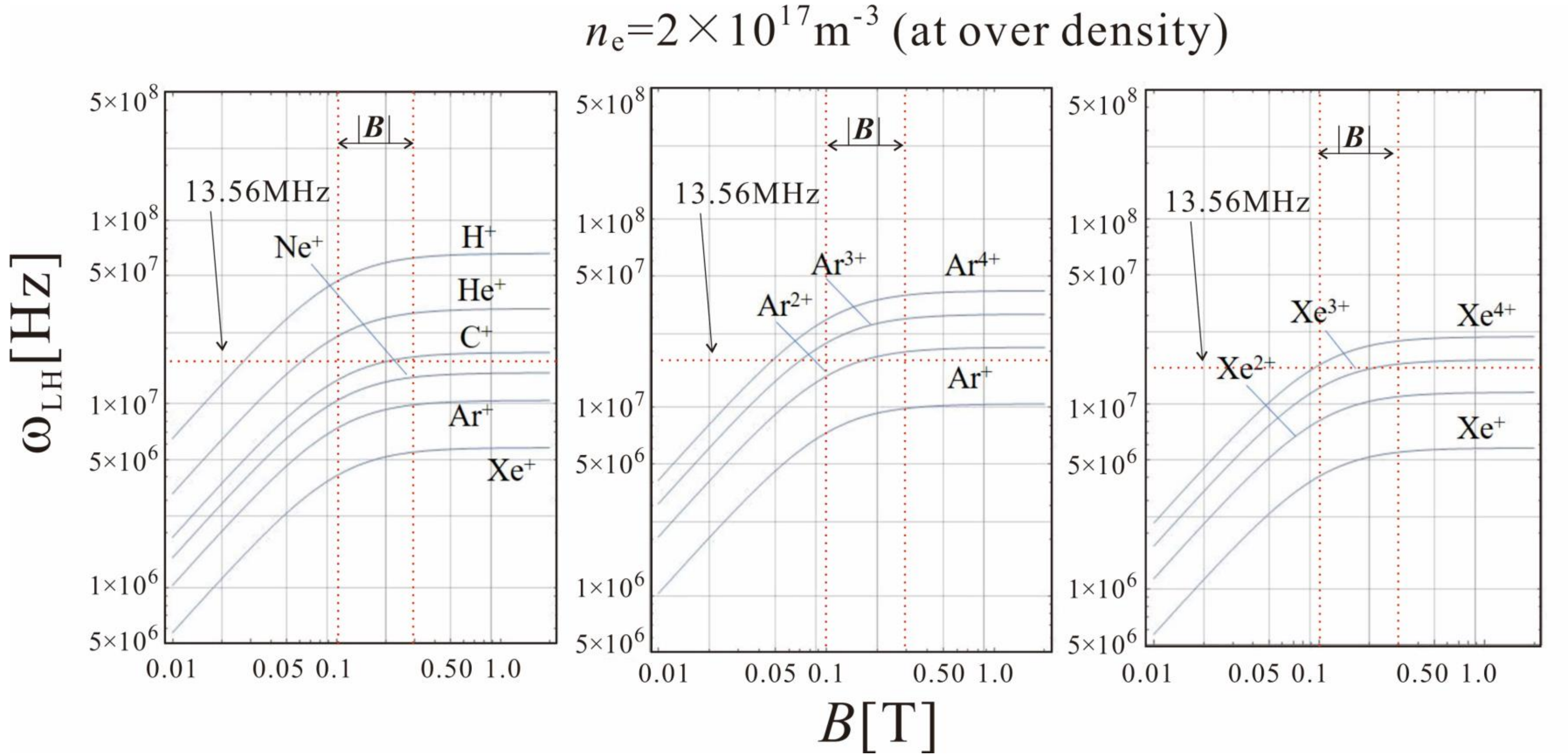

- By using available13.56 GHz RF source in the initial experiment,
- The |***B***| around our 2.45 GHz ECRIS ($|\boldsymbol{B}_{\mathrm{ECR}}|$=0.0875G) is about 0.1-0.3 T.
- Ion species in which the LHR region exists are ones lighter than C^+, $Ar^{2+\sim}$, $Xe^{3+\sim}$.
- In our ECRIS, averaged Ar <q^+> is about 2~4, so the LHR is sufficiently possible.

Guiding principles of saddle-coiled antenna for LHR via exciting helicon waves

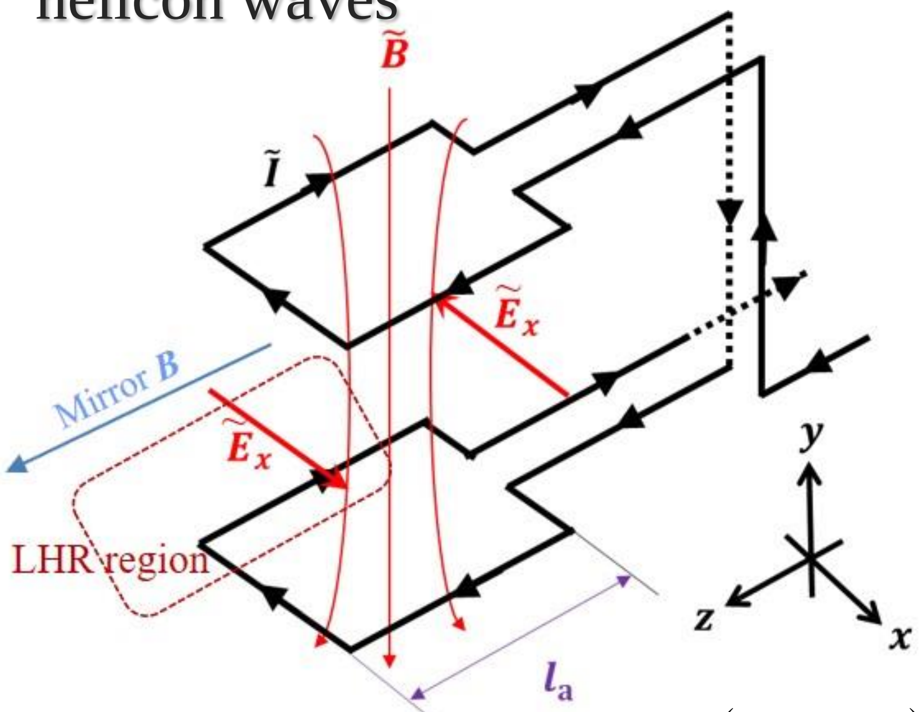

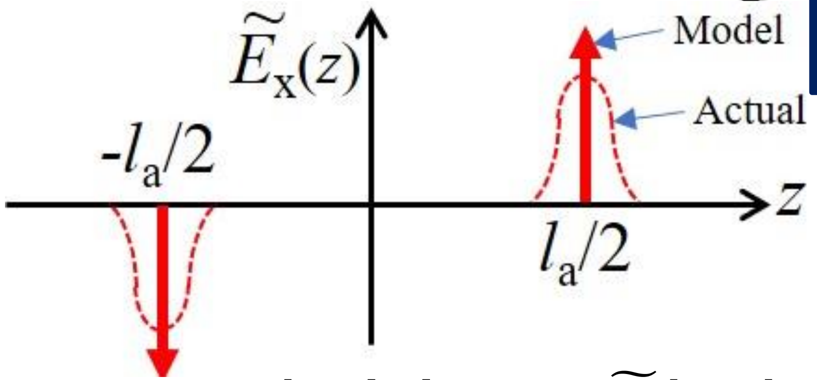

- Assuming the ideal antenna $\widetilde{E_x}$ has sharp δ-function peaks at both ends of the coil, we consider the following electric field:

$$\widetilde{E_x}(z) \approx \widetilde{E_{x1}}\Delta z\left[\delta\left(z+\frac{l_a}{2}\right)-\delta\left(z-\frac{l_a}{2}\right)\right]$$

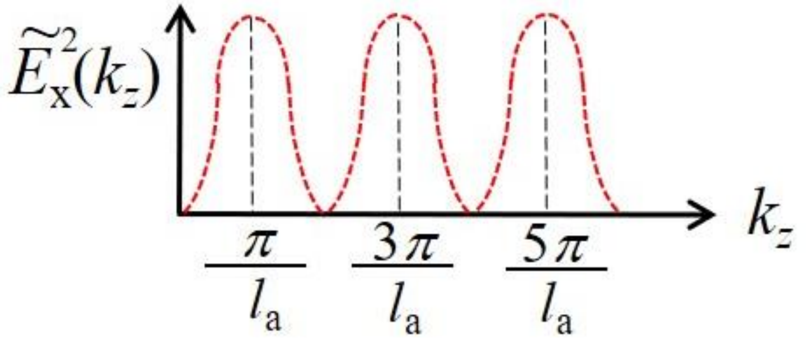

- Helicon wave modes: mixtures of EM $(\nabla\cdot\boldsymbol{E}\approx 0)$ and quasi-static $(\nabla\times\boldsymbol{E}\approx 0)$ fields having form:

$$\boldsymbol{E},\boldsymbol{H}\propto \exp i\,(\omega t - k_{/\!/}\, z - m\theta),$$

where integer m specifies azimuthal modes.

- Assumption: uniform n_e and the boundary condition (Chen[9]):

$$mkJ_m(k_\perp R)+k_{/\!/}J_m'(k_\perp R)=0,$$

- where J_m' denotes derivative of Bessel function J_m.
- Here we apply a typical saddle-coiled antenna with m=1 mode excitation according to Leiberman. [7]

- By Fourier transforming and squaring, the spatial power spectrum can be obtained as follows: $E_x^2(k_z)\approx 4\widetilde{E_{x1}}^2(\Delta z)^2\sin^2\frac{k_z l_a}{2}$.
- When $k_z\approx\pi/l_a$, $3\pi/l_a$, etc., and then when $\lambda_z\approx 2l_a$, $2l_a/3$, etc., the antenna is well coupled to the helicon mode, and $E_x^2(k_z)$ is maximized.

Wavelength matching condition for helicon wave excitation

(This fig. shows dispersion relations for typical densities & 13.56MHz RF freq.)

Dispersion relations of helicon modes:

Fast wave($N_\perp$: small $(k_\perp \lesssim k_{/\!/})$):

$$c^2 k_\parallel \sqrt{k_\parallel^2 + k_\perp^2} \simeq \omega\omega_{\mathrm{pe}}^2 / \omega_{\mathrm{ce}}$$

Slow wave($N_\perp$: Large $(k_\perp \gg k_{/\!/})$):

$$\omega \simeq \sqrt{\frac{\omega_{\mathrm{pe}}^2\omega_{\mathrm{ce}}^2}{\omega_{\mathrm{pe}}^2 + \omega_{\mathrm{ce}}^2}}\frac{k_\parallel}{k_\perp}$$

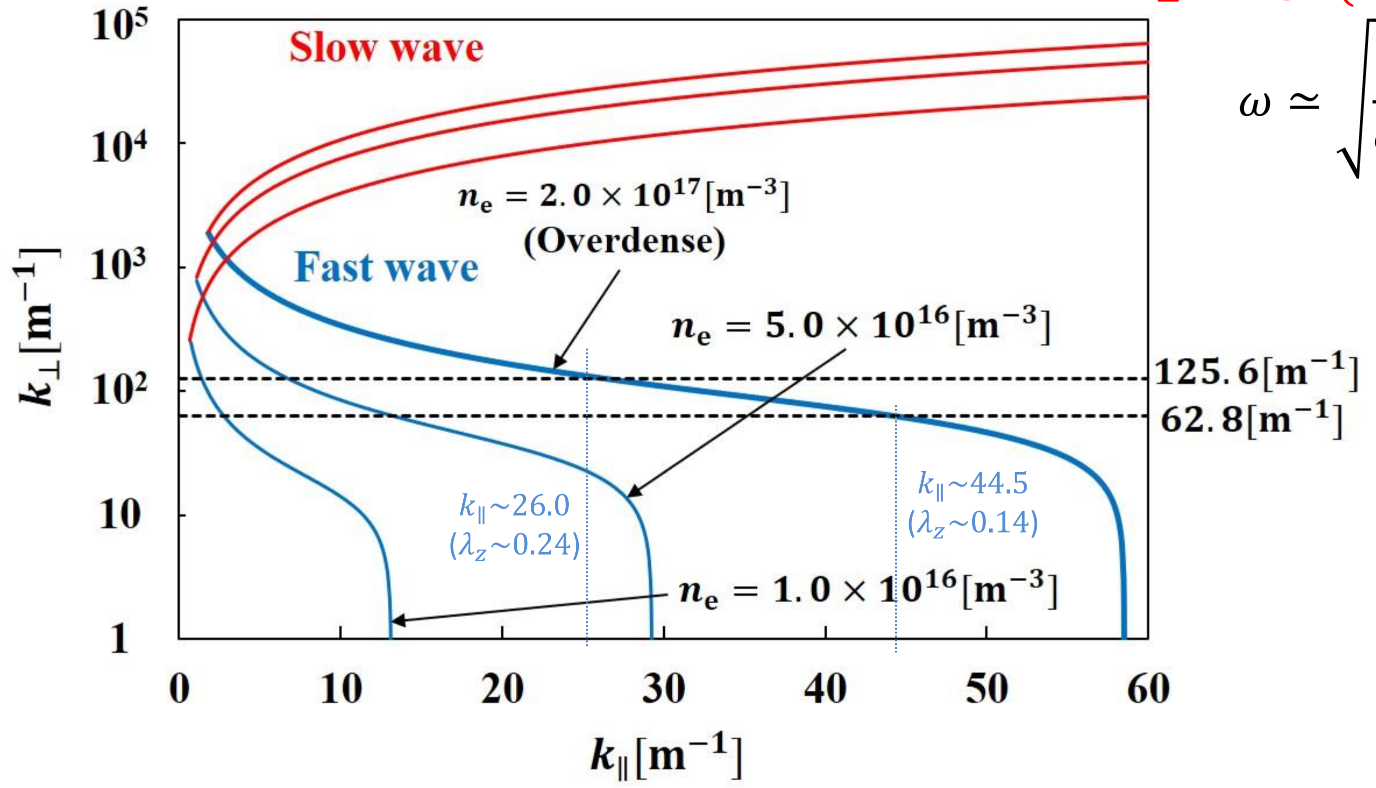

($\lambda_\perp\sim0.05\sim0.1$m ∵ Considering the plasma diameter)

- Assuming the wavelength of the radial electric field is about $\lambda_\perp$≒**0.05~0.1m, *i.e.*, $k_\perp$≒125.6~62.8m^{-1}**, considering the plasma diameter.
- We aim to excite helicon wave at high density n_e **= 2 × 10^{17} m^{-3}** in high microwave power operation, we obtained the corresponding **$k_{/\!/}$≒26.0~44.5m^{-1}, and λ_z≒0.24~0.14**.
- By using $E_x^2(k_z)$ maximized conditions (**k_z≈π/l_a, 3π/l_a, etc.**, and then **λ_z≈2l_a, 2l_a/3, etc.**), We determined **the axial coil length l_a = 0.12m and the radial length l_b = 0.1m actually**.

Saddle-coiled LHR antenna exciting helicon waves

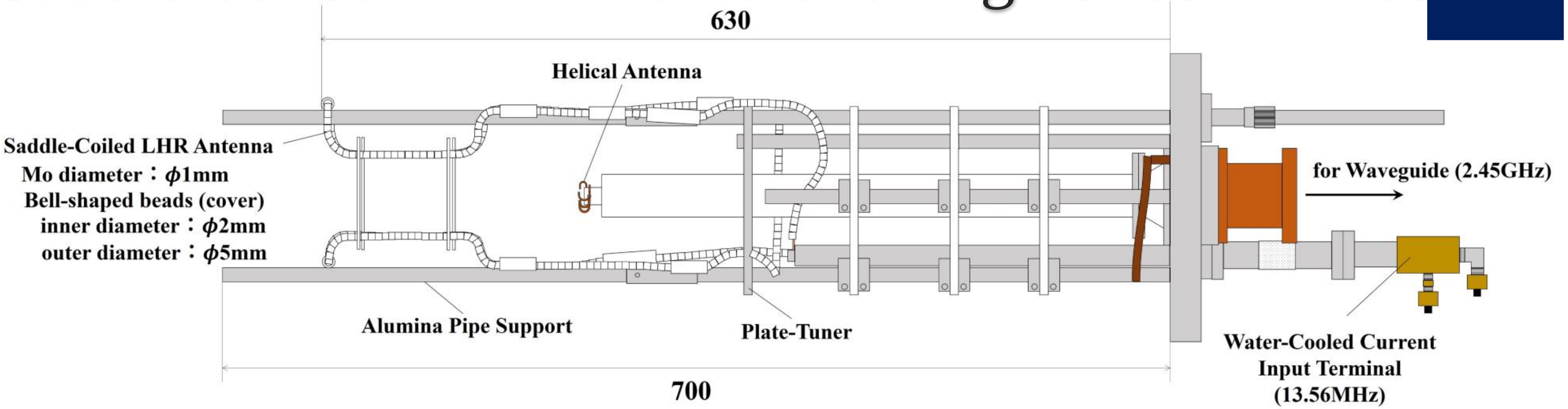

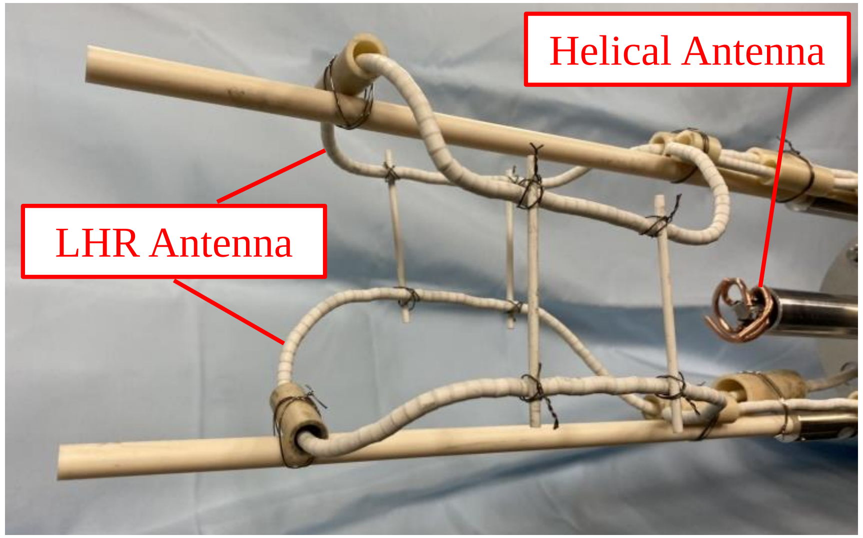

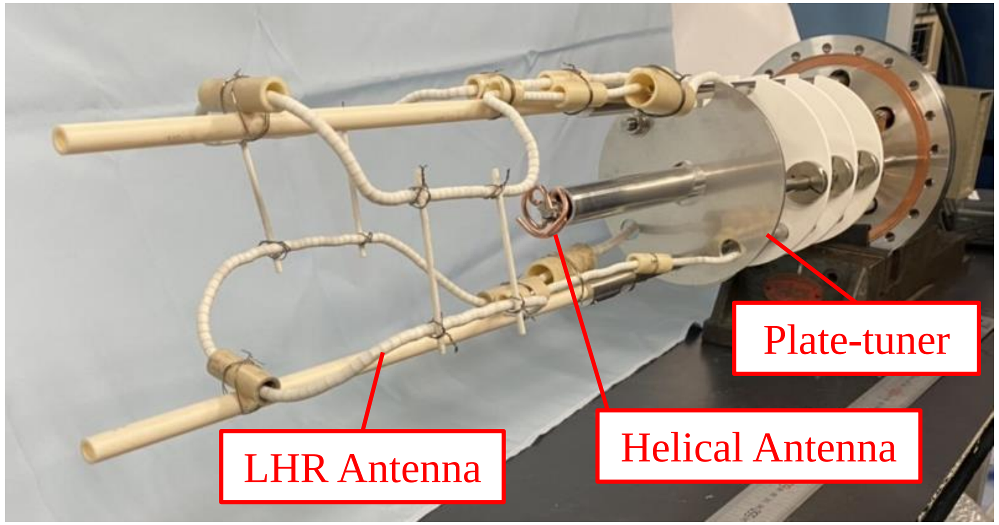

Connections of the saddle coil are made behind the plate tuner,
so as not to affect the X-mode electric field as much as possible.

Please refer to Y Kato, et, al, Journal of Physics: Conference Series 2743 (2024) 012004, doi:10.1088/1742-6596/2743/1/012004

13.56MHz RF power source & matching box

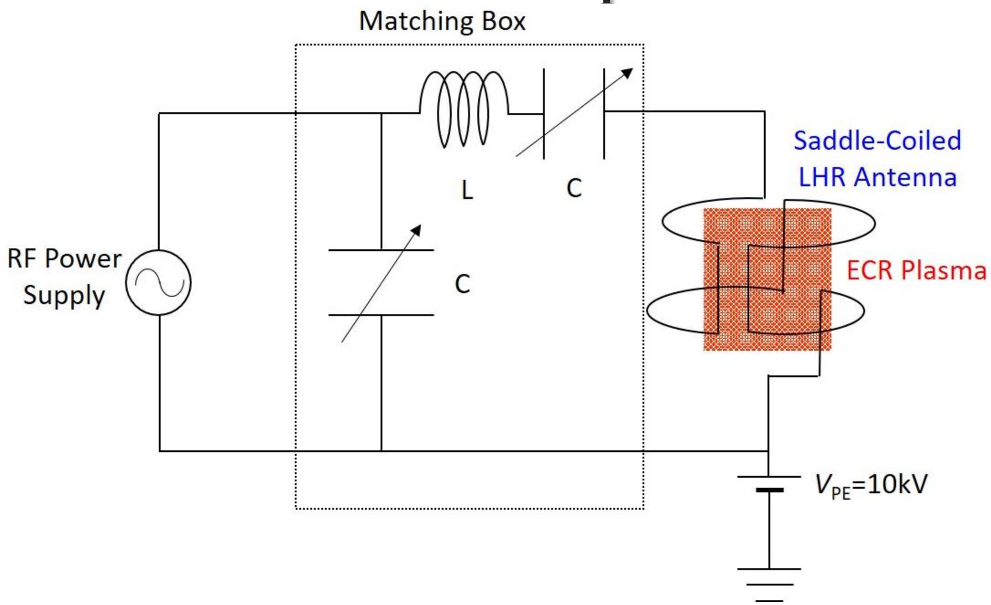

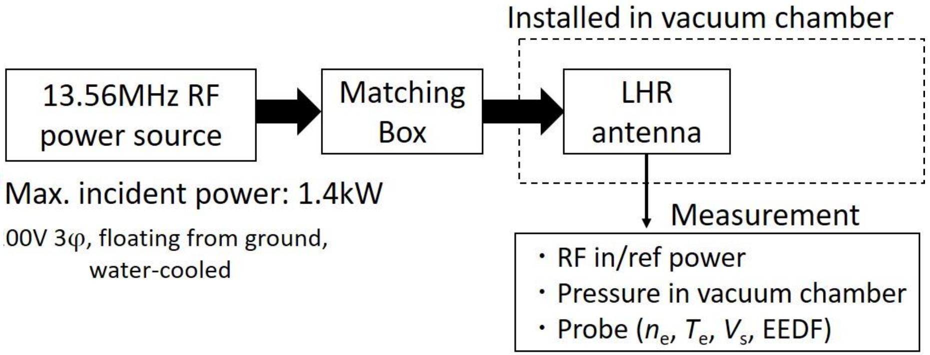

Max. incident power: 1.4kW

00V 3φ, floating from ground, water-cooled

We conducted the initial experiment from February to March 2021 by fabricating the RF lead-in, after initial ICR and measurement experiments to verify L-cutoff.

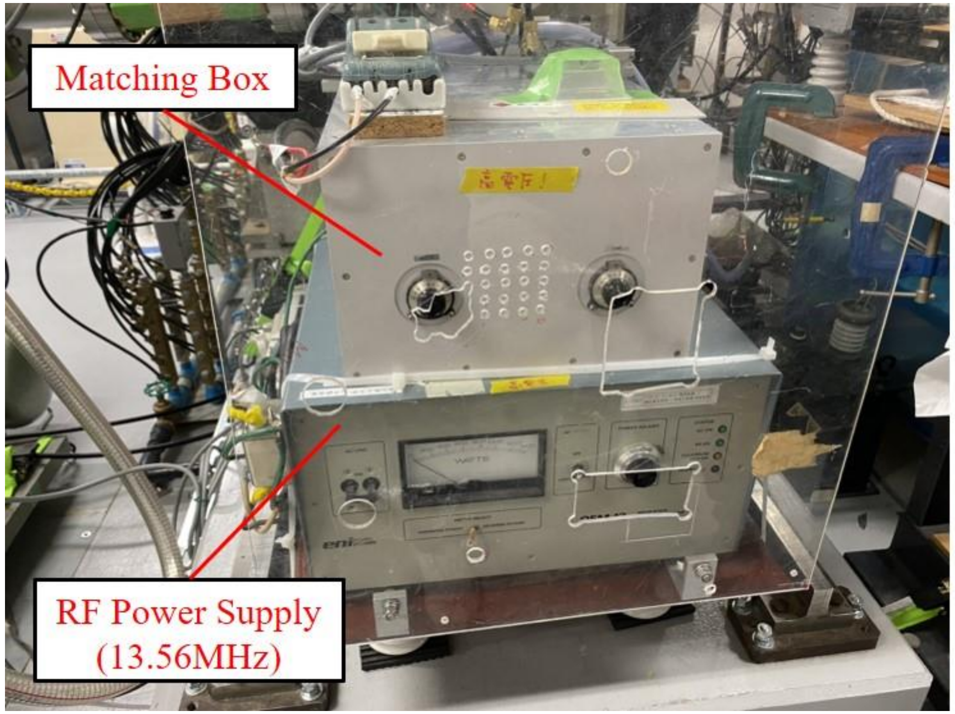

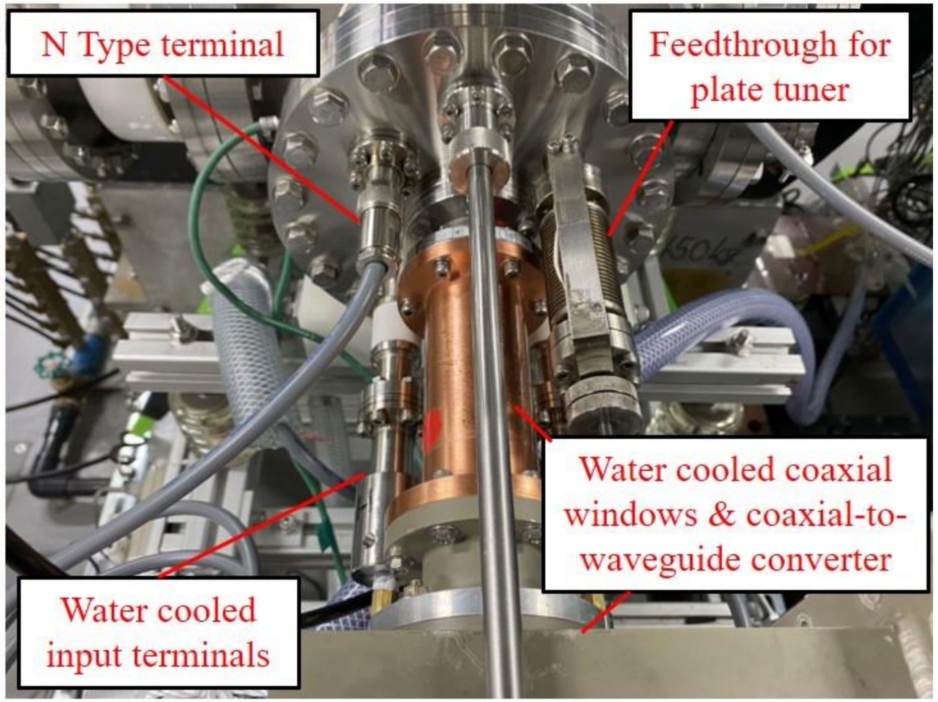

Typical CSD (in first experiment (best condition))

It indicates the effect of RF application with good reproducibility.

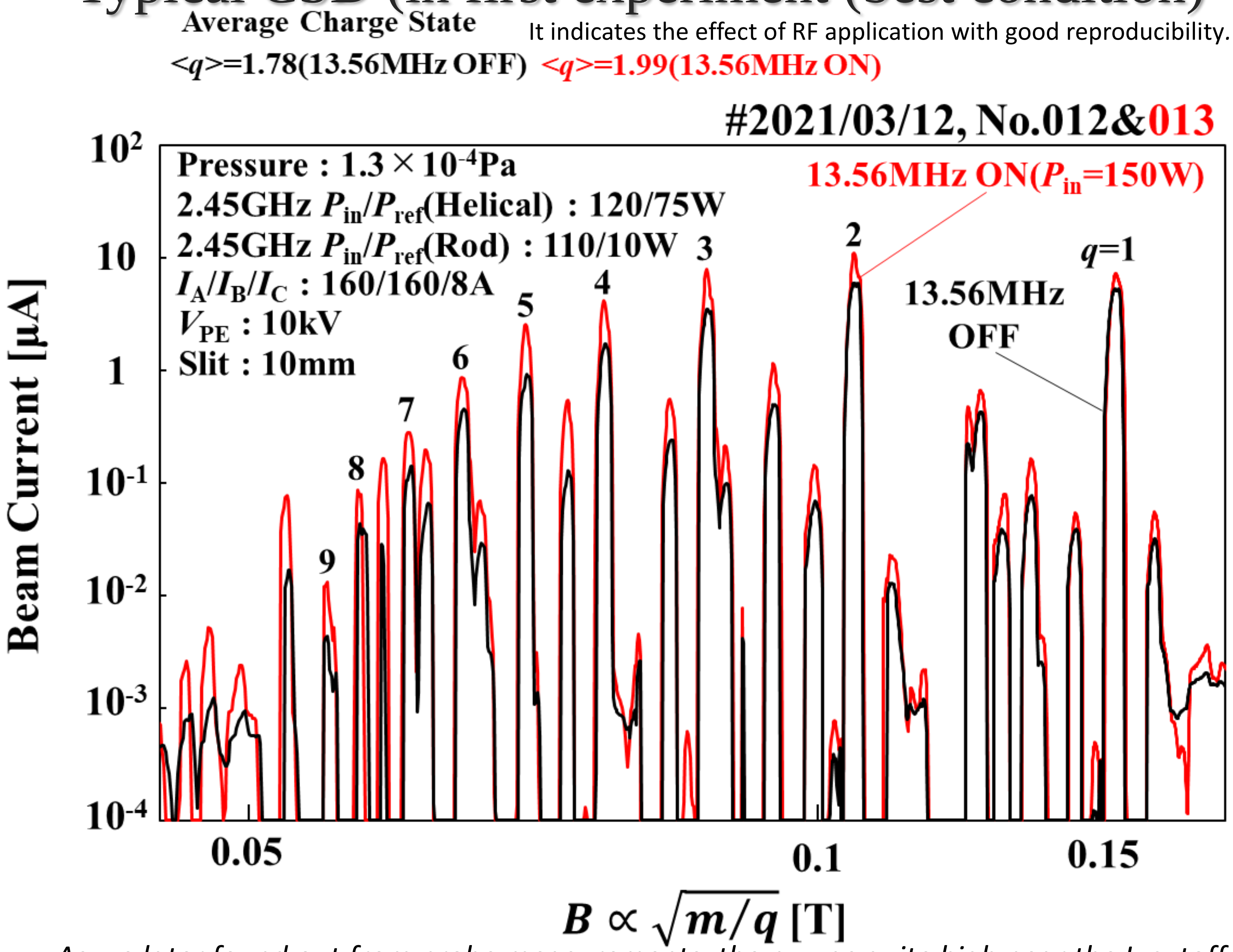

As we later found out from probe measurements, the n_e was quite high near the L-cutoff.
The RF application clearly increases multiply charged ion currents and shifts the average charge state to the higher side, and these results suggest an increase of the electron temperature T_e.

The Low Frequency RF Power Dependences of $Ar^{8+,9+}$ Currents.

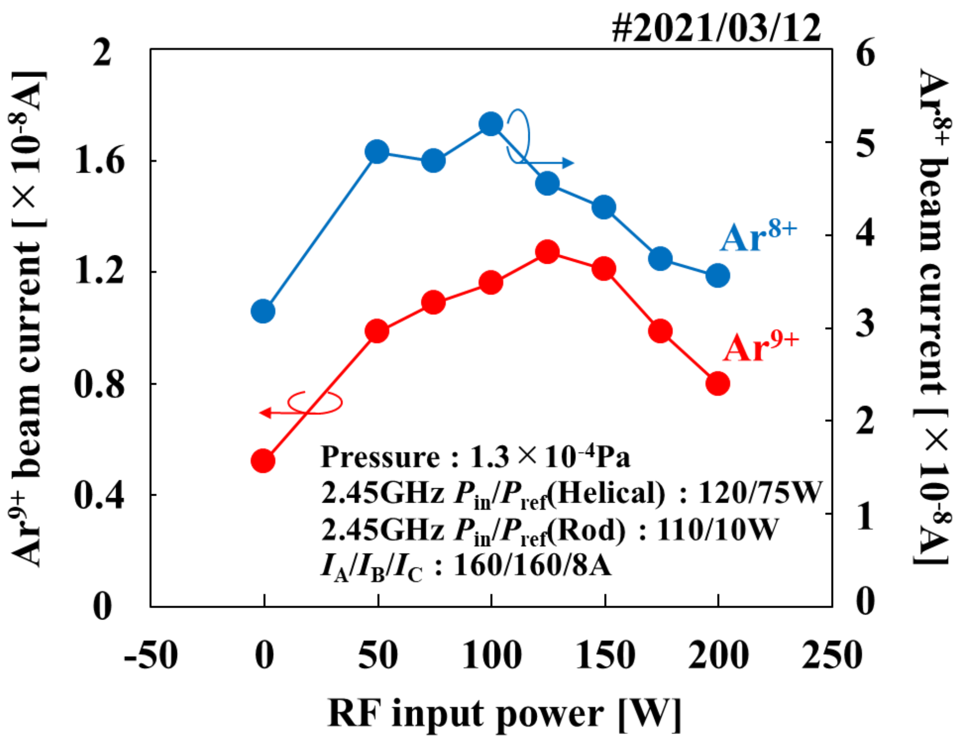

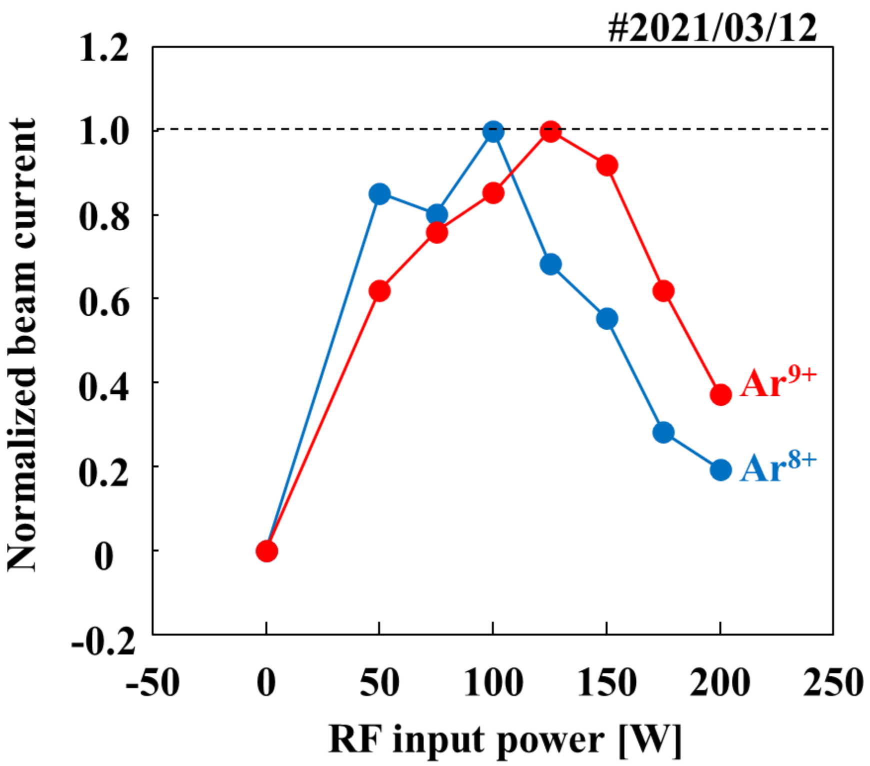

From 100W to 150W, the charge state clearly shifts to the higher side.
It suggests an increase of T_e due to LHR based on helicon wave excitation.

We Measured Electron Energy Distribution Function (EEDF)

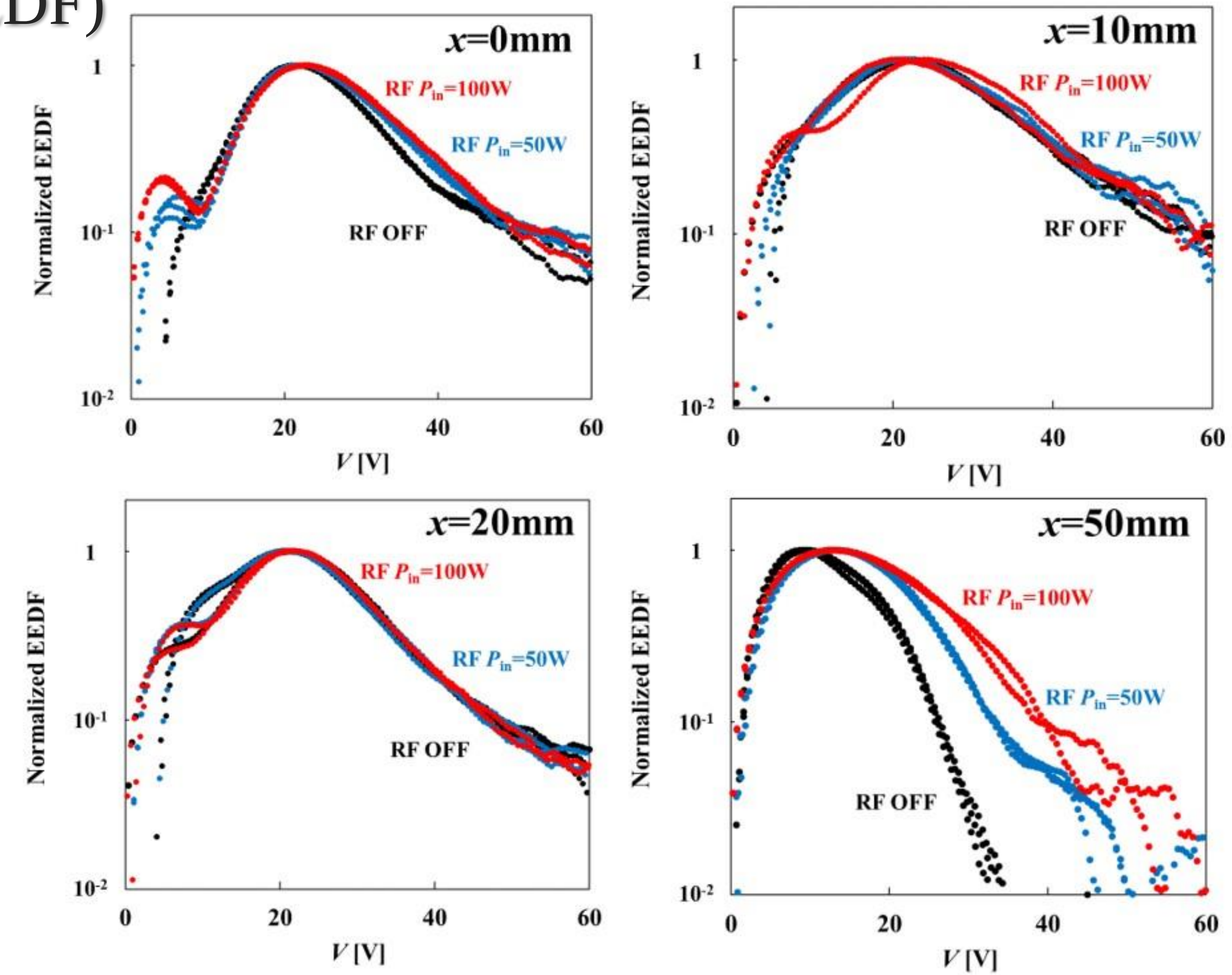

A distinct shift to the higher energy side was observed in the periphery compared to that in the center.
This result has a good correspondence with conventional T_e measurements. From the later accessibility considerations, it corresponds to the presence of LHR region in the periphery, suggesting the increase in T_e due to the LHR.

Typical Probe Measurements (high RF power)

A15

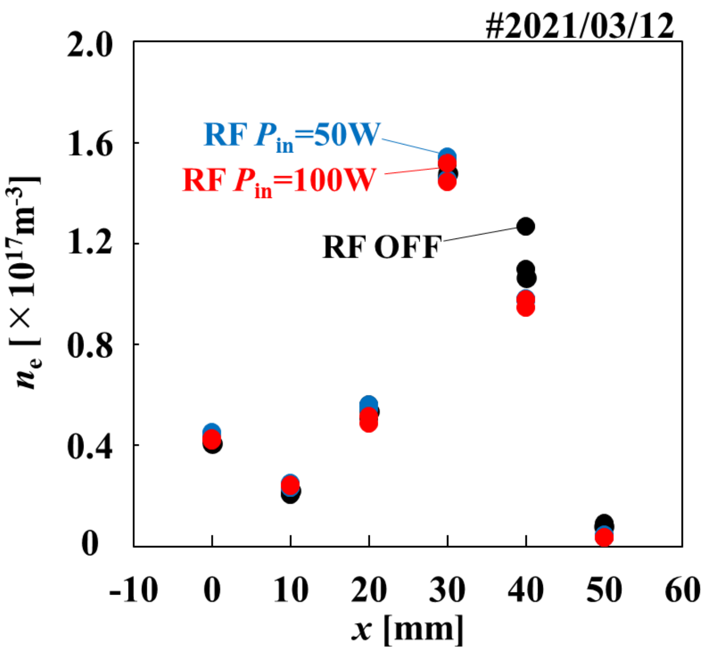

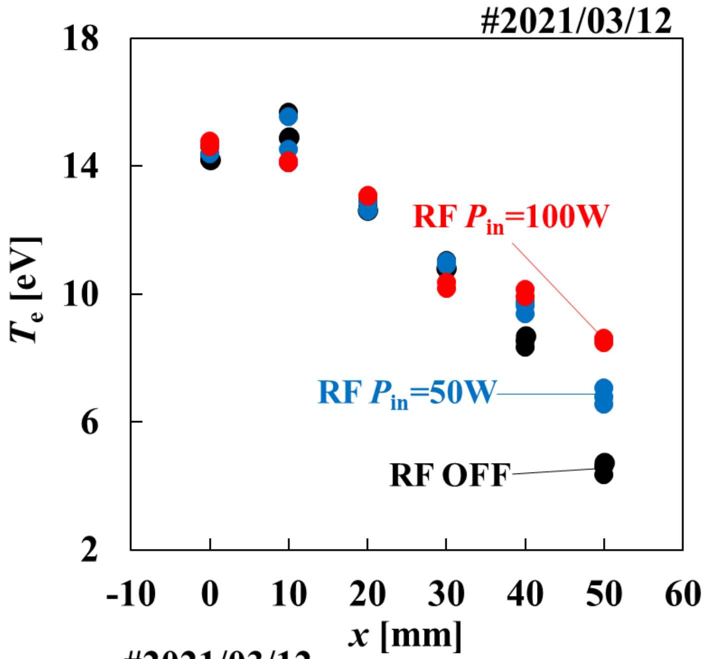

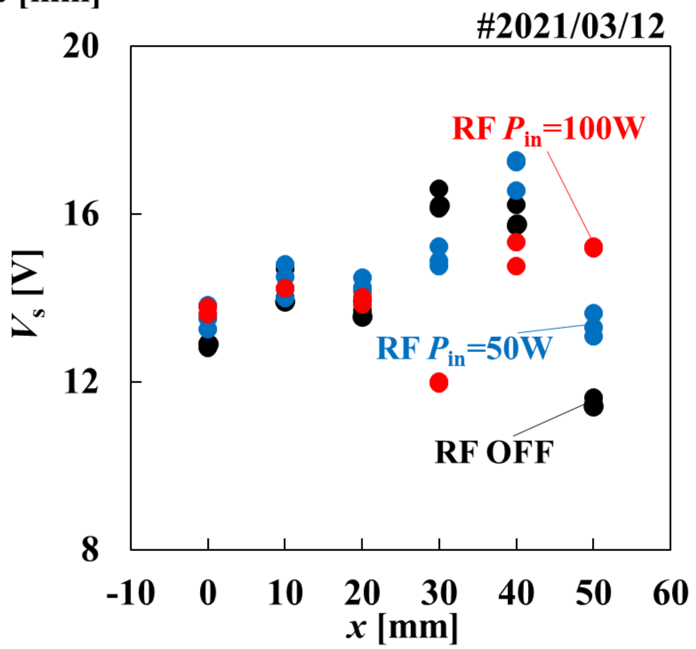

Accessibility Condition
(corresponding to the best condition CSD)

n_e= 2.50 × 10^{17}m^{-3} (obtained by measurements as the same conditions)

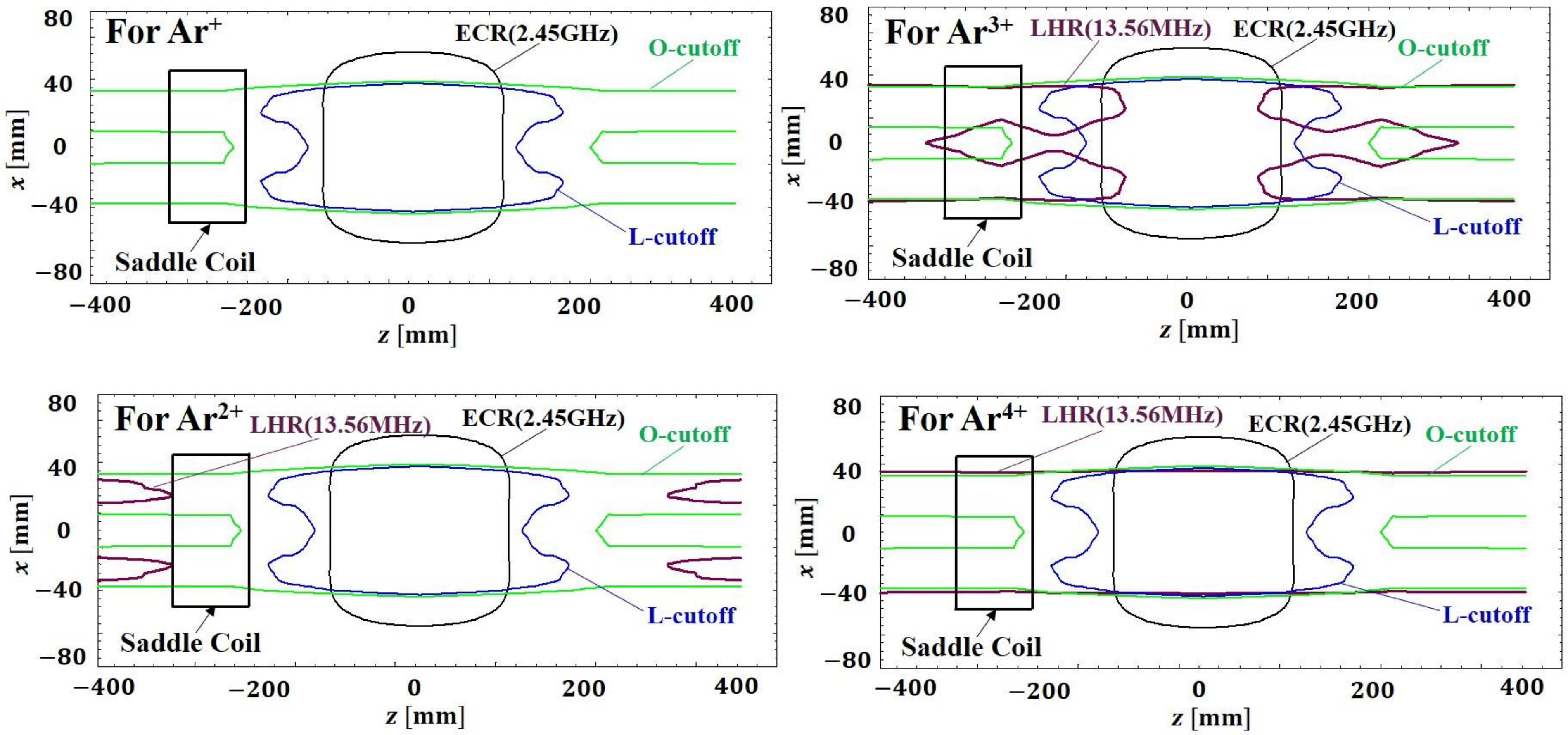

Because the average charge state is about 2+~4+,

the LHR may be generated by the X-mode electric field of the helicon wave.

The electron heating by the LHR should be effectively contributed to produce multiply charged ions.

This result shows a good agreement with the result of EEDF and the T_e measurements.

Future aspects for further improving their performances

Increasing freq. & B,

and multi-frequencies including dual-modes with helical antenna exciting R-waves

‘Plasma diagnostics’: European trend of ECRIS

Additional Electron (or plasma) beams

Measurements on high performance ECRIS’s

EMS emittances and Ion sensitive probes & multi-grid FC

Summary

- Acting directly towards electrons (royal road!)
  - Enhancing ECR efficiency:
    - Overcoming R-cutoff constraint: *Dual ECR*
    - R-wave efficient excitation: *Helical antenna*
    - Differences from multi-f. μWs introduction / Stabilization for instabilities
    - Upper/*Lower hybrid resonance* (UHR/*LHR*)
- Acting directly towards ions (maverick?)
  - Overcoming L-cutoff constraint: Low frequency RF
    - ICR: Selectively heating Low Z ions / Relaxation of *Potential well*
      - Ar + He (f = 400kHz), Xe + Ar (f = 40kHz) , Xe + He (f = 400kHz)
    - LHR: X-mode resonance via Helicon wave / or other way ? (MHz) (*e.g.* 13.56MHz)
    - Stabilization for instabilities?/ ion sensitive probes, Multigrid FC, erms ,interferometer, VUV, etc.
- Gas phase synthesis of Fe@C_{60}
  - Fe & C_{60} evaporation sources in the ECRIS
- Introducing electron beam/beam plasma with *EBEP*
  - Lowering the plasma potential (*i.e.* Drilling a hole in the potential well?)

→Please refer to Ide-san's poster presentation!

Reference books

- Magnetics & Equilibrium:
  - A.I. Morozov and L.S. Solov’ev, `The structure of magnetic fields`; Review of Plasma Physics II
  - V.D. Shafranov, `Plasma equilibrium in magnetic field`, *ibid*.
- Mirror Confinement: *ibid*, XII
- Transports:
  - B.A. Trubnikov, `Particle interactions in fully ionized plasma`, Review of Plasma Physics I
  - S.I. Braginskii, `Transport processes in a plasma`, ibid
  - L. Spitzer, Jr, `Physics of fully ionized gases`, Chap. 5.
- Accessibility conditions of μW:
  - Stix T H, *The Theory of Plasma Waves* (McGraw-Hill, New York, 1962).
  - Lieberman M A and Lichtenberg A J, *Principle of Plasma Discharges and Materials Processing*, 2nd Edit., A John Wiley & Son, Inc Publications, 2005, Chap.4, pp.110; *ibid*, Chap.13, pp.514.
  - F. F. Chen, *Plasma Phys. Controlled Fusion*, 33(1991)pp.339.
- Plasma diagnostics:
  - R. H. Huddelestone and S. L. Leonard, `Plasma Diagnostics Techniques`,
  - `Vacuum Ultra Violet Spectroscopy`
- Miscellaneous:
  - R. Geller, ‘Electron Cyclotron Resonance Ion Sources and ECR Plasma ’
  - J.S.Chang, R.M. Hobson, 市川幸美，金田輝男，`電離気体の原子・分子過程`
  - K. Miyamoto, `Plasma physics for nuclear fusion`
  - 提井信力「プラズマ基礎工学」

Acknowledgements:

The authors would like to thank

Emeritus Prof *Ishii S* (Toyama Pref Univ) and Emeritus Prof *Kawai Y* (Kyusyu Univ) for their valuable suggestions.

The authors would like to thank

Prof *Yoshida Y* (Nagano Univ), Dr *Kitagawa A* (QST), and Dr *Muramatsu M* (NIRS,QST) for provided informative discussion and continued encouragement.

The authors would like to thank all previous staff and graduated students, Osaka Univ for their great efforts in preparing and constructing this experimental device.

The authors would like to thank Dr *Asaji T* (The University of Siga Prefecture) for providing solid-state amplifiers and Mr *Yano K* (Osaka Univ) for the preparation of the experiment.

This presentation is the result of experiments before/after receiving the support of the Grants-in-Aid (JP) for Scientific Research.


Thank you for your attentions
If any of you are interested,
please feel free to comment, discuss,
and join us in the research.